A STUDY OF FAST REACTIONS IN NOZZLE TYPE REACTORS

BY

AKINTUNDE KAYODE COKER, B.Sc.(Hons), M.Sc.
M.A.I.Ch.E., M.I.Chem.E.

A Thesis submitted to

The University of Aston in Birmingham

for the Degree of

Doctor of Philosophy

Department of Chemical Engineering

University of Aston In Birmingham

October 1985

THE UNIVERSITY OF ASTON IN BIRMINGHAM

'A STUDY OF FAST REACTIONS IN NOZZLE TYPE REACTORS'

AKINTUNDE KAYODE COKER Ph.D. October 1985

SUMMARY

A study of fast reactions in three nozzle reactors of the same geometry has been investigated. The nozzle reactors are Ø.55 x $1Ø^{-3}m^3$, 1.52 x $1Ø^{-3}m^3$ and 5.13 x $1Ø^{-3}m^3$ respectively, and flow visualizations have been studied by injecting a tracer into the inlet and at the walls of the reactors. A mathematical model which has been developed, suggests that the flow characteristics in the systems consisted mainly of a series of continuous stirred tanks (CSTR's) with a plug flow between them, and a parallel stream of a plug flow.

Fast reactions studies involving aqueous solutions of sodium carbonate (Na_2CO_3) and sulphuric acid (H_2SO_4) were carried out at varying molar ratios and flow rates in Ø.55 x $1Ø^{-3}$ m^3 and 5.13 x $1Ø^{-3}$ m^3 nozzle reactors respectively. The product samples were determined volumetrically; the yield of the product and the amount of the excess acid reacted in each reactor were determined from stiochiometry. A modified residence time distribution model was developed with the designed equations for a CSTR and plug flow to determine the conversion of the limiting reactant concentration.

Neutralization reaction was carried out involving Linear alkyl sulphonic acid (Dodecylbenzene sulphonic acid) with aqueous solution of sodium carbonate and at varying viscosity of the surfactant in Ø.55 x $1Ø^{-3}$ m^3 nozzle reactor. Studies were conducted at varying flow rates of Dobanic acid and sodium carbonate, and the percentage of the active detergent was analyzed volumetrically.

KEY WORDS:

Air core
Residence Time Distribution
Linear alkylbenzene sulphonic acid (Dobane JN)
Alkylbenzene sulphonate (ABS)

To

The Memory Of My Father

To My Mother,

My Wife, Omolara for her patience,

encouragement and support,

and my Sons

Akintunde

and

Ebunoluwa

The most

beautiful gift

we can give

each other

is the truth

--- Anonymous

ACKNOWLEDGEMENTS

I wish to express my gratitude to the following:

Professor G.V. Jeffreys for his encouragement, expert guidance and personal supervision during the course of this work.

Dr. C.J. Mumford for his technical and helpful suggestions from time to time.

Mr. J. Holloway for the photographs.

Mr. N. Roberts and the entire staff of the Workshop, Analytical Lab. and Stores.

The Lagos State and Federal Governments of Nigeria for their financial support.

Above all, to the elemental beings and forces in the beyond.

CONTENTS

LISTS OF FIGURES

LISTS OF TABLES

LISTS OF PHOTOGRAPHS

CHAPTER ONE

INTRODUCTION

1.Ø INTRODUCTION

Fluid mixing is perhaps the most common unit operation in the chemical process and allied industries. Yet, it is still to be fully accepted that mixing is an operation which is totally dependent on the mechanics of motion of fluids. However, its importance is greatly acknowledged in the mining, food, petroleum, chemicals, phamaceuticals, pulp and paper, and industrial waste treatment, to name a few. The physical interaction of a fluid body with the entire range of physical species, from particulate solids to viscous masses and to low density gases is encountered in mixing. Mixing on a microscopic scale results in molecular diffusion or of repeated movement of small particles adjacent to others. On a macroscopic scale, mixing is the result of the movement of large masses of fluid made up of one or more phases. Thus, a desired distribution of molecular species will result from the mixing caused by applying fluid motion to the system and allowing molecular diffusivity to become rapidly effective.

There are many different ways to provide mixing action in a vessel. A study of the mixing process includes several basic considerations, such as the effect of the vessel on the mixing process. Vessel geometry and structure may also dictate selection and mixing performance. Some vessels are sometimes chosen in process operations which give unsatisfactory performance because

some mixing operations are accomplished in vessels of specific geometry.

Many reactions are sufficiently slow that their rates are determined by chemical kinetics. Reagent streams can first be well mixed before significant conversion takes place and mixing on the molecular scale (micromixing) does not require much attention. Fast reactions on the other hand are characterised by steep concentration gradients on the molecular scale, which ensure that the rate of reagent diffusion matches the high consumption rate due to reaction. Fast reactions are termed as those for which the half - life time of the reaction, determined by chemical kinetics, is of the same order of magnitude as the half - life time of the mixing process resulting in homogeneity on the molecular scale. Reactions of this nature are found in the combustion of fuel, neutralization of acid - base or an alkali and the sulphonation of dodecylbenzene with sulphur trioxide, oleum or sulphuric acid.

The design of mixers and chemical reactors for fast reaction are chiefly characterized from a knowledge of basic hydrodynamic parameters, geometry and molecular properties. Although molecular properties, such as viscosity, density, diffusivity and reaction rate constants are not perturbed by the mixing process; however, the hydrodynamic parameters and geometry determine the intensity of the turbulence, the intensity of the turbulence

determines the rate of mixing, and the rate of mixing in many cases determines the conversion within a reactor.

The reactors to be considered in this study are three geometrically similar cylindrical nozzle vessels of a 'cyclonic' shape, and the objectives of this study are therefore defined as follows:

(i) To design and construct a suitable reactor for the study of flow characteristics, and to investigate the neutralization reactions between sodium carbonate and sulphuric acid, and dodecylbenzene sulphonic acid and sodium carbonate.

(ii) To investigate various reactor and reaction parameters on the conversion and product yield in order to further the understanding of reaction mechanism in the nozzle vessels.

(iii) To investigate and establish scale - up criteria for the nozzle vessels with a view to commercial usage.

CHAPTER TWO

LITERATURE REVIEW

2.1 FLUID MIXING IN REACTION VESSELS

2.1.1 TYPES OF REACTOR

2.2 THEORY AND A REVIEW OF PREVIOUS WORK

2.2.1 SWIRLING FLOW IN HYDRAULIC CYCLONES

2.2.2 SWIRLING FLOW IN CONVERGING CROSS SECTIONS

2.2.3 SWIRLING FLOW IN SWIRL ATOMIZERS

2.2.4 SWIRLING FLOW IN A TUBE

2.2.4.1 VORTEX BREAKDOWN

2.2.5 SWIRLING FLOW IN A GAS-LIQUID CYCLONE REACTOR

2.3 MIXING IN AN ISOTROPIC TURBULENT HOMOGENEOUS FIELD WITH CHEMICAL REACTION

2.3.1 STATISTICAL THEORY OF TURBULENT SCALAR MIXING

2.3.2 MECHANISM OF MIXING

2.3.3 TURBULENCE STUDIES IN MIXING REACTORS

2.3.3.1 STIRRED TANK TURBULENCE AND MIXING

2.3.3.2 FLUID JET TURBULENCE AND MIXING

2.3.3.3 TUBULAR REACTOR TURBULENCE AND MIXING

2.3.4 DIFFUSION CONTROLLED CHEMICAL REACTIONS

2.4 MIXING WITH FAST CHEMICAL REACTIONS

2.1 FLUID MIXING IN REACTION VESSELS

The term mixing is applied to operations which reduce nonuniformities and variations in the composition, physical properties, or temperature of material in bulk. Such mixing is accomplished by movement of material between various parts of the whole mass. Thus, a mixing process is generally considered to mean any blending into a homogeneous mass.

In some cases, a mixing operation involves the movement or transfer of materials to, or from, surfaces of fluid particles or phases. Such operations are encountered in gas absorption, liquid-liquid extraction, leaching and crystallisation (1). In these operations, fluid motion effectively increases the concentration gradient immediately adjacent to the particle or phase surfaces of the transferring components in the liquid. Hence, the performance of equipment for such interfacial mass transfer operations is determined by an interfacial mass transfer coefficient.

An important mixing operation involves bringing different molecular species together to obtain chemical reaction. The components may be (a) miscible liquids, (b) immiscible liquids, (c) solid particles and a liquid, (d) a gas and a liquid, (e) a gas and solid particles, or (f) two gases. In these cases, performance of the equipment involving chemical reaction can be determined in terms of

reaction conversion or yields, and the chemical species of the products obtained. The main mechanisms by which mixing occurs are bulk flow, eddy diffusion and molecular diffusion (1,2). If two miscible liquids are placed together, they will gradually intermix due to the diffusion (or natural convection) of the molecules. Such mixing may take place very slowly, as this type of diffusion is usually a slow process. In turbulent flow, there is bulk motion of large groups of molecules. These groups are termed eddies and their movement results in the material transport called eddy diffusion or eddy dispersion. However, non molecular and non eddy diffusional processes are classified as bulk diffusion convection or dispersion. This is a result of large scale motions that are causing the dispersion. Thus, in each case of fluid mixing, there is bulk motion or convection, which gives rise to dispersion and is superimposed on either molecular or eddy diffusion or both.

2.1.1 TYPES OF REACTORS

Industrial chemical reactors cover a wide range of forms and geometries, such as stirred tanks, pipe lines, jet mixers, packed beds, fluidised bed or circulation loops. Generally, there appears to be no direct correlation between the type of reaction being carried out (e.g. oxidation, reduction, neutralization, combustion,

polymerization) or the complexity of the reaction (e.g. consecutive, parallel and chain reactions), and the geometric arrangement and operating conditions of the equipment in which the reaction is performed.

A survey of the reactors in use in the chemical industry follows two main criteria, which are related to the handling of reactants and products (3).

(1) One or more phases are needed for carrying out the desired reaction; these involve homogeneous and heterogeneous reaction systems.

(2) The reaction mixture is in intermittent or in uninterrupted operations.

If in the former case, no material is supplied or withdrawn during the reaction cycle, the reaction is carried out batch- wise. The other case is that of the continuous flow reactor. Continuous flow reactors for homogeneous reaction systems are of widely different configuration. These extreme shapes are the tubular reactor and the mixed tank reactor, which exhibit different characteristics. These are illustrated in Figure 2.

Recently, hydrocyclone, cyclone, venturi and nozzle type reactors have found increasing industrial use. In particular the hydrocyclone and cyclone reactors (4,5) are claimed to give high liquid mass transfer coefficients when used as gas-liquid reactors. The successful quality and yields of the products from chemical reactors have

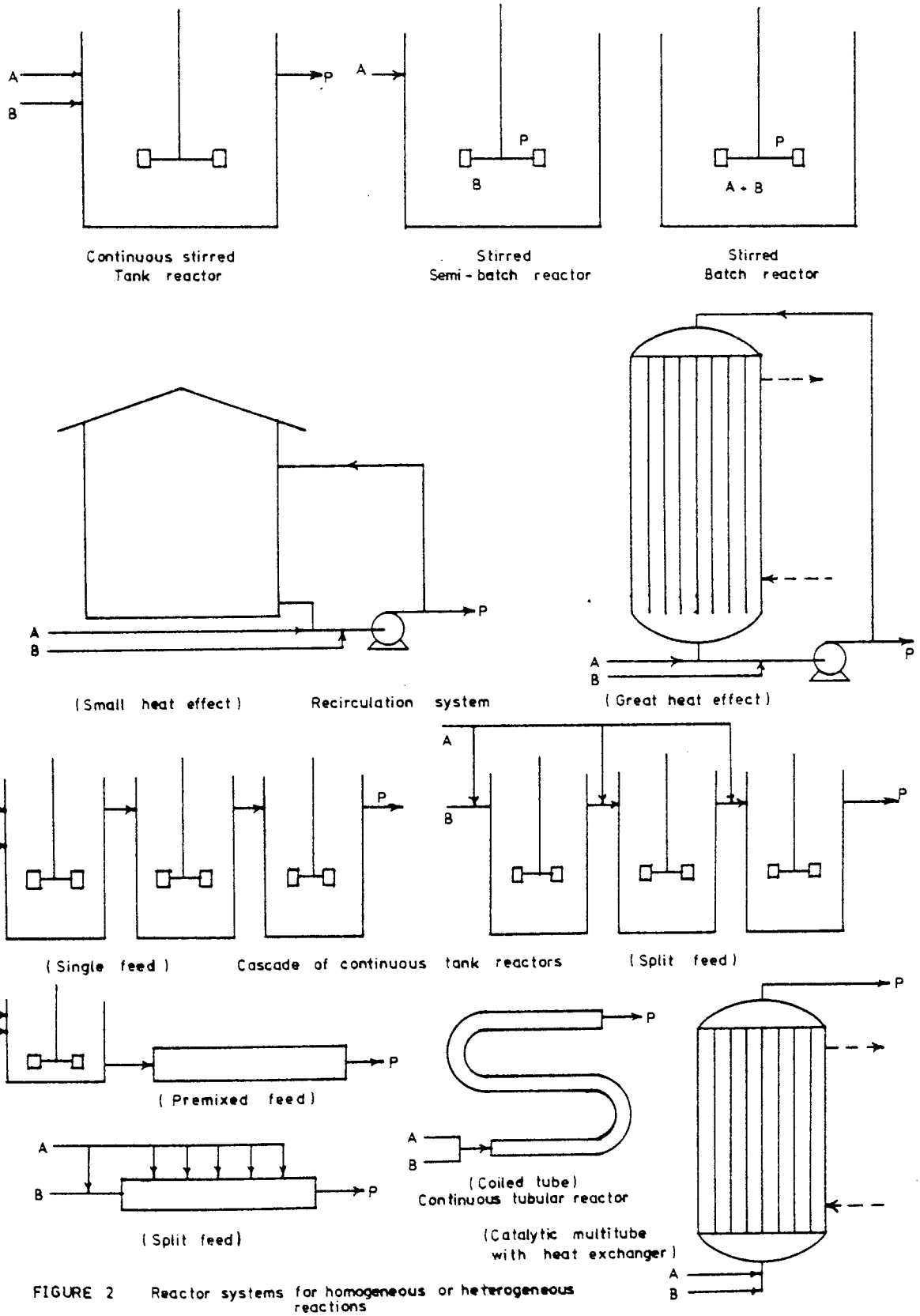

FIGURE 2 Reactor systems for homogeneous or heterogeneous reactions

been shown to be dependent on the level of agitation and type of mixing achieved. Goldstein (6) indicated in Figure 2.1, that three general approaches can be applied to solve an industrial mixing problem. In this work, emphasis is made on the third approach, comprising of developing a mathematical model and carrying out a simulation mixing study to investigate the perfomance of the nozzle reactors.

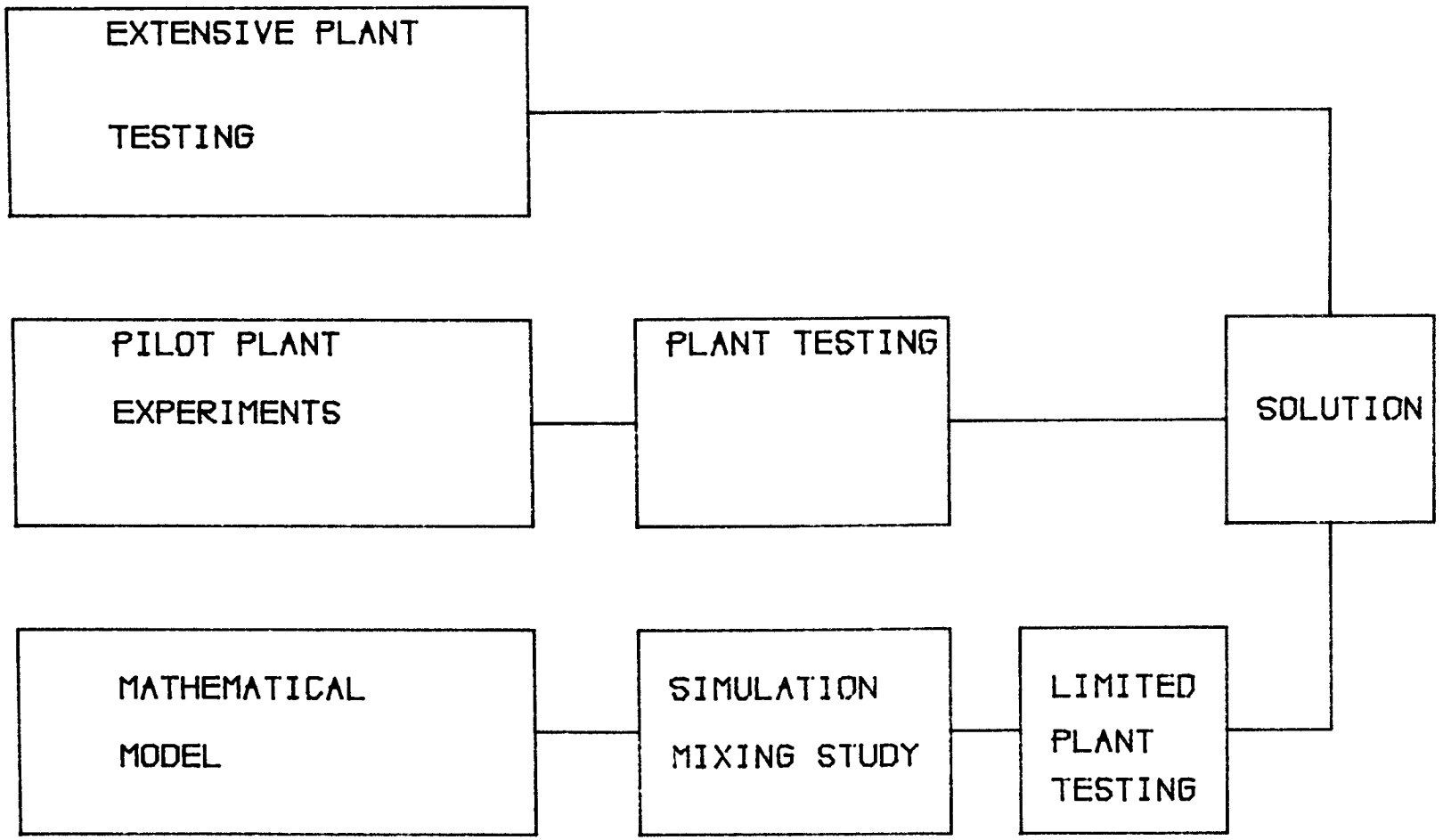

FIGURE 2.1 ALTERNATIVE METHODS FOR SOLVING AN INDUSTRIAL MIXING REACTOR

2.2 THEORY AND A REVIEW OF PREVIOUS WORK

2.2.1 SWIRLING FLOW IN HYDRAULIC CYCLONES

The type of nozzle reactor used in this work is analogous to the liquid cyclone with a cylindrical extension at its base. Figure 2.2 illustrates detailed flow patterns encountered during the flow of fluid particles in a liquid cyclone. Initially, the feed enters tangentially in the cylindrical section to set up a centrifugal force flow pattern. Fluid particles are thrown to the outer radii by the centrifugal force and are conducted by spiral flow currents to the apex of the conical section where they are discharged as an underflow product. The bulk of the fluid and extremely fine fluid particles migrate to the vortex finder called an overflow. The salient operation of the liquid cyclone is the forming of a free vortex, resembling the natural phenomena of whirlpools and atmospheric cyclones.

Dahlstrom (7) indicated that two spiral flow patterns exist within the cyclones (Figure 2.2). The outer spiral travels towards the apex of the cyclone while the inner spiral rotates in the same manner towards the vortex finder. This movement infers that the outer radius of the inner spiral and the inner radius of the outer spiral appear to increase until they are slightly larger than the vortex finder radius at the plane of entrance to the overflow. Because the direction of the inner spiral is towards the vortex finder, an air core 'i.e. a

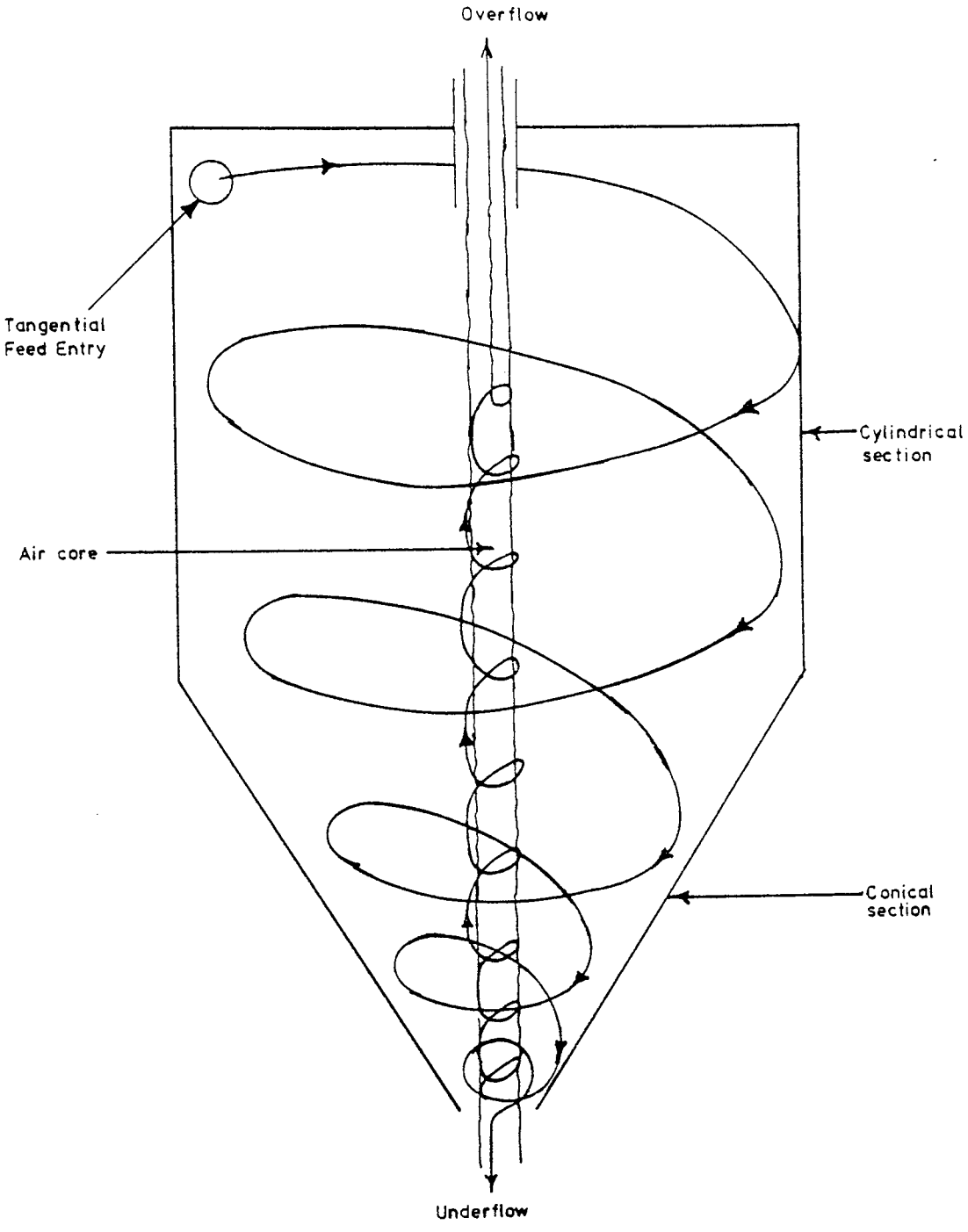

FIGURE 2.2 FLOW PATTERNS IN A LIQUID CYCLONE

cylindrical cavity' is present in the cyclone if both overflow and underflow discharges are at atmospheric pressure. Dahlstrom deduced that correct application of back pressure to the underflow would eliminate the air core.

Kelsall (8,9) undertook detailed studies in a hydraulic cyclone. Using an optical method involving Ultramicroscope illumination and a microscope fitted with a rotating device, he measured tangential and vertical velocity components of fine aluminium particles. The radial velocity components were calculated from continuity considerations. A picture was formed of the flow patterns based upon the results presented as tangential, vertical and radial profiles. Other observations included recirculations of liquid and solid particles at levels above the bottom of the vortex finder, and a short circuit flow down the outside wall of the vortex finder to the overflow.

Bradley and Pulling (10) examined the flow patterns of fluid in hydraulic cyclones by visual and photographic observation of the movement of injected dye. Their transparent perspex cyclones were 38.6 mm and 76.2 mm diameter respectively and the dye was methylene blue solution. The formation of a stationary annular layer in the cyclone was observed, and this effect was attributed to the reversal of flow within the point of transition from downward to upward flow marked by the mantle. Such

an effect was previously observed by Binnie and Teare (11) in their studies of swirling flow in nozzles where the mantles of colour were observed; although there was no top outlet for the liquid. Bradley and Pulling had inferred that such a mantle located the position of zero vertical velocity.

2.2.2 SWIRLING FLOW IN CONVERGING CROSS SECTIONS

A well defined secondary flow sometime occurs in convergent nozzles within the boundary layer of a swirling fluid. For small nozzles almost all of the fluid passing through the throat arrives there by way of the boundary layer. Binnie et al.(11,12,13,14) have reported many experiments in which swirling water, with a nearly free vortex tangential velocity distribution, was passed through convergent nozzles. It was found that water near the axis moved counter to a net forward flow direction.

A secondary flow which has not been explained by Binnie, was treated theoretically and experimentally by Long (15) who considered the case of an inviscid fluid in solid body rotation moving through a tube toward a point sink on the tube axis. Long found that fluid near the axis was accelerated toward the sink, while fluid near the tube wall was decelerated. This effect became more pronounced as the swirl ratio was increased until, at a critical swirl ratio, a region of reversed flow appeared near the wall with a highly accelerated forward flow along

the axis. There are contrasting results between those obtained by Binnie et al., and those by Long. Binnie's small nozzle with an opening angle of 30° suggests the possibility of viscous wall effects than Long's, whose converging nozzle has an opening angle of 180°. Also, the results in Binnie's experiments were for a free vortex distribution of tangential velocities as supposed to Long's, whose experiments were for rigid body rotation.

2.2.3 SWIRLING FLOW IN SWIRL ATOMIZERS

In a swirl atomizer, liquid under high pressure enters through one or a number of tangential entry ports into a cylindrical swirl chamber and after passing through a conical spin chamber gets discharged through the orifice. The liquid entering the atomizer tangentially has a tendency to attain a free vortex motion. This gives rise to very high tangential velocities and very low pressures near the axis, inducing a central air core running through the atomizer. Due to the formation of the air core the liquid comes out through the orifice as thin peripheral liquid film. The air core formed thus has a predominant effect in a swirl atomizer.

Som and Sen (16) investigated the formation of the air core in swirl atomizers, and found that the air core diameter varies considerably with the injection pressure which could be predicted by an analysis of the flow.

Harvey and Hermandorfer (17) described the actual vortex within a swirl chamber as a combination of a free

vortex and a forced vortex. They observed that the flow of oil entering a swirl chamber tangential to the chamber wall by the supply pressure, creates a free vortex, such that the angular momentum which is proportional to RV_t is constant; that is, the velocity increases hyperbolically. They determined the number of revolutions an oil particle makes in the swirl chamber from time of entry to exit, and noted that a particle will revolve less in passing through the chamber under a forced vortex than under a free vortex.

Place et al. (18) found a region in their spray drier where a core of velocities opposite in direction to the primary upward flow existed. They constructed a 1/8Ø scale model in which water was the fluid, and in their study; they observed a region of downward vertical velocity located between an upward central core and an upward velocity region adjacent to the velocities. They noted this as being analogous to a 'Regime III' type of flow as previously observed by Binnie (19). In this regime, the flow was upward near the centre and the walls and downward in an intermediate zone. This phenomenon had earlier been reported by Nuttal (2Ø) in his investigation of swirling fluid flow in a circular pipe. Binnie's method of producing tangential swirl was by rotation of the cylinder wall in constrast to Nuttal's approach, who employed a tangential feed system.

Several studies (21,22,23,24) have been conducted on the formation of a boundary layer in nozzles and cyclones. Taylor (24) studied the boundary layer flow in a swirl atomizer by considering the secondary motion due to a free vortex on the axis of the cone. His application was based upon more approximate methods, based on a technique due to Pohlhausen, which made use of the momentum integral equations. Ashton (25) improved on the technique in his studies of liquid dispersion in a spray drying tower, and deduced that his method was more generally applicable irrespective of the geometry of nozzles.

Binnie and Harris (12) had examined Taylor's earlier work to include a radial sink flow outside the boundary layer. They inferred that the boundary layer in a nozzle may exert an influence upon the discharge of swirling flow of a liquid. Binnie and Teare (11) studied the pressure and velocity distributions inside a convergent nozzle discharging water downwards under pressure. They observed a boundary layer of forced vortex motion on the free surface of the air core. Their findings indicated that with a low supply pressure and a considerable amount of swirl, the axial velocity was reversed in the upper part of the nozzle. Binnie (26) had earlier noted that the axis of the core commonly formed a helical shape with a displacement up to half the core's diameter.

2.2.4 SWIRLING FLOW IN A TUBE

Secondary flows have been observed when swirling water is passed through a round tube of constant cross section. At low swirl ratios, that is at low values of the ratio of a characteristic tangential velocity to axial velocity, the flow is forward everywhere. However, at higher swirl ratios, a cylindrical core of backflow along the tube axis is observed. At still higher swirl ratios, the cylindrical core changes to an annular ring of backflow.

Nissan and Bresan (27) inferred that more complicated flows can occur, depending on initial distribution of tangential velocities and tube diameter. In their study, involving rotating water in a short, 9 in. diameter tube with two 3/8 in. tangential inlets at 1/2 in. from the wall; they observed a central core and an annulus region of backflow sandwiched between two annular regions of forward flow. Although, there have been no theoretical solutions for reversed flows of this kind, it has been noted (27,28,29,30) that these reversed flows depend on viscous action. The phenomena exhibited in such flows are often described as vortex breakdown.

2.2.4.1 VORTEX BREAKDOWN

The phenomenon known as 'vortex breakdown' or 'vortex bursting' is referred to abrupt and drastic change of structure which sometimes occurs in a swirling flow particularly in the leading - edge vortex, formed above a sweptback lifting surface.

Harvey (28) performed experiments on the swirling flow within a long cylindrical tube and observed a region of reversed flow on the axis which had the form of a sphere at one condition. The position of this region was maintained by careful adjustment of the inlet angle of the pheripheral vanes in the swirl generator. Harvey varied the amount of swirl imparted to the fluid before entering the tube, and established that the breakdown formed an intermediate stage between the two types of rotating flows, involving those that did and did not exhibit axial velocity reversal.

Benjamin (29) gave theoretical support to Harvey's conclusion, by considering the change of flow direction on the axis as analogous to the hydraulic - jump in open channel flow. He surmised that the vortex breakdown is not a manisfestation of instability, but a finite transition between two conjugate flow states.

Following the occurence of the vortex breakdown, two main flows have been observed. These are namely, flows containing a large three dimensional time dependent instability called the precessing vortex core (PVC), and

flows in which the amplitude of the PVC is damped . The PVC lies on the boundary of the mean reverse flow zone between the zero velocity and zero stream line. Previously, Gore and Ranz (31) observed oscillations in a swirling fluids moving axially through expanding cross sections, although they were unable to describe the nature.

Chanaud (32) observed such periodic motion in his investigation, comprising both air and water in the vortex whistle and cyclone separator. At higher Reynolds number, he noted that the periodic motion was of large amplitude and injecting a dye near the axis from upstream, produces a flow pattern as shown in Figure 2.3. The shaded region represents a cylindrical sheet of dye which had moved from upstream and then deformed into a rotating spiral pattern. Chanaud observed that at this amplitude the dye represented the central region of a precessing spiral vortex.

2.2.5 SWIRLING FLOW IN A GAS-LIQUID CYCLONE REACTOR

Lately, a gas - liquid cyclone reactor (GLCR) has been developed (5,33) to achieve high mass transfer coefficients in fast consecutive reactions. A particular interest is the sulphonation process, in which the yield of the product is favoured by a high value of the liquid mass transfer coefficient. Furthermore, the selectivity of the reaction has a strong influence on the economy of the process and tends to increase with increase in the

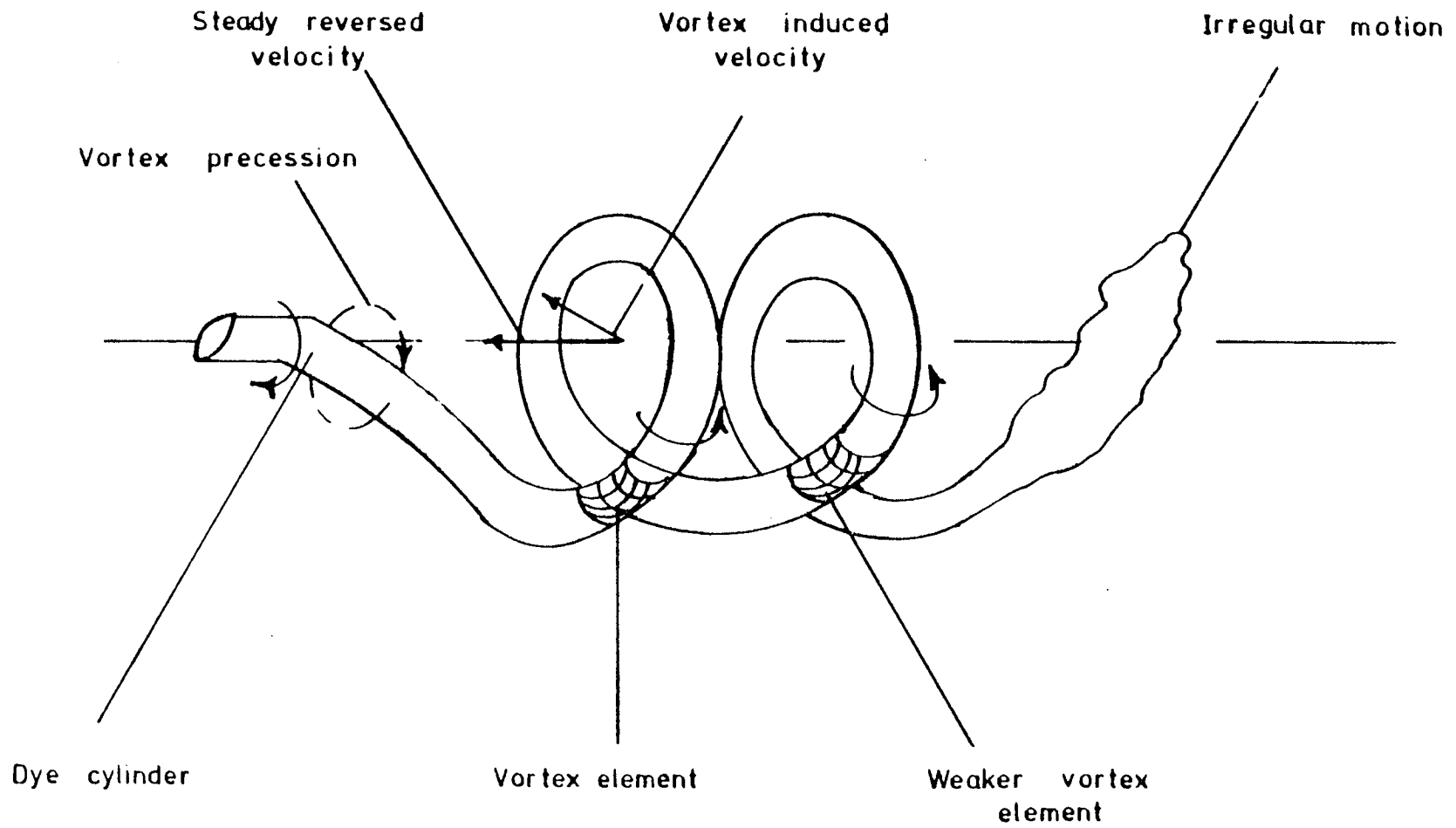

FIGURE 2.3 THE MOTION OF A ROTATING SPIRAL VORTEX

liquid mass transfer coefficient. Recent investigations by Beenackers and Van Swaaij (34) have shown that GLCR has produced high mass transfer coefficient because of the strong centripetal forces on the gas bubbles.

2.3 MIXING IN AN ISOTROPIC TURBULENT HOMOGENEOUS FIELD WITH CHEMICAL REACTION

Turbulence is viewed to comprise of eddies of various sizes and vortices. The upper size limit of eddies is of the order of the characteristic dimension of the apparatus. The effect of conversion and diffusion causes the larger eddies to break and are reduced to smaller sizes. The lower size limit of the eddies is governed by viscosity effects. A larger velocity gradient in a smaller eddy gives rise to a larger shearing stress which subsequently limits the further reduction in size.

Since turbulent mixing of stream components relies upon the action of turbulent motion, hence theoretical development of turbulent mixing is closely interacted with that of turbulence theory. Turbulent mixing and chemical reactions are often involved in the analysis of industrial reactors. In such cases, chemicals react only to the extent that turbulent stretching and mixing bring the components close enough for diffusion to ensure contact of the individual molecules and subsequent reaction. Hence, a basic understanding of turbulent motion, mixing and kinetics with reactor modelling and design is not available, since the mechanism of turbulent motion is of a complex nature. However, studies of turbulent motion involve experimental observation of phenomena coupled with theoretical concepts such as statistical description by

correlation and spectra analysis, homogeneity, isotropy and asymptotic solution of relevant equation.

Certain terms such as isotropy and homogeneity have been associated to the turbulent field. These terms have reduced the complex problem of turbulence suitable to theoretical analysis. The term homogeneous turbulence implies that the average fluctuations in the system are random, and that the average turbulent characteristics are independent of the position in the fluid. Thus homogeneous system can be restricted by assuming that in addition to its homogeneous nature, the velocity fluctuations are independent of the axis of reference, that is invariant to the axis of rotation and reflection. This restriction forms isotropic turbulence, which is always homogeneous (1). The difference between the two types of turbulence is illustrated by considering the root mean - squared (r. m. s.) velocity fluctuations in x, y, z - directions respectively.

$$u' = \sqrt{\bar{u}^2}, \quad v' = \sqrt{\bar{v}^2}, \quad w' = \sqrt{\bar{w}^2}$$

In homogeneous turbulence, the r.m.s values could all be different, however each must be constant over the entire turbulent field. In isotropic turbulence, the spherical symmetry requires that the fluctuations be independent of the direction of reference or the r.m.s values all be equal, that is,

$$\sqrt{\bar{u}^2} = \sqrt{\bar{v}^2} = \sqrt{\bar{w}^2}$$

or $u' = v' = w'$

Chemical reactions in turbulent fields can be viewed in several ways. In the deterministic approach, the time average diffusion equations for the species are developed with the appropriate boundary conditions and the mean concentration profiles are obtained by solving the equations either analytically or numerically after introducing the information about the fluctuations into the equations. Generally, the experimental information is required in determining the behaviour of the fluctuating terms. The other approach is the statistical theory based on the random behaviour of eddies in a turbulent field. In this approach, several statistical parameters, such as the Kolmogoroff number for species fluctuation, the rate of destruction of the turbulent kinetic energy, energy containing wave numbers, root mean square velocity fluctuations, dissipating length and velocity auto correlations are introduced in the basic conservation equation for turbulent mixing. This in effect gives rise to a term called ' the closure problem of turbulence theory' since the number of unknowns are always more than the number of equation. Thus the remaining unknown and parameters are determined by the relationships which are based on intuitive approximations and trial - error.

Finally, there are many phenomenological theories such as the Prandtl mixing length theory based on physical intuition, but limited in its possibilities for further

development. Also, there are the phenomenological models which may predict the average conversion over the cross section of a reactor quite adequately. Such models tend to give much insight into the fundamental mechanism of the process which is often useful for practical work. This category includes the models based on macromixing (measured by the residence time distribution) and micromixing (representing the immediate environment of the reacting fluid element and measured by e.g. the number of coalescence the fluid element experiences before exit from the reactor).

2.3.1 STATISTICAL THEORY OF TURBULENT SCALAR MIXING

The study of turbulent motion was initiated by Reynolds (35) and Taylor (36) later employed statistical concepts to represent the first significant step in the analysis. Van Karman and Howarth (37) obtained a one dimensional form for the velocity correlation function which has been transformed by Fourier analysis into a spectral form. Subsequent theoretical investigation has suggested three categories of solutions for these equations. Namely, dimensional analyses surveyed by Kolmogoroff (38), intuitive solutions proposed by Heisenberg (39) and direct approximations exemplified by Kraichnan (40).

The study of turbulent mixing theory began with the work of Obukhov (41), who, using the concepts developed

for turbulent motion, derived the basic equations. The solutions of these equations are classified similar to those of turbulent motion:
dimensional analyses formulated by Obukhov (41) and Batchelor (42), intuitive solutions suggested by Beek and Miller (43) and direct approximation solutions established by Lee (44).

Obukhov (41) and Corrsin (45) developed the turbulent mixing problem starting with the scalar conservation equation.

$$\frac{\partial C}{\partial t} + \underline{V} \cdot \nabla C = D \nabla^2 C \qquad 2.1$$

For an isotropic, homogeneous turbulence the following equation in physical space describes the behaviour of C'.

$$\frac{\partial \overline{C'^2}}{\partial t} g_s(r) - 2 \overline{C'^2} \overline{U'} \{ \frac{\partial K_s(r)}{\partial r} + 2 \frac{K_s(r)}{r} \} = 2 D \overline{C'^2} \cdot$$

$$\{ \frac{\partial^2 g_s(r)}{\partial r^2} + \frac{2}{r} \frac{\partial g_s(r)}{\partial r} \} \qquad 2.2$$

$K_s(r)$ is the triple correlation function

For isotropic conditions the basic differential equation when converted into wave number space becomes

$$\frac{\partial E_s(K)}{\partial t} = T_s(K) - 2 D K^2 E_s(K) \qquad 2.3$$

where K is the wave number
$E_s(K)$ is the scalar spectrum

and $T_s(K)$ is the scalar associated with transfer of energy between wave numbers or eddy sizes. Since $T_s(K)$ is unknown, equ. 2.3 is indeterminate and results to a familiar closure problem of turbulence. Hence, a relation between $E_s(K)$ and $T_s(K)$ is assumed, using experimental results. Thus the conservation of matter relation, which was used to obtain equ. 2.3 can be reduced to

$$\frac{da'^2}{dt} = -12\frac{Da'^2}{\lambda_s^2} \qquad 2.4$$

where λ_s is the scalar microscale mixing and D is the molecular diffusivity.

Integrating equ. 2.4, gives an expression for the intensity of segregation.

$$I_s = e^{-t/\tau} \qquad 2.5$$

where $$\tau = \frac{\lambda_s^2}{12D}$$

and is the time constant of mixing.

Corrsin (46) had obtained τ for both the low and high Schmidt number ranges.

For the low Schmidt number case,

$$\tau = \frac{\lambda_s^2}{12D} = \frac{2}{(3 - N_{Sc}^2)(\epsilon k_{o,s})^{1/2}}$$

$$= \left\{\frac{5}{\pi}\right\}^{2/3} \frac{2}{(3 - N_{Sc}^2)} \left\{\frac{L_s^2}{\epsilon}\right\}^{1/3} \qquad 2.6$$

where

L_s is the scalar macroscale

ϵ is the velocity energy dissipation per unit mass

and $k_{o,s}$ is the wave number representative of the large scalar blobs.

For the high Schmidt number, the time constant can be obtained by integration of the spectrum curve (a composite of the - 5/3 and - 1 subranges) to give

$$\tau = \frac{\lambda_s^2}{12 D} = \frac{1}{2}\left\{ \frac{3}{(\epsilon k_{o,s})^{1/3}} + \left[\frac{\nu}{\epsilon}\right]^{1/2} \ln N_{Sc} \right\}$$

$$= \frac{1}{2}\left\{ 3\left[\frac{5}{\pi}\right]^{2/3} \left[\frac{L_s^2}{\epsilon}\right]^{1/3} + \left[\frac{\nu}{\epsilon}\right]^{1/2} \ln N_{Sc}\right\} \qquad 2.7$$

2.3.2 MECHANISM OF MIXING

The type of mixing considered is the mixing between two or more streams. In this case, if two mutually soluble liquids are mixed together; the liquids are broken up into 'clumps' which are intermingled and the shape of the clumps will depend on the mechanism of the mixing process. These may be contracted or in the form of long streaks. Also, the average size of these clumps will continue to decrease as mixing is advanced.

At the same time, molecular inter - diffusion of the two liquids occurs across the boundaries of the clumps.

This occurs rapidly and will continue even if the mechanical mixing is stopped. Diffusion will ultimately reduce any mixture of mutually soluble liquids to complete homogeneity, but the process is slow unless the liquids have been broken up into small clumps. However, unless diffusion occurs, continuous stirring will not produce a homogeneous mixture. The composition at any point will vary from one region to another. The breaking up and the interdiffusion are largely independent processes which produce discernible results (47).

Danckwerts (47) proposed a set of criteria to provide a measure of the level of mixing 'goodness of mixing'. This would enable mixing tasks to be specified and the efficiency of mixing process to be compared. The two criteria are the scale of segregation (L_s) and the intensity of segregation (I_s) respectively. The scale of segregation is defined as a measure of the size of the regions of segregation, or 'clump' of the unmixed components, in an imperfect mixture. It is also a measure of some average size. In Figure 2.4, along the top from left to right, as the clumps are pulled and contorted, the scale of mixing is reduced. The second criteria is the intensity of segration, which describes the effect of molecular diffusion on the mixing process. It is a measure of the difference in concentration between neighbouring clumps of fluids. The intensity for each value of the scale is illustrated by the columns in Figure 2.4.

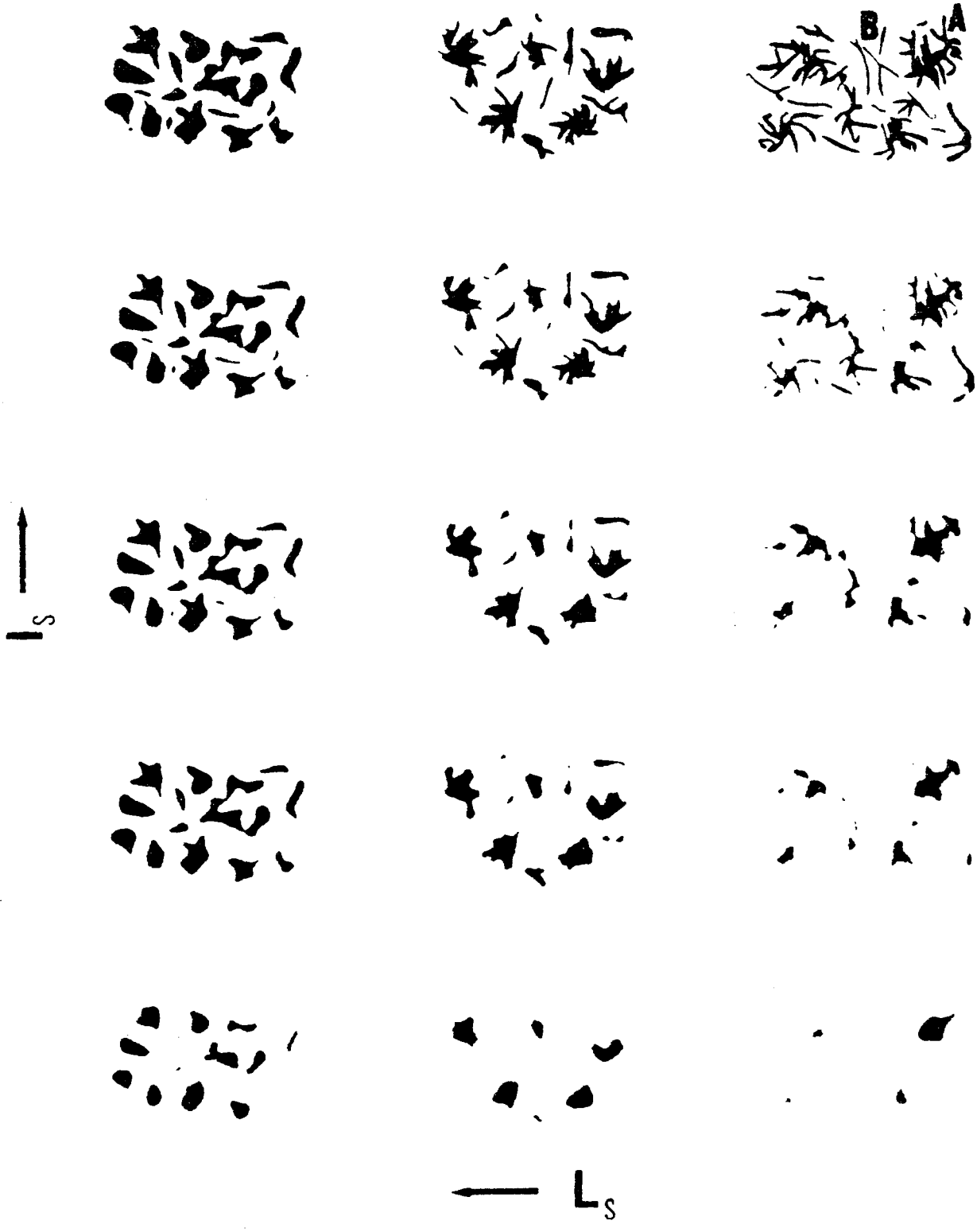

FIGURE 2.4 A VISUALIZATION OF THE SCALE AND INTENSITY OF MIXING

In general, the turbulent process can be used to break up fluid elements to some limiting point, although the level of break up or scale is not close to molecular size because of the microscopic nature of turbulence. However, since energy is necessary for this reduction in scale, the limiting scale is associated with the smallest of the energy containing eddies. The size will remain large when compared with molecular dimensions and without molecular diffusion, this ultimate mixing can not be obtained.

Molecular diffusion allows the movement of the different molecules across the boundaries of the elements, thus reducing the difference between molecules. This reduction in intensity will occur with or without turbulence. Hence, turbulence can accelerate the process by breaking the fluid into many small clumps and thus creating more area of molecular diffusion. When diffusion has reduced the intensity of segregation to zero, the system is then classified as being mixed. The molecules are distributed uniformly over the field, and various degrees of this combined process are illustrated in Figure 2.4.

2.3.3 TURBULENCE STUDIES IN MIXING REACTORS

2.3.3.1 STIRRED TANK TURBULENCE AND MIXING

Various techniques have been used to elucidate the turbulent mixing occuring in stirred tanks. The simplest approach involves a stimulus response method, which

measures the response of the concentration in the exit stream to a change in the entrance stream concentration, and relates the response to parameters of the vessel such as capacity, impeller speed, impeller design or vessel design. However, detailed information about turbulent flow patterns is one in which the concentration and velocity are measured at various points in the system.

Sachs and Rushton (48) attempted to measure the velocity of the fluid leaving a turbine by photography of tracer particles suspended in a fluid. The particles appeared as streaks whose lengths were directly proportional to the velocity. They found that the maximum radial velocity did not occur at the impeller tip, but at a distance from the tip, because of the axially moving fluid being entrained by the discharge stream.

Cutter (49) studied turbulence in a stirred batch tank by means of a photographic technique, focussing his investigation about the impeller stream. The turbulence parameters obtained were intensities of turbulence, macroscales in the radial and tangential directions, and estimates of energy dissipation based on turbulence intensity and macroscale in various sections of the vessel. He inferred that half of the total dissipation in the tank occurred in the impeller stream, a fifth in the impeller region and the remaining in the rest of the tank.

Manning and Wilhelm (5Ø) measured concentration fluctuations using a conductivity probe. The traced

solution was injected directly under the impeller and water was fed into the bottom of the tank with measurements at various positions. These researchers focussed their study on measurements at 15ØØ r.p.m., a speed at which average concentration is nearly uniform and the concentration fluctuations are near zero at all points except those near the injection point at the impeller. They found that the r.m.s. concentration fluctuations varied with respect to angular position as did the average concentration, except near the baffles.

Similar measurements were made with a smaller probe by Reith (51); who found that the spectrum of concentration fluctuations contained a Kolmogroff -5/3 wave number region and that the spectra were not similar at a fixed position for several impeller speeds. Reith reported integral concentration scales of the order of twice the impeller diameter and he inferred that the principles of Reynolds number similarity could predict correctly the influence of impeller speed on the turbulence decay rate.

Kim and Manning (52) measured the radial components of the turbulence energy within a stirred, baffled tank with a piezo - electric transducer probe. Results of their spectral measurements over the frequency range of 19 to 1,1ØØ Hz showed that the energy spectra were proportional to $k^{-1Ø/3}$ over one decade. However, they were unable to determine the absolute levels of the intensity due to a limitation on their technique.

Rao and Brodkey (53) studied mixing in a continuous flow tank stirred by a flat bladed open impeller. They measured the mean and fluctuating radial, axial and tangential velocities in the impeller stream by a hot film anemometer. Auto correlations and one - dimensional spectra of the velocity fluctuations, obtained at various positions in the stream, revealed the presence of periodic velocities close to the impeller, generated by the rotating blades.

Mujumdar et al. (54) used hot wire and hot film anemometry to measure mean and fluctuating radial velocities in the impeller stream in stirred tanks. Air was used as the working fluid, based on the assumption that small scale turbulence characteristics would be the same at equal Reynolds number, regardless of the fluid in the tank. Their results indicated that the intensity of the turbulence rapidly increased from a level of 5% near the impeller tip to 35% at radial position of one - third of the distance from the impeller to the wall. However, they were unable to observe the Kolmogoroff -5/3 range due to the presence of the non - random component.

Techniques involving the use of a laser Doppler anemometry and a self scanning photodiode array, have provided a valuable tool for studying turbulent parameters. Reed et al. (55) investigated the turbulent flow in the impeller stream using a laser Doppler anemometry, as no interference with the flowing fluid.

The average and r.m.s. velocities were measured, and these showed the absence of a symmetry plane in the impeller stream of a flat blade, disk type turbine located one - third the way up from the base of the tank.

2.3.3.2 FLUID JET TURBULENCE AND MIXING

When a turbulent free jet mixes with its environment, macroscopic elements of the two fluids are interspersed, with the result that molecular diffusion tends to reduce the resulting variations in concentration between neighbouring regions. Also the instantaneous concentration of the jet fluid at any point in the mixing zone fluctuates about its mean value. The more complete the degree of mixing on the molecular scale, the less the fluctuations. Jets may be moving in the same or opposite directions, in cross flow or in a swirling motion. The eddies on the tangential surfaces cause an exchange of momentum, heat and mass transfer across the jet.

Turbulent mixing studies in fluid jets have been well documented (56,57,58,59). Rosensweig et al. (60) studied the behaviour of a smoke jet, using the intensity of light scattered from a small region in the mixing zone to measure local r.m.s. concentration fluctuations for a jet Reynolds number 26,000.

Kristmanson and Danckwerts (61) introduced a photographic technique to determine the concentration distribution of jet fluid when a circular turbulent jet of liquid mixes with a liquid in the environment. They

investigated the decay of segregation and the dilution process on the molecular scale of the jet fluid in the mixing zone, using aqueous solutions of hydrochloric acid and sodium hydroxide with an indicator at Reynolds number of 12,ØØØ. Subsequently, Wilson and Danckwerts (62) focussed on the mixing and dilution of a turbulent hot air jet with its surroundings by measuring the time average temperatures and temperature fluctuations with Reynolds number of 2 to 4Ø,ØØØ. They presented their results in terms of the r.m.s. temperature fluctuations at different points in the jet, and compared the intimacy of mixing at different points with the effect of the magnitude of molecular diffusivity on the intimacy of mixing.

2.3.3.3 TUBULAR REACTOR TURBULENCE AND MIXING

Radial mixing has been applied to fluid homogeneity in a tubular reactor which determines the conversion rate and selectivity of the desired product (63). Several techniques have been considered to promote radial mixing in tubular reactors. These include helically coiling a tubular reactor (64), rotating an annular reactor (65) and employing tubular reactors as mixing heads (66,67,68,69,7Ø).

Fisher (68) and Ou (69) have achieved radial mixing in a tubular flow reactor by attaching mixing heads to their reactors. Fisher's reactor was preceded by a multi-jet mixing head to mix the reactants of aqueous solutions

of hydrochloric acid and sodium hydroxide. He examined the effect of Reynolds number, mixing heads, mixing head spacing, stoichiometry of the reacting fluids, chemical diffusion and common ion effect on the rate of reaction. Ou on the other hand, considered nitric oxide formation in combustion during a mixing quench with colder gases and cases of competitive reactions where chemical selectivity is disguised by mixing.

Ou et al. (7Ø) have recently employed mixing of chemically reactive fluids by swirling in a tubular reactor. They achieved a varying degree of radial mixing in a single phase fluid by two non premixed fluid streams tangentially entering a tubular reactor, which subsequently formed a stable laminar swirl. They indicated the formation of vortex created by the tangential entry of the fluids of no interfacial tension that enter a tube in opposite directions with result that the fluid swirls downstream with simultaneous mixing. They employed the material stretching co-ordinates technique to describe the laminar swirling induced by the tangential inflow of two fluid streams and deduced the effect of mixing on the conversion of an infinitely fast second order reaction involving non premixed feeds.

2.3.4 DIFFUSION CONTROLLED CHEMICAL REACTIONS

Chemical reactions carried out in turbulent flow systems are often analysed into two limiting cases and one

intermediate case. The two limiting cases occur when either hydrodynamics or kinetics completely dominate a combined mixing reaction system. In the first limiting case, the kinetics of the reaction are so rapid that the reaction is complete when mixing is complete. Reactions of this type are referred to as diffusion - controlled reactions, since the molecular diffusivity is the sole reaction - limiting factor in the flow field. The second limiting case is the situation in which the kinetics of the chemical reaction are so slow that the reactants are completely and thoroughly mixed before any reaction has taken place. This relates to the most encountered case in reactor design. However, the intermediate case, employs the hydrodynamics of mixing and the kinetics of reaction to determine reaction yield (71,75).

Generally slow reactions allow reactants be mixed on a molecular scale before appreciable reaction takes place. For fast reaction, the rate of conversion depends only on the rate of reactant mixing. The reaction of this type is noted as diffusion controlled reactions, and in turbulent flow, the rate of conversion depends on turbulent mixing at large scales as well as molecular diffusion at the small scales. The treatment of the rate of diffusion controlled reaction in solution was initiated by Smoluchowski (72) for the rates of coagulation of colloids. Recently, numerous studies on turbulent mixing reaction problems have been carried out, theoretical or

experimental by Toor (73,74), Keeler et al. (75), Toor and Chiang (76), Mao and Toor (77), Singh (78), Torrest et al. (79), Brodkey (8Ø) and Mckelvey et al. (81).

Toor employed transformations first proposed by Burke and Schumann (82) to solve mathematically the limiting case of an instantaneous or diffusion - controlled reaction, and later applied them to turbulent flow systems. For such systems, Toor suggested that in diffusion - controlled reactions, solutions could be expressed in terms of the r.m.s. concentration fluctuations as previously proposed by Beek and Miller. After assuming that the fluctuating component of concentration is normally distributed around the mean, Toor obtained the solution for the yield of a diffusion controlled reaction in terms of the mixing problem, even when reactants were present in non stoichiometric amounts. For the diffusion controlled reaction, with reactants

$$aA + bB \text{ -----> } \text{Products} \qquad 2.8$$

a, b stoichiometic coefficients present in stoichiometric amounts,

$$F = 1 - \sqrt{I_s} = 1 - \frac{\sqrt{\bar{c}^2}}{\sqrt{\bar{c}^2_o}} = \eta \qquad 2.9$$

where F = Fractional conversion of reactant

$\sqrt{\bar{c}^2}$ = root mean square concentration fluctuations

$\sqrt{\bar{c}_o^2}$ = initial root mean square concentration fluctuations

I_s = Intensity of segregation

For the case where the reactants are not present in stoichiometric quantities, Toor arrived at a more complex expression.

$$F = 1 + (\beta - 1)\{1 + g[\gamma(1 - n)]\} \qquad 2.10$$

where $g(x) = \frac{x}{\sqrt{2}}\ \text{ierfc}\left(\frac{1}{\sqrt{2}x}\right)$

β = stoichiometric parameter

$$\beta = \frac{a\,\bar{c}_B}{b\,\bar{c}_A}$$

γ = initial value of r.m.s. reactant concentration

x = distance

The statistical theory of Toor was confirmed experimentally by Keeler et al. who measured the scalar decay law and fractional conversion for Ammonium hydroxide - Acetic acid reaction in the turbulent field behind a grid. Vassilatos and Toor used a multiple jet mixing head to produce a turbulent field, homogeneous on a coarse scale after about four jet diameters from the inlet. They studied four very rapid acid - base reactions, two rapid reactions and one slow reaction. For the case of very

slow reactions, they found that mixing had very little effect on the reaction. However, the predictions of very fast reaction conversion were in agreement with the experimental values for various values of the initial concentrations and the theory of Toor was verified.

2.4 MIXING WITH FAST CHEMICAL REACTIONS

Previous investigation of the rates of chemical reactions in solution were studied by relatively simple methods. Initially, the reaction was initiated by mixing the solutions, and its progress was followed by either titrating samples or making measurements of some physical property after various time durations. In the process, the time required for mixing and for observation had to be short compared with the half life time of the reaction. Consequently, the fastest reactions that could be measured had half life times of minutes or sometimes seconds. Also many reactions, especially those containing ions, were immeasurably fast such that their mechanisms could not be kinetically studied, and are termed fast reactions. Hence, fast reactions are defined as those for which the half - life time of the reaction, determined by chemical kinetics, is of the same order of magnitude as the half life time of the mixing scale, principally due to molecular diffusion. Further reviews in the study of fast reactions are well illustrated by Caldin (83), Hague (84), Frost and Pearson (85).

Generally many chemical reactions are sufficiently slow compared to mixing, such that homogeneous reaction to the molecular scale (micromixing) occurs when contacting reagents before any significant reaction can take place. Also the reactor has no influence on the course of the reaction whether the solutions are premixed or added in

separate streams. However, in fast reactions (e.g. neutralization, precipitation and combustion), the conversion occurs locally in regions where steep concentration gradients are formed (reaction zones) and separate solution feeds are employed. Bourne (86) stated that inhomogeneity at the molecular scale (segregation) causes:-

(i) a reduction in reaction rate relative to perfect mixing, hence calling for more reactor volume in order to obtain a given output, and

(ii) a frequent change in the relative amounts of the products from multiple reactions, so that the selectivity depends upon mixing.

Bourne emphasized that this change can result in a loss of raw materials in manufacturing unwanted products, increased load on the separation stages after the reactor when working up the desired product and the difficulties in scale - up, since the agitation intensity and thus the product distribution often vary with scale.

2.4.1 TECHNIQUES FOR STUDYING FAST REACTIONS

Several methods have been investigated to follow fast reactions, involving rapid mixing of two reactants solutions, within a fraction of a second. The flow techniques, namely the continuous flow, accelerated flow and the stopped flows are the earliest of the methods developed for such studies.

Hartridge and Roughton (87) first applied the continuous flow method to measure the rate of reaction between oxygen and haemoglobin in water. They passed the two reactant solutions from large reservoirs held at a constant head along two capillary tubes arranged to form a T - piece mixer and determined the concentration of one or more of the reactants along the tube. Eight jets were arranged tangentially around the outlet tube in the mixer, and it was found that mixing was complete within a millisecond at a distance of 3 mm from the mixer. Their device depends upon achieving efficient mixing and the flow is such that the composition of the liquid must be uniform at any cross section of the observation tube. However, the drawback on the continuous flow method is the requirement for vast amounts of reactant solution.

Chance (88) overcame this disadvantage in the flow method, by introducing a variation of the unstirred flow method in which the reaction time is continuously varied by changing the throughput and holding the volume constant. In the accelerated flow technique, the output from a photoelectric colorimeter is fed to a cathode - ray oscilloscope, which then sweeps out a complete time concentration record and may be photographed. The method was applied for very rapid enzyme reactions which require small amounts of reactants.

Chance (89) further used a simple device consisting of two hypodermic syringes of equal volume, with the

plungers pushed together to deliver equal amounts of the two solutions to the mixer. The reactant liquids were made to flow and then suddenly stopped. He employed oscilloscopic methods to study the concentration as a function of time after the flow ceased. Gibson (90) also developed the method of Chance, but showed prominent differences pertaining to the electronic arragements and the stopping device. Dalziel (91) applied photoelectric spectrophotometer analysis to the constant flow method in the kinetic study of rapid reactions on the dissociation of oxyhaemoglobin. Analyses on the accuracy of the kinetic measurements, and the factors in assessing the validity or accuracy of any particular application, namely; the slit length, the equivalent mixing length and the character of flow in the tube were studied. He inferred that the equivalent mixing length general decreases as the rate of flow increases and as such; in measurements on a particular reaction, the error, must decrease as the flow rate increases and the reaction spreads over a greater length of the observation tube.

Other methods have been explored to study reactant solutions with no specific fast techniques of observation. Pinsent (92) presented a rapid quenching technique to measure the reaction rate of carbon dioxide with hydroxyl ions in a carbon and bicarbonate buffer solutions. Pearson et al. (93) developed a thermal method to measure the rate of fast reactions which have an appreciable heat

of reaction. They studied the reaction rate of carbon dioxide in solution with hydroxide ions and ammonia. Denbigh and Page (94) proposed a capacity flow method which formed a steady state of constant uniform concentration in a well stirred vessel that operated continuously. Reactions were studied at times of passage between 1 and 4000 secs. Their technique was suitable for the measurement of reaction rates which are too fast for investigation by the conventional static methods, but too slow for convenient application of the Hartridge and Roughton technique.

Young and Hammett (95) studied the kinetics of the alkaline bromination of acetone in a stirred flow reactor, based on the earlier investigations by Denbigh et al. (96). Saldick and Hammett (97) presented a method of investigating reaction kinetics in solution by applying a scheme of continuous titration to the output of the reactor when aqueous solutions of sodium hydroxide and of sodium acetate were introduced in separate streams of constant flow rate in a closed stirred reactor. Their method avoided the difficulty of quenching and analyzing a considerable volume of reaction mixture at a known time. Rand and Hammett (98) studied the measurement of reaction rate through determining the temperature rise in a stirred flow reactor and applied the same technique to measure reaction heats in systems whose rates of reaction are difficult to measure.

Protons transfer reactions are extremely fast and Eigen (99) has investigated possible method for studying ionic reactions in solutions. His studies were applied to neutralization and hydrolysis reactions, and the methods are based upon measurements of the chemical relaxation of an electrolytic dissociation equilibrium effected by rapid variation of pressure, electrical field density and temperature. Eigen's studies have shown that bimolecular reactions in aqueous solutions involving H^+ or OH^- ions are characterized by extremely high rate constants in the order of 10^{10} to 10^{11} l/mole sec. He found that the rate constants of the reaction

$$H^+ + SO_4^{2-} \text{ --------> } HSO_4^- \qquad 2.11$$

was 10^{11} l/mole.sec. and for

$$NH_4^+ + OH^- \text{ ---------> } NH_3.H_2O \qquad 2.12$$

was 4×10^{10} l/mole.sec. His findings were in fair agreement with other methods.

2.5 RESIDENCE TIME DISTRIBUTION AND FLOW PATTERNS IN CONTINUOUS FLOW SYSTEMS

A knowledge of the residence time distribution functions (RTD) of fluid flows in steady state flow systems is an important phenomenom in the choice, the development and the upscaling of reactors and contactors, as it may influence to a great extent, conversions and efficiencies of the chemical and physical processes in these systems. In any continuous flow system with one or more entrances and exits, conserve particles enter the system, remain in it for some period of time and may be either deterministic or probabilistic, and eventually leave. Fluid elements which first enter the system have zero age and subsequently acquire age at a rate equal to the time spent within the system boundaries. The age of a fluid element is the time that is has spent in the system; and thus, the age of an element at its last exit from the system is called the residence time.

At a molecular level of scrutiny, the residence time is a stochastic variable when applied to a probability distribution. This distribution is also suitable if conserved entities are Brownian particles or fluid elements in a turbulent flow field. However, in the instance of fluid elements in laminar flow, residence times may be completely deterministic in nature (100).

In general, there is always a distribution of residence times, and probability functions are used to characterize

this distribution whether intrinsicly stochastic or deterministic. Tracer methods have found immense uses in investigating flow systems, and to determine the physical parameters of systems such as diffusion, dispersion and dilution coefficients; modelling of flow systems, and to evaluate some parameters of a model representing the system.

The first systematic attempt to develop a theory of residence time distribution for the case of a number of identical, completely mixed tanks in series was initiated by Mac Mullin and Weber (101). Later, Bosworth (102,103) applied the concept of the RTD to laminar and turbulent flows in cylindrical reactors. However, Danckwert's (104) work heralded the application of the RTD to flow systems. He analysed the relationship between the various age distributions and the relationship of the residence time distributions (i.e. $F(\theta)$) and the residence time probability density (i.e. $E(\theta)$) to other representations of the dynamic behaviour of flow systems, such as pulse, step and frequence response. From his critical work, have resulted in further established differential equations and transfer functions derived by many researchers (105,106,107).

2.5.1 FLOW VISUALIZATION IN CONTINUOUS STIRRED VESSELS

Studies have been carried out on various methods of characterizing flow through vessels. An important reason for this is the need to predict the performance of a vessel when processing a chemical reaction with non linear kinetics. Flow patterns exhibiting deviations from plug flow have been represented by a dispersion model (108). In systems of small height to diameter ratio, such that the inlet diameter is a fraction of the vessel diameter, stagnant zones and short circuiting phenomena have been observed. Such flow systems have been modelled by networks of idealized flow systems which often involved the use of mixed models (109). Recirculation effects have been encountered in some systems and are also included in some theoretical models. However, experimental investigations involving recirculation which featured greatly in turbine stirred tanks (110) have been extended to cylindrical vessels and circular confined jets (111,112).

2.5.2 MIXING TIME STUDIES IN STIRRED VESSELS

Flow visualization and RTD involving tracer experiments have been extensively investigated by many workers. The development of the RTD models, to account for the behaviour of different geometrical vessels has been postulated. However, the effectiveness of mixing in system, was evaluated as the time required to bring a non homogeneous mixture to a level of homogeneity. The acid - base neutralization followed visually with an indicator dye has been reviewed by a number of workers

(113,114,115). The method has the advantage of providing a visual indication of the last point in the system where homogeneity is achieved, as no probes are required and any dead regions can be reasonably identified.

Coker (116) investigated fluid mixing in three geometrically similar nozzle vessels, using tap water as the vessel fluid and a tracer of potassium permanganate solution, with the object of determining the mixing time of the tracer in the fluid vessel. Mixing times were determined visually with a stop watch. A correlation was formulated involving mixing time, geometric parameters and physical properties of the fluid. For this case, however, mixing time was seen to be dependent on the inlet nozzle diameter, diameter of the vessel, depth of fluid in the vessel, nozzle velocity, fluid viscosity and density, and the acceleration due to gravity.

$$T = f(D_i,\ D_t,\ H,\ V_i, \mu, \rho,\ g) \qquad 2.13$$

A dimensional analysis was used to correlate the mixing time and the parameters. It was established, that the dimensionless mixing time $\left(\frac{TV_i}{D_i}\right)$ is solely dependent on the nozzle Reynolds number $\left(\frac{\rho V_i D_i}{\mu}\right)$ and Froude number $\left(\frac{V_i^2}{D_i g}\right)$, although it has been observed

i.e.

$$\Theta = K\ Re^{x}\ Fr^{-y} \qquad 2.14$$

x, y is dependent on the vessel geometry.

x : 1.6Ø17, y : Ø.7568 for 5.13 x $1Ø^{-3} m^3$

x : 1.2246, y : Ø.2851 for Ø.55 x $1Ø^{-3} m^3$

that vortex formation (117) nullifies the effect of the Reynolds number.

Fox and Gex (113) using the alkaline fluids coloured deep red by phenolpthalein, measured visually the time required to discharge the colour after an instantaneous addition of an exactly equivalent amount of neutralizing acid. Their results indicated that mixing time was dependent on the jet Reynolds number. However, the effect of the dependence was found to be strong in the laminar jet regime than in turbulent jet regime.

For the laminar regime

$$T = C_1 \frac{y^{Ø.5} D_t^{1.Ø}}{Re_j^{1.33} (V_o D_o)^{Ø.67} g^{Ø.17}} \qquad 2.15$$

For the turbulent regime

$$T = C_2 \frac{y^{Ø.5} D_t^{1.Ø}}{Re_j^{Ø.17} (V_o D_o)^{Ø.67} g^{Ø.17}} \qquad 2.16$$

Further studies involving mixing time in various vessels have been investigated. Okita and Oyama (118) obtained the mixing time for two different size tanks (D = Ø.4 m, 1.Ø m) respectively, by measuring the concentration differences at two points with electrolyte conductivity

probes placed in each tank. On the basis of dimensional analysis of the mean circulation time, Okita and Oyama correlated the results by the following expression.

$$T = \text{Ø}.55 \left(\frac{d}{u}\right) \left(\frac{D}{d}\right)^{1.5} \left(\frac{H}{d}\right)^{\text{Ø}.5},$$

$$5 \times 1\text{Ø}^3 < Re_j < 1 \times 1\text{Ø}^5 \qquad 2.17$$

Van de Vusse (119) compared the time of blending two benzene fractions in a $12 \times 1\text{Ø}^3 m^3$ vessel, using an inclined side entry jet, a paddle stirrer and a jet eductor. Mixing time was monitored by a density technique and found that mixing time T can be expressed as :-

$$T = 3.68 \frac{D^{2.\text{Ø}}}{(V.d)^{1.\text{Ø}}} \qquad 2.18$$

Both Okita and Oyama, and Van de Vusse concluded that in the turbulent jet regime, mixing time was independent of the jet Reynolds number.

In all the above studies, the degree of mixing was defined qualitatively, such as terminal mixing or complete mixing and consequently, the mixing time has been determined from the time when the uniformity of composition (or colour) in the specified sample size, within the precision of the instrument used (or of visual interpretation) was not further changed by additional mixing. Therefore, the mixing time is not sufficient to predict quantitatively the time required to achieve a desired degree of mixing.

Recently, alternative designs for jet mixing have been published. Such studies were by Hiby and Modgell

(12Ø), who using a flat base cylindrical tank, a capacity of 33.7 x $1Ø^{-3}m^3$ with an axial vertical jet, studied mixing times by a conductivity tracer method. They found that the mixing time was dependent on a jet Reynolds number when the tank Reynolds number was less than 1 x $1Ø^6$. From their results, Hiby and Modigell proposed a dimensionless mixing time:-

$$T^* = \frac{T.v.d}{D^{2.Ø}} \qquad 2.19$$

$T^* = 2.3$ for 95% homogeneity when the tank Reynolds number was greater than 1 x $1Ø^6$.

$$T_{95\%} = T^* \frac{D^{2.Ø}}{V^{1.Ø} . d^{1.Ø}} \qquad 2.2Ø$$

$$Re_t > 1 \times 1Ø^6 \quad T^* = \text{constant} = 2.3$$

$$Re_t > 1 \times 1Ø^6 \quad T^* \propto Re_j$$

Lane and Rice (121) conducted experiments on Ø.31 m diameter and Ø.91 m diameter tanks with a hemispherical base, using a vertical jet. Water was the process fluid and its viscosity was altered using sodium carboxymethyl cellulose. A tracer injection was applied, and the mixing time was measured by a conductivity technique. They showed that the mixing time is strongly dependent on the jet Reynolds number in the laminar jet regime and only slightly dependent in the turbulent jet regime.

$$T_{95\%} = C_1 \frac{Y^{0.5} D^{0.75}}{Re_j^{1.30} (V_o D_o)^{0.5} g^{0.25}} \qquad 2.21$$

$Re_j < 1800$

$$T_{95\%} = C_2 \frac{Y^{0.5} D^{0.75}}{Re_j^{0.15} (V_o D_o)^{0.5} g^{0.25}} \qquad 2.22$$

$Re_j > 1800$

A recycle model for tracer reponse has been found to analyze the mixing characteristics quite adequately. However, when the Reynolds number of the jet is so large that the circulating flow in the tank dominates the mixing and the variance of circulation time is small, an output curve of the impulse response shows a damping oscillation. As such, Khang and Levenspiel (122) proposed an approximate expression for the decaying amplitude of the damping oscillation.

$$A = 2 \exp\left(\frac{-2\pi^2 \sigma_c t}{T}\right) \qquad 2.23$$

That is, a concentration deviation from a mixed mean value decreases exponentially in time and the time elapsed to a certain value of A depends on the mean circulation time t_c, and the dimensionless variance of the circulation time, σ_c^2. Maruyama et al. (123) showed that in circulation flow regime ($Re \geq 3 \times 10^4$) of mixing, the dimensionless mixing time depended solely on liquid depth,

nozzle height and nozzle elevation angle, and shows a value between 2.5 and 7.

The study of mixing times has been investigated in unbaffled vessels. Van de Vusse (119) used several types of agitators for the mixing of miscible liquids in batch cylindrical flat bottomed vessels of diameter 208 mm and 262 mm respectively. He employed a Schlieren method to determine when refractive index differences disappeared and determined the mixing time from an initial condition where impeller and fluid were static. Such a situation showed considerable changes in flow pattern, which occurred with radial and axial components decreasing in favour of tangential components as mixing continued. Van de Vusse found that the dimensionless mixing time was essentially independent of the Reynolds number, but greatly dependent on the speed of the impeller,

i.e.

$$N\theta \propto N^{-0.6} \text{ for } N < N_{crit} \qquad 2.24$$

where N_{crit} is the critical impeller speed in unbaffled vessel at which air entrainment commences.

Kafarov et al. (124) on the otherhand, employed a cylindrical conical bottom of sizes $5.3 \times 10^{-3} m^3$, $42 \times 10^{-3} m^3$ and $339 \times 10^{-3} m^3$ repectively with the base as vessel inlet and the overflow at the top of the vessel wall as exit. The operation was continuous, and a flat blade disc turbine stirrer was used as the impeller with

water as the process fluid. A conductivity probe located within the vessel at the overflow, was used to measure the mixing time from the moment of introducing the electrolyte, and was defined as the time when the concentration of the exit stream varied by 1% of its maximum value. Fakarov et al. showed that the dimensionless mixing time was independent of Reynolds number as did Van de Vusse, but on the impeller rotational speed, and in their results showed that,

$$N\theta \propto N^{0.24} \qquad \text{for } N < N_{crit} \qquad 2.25$$

and

$$N\theta \propto N^{1.60} \qquad \text{for } N > N_{crit} \qquad 2.26$$

Lastly, Brennan and Lehrer (125) observed that the mixing time determinations in unbaffled vessels showed a well defined depression in the liquid surface which resulted from the combined vortex established in the liquid. It has been noted that the depth of the liquid at the shaft and elevation at the wall increased with increasing in impeller speed. However, beyond a certain critical impeller speed N_{crit}, air was entrained by the impeller and dispersed in the liquid as small bubbles. However, at speeds lower than N_{crit}, a cylindrical core was shown after the remainder of the liquid in the vessel had decoloured; although the core was symmetrical about the shaft at the vessel axis and extended from the liquid surface towards the impeller. Their flow visualization

studies, using polystyrene tracer particles in the fluid, revealed a difference in flow patterns in the core region above and below the impeller. Above the impeller, particles travelled in circular paths with no discernible axial or radial motions. Below the impeller, particles moved in a slow upward spiral from the base of the vessel to the impeller. Because of stability in the core region, Brennan and Lehrer determined mixing times with reference to fluid outside this region. Although reproducibility of their results was not satisfactory due to the nature of flow patterns created; however, their limitations were considered favourable as compared to the insertion of probes in the vessel fluid which could have encountered more deleterious effects. As such, the cylindrical core region might not have been revealed, as flow patterns and hence mixing times could have been greatly affected.

In general, any attempt to compare the mixing time from any of the published investigations can lead to widespread discrepancies in the results obtained. This is because investigators have used a number of different experimental techniques to determine mixing times to unspecified degrees of homogeneity.

2.5.3 RESIDENCE TIME STUDIES IN STIRRED VESSELS

A stirred vessel is generally conceived to be ideal when the conditions such as temperature and concentration at any point in the system is the same as the outlet

conditions. In most continuous stirred reactors, this ideal situation may be attained with a suitable stirrer design or jet stirred design and by appropriate stirrer speeds, which make the mixing time small as compared with the residence time. However, in rate processes where high conversions are required, especially with a high reaction order, the reaction time can be reduced considerably, if there is some staging in the reactor.

Denbigh et al. (126) first suggested an interesting tracer technique of using the 'time reaction' for flow visualization in RTD studies. They used potassium iodate and a solution of sodium sulphite with a little starch paste to liberate iodine starch solution. On mixing the solutions, at first, there was no visible change during an induction period; but when this was complete, there was a very sudden liberation of iodine which resulted in an instantaneous colouration of the starch. Later, Danckwerts et al. (127) extended the work by using sodium persulphate, potassium iodide, sodium thiosulphate and starch, in a cylindrical vessel of $Ø.2 \times 1Ø^{-3}$ m^3 of diameter 5Ø mm and height 1ØØ mm. One was with an inlet and an outlet radially directed and at opposite sides and ends and the other vessel with a tangential inlet and an axial outlet. In this case, the reaction between persulphate and iodide ions yielding iodine is a slow process.

$$Na_2S_2O_8 + 2\ KI \text{ -----> } Na_2SO_4 + K_2SO_4 + I_2 \quad \text{slow} \quad 2.27$$

The iodine reacts instantaneously with thiosulphate and is reduced back to iodide.

$$2Na_2S_2O_3 + I_2 \text{ ----> } Na_2S_4O_6 + 2NaI \quad \text{(Instantaneous)} \qquad 2.28$$

When all the thiosulphate has been consumed, free iodine is liberated and the solution immediately turns blue because of the starch - iodine reaction. From this, the portion which has the average older or younger than the reaction time could be detected by the colour. Photographs were taken at different times to visualize the flow pattern. Although no RTD model was proposed, the technique has been found suitable when there is no molecular interdiffusion between different parts of the liquid. The effect of molecular diffusion causes a small amount of the coloured liquid to alter the colour of a large amount of liquid even when the residence time of the liquid is still very small.

Coker (128) studied the RTD in two hydraulic nozzle vessels of $\emptyset.31 \times 1\emptyset^{-3} m^3$ and $1.48 \times 1\emptyset^{-3} m^3$ respectively, using tap water as the process fluid with acidified potassium permanganate ($KMnO_4$) as a self acting tracer to the step change in the vessels. A conductivity bridge meter was used to measure the effluent concentration, which was converted to the $F(\theta)$ function. A tank in series, incorporating a delay time was successfully used to simulate the experimental results. Further RTD studies

involving hydrogen peroxide solution and acidified $KMnO_4$ to a step downward change were investigated. For this case, models reviewed by Cooper and Jeffreys (129) were employed to ascertain the extent of non ideality of the systems.

Jet stirred vessels made of silica or pyrex other than high speed stirred reactors have now been used to study the kinetics of fast, combustion or neutralization reactions, while still preserving the principle of a well mixed reaction volume. Such reactors are based on the principle of the entraining property of free jets. These reactors are free of the mechanical complication of a rotating stirrer and its bearing, which invariably become contaminated with organic compounds present in the reactor.

Stainthorp and Clegg (130) used a jet stirred cylindrical vessel of 88.9 mm and 139.7 mm diameter respectively, with an inlet and an outlet nozzle offset from the axis to investigate a second order reaction between the diazonium salt of sulphanilic acid and sodium 1 napthol - 4 sulphonate to produce a dye stuff. They inferred that the vessel geometry caused a large recirculating entrained flow pattern, while allowing very little direct by - passing of fluid. Clegg and Coates (111) using geometrically similar vessels as in Stainthorp and Clegg's work , employed an impulse injector device to introduce a tracer of nigrosine into the water fluid

the outlet response was continuously monitored by a photoelectric cell. Two broadly differing flow regions within the recirculating flow pattern were noted, and a simple model proposed, accounted for these regions.

Sinclair and Mc Naughton (131) used three geometrically cylindrical vessels with length to diameter ratios of 1:1, 2:1 and 3:1 respectively, having co - linear axial inlet and outlet nozzles to study the RTD. A step change from water to a tracer solution at the inlet with Reynolds number of the inlet nozzle ranging from 3ØØØ to 1Ø,ØØØ was employed. The flow pattern which was made up of a fully turbulent conical jet in the centre with a slow moving recirculating flow in the outer section of the vessel was noted, and the proposed model was based on the general form of Wolf and Resnick (132).

Bush (133) proposed a design procedure of single phase jet - stirred reactors for chemical kinetic studies, applying a hydraulic model to analyse the fluid flow in the reactor. Analysis of the formulated mathematical model and dispersion, resulted in an expression for the fluid recirculation and the mixing time in the reactor. Bush realised that the presence of the velocity gradients caused an effective dispersion coefficient to 2Ø times the local turbulent diffusivity.

Moeller and Dealy (112) studied the RTD in a circular confined jet by monitoring the concentration in the outlet stream of a saturated sodium chloride solution which was

injected into the primary jet tube. Two possible mixing patterns were discernible, depending on whether there was recirculation or not. For flows without recirculation, the flow pattern was along the solid lines. Also, the secondary flow combined with the jet flow in a continuous manner, at various times and positions along the jet. As such, part of the total available mixing volume was in dispersed plug flow and the other part, perfectly mixed. Moeller and Dealey inferred that the recirculation eddy was effective in the mixing process and with an increased recirculation rate in the eddy, the amount of dead space in the confined jet system increased. This however, reduces the efficiency of the cylindrical confined jet as a mixer of different fluids for industrial purposes; although, its suitability could be justified for autocalytic and autothermal reactions because these types favour recycle flow.

Wood (134) considered the problem of predicting the amount of mixing caused by a turbulent jet of water flowing horizontally through a cylindrical or rectangular vessel with axially opposed inlet and outlet. Sodium chloride (NaCl) was used as the process fluid and at a steady state condition, applied a step change to pure water. The effluent was collected and a titremetric analysis was employed to evaluate a cumulative distribution of 'NaCl displaced' against the 'time measured from

the step change'. Wood proposed a model that was consistent with the results and observed that as the inlet diameter to the vessel decreases, the entrainment rate increases with subsequent increase in the intensity of mixing. However, complete mixing was achieved with further reduction in inlet diameter.

Gas mixing in Jet - stirred reactors involving homogeneous and heterogeneous reactors with short residence times (about one second) has been reported by David et al. (135). They used jet - stirred reactors of spherical and cylindrical geometries in their kinetic studies of organic compounds. Their results showed that the kinetic constants determined in the transient state gave good agreement with published work. Also, the micromixing state in the reactor which was evaluated was found to be very close to the maximum mixedness state, and as such the reaction rate and the kinetic constants could be applied to the design equation of a continuous stirred tank. The RTD studies of David et al., showed that perfect mixing was attainable and a cascade of 1Ø stirred reactors in series would tend to approach plug flow. They also pointed out the high efficiency of jet stirred reactors as excellent heat or mass exchangers.

The effect of the RTD has been investigated to predict the performance and efficiency of combustors. The concept of a well - stirred reactor coupled to a plug flow

reactor has proven to be a powerful model for the performance and efficiency of swirl burners. It has been shown that the performance can be optimized for a highly loaded burner by varying the proportions of the mean residence time spent in well stirred and plug flow parts respectively. Syred and Beer (136) have reviewed the combustion in swirling flow systems, high-lighting on the importance of visual flow studies and the RTD. In this review, emphasis was laid on the effects of swirl to improve flame stability as a result of the formation of toroidal recirculation zones, and to reduce combustion lengths by producing high rates of entrainment of the ambient fluid and fast mixing particularly near the boundaries of recirculation zone.

Beer and Lee (137) employed the RTD to elucidate the performance and efficiency of a furnace. They used a 1/10 scale water model of the IJmuiden furnace and IJmuiden tunnel furnace. A salt solution was the tracer, injected into the burner fluid of the water model and the RTD was determined by measuring the decay of the salt concentration with time in the exit stream, after cutting off the tracer flow. The profile of the RTD curves showed that the combustor volume consisted of two parts, a well stirred and a plug flow type volume fraction in series.

2.6 MACROMIXING AND MICROMIXING IN FLOW SYSTEMS

The residence time distribution (RTD) by itself does not completely define a state of mixing. It does however, define macromixing and not mixing between molecules, termed micromixing. Macromixing refers to those gross flow processes which cause different fluid elements to have different residence times. These same processes may or may not cause any mixing at a molecular level of scrutiny.

If individual fluid elements are enveloped they could flow through the system and have a distribution of residence times without any mixing on the molecular scale. Such a system is completely segregated, and complete segregation represents a lower limit on micromixing; that is, where there is no mixing. An upper limit corresponds to the maximum amount of molecular level mixing possible with a given RTD. This condition is referred to as maximum mixedness (138).

Segregation phenomena and micromixing in chemical reactors have become widely investigated by theoretical and experimental studies. These investigations are required, both from the theoretical and practical point of view. In practice, micromixing significantly affects the course of several types of reactions such as very rapid reactions, precipitation reactions, complex reactions and reactions in highly viscous fluids.

2.6.1 MACROMIXING THEORY

The incoming fluid is dispersed into discrete fragments which are small compared to the volume of the reactor and uniformly dispersed in it. Furthermore, the molecules that enter the system remain together indefinitely. Thus the fluid stays completely segregated and such a fluid is termed 'macrofluid' and the type of mixing is 'macromixing'. As such, macromixing implies that fluid elements of a scale orders of magnitude larger than molecular scale may be mixed with one another, but no diffusion may be possible between them.

Macromixing is thus the aspect of mixing accompanied by gross fluid or particle motion in a flow chemical reactor, induced by the combination effects of convective flow, motion of eddies and molecular diffusion. The macromixing component specifies the variation in the residence times experienced by molecules or particles flowing through the reactor. The time elapsed between the entry of a fluid molecule or flowing particle into a reactor and its exit from the reactor, is its residence time. Hence as different fluid elements or particles generally remain in the flow system for varying lengths of time, the residence times are usually distributed. In general, a knowledge of macromixing as represented by the RTD is sufficient to determine two limits between which the conversion must lie. The two limits thus correspond to two extreme conditions of micromixing:- complete segregation and maximum mixedness.

2.6.2 MICROMIXING THEORY

The entering fluid flow is dispersed on the molecular scale in a time much less than the mean residence time. Such a fluid is termed 'microfluid' and the type of mixing encountered in the system is micromixing. Micromixing thus implies that elements of fluid in proximity become completely mixed to the molecular scale.

Danckwerts (139) elucidated the effect of the state of micromixing on the performance of a continuous stirred tank reactor with a second order reaction. He considered a well stirred tank reactor in which the elements of fluid entering the reactor were uniformly dispersed through its volume in a time much less than the average residence time. The distribution of residence times was that of ideal mixed system, and Danckwerts suggested a line of approach, based on two limiting circumstances.

(i) The incoming fluid is broken up into discrete fragments or streaks which are small compared to the reactor volume and uniformly dispersed in it, but in which molecules entering together remain together indefinitely. The fluid remains completely segregated.

(ii) The incoming material is dispersed on the molecular scale in a time much less than the mean residence time; the environment of any particular molecule does not tend to contain an excess of molecules which entered at the same time as itself and the mixture is chemically uniform or completely micromixed.

Micromixing provides information regarding the environmental variation experienced by the reacting fluid elements or particles during their passage through the reactor. Micromixing embraces all aspects of mixing not defined by macromixing or the RTD, and is concerned with the extent of mixing on a molecular level. Danckwerts introduced the concept of a 'point' of fluid as a volume of fluid very small in size in comparison with the total volume of the reactor, but still sufficiently large to contain many molecules. Molecules entering the reactor have an age α = Ø and various life expectations described by the RTD. Molecules leaving the reactor, however have a life expectation λ = Ø and various exit ages given by the RTD, E(α) or E(λ). Thus within the reactor a transition takes place from a grouping of molecules with identical life expectations. This transition between the molecular groupings is regarded as micromixing. The micro - mixed and macromixed cases are illustrated in Figures 2.51 and 2.52 respectively.

The extent of micromixing depends on the association of entering molecules with older molecules already within the reactor. Thus, models respresenting the two extreme conditions of micromixing are complete segregation and maximum mixedness models.

Complete segregation:- Mixing occurs as late as possible and a fluid element entering the reactor breaks into small, but finite discrete fragments in which a fluid

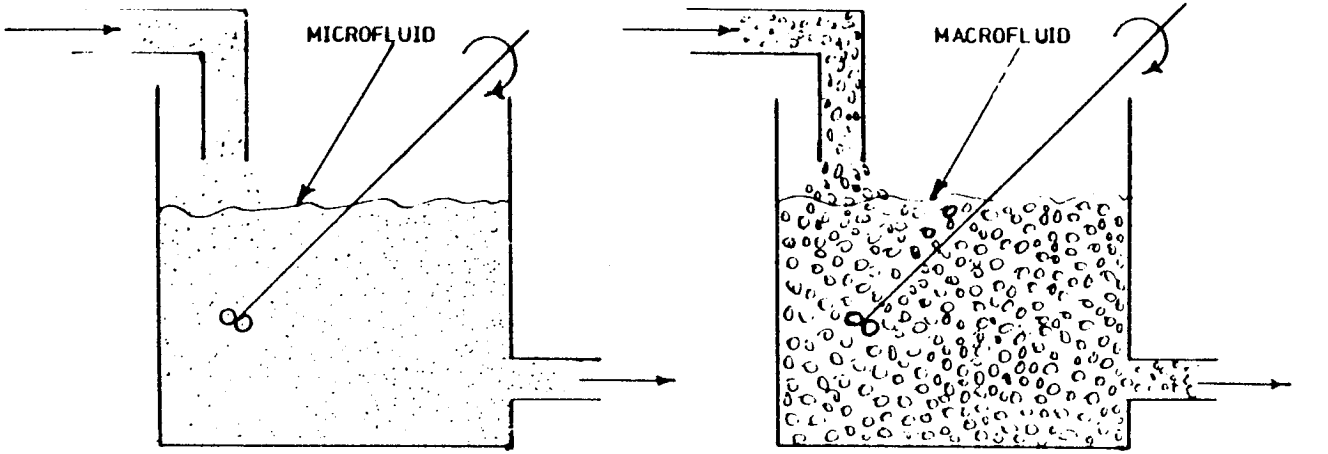

FIGURE 2.51 Schematics of micromixed and macromixed reactors with premixed feeds

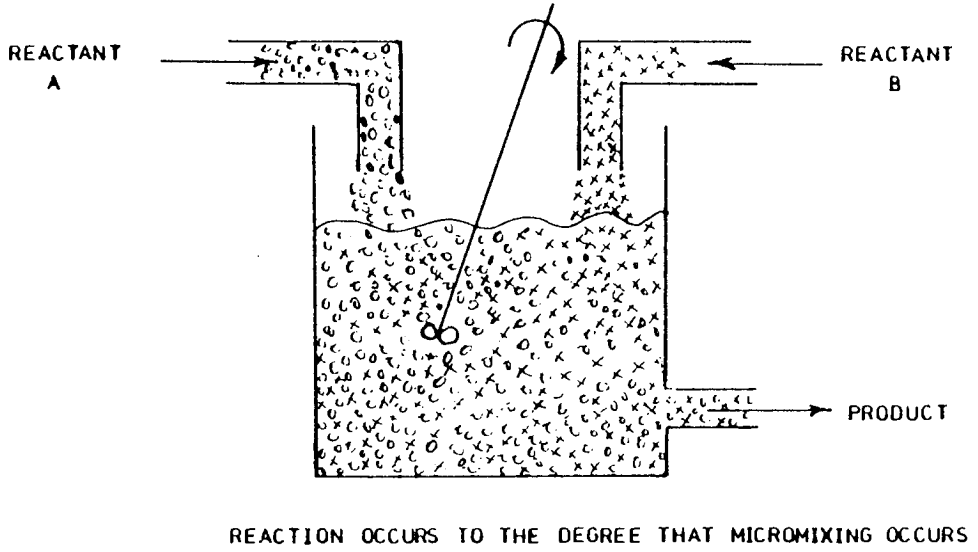

FIGURE 2.52 Schematic of reactor with non-premixed feeds

element entering together remain together. Under these conditions, each fluid element is totally isolated or segregated from the other points in the system.

Maximum mixedness :- Mixing occurs as early as possible, and an incoming fluid element is dispersed on a molecular scale in a time much less than the mean residence time of the reactor. Thus any molecule on entering a maximum mixedness chemical reactor immediately becomes associated with other molecules with which it exits from the reactor, that is, the molecules of the same life expectation are completely mixed regardless of their ages. These two extremes models are shown in Figures 2.61 and 2.62 respectively. Danckwerts (139) and Zwietering (140) have postulated a measure for micromixing in a flow reactor, the 'degree of segregation'. It is defined as the ratio of the variance of the ages between the points in the reactor to the variance of the ages of all the molecules in the reactor. Hence,

$$J = \frac{\text{var}\,\alpha_p}{\text{var}\,\alpha} = \frac{\overline{(\alpha_p - \bar{\alpha})^2}}{\overline{(\alpha - \bar{\alpha})^2}} = \frac{1}{V}\,\frac{\int_V (\alpha_p - \bar{\alpha})^2 dV}{\int_0^\infty (\alpha - \bar{\alpha})^2\, I(\alpha) d\alpha} \qquad 2.29$$

where

α = age of a molecule in the flow reactor

$\bar{\alpha}$ = mean age of molecules in the flow reactor

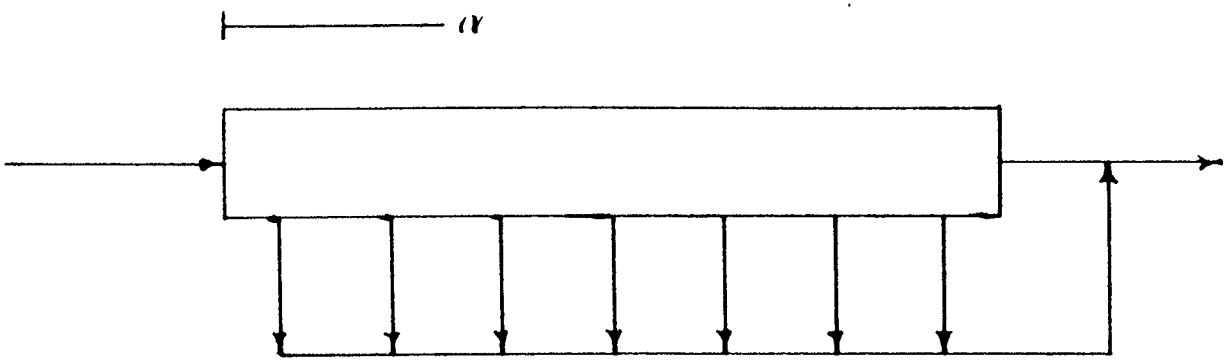

FIGURE 2.61 Plug flow reactor with side exits. A case of complete segregation

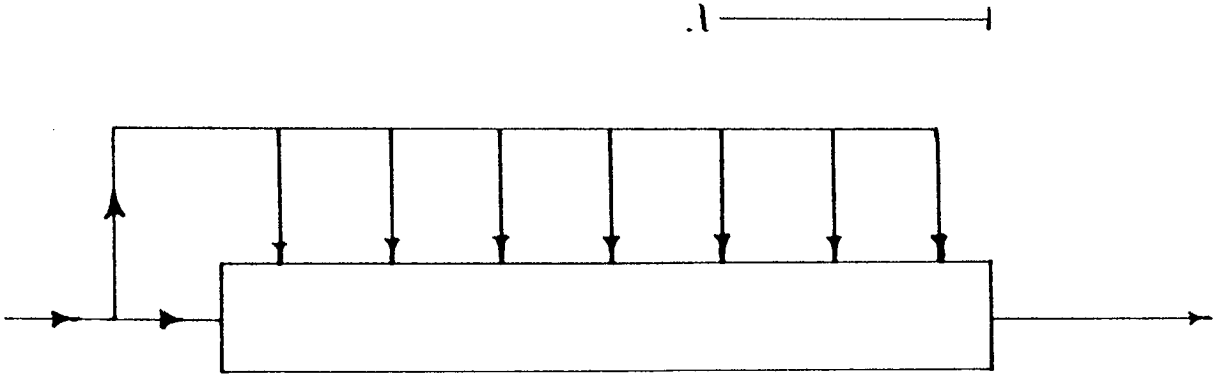

FIGURE 2.62 Plug flow reactor with side entrances. A case of maximum mixedness

$$= \int_0^{\infty} \alpha \, I(\alpha) d\alpha$$

α_p = mean age of molecules within a point in the flow reactor

$\int_V$ = the volume integral represents the sum over all points.

The degree of segregation for a system with the residence time distribution of an ideally mixed tank lies betweeen J = Ø for complete micromixing and J = 1 for complete segregation.

Zwietering (14Ø) stated that for systems with some other RTD, the upper limit for the degree of segregation is always J = 1, for the concept of complete segregation is applicable, but a value J = Ø is impossible because there must be a difference in ages at various points in the system. He proceeded to explain a condition of maximum mixedness, compatible with a given residence time distribution which makes possible the evaluation of a lower limit for J as well as a conversion limit. A steady flow system is in a state of maximum mixedness when the flollowing criteria are ascertained.

(i) All molecules within a point have the same life expectancy λ (defined as the time a molecule will spend in the system from a specified moment until it leaves).

(ii) Points with equal life expectation are mixed, or at least the molecules within them have identical age distributions.

The first condition is also a requirement for complete segregation where the molecules at each point have entered the system at the same time. These conditions together express, the requirement for any degree of micromixing, because if molecules of different life expectancies mix they will later have to unmix so that those with lower values of λ may leave the system. This spontaneous unmixing would be necessary in order to maintain the RTD, but would violate the Second Law of Themodynamics and cannot be permitted (141). In view of the Second Law of Thermodynamics, which eliminates the possibility of "unmixing", a model (Figure 2.63) is proposed that gives a general representation of micromixing. Zwietering showed that this condition was not satisfied by an ideal mixer with an exponential residence time distribution because every point would contain molecules with different life expectancies. He indicated that this RTD is a degenerate case where condition (i) could be dropped. The two conditions together express the requirement that all molecules which will leave the system together are mixed during the whole of their stay in the system. Hence the mixing prescribed by the RTD is performed as early as possible.

The two extremes of micromixing, namely complete segregation and maximum mixedness can be represented by

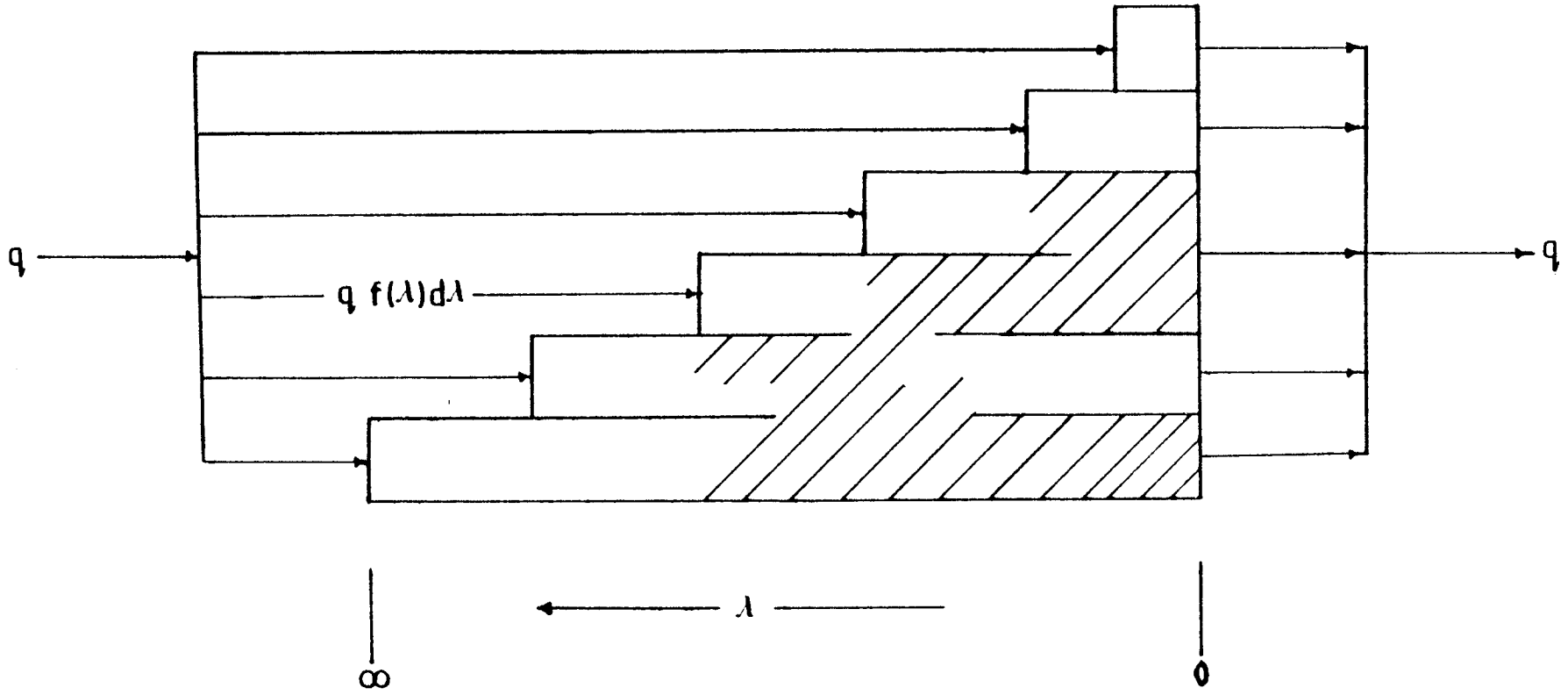

FIGURE 2.63 General micromixing model

two plug flow models. Figure 2.61 indicates the model of complete segregation, such that the feed stream enters the reactor with side exits through which portions of the flow leave after their sojourn of the residence time distribution. This model, represents molecules within the flow reactor according to their ages, α, satisfying the condition that mixing occurs as late as possible. As such, each fluid element containing molecules of the same age during its passage through the reactor can be considered as a batch reactor. The mean concentration at the reactor outlet is:-

$$\bar{C} = \int_{\emptyset}^{\infty} C_b(\alpha)\ E(\alpha)\ d\alpha \qquad 2.3\emptyset$$

where $C_b(\alpha)$ is the batch concentration at age α.

The maximum mixedness model indicates that the feed streams enter side entrances of a plug flow reactor to satisfy the residence time distribution. Figure 2.62 illustrates that the model classifies molecules within the flow reactor according to their life expectation. Such mixing within the system leads to the earliest possible mixing of elements in the feed streams with elements of equal life expectation already in the reactor.
Zwietering's derivation for the maximum mixedness condition is:-

$$\frac{dC}{d\lambda} = r(C) + \frac{E(\lambda)\{C(\lambda) - Co\}}{1 - F(\lambda)} \qquad 2.31$$

The boundary condition is such that C(λ) is bounded and positive for all λ,

$$\text{i.e.} \qquad \frac{dC}{d\lambda} = \emptyset \text{ at } \lambda = \infty.$$

The outlet concentration from the reactor is obtained by evaluating the solution of equ. 2.31 at $\lambda = \emptyset$.

In general, the extent of micromixing has been found to have a pronounced influence on the conversion of reaction of the order greater than one. For an n th order chemical reaction with reaction rate $r(C) = kC^n$, where C is the concentration of the limiting reactant; complete segregation or lateness of mixing yields the highest conversion for concave - up rate reaction when $n > 1$ or $\frac{d^2r}{dC^2} > \emptyset$. Alternately, maximum mixedness or earliness of mixing yields the highest conversion for concave - down rate reaction when $n < 1$ or $\frac{d^2r}{dC^2} < \emptyset$. However, for a first order rate reaction conversion or yield is independent of micromixing i.e. $\frac{d^2r}{dC^2} = \emptyset$.

2.6.3 MODELS FOR MICROMIXING

The residence time distribution is classified as being a multiparameter representation of macromixing. The parameters are infinite in number and are the moments of the distribution. Some of the macromixing models are well

illustrated in section 2.5. However, analogous to macro-mixing models are micromixing models which also require an infinite parameter discriptor necessary to completely characterize micromixing in systems, even when constrained with a fixed residence time frequency function E(t). Although the development of such a discriptor is yet to be published, however, various models have been formulated which attempt limited characterization of micromixing using a finite number of parameters. Such models have been analysed by Wen and Fan (142) and extensively reviewed by Ritchie and Tobgy (143). Most of these employ a single adjustable parameter to characterize micromixing within the bounds of complete segregation and maximum mixedness that have been discussed, since they do not project a clear physical understanding of the actual phenomena.

CHAPTER THREE

HYDRODYNAMICS OF SWIRLING FLUID IN CYLINDRICAL NOZZLE VESSEL

3.1 VORTEX FORMATION

3.2 CHARACTERISTICS OF SWIRLING FLUID IN A CYLINDRICAL VESSEL

3.2.1 THE FORCED VORTEX MOTION

3.2.2 THE FREE VORTEX MOTION

3.2.3 THE COMBINED VORTEX MOTION

3.1 VORTEX FORMATION

An insight into the mixing behaviour of fluid elements in a cylindrical nozzle can be gained by reviewing the flow patterns of liquid in the vessel. Taylor (24) explained that when a liquid which is not swirling approaches an orifice through a convergent chamber, it converges from all points of a cross section only decreasing in velocity in the boundary layer near the wall. When the liquid is swirling, the radial pressure gradient which accompanies the swirling or tangential motion and holds the liquid elements in their circular paths; acts on the retarded boundary layer, driving it along the surface of the chamber towards the orifice. Furthermore, the elements are acted upon by tangential acceleration and the magnitude is determined by the centrifugal force. Once the action of the centrifugal field becomes visible, the liquid level exhibits a depression, which is termed a vortex. The condition for vortex formation is the effect of centrifugal acceleration upon the gravitational acceleration in which the circular motion of the fluid contents acts.

Other industrial processes in which a sound knowledge of vortex motion is important for proper design and operation are cyclone dust separators, gas scrubbers, spray coolers, centrifugal burners and recently, plasma flame stabilization. In this section, characteristics of vortex

motions in stirred vessels are reviewed from the hydrodynamic viewpoint, using the Navier - Stokes equation of motion.

3.2 CHARACTERISTICS OF SWIRLING FLUID IN A CYLINDRICAL VESSEL

The cylindrical vessel considered here is one in which the liquid enters the swirl chamber tangentially and passes through a cylindrical section down a conical section to emerge through an orifice. Assuming a fluid of constant density ρ, and viscosity μ in a cylindrical portion of the vessel of radius R. The equation of continuity in the cylindrical co - ordinates (r, θ, z) then becomes:-

$$\frac{\partial \rho}{\partial t} + \frac{1}{r}\frac{\partial}{\partial r}(\rho r V_r) + \frac{1}{r}\frac{\partial}{\partial \theta}(\rho V_\theta) + \frac{\partial}{\partial z}(\rho V_z) = \emptyset \qquad 3.1$$

In steady state laminar flow, the fluid moves in a circular pattern with an angular velocity ω, and the velocity components V_r and V_z are zero. Also there is no pressure gradient in the θ - direction. Therefore the terms of the equation of continuity are zero (144).

the equation of motion in the cylindrical co - ordinates (r, θ, z) becomes :-

r - component

$$\rho\left(\frac{\partial V_r}{\partial t} + V_r \frac{\partial V_r}{\partial r} + \frac{V_\theta}{r} \frac{\partial V_r}{\partial \theta} - \frac{V_\theta^2}{r} + V_z \frac{\partial V_r}{\partial z} \right) = - \frac{\partial p}{\partial r}$$

$$+ \mu\left(\frac{\partial}{\partial r} \left(\frac{1}{r} \frac{\partial}{\partial r} (r V_r) \right) + \frac{1}{r^2} \frac{\partial^2 V_r}{\partial \theta^2} - \frac{2}{r^2} \frac{\partial V_\theta}{\partial \theta} + \frac{\partial^2 V_r}{\partial z^2} \right) + \rho g_r$$

3.2

θ - component

$$\rho\left(\frac{\partial V_\theta}{\partial t} + V_r \frac{\partial V_\theta}{\partial r} + \frac{V_\theta}{r} \frac{\partial V_\theta}{\partial \theta} + \frac{V_r V_\theta}{r} + V_z \frac{\partial V_\theta}{\partial z} \right) = - \frac{1}{r} \frac{\partial p}{\partial \theta}$$

$$+ \mu\left(\frac{\partial}{\partial r} \left(\frac{1}{r} \frac{\partial}{\partial r} (r V_\theta) \right) + \frac{1}{r^2} \frac{\partial^2 V_\theta}{\partial \theta^2} + \frac{2}{r^2} \frac{\partial V_r}{\partial \theta} + \frac{\partial^2 V_\theta}{\partial z^2} \right) + \rho g_\theta$$

3.3

z - component

$$\rho\left(\frac{\partial V_z}{\partial t} + V_r \frac{\partial V_z}{\partial r} + \frac{V_\theta}{r} \frac{\partial V_z}{\partial \theta} + V_z \frac{\partial V_z}{\partial z} \right) = - \frac{\partial p}{\partial z}$$

$$+ \mu\left(\frac{1}{r} \frac{\partial}{\partial r} \left(r \frac{\partial V_z}{\partial r} \right) + \frac{1}{r^2} \frac{\partial^2 V_z}{\partial \theta^2} + \frac{\partial^2 V_z}{\partial z^2} \right) + \rho g_z$$

3.4

At steady state, $V_r = V_z = \emptyset$ and V_θ is a function of r alone. Also the pressure will depend upon r because of

the centrifugal force and upon z because of gravitational force.

Hence from equs. 3.2 ,3.3 and 3.4 respectively

r - component $$\rho \frac{V_\theta^2}{r} = \frac{\partial p}{\partial r} \qquad 3.5$$

θ - component $$\emptyset = \frac{\mu \partial}{\partial r}\left(\frac{1}{r}\frac{\partial}{\partial r}\left(rV_\theta\right)\right) \qquad 3.6$$

z - component $$\emptyset = -\frac{\partial p}{\partial z} - \rho g \qquad 3.7$$

Integrating equ. 3.6,

$$\frac{\mu \partial}{\partial r}\left(\frac{1}{r}\frac{\partial}{\partial r}\left(rV_\theta\right)\right) = \emptyset$$

$$\frac{d}{dr}\left(\frac{d}{dr}\left(rV_\theta\right)\right) = \emptyset \qquad 3.8$$

$$\int_\emptyset^{V_\theta} r \frac{d^2 V_\theta}{dr^2} \cdot dr = C_1 \int_\emptyset^r dr \qquad 3.9$$

Therefore

$$r \frac{dV_\theta}{dr} = C_1 r \qquad 3.1\emptyset$$

Further integration of equ. 3.1Ø

$$\int_\emptyset^V \frac{r dV_\theta}{dr} = C_1 \int_\emptyset^r r dr + C_2 \qquad 3.11$$

$$rV_\theta = C_1 \frac{r^2}{2} + C_2 \qquad 3.12$$

Hence $$V_\theta = C_1 \frac{r}{2} + \frac{C_2}{r} \qquad 3.13$$

where C_1 and C_2 are constants of integration. Because V_θ cannot be infinite at r = Ø, the constant C_2 must be zero. At r = R , the velocity V_θ is $R\omega$

From equ. 3.13

$$R\omega = C_1 \frac{R}{2}$$

therefore $C_1 = 2\omega$ 3.14

and $V_\theta = 2\omega \cdot \frac{r}{2}$

$= r\omega$ 3.15

3.2.1 THE FORCED VORTEX MOTION

This states that each element of the rotating fluid moves as the element of a rigid body. Substituting equ. 3.15 in the r - component of the equation of motion, equ. 3.5.

$$\frac{\partial p}{\partial r} = \rho \frac{r^2}{r} \omega^2$$

$$= \rho r \omega^2 \qquad 3.16$$

$$\frac{\partial p}{\partial z} = -\rho g \qquad 3.7$$

Since p is a function of position r and z, p=p(r,z). Applying total differential equation

$$dp = \frac{\partial p}{\partial r} dr + \frac{\partial p}{\partial z} dz \qquad 3.17$$

substituting equs. 3.7 and 3.16 in equ. 3.17

$$dp = \rho r\omega^2 dr - \rho g dz \qquad 3.18$$

Integrating equ. 3.18

$$\int_{dp}^{p} = \int \rho r\omega^2 dr - \int \rho g dz$$

$$p = \rho\omega^2\frac{r^2}{2} - \rho gz + C_3 \qquad 3.19$$

where C_3 is a constant

at $p = p_o$, $z = z_o$ and $r = \emptyset$

therefore

$$p_o + \rho g z_o = C_3 \qquad 3.2\emptyset$$

substituting equ.3.2Ø in equ. 3.19

Hence

$$p - p_o = \rho\frac{r^2\omega^2}{2} - \rho g(z - z_o) \qquad 3.21$$

This equation decribes the motion of the forced vortex as shown in figure 3.1. The locus of the free surface consists of all points on the free surface, that is the

surfaces of constant pressure are therefore the paraboloids of revolution.

where $p = p_o$, equ. 3.21

$$\phi = \frac{r^2 \omega^2}{2} - g(z - z_o) \qquad 3.22$$

therefore

$$z - z_o = \left(\frac{\omega^2}{2g} \right) r^2 \qquad 3.23$$

Equ. 3.23 is the equation of a parabola.

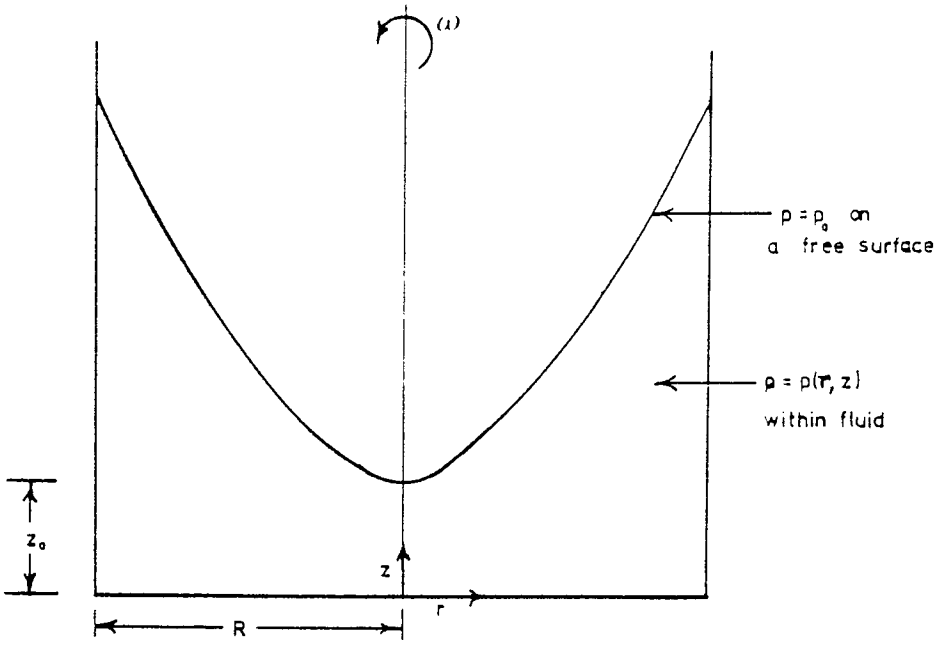

FIGURE 3.1 FORCED VORTEX

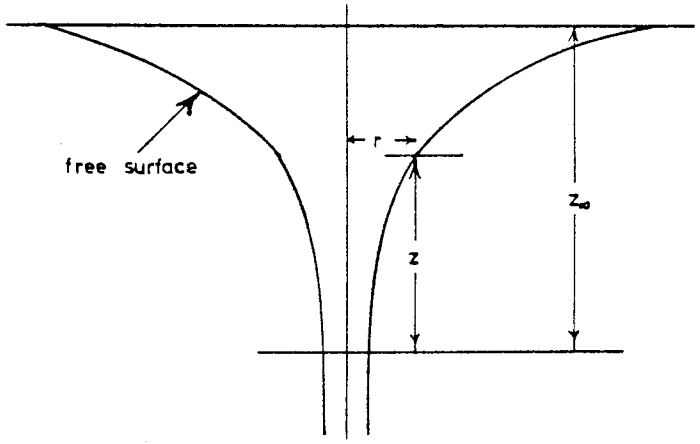

FIGURE 3.2 FREE VORTEX

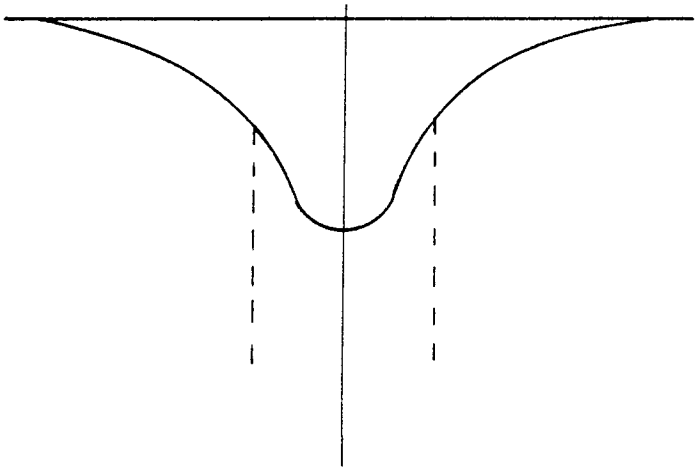

FIGURE 3.3 COMBINED VORTEX

3.2.2 THE FREE VORTEX MOTION

In the case of the free vortex, the motion of fluid is irrotational, which means that although each small element of fluid describes a fixed circular path, it has zero rate of spin about its own axis (145). The circulation in the circular path is independent of the radius. Thus, the product of velocity of flow and the circumference of the circle is constant and hence the velocity varies as the radius.

$$\omega \propto \frac{1}{r^2} \qquad 3.24$$

and $$\omega = \frac{C}{r^2} \qquad 3.25$$

where C is a constant.

subsituting equ. 3.25 in equ. 3.21

$$p - p_o = \frac{\rho C^2}{2r^2} - \rho g(z - z_o) \qquad 3.26$$

therefore

$$z - z_o = \frac{C^2}{2r^2 g} - \left(\frac{p - p_o}{\rho g} \right) \qquad 3.27$$

The form of the surface of a free vortex is hyperbolic provided that the vertical velocity is zero everywhere. When r is large the surface approaches a horizontal plane, but when r is very small $(z - z_o)$ is

large and negative. The surface resembles a trumpet with its mouth upward forming into a horizontal plane as shown in Figure 3.2.

3.2.3 THE COMBINED VORTEX MOTION

The combined vortex consists of an inner cylindrical core of radius a, rotating as a solid with an angular velocity ω, surrounded by a free vortex, the velocity being continuous at the radius a.

From equ. 3.25

$$c = \omega a^2 \qquad 3.28$$

The pressure in the core ($a \geq r \geq \emptyset$) is given by equ. 3.19.

$$p = \frac{1}{2}\rho r^2 \omega^2 - \rho g z + C_3$$

at $p = p_o$, $r = \emptyset$, $z = \emptyset$

therefore $C_3 = p_o$

Thus

$$p = \frac{1}{2}\rho r^2 \omega^2 - \rho g z + p_o \qquad 3.29$$

The pressure at radius a is

$$p(a) = \frac{1}{2}\rho a^2 \omega^2 - \rho g z + p_o \qquad 3.30$$

But the pressure is continuous at this radius (145), hence

$$p(a) = C_4 - \frac{\rho c^2}{2a^2} - \rho g z \qquad 3.31$$

$$C_4 = p(a) + \frac{\rho c^2}{2a^2} + \rho g z \qquad 3.32$$

substituting equs. 3.28 and 3.30 in equ. 3.31.

$$C_4 = \frac{1}{2}\rho a^2\omega^2 - \rho g z + p_o + \frac{1}{2}\rho a^2\omega^2 + \rho g z \qquad 3.33$$

$$C_4 = \rho a^2\omega^2 + p_o \qquad 3.34$$

Thus the pressure when r > a

$$p(r) = C_4 - \frac{\rho c^2}{2r^2} - \rho g z \qquad 3.35$$

substituting equs. 3.28 and 3.34 in equ. 3.35

$$p(r) = \rho a^2\omega^2 + p_o - \rho\omega^2\frac{a^4}{2r^2} - \rho g z \qquad 3.36$$

$$p(r) - p_o = \rho a^2\omega^2\left(1 - \frac{a^2}{2r^2}\right) - \rho g z \qquad 3.37$$

Equ. 3.37 shows that the free surface has a dimpled form (or embryonic vortex) as shown in Figure 3.3. The combined vortex is a combination of a free vortex with a forced vortex inside it.

CHAPTER FOUR

MATHEMATICAL SIMULATION OF THE FLOW CHARACTERISTICS

4.1 INTRODUCTION

4.2 DEVELOPMENT OF THE RTD MODEL

4.2.1 SIMULATION PROGRAM

4.1 INTRODUCTION

Various models have been developed to express continuous flow systems. These vary from the basic mass,momentum and energy balances, ranging from the detailed microscopic transport phenomena models to macroscopic models. For turbulent flow, models using effective coefficients have been described (108,146). These dispersion models are from microscopic considerations based on the assumption that the flow consists of small random fluctuations of the dependent variables. The transport phenomena models might be expressed for local regions for any process and then integrated throughout the vessel with varying coefficient used to introduce the detailed flow and mixing patterns (147).

In addition to the age - distribution analysis of flow systems, is the introduction of the population balance models for countable entities. The application of population balance principles to the modelling of flow and mixing characteristics in vessels was initiated by Danckwerts(104). Wen and Chung (109) presented transient equations based on impulse, step, ramp, parabolic and sinusoidal inputs of tracer for reactors of various flow models. Indeed, Wen and Fan (142) have provided excellent review on the models for flow system in various reactors. A generalized RTD model is proposed, that can be greatly

utilized in any continuous flow system involving tracer input.

4.2 DEVELOPMENT OF THE RESIDENCE TIME DISTRIBUTION MODEL

The residence time distribution model adopted here comprises a network of stirred tanks and plugflows, and is made up of three flow sections. The first consists of a stream of two well stirred tanks separated by a plug flow. The second consists of a plug flow followed by a well stirred tank and the third section is a stream of plug flow. The RTD model involves seven parameters and linear first order differential equations are employed. The models, with its assumptions,is shown in Figure 4.1. A pulse of tracer was injected to the water flow rate at the inlet, top and bottom walls to the nozzle vessel. The exit concentration profile of the tracer was monitored by a high speed camera.

ASSUMPTIONS USED IN THE MODEL :-
A+B+C=1.0
I+J+K+M+N+L=1.0
ANY OF THE PARAMETERS CAN BE ZERO

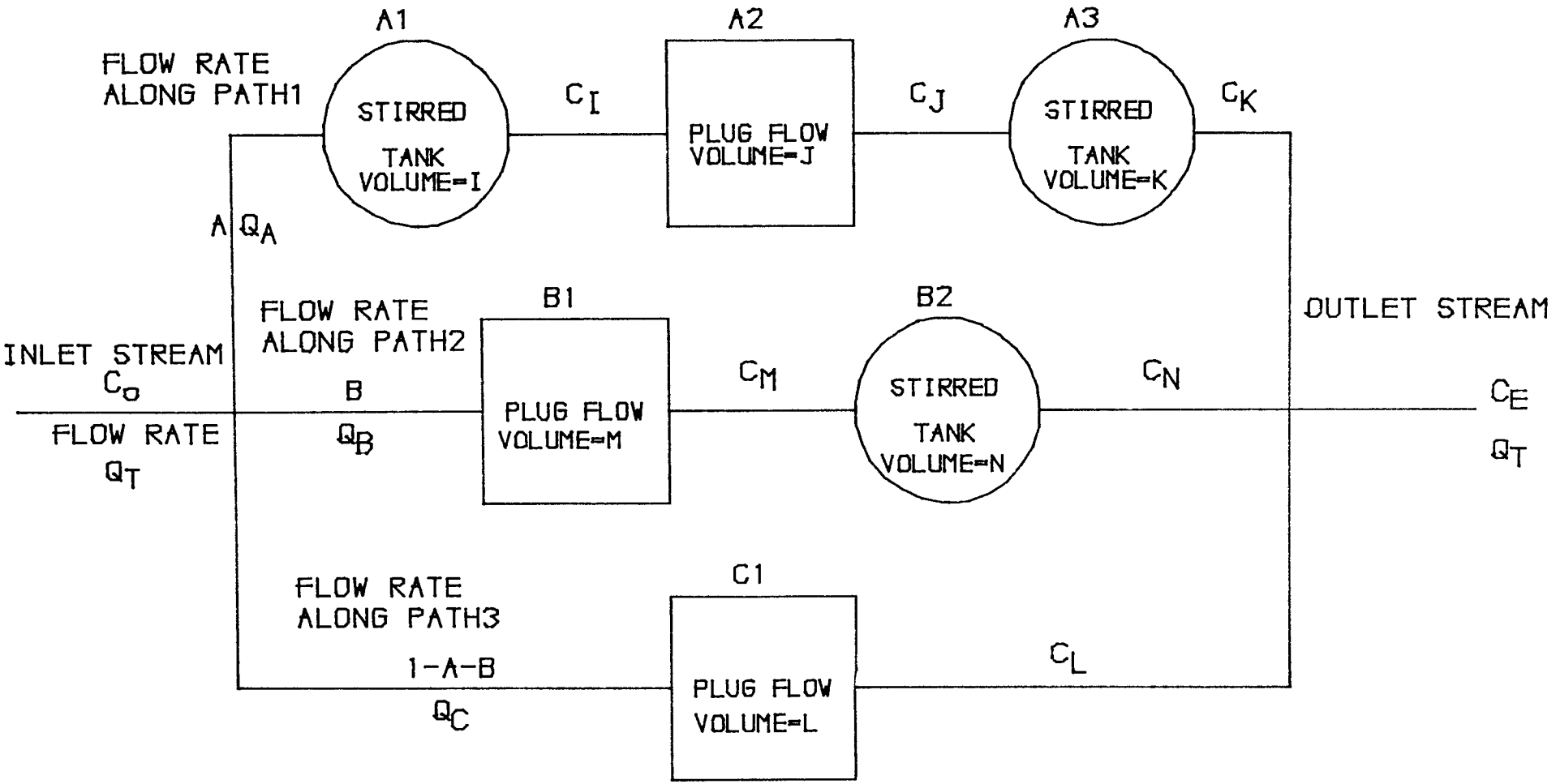

FIGURE 4.1: RESIDENCE TIME DISTRIBUTION MODEL

With respect to Figure 4.1, the following notations are used:

(1)

A1	1st Stirred Tank in Section 1 Volume	V_I
A3	2nd " " " " " "	V_K
B2	Stirred Tank in Section 2 "	V_N
A2	Plug Flow in Section 1 "	V_J
B1	" " " " 2 "	V_M
C1	" " " " 3 "	V_L

(2) A,B,C, - The ratio of the flow of the tracer into sections 1,2 and 3 respectively.

(3)

J	Fraction by Volume of A2
K	" " " " A3
M	" " " " B1
N	" " " " B2
L	" " " " C1

(4) Q_A, Q_B, Q_C, - the flow rates into sections 1,2 and 3 respectively.

(5) V_T and Q_T - the volume of the nozzle reactor and the flow rate respectively.

From (2), (4) and (5)

$$A = \frac{Q_A}{Q_T} \qquad 4.1$$

$$B = \frac{Q_B}{Q_T} \qquad 4.2$$

$$C = \frac{Q_C}{Q_T} = 1-A-B \qquad 4.3$$

From (1), (3) and (5)

$$J = \frac{V_J}{V_T} \qquad 4.4$$

$$K = \frac{V_K}{V_T} \qquad 4.5$$

$$M = \frac{V_M}{V_T} \qquad 4.6$$

$$N = \frac{V_N}{V_T} \qquad 4.7$$

$$L = \frac{V_L}{V_T} \qquad 4.8$$

Therefore, the fraction by volume in Al

$$= 1-J-K-M-N-L$$

$$\text{Hence } I = \frac{V_I}{V_T} = 1-J-K-M-N-L \qquad 4.9$$

Material Balances :-

A WELL STIRRED TANK ZONE A1

$$Q_A C_o = Q_A C_I + V_I \frac{dC_I}{dt} \qquad 4.10$$

$$V_I \frac{dC_I}{dt} = Q_A (C_o - C_I) \qquad 4.11$$

Therefore

$$\frac{dC_I}{dt} = \frac{Q_A}{V_I} (C_o - C_I) \qquad 4.12$$

From equations 4.1 and 4.9

$$\frac{Q_A}{V_I} = \frac{A\, Q_T}{V_T (1-J-K-M-N-L)} \qquad 4.13$$

But $$\bar{t} = \frac{V_T}{Q_T} \qquad 4.14$$

Therefore equation 4.13 becomes

$$\frac{Q_A}{V_I} = \frac{A}{\bar{t}\,(1-J-K-M-N-L)} \qquad 4.15$$

substituting equation 4.15 in equ. 4.12

$$\frac{dC_I}{dt} = \frac{A\,(C_o - C_I)}{\bar{t}\,(1-J-K-M-N-L)} \qquad 4.16$$

In terms of the dimensionless time domain

$$\theta = \frac{t}{\bar{t}} \qquad 4.17$$

therefore $dt = \bar{t}\, d\theta$ 4.18

substituting equ. 4.18 in equ. 4.16

$$\frac{dC_I}{d\theta} = \frac{A\,(C_o - C_I)}{1-J-K-M-N-L} \qquad 4.19$$

A DELAY ZONE A2

This zone constitutes a time delay and the only requirement in the derivation is to calculate the delay time T_j.

T_j is the real time delay

Thus in zone A2,

$$T_j = \frac{V_j}{Q_A} \qquad 4.20$$

From equs. 4.1 and 4.4

$$T_J = \frac{J\ V_T}{A\ Q_T} \qquad 4.21$$

$$T_j = \frac{\bar{t}\ J}{A} \qquad 4.22$$

In terms of the dimensionless time domain,

$$\theta_j = \frac{T_j}{\bar{t}} = \frac{J}{A} \qquad 4.23$$

A WELL STIRRED ZONE A3

$$Q_A\ C_J = Q_A\ C_K + V_k \frac{dC_k}{dt} \qquad 4.24$$

$$\frac{dC_K}{dt} = \frac{Q_A}{V_K} (C_J - C_K) \qquad 4.25$$

From equs. 4.1 and 4.5 respectively,

$$\frac{dC_K}{dt} = \frac{A\ Q_T}{K\ V_T} (C_J - C_K) \qquad 4.26$$

$$\frac{dC_K}{dt} = \frac{A}{k\bar{t}} (C_J - C_k) \qquad 4.27$$

substituting equ. 4.18 in equ. 4.27

In dimensionless time domain

$$\frac{dC_K}{d\theta} = \frac{A}{K} (C_J - C_K) \qquad 4.28$$

A DELAY ZONE B1

This zone also constitutes a time delay

$$T_M = \frac{V_M}{Q_B} \qquad 4.29$$

subsituting equs. 4.2 and 4.6 in equ. 4.29

$$T_M = \frac{M}{B}\frac{V_T}{Q_T} \qquad 4.30$$

$$T_M = \bar{t}\frac{M}{B} \qquad 4.31$$

In dimensonless time,

$$\theta_M = \frac{T_M}{\bar{t}} = \frac{M}{B} \qquad 4.32$$

A WELL STIRRED TANK ZONE B2

$$Q_B C_M = Q_B C_N + V_N \frac{dC_N}{dt} \qquad 4.33$$

$$\frac{dC_N}{dt} = \frac{Q_B}{V_N}(C_M - C_N) \qquad 4.34$$

From equs. 4.2 and 4.7

$$\frac{dC_N}{dt} = \frac{B}{N}\frac{Q_T}{V_T}(C_M - C_N) \qquad 4.35$$

$$\frac{dC_N}{dt} = \frac{B}{N\bar{t}}(C_M - C_N) \qquad 4.36$$

substituting equ. 4.18 in equ. 4.36

In dimensionless time,

$$\frac{dC_N}{d\theta} = \frac{B}{N}(C_M - C_N) \qquad 4.37$$

A DELAY ZONE C1

zone C1 constitutes the final time delay in the model.

Thus, real time delay in C1

$$T_L = \frac{V_L}{Q_T - Q_A - Q_B} \qquad 4.38$$

From equs. 4.1, 4.2 and 4.8 respectively

$$T_L = \frac{L\, V_T}{Q_T\,(1 - A - B)} \qquad 4.39$$

substituting equ. 4.14 in equ. 4.39

$$T_L = \frac{\bar{t}\, L}{1 - A - B} \qquad 4.40$$

In dimensionless time

$$\theta_L = \frac{T_L}{\bar{t}} = \frac{L}{1 - A - B} \qquad 4.41$$

The total exit response C_E to a square pulse tracer input is the summation of the individual concentration from each zone, and is given by

$$C_E = C_K + C_N + C_L \qquad 4.42$$

4.2.1 SIMULATION PROGRAM

The exit concentration profile of tracer in the liquid effluent was captured by a high speed camera, and analysed using an Atomic Absorption Spectrophotometer as described in Chapter 5. The data were converted into dimensionless parameters and the mean residence time $\bar{t}$, for each liquid flow rate was determined from the size of the of the reactor V_T and the flow rate Q_T.

Runge Kutta - Merson routine was used to solve all the linear first order differential equations (4.19), (4.28) and (4.37). The whole simulation exercise was carried out using a fortran IV program, run on Aston University Harris 500 computer system. Values for A,B,J,K,M,L were obtained by trial and error until a close fitting occurred between the overall exit response C_E obtained from simulation and experimental response data. A full listing of the program is presented in Appendix C.

CHAPTER FIVE

EXPERIMENTAL WORK AND EQUIPMENT

5.1 DESIGN AND CONSTRUCTION

5.1.1 CONSTRUCTION OF THE CYLINDRICAL NOZZLE REACTORS

5.2 DESCRIPTION OF EXPERIMENTAL APPARATUS

5.3 EXPERIMENTAL PROCEDURE

5.4 THE ATOMIC ABSORPTION SPECTROPHOTOMETER ANALYSIS TECHNIQUE

5.5 RESIDENCE TIME DISTRIBUTION CURVE ANALYSIS

5.1 DESIGN AND CONSTRUCTION

5.1.1 CONSTRUCTION OF THE CYLINDRICAL NOZZLE REACTORS

The plan and elevation of the cylindrical nozzle reactor are illustrated in Figure 5.1a, where the principal dimensions are shown. The vessel consisted of a top cylindrical section and a bottom conical section. The conical section was fabricated from acrylic perspex rod machined to fit a hollow cylindrical section of the same material. Plate 5.1 shows the three geometrical sizes of the cylindrical nozzle reactors, and detailed calculation of each capacity is presented in appendix A. The capacity of each reactor was $Ø.55 \times 1Ø^{-3} m^3$, $1.52 \times 1Ø^{-3} m^3$ and $5.13 \times 1Ø^{-3} m^3$ respectively. The $5.13 \times 1Ø^{-3} m^3$ vessel of the same geometry was fabricated from polyvinylchloride (PVC), by British Construction Ltd., Birmingham. Each reactor had two inlet nozzles of 6 mm diameter, which projected tangentially into the wall of the vessel and at approximately 1Ø mm from the top of the cylindrical section. Along the side walls were constructed 4 - 5 injection ports for inserting tracer solution by the use of a hypodermic syringe. The dimensions of the nozzle reactors are summarised in Table 5.Ø

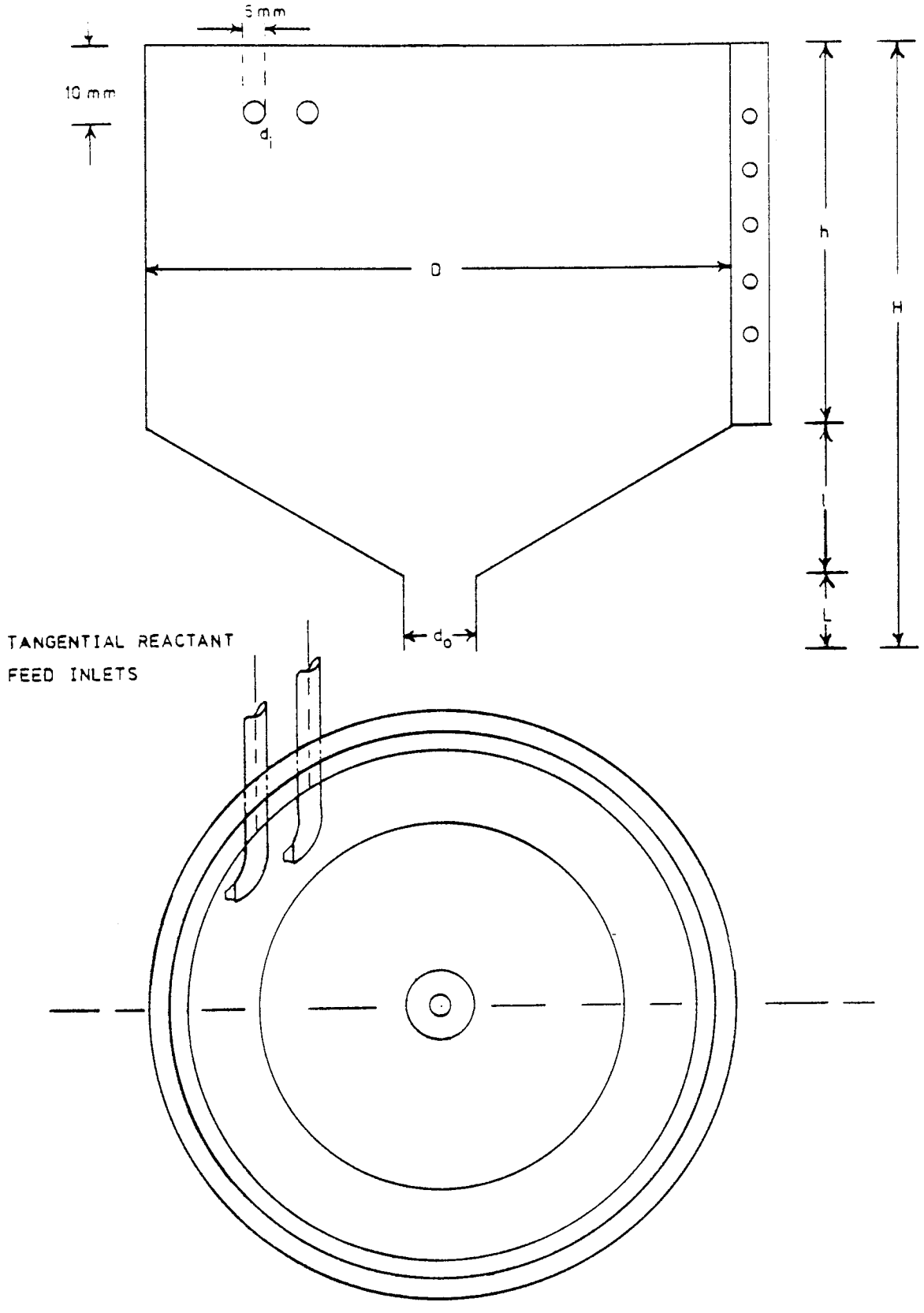

FIGURE 5.1.a
PLAN AND ELEVATION OF CYLINDRICAL NOZZLE REACTOR

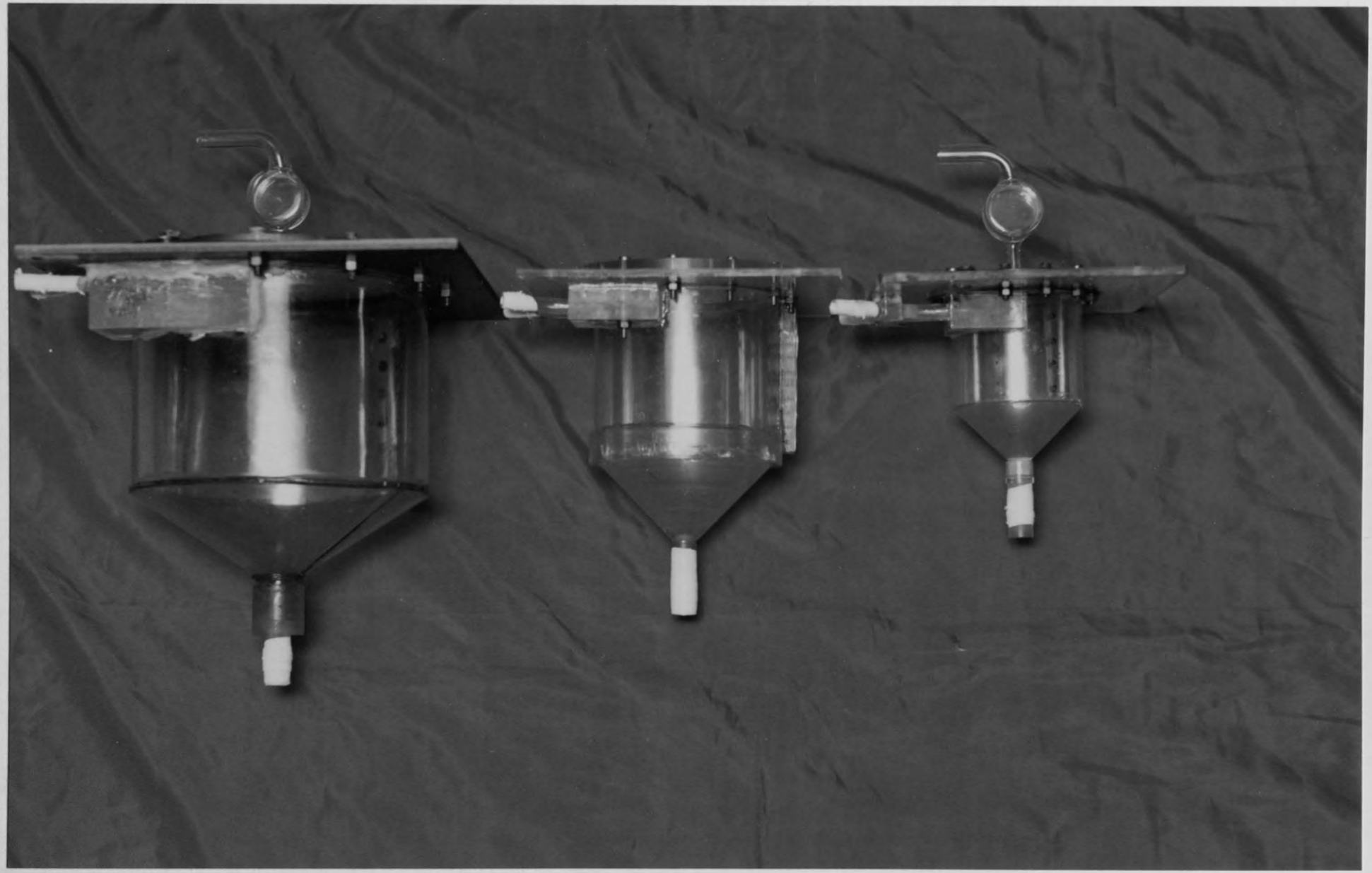

PLATE 5.1 CYLINDRICAL NOZZLE REACTORS

TABLE 5.Ø

DIMENSIONS OF THE CYLINDRICAL NOZZLE REACTORS

CYLINDRICAL NOZZLE REACTORS			1	2	3
MATERIAL OF CONSTRUCTION			Acrylic	Acrylic	PVC
Volume of the vessel $1Ø^{-3}m^3$			Ø.55	1.52	5.13
CYLINDRICAL SECTION					
Height of the hollow cylinder	h	mm	81	114	144
Diameter of the cylinder	D	mm	85	12Ø	2ØØ
CONICAL SECTION					
Height of the solid cone	l	mm	38	55	54
Length of the outlet orifice	L	mm	53	5Ø	72
Diameter of the outlet orifice	d_o	mm	1Ø	1Ø	1Ø
Diameter of the inlet orifice	d_i	mm	6	6	6
Cone Angle	o		96.4^o	$95.Ø^o$	123.3^o

5.2 DESCRIPTION OF EXPERIMENTAL APPARATUS

The salient features of the experimental apparatus are shown on plate 5.2. The schematic diagram is shown in Figure 5.2a and consists of a nozzle type reactor constructed from Q.V.F. glass section which was connected to two feed tanks, each of capacity of 2Ø litres. The pipe lines from the feed tanks were connected to two Number 12 Stuart Turner centrifugal pumps of capacity of Ø.9Ø8 x $1Ø^{-3}m^3$ per sec. and two pressure gauges capable of recording a maximum pressure of 1.961 bar. The flow rates from the pumps were controlled by two 12.7 mm diameter needle valves and metered by two metric type 18S rotameters with stainless steel floats. finally two 3-way glass valves were installed in each feed line to control the flow rate to the reactor or divert the flow back to the feed tanks.

The exit from the vessel contained an optical flat glass test section shown in plate 5.3, suitably illuminated so that any change in colour of the liquid effluent with time could be followed by cine photography. The location of the light source and the disposition of the camera are illustrated in Figure 5.2a. The study of the flow characteristics and measurements of the residence time distribution at different liquid rates, required monitoring the effluent response to either a step-input or

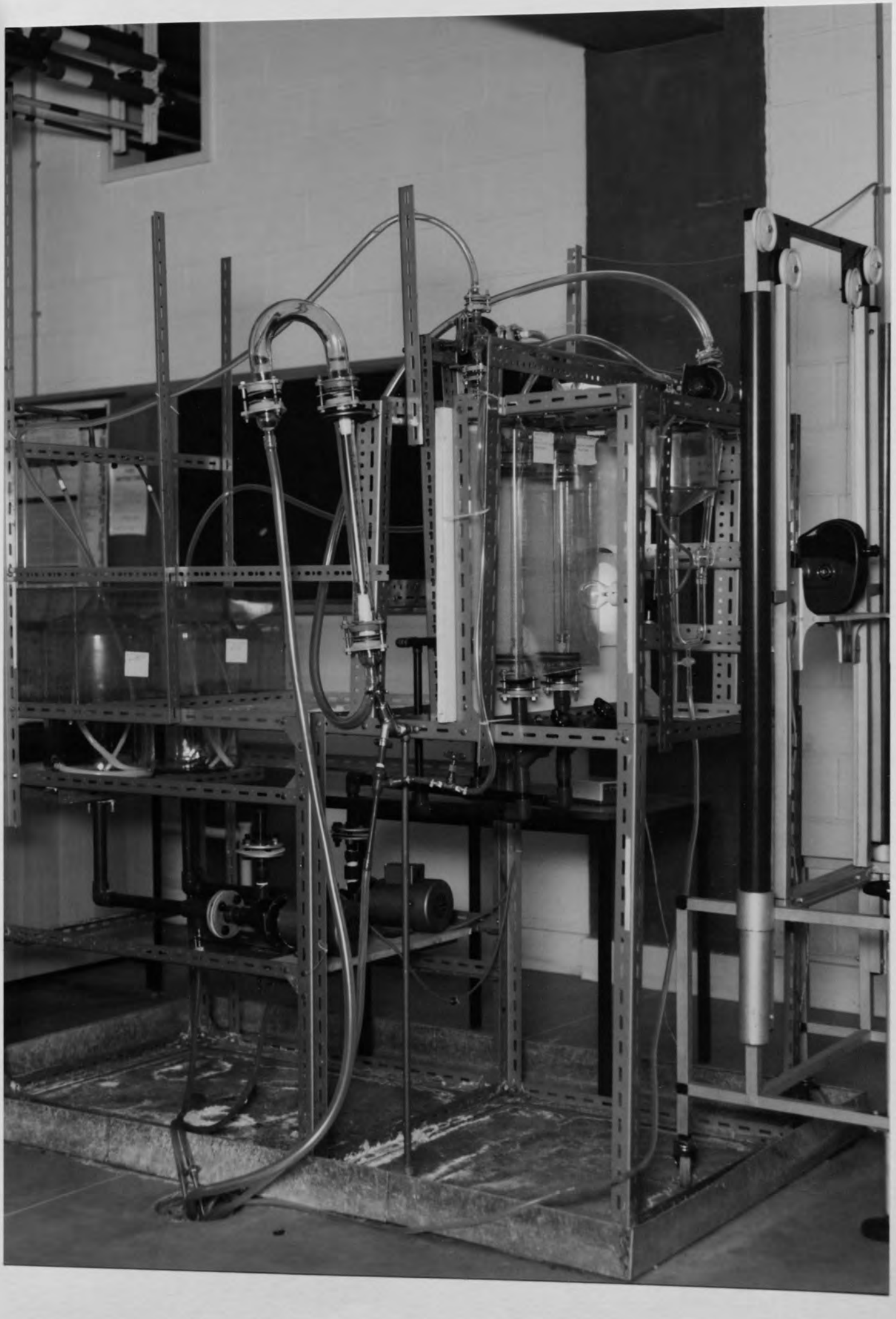

PLATE 5.2 EXPERIMENTAL APPARATUS

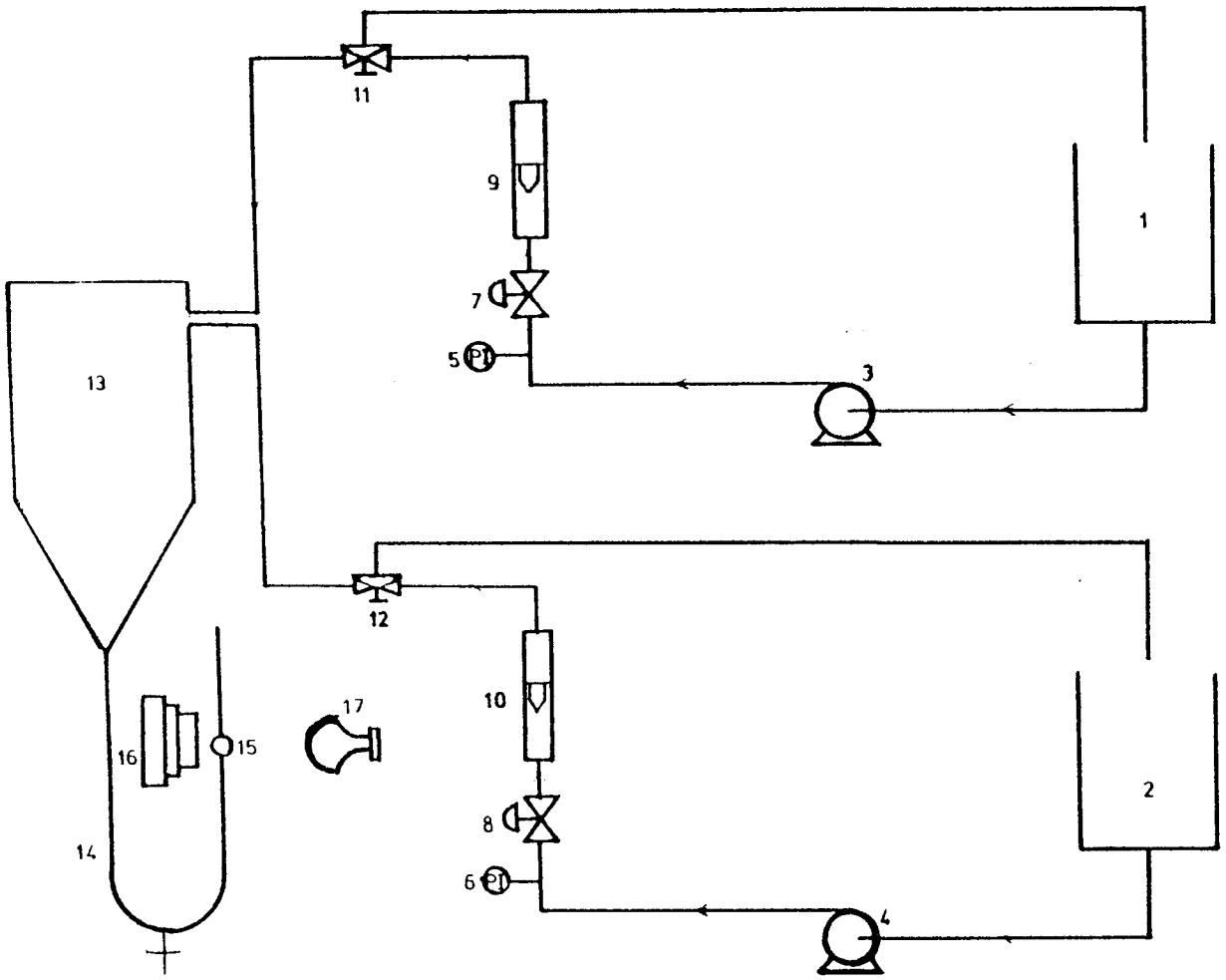

KEY

1, 2	20-LITRE GLASS HOLDING TANKS
3, 4	STAINLESS STEEL SIZE 12 CENTRIFUGAL PUMPS
5, 6	PRESSURE GAUGES
7, 8	1/2 INCH DIAMETER NEEDLE VALVES
9, 10	ROTAMETERS WITH STAINLESS STEEL FLOATS
11, 12	1/4 INCH DIAMETER THREE-WAY GLASS VALVES
13	CYLINDRICAL REACTOR NOZZLE
14	1/2 INCH DIAMETER GLASS U-TUBE
15	1 2/5 INCH DIAMETER OPTICAL PYREX GLASS
16	CINÉ - CAMERA
17	LIGHT - SOURCE

FIGURE 5.2.a FLOW DIAGRAM OF THE EXPERIMENTAL APPARATUS

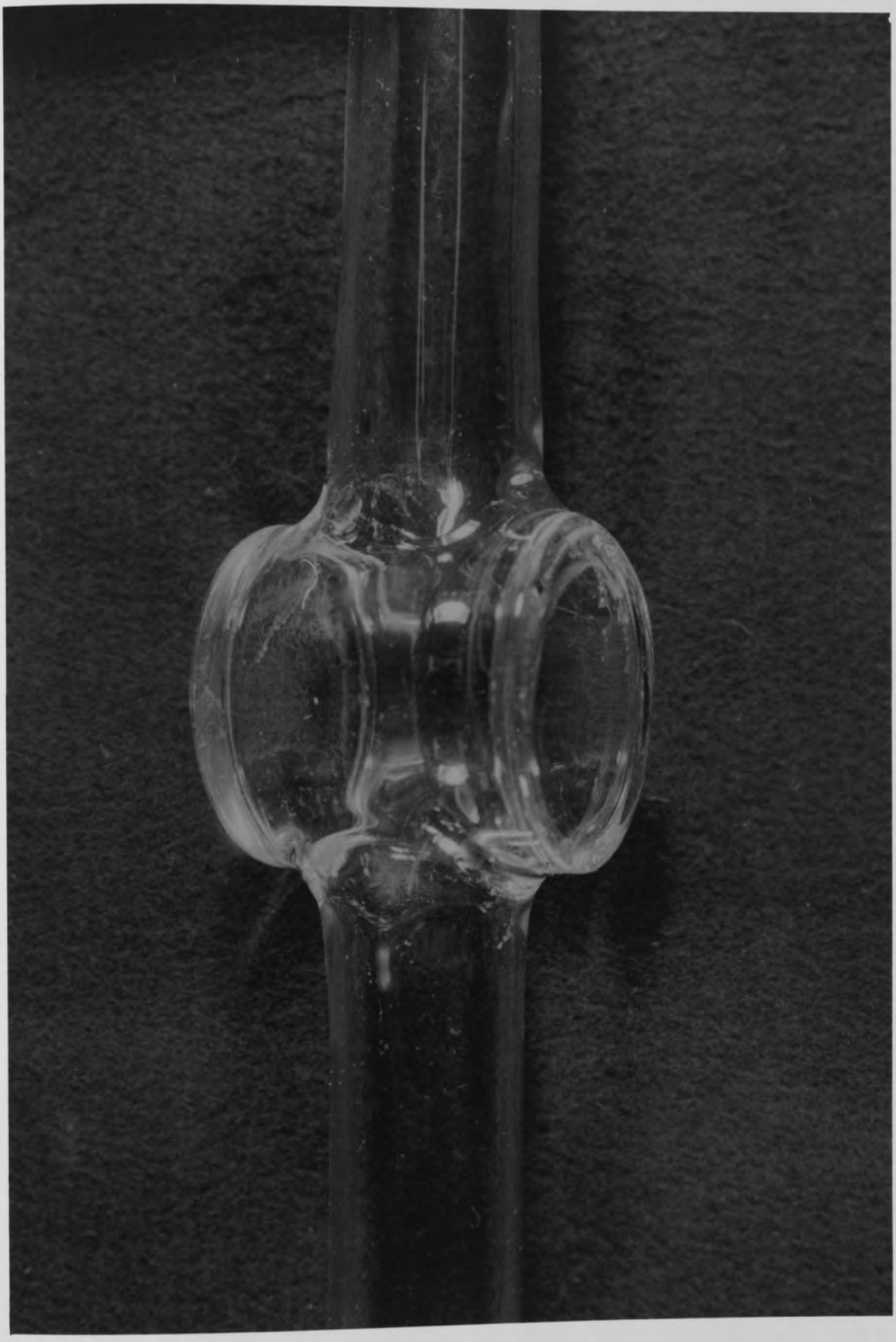

PLATE 5.3 AN OPTICAL FLAT GLASS TEST SECTION

a pulse input of the feed of the reactor. In this experimentation, a square wave pulse input of tracer solution of a known time duration was adopted. The liquid used to investigate the flow patterns was tap water, and the tracer solution was Ø.2 M potassium permanganate. It was also confirmed that the density and viscosity differences between the tracer solution and water flowing through the reactor was negligible.

A cine - photographic technique was developed to capture the response of the tracer solution of the effluent from the vessel. A Beaulieu R16 camera was placed about 25Ø mm from the optical glass section and a 75W reflector lamp provided illumination via a re- enforced mounted glass plate. The aperture settings on the cine-camera were f16-22, over a range of film speed from 2 to 8 frames per sec. and Kodak 4Ø type A KMA449P,16mm x 3Ømm coloured film was used.

5.3 EXPERIMENTAL PROCEDURE

An experiment was started by switching on the pumps and opening the needle valves in the process lines; then adjusting the 3 way glass valves so that the liquid would circulate the pipeline systems and be returned to the feed tanks. The 3 way glass valves were next adjusted to direct the flow of water, metered via the calibrated rotameters, to the inlets of the reactor. The needle valves were then adjusted to control the flow rate to that desired for the experiment.

The reflector lamp was switched on, and a beam of light was directed through to the optical glass. The camera, which was focussed onto the optical glass, was then set in motion. The camera was set at a film speed of 2 frames per sec. with an aperture setting of f22 for the $5.13 \times 10^{-3} m^3$ capacity reactor. When a steady water flow rate had been attained, 10 mls of 0.2 M potassium permanganate solution was injected continuously for about 3 seconds, into the inlet stream to the reactor from a hypodermic syringe. It was found that, after a period of three times the nominal residence time, a substantial amount of the tracer had passed through the reactor and been photographed. The filming process was however only stopped, when negligible amounts of the tracer, formed a thin layer at the vortex of the air - core in the nozzle reactor. The experiments were repeated for different

water flow rates using $\emptyset.55 \times 1\emptyset^{-3} m^3$ and $1.52 \times 1\emptyset^{-3} m^3$ reactor sizes respectively.

Further experiments were also conducted on $\emptyset.55 \times 1\emptyset^{-3} m^3$ nozzle reactor, to investigate more critically the nature of the flow characteristics by injecting tracer solution at varying liquid rates at both top and bottom respectively, of the wall of the nozzle reactor. A video film of the flow patterns from the cylindrical nozzle vessels has been deposited in the Chemical Engineering Department. Tables 5.1 - 5.5 show the range of liquid and the Reynolds number calculated for the different nozzle sizes.

TABLE 5.1

EXPERIMENTAL RUN FILM CODE	REACTOR SIZE LITRE	FLOW RATE LITRE/MIN	AVERAGE REYNOLDS NUMBER OF INLET NOZZLES
F91	.550	2.900	5119
F92	.550	3.500	6178
F93	.550	4.100	7237
F94	.550	4.750	8385
F95	.550	5.350	9444
F96	.550	5.980	10556
F97	.550	6.600	11650
F98	.550	7.300	12890
F99	.550	7.930	13998

TABLE 5.2

EXPERIMENTAL RUN FILM CODE	REACTOR SIZE LITRE	FLOW RATE LITRE/MIN	AVERAGE REYNOLDS NUMBER OF INLET NOZZLES
F31	1.520	2.900	5119
F32	1.520	3.500	6178
F33	1.520	4.100	7237
F34	1.520	4.750	8385
F35	1.520	5.350	9444
F36	1.520	5.980	10556
F37	1.520	6.600	11650
F38	1.520	7.300	12886
F39	1.520	7.960	14051

TABLE 5.3

EXPERIMENTAL RUN FILM CODE	REACTOR SIZE LITRE	FLOW RATE LITRE/MIN	AVERAGE REYNOLDS NUMBER OF INLET NOZZLES
F81	5.130	2.900	5119
F82	5.130	3.500	6178
F83	5.130	4.100	7237
F84	5.130	4.750	8385
F85	5.130	5.350	9444
F86	5.130	5.980	10556
F87	5.130	6.600	11650
F88	5.130	7.300	12886
F89	5.130	7.900	13998
F810	5.130	8.640	15251
F811	5.130	9.330	16469
F812	5.130	10.040	17723
F813	5.130	10.800	19064
F814	5.130	11.530	20353
F815	5.130	12.300	21712
F816	5.130	13.100	23124

TABLE 5.4

EXPERIMENTAL RUN FILM CODE	REACTOR SIZE LITRE	FLOW RATE LITRE/MIN	AVERAGE REYNOLDS NUMBER OF INLET NOZZLES
F11	.550	2.900	5119
F12	.550	3.500	6178
F13	.550	4.100	7237
F14	.550	4.750	8385
F15	.550	5.350	9444
F16	.550	5.980	10556
F17	.550	6.600	11650
F18	.550	7.300	12886
F19	.550	7.930	13998
F110	.550	8.640	15251
F111	.550	9.330	16469

TABLE 5.5

EXPERIMENTAL RUN FILM CODE	REACTOR SIZE LITRE	FLOW RATE LITRE/MIN	AVERAGE REYNOLDS NUMBER OF INLET NOZZLES
F21	.550	2.900	5119
F22	.550	3.500	6178
F23	.550	4.100	7237
F24	.550	4.750	8385
F25	.550	5.350	9444
F26	.550	5.980	10556
F27	.550	6.600	11650
F28	.550	7.300	12886
F29	.550	7.930	13998

5.4 THE ATOMIC ABSORPTION SPECTROPHOTOMETER ANALYSIS TECHNIQUE

The technique adopted to analyse the coloured cine film, to determine the response signals of the tracer solution, involved the use of an Atomic Absorption Spectrophotometer, a Photo - Optical Data Analyser projector and a chart recorder. The light source chosen for the A.A.S analysis was assessed as follows:-

One millilitre of Ø.25 M potassium permanganate solution was diluted to 5ØØ mls and a sample of the diluted solution was then tested in an Ultra - violet spectrophotemeter. This produced an absorbance peak height of 53Ø nm that was close to the wave length of sodium lamp (589 nm). Therefore a sodium light source was fitted into the A.A.S.

The measuring technique is illustrated as shown in plate 5.4 and involved estimating the absorbance intensity of colour of the film and transferring this onto a chart recorder. The flame holder, normally used in spectrophometer analysis was replaced by the pulley device shown on plate 5.5 which functioned as the film guide. This was adjusted until a beam from the sodium lamp passed once through the central section of the film. The film was then displaced from the light beam as it was returned to the take-up reel.

PLATE 5.4 ATOMIC ABSORPTION SPECTROPHOTOMETER WITH 16mm CINE PROJECTOR IN PLACE

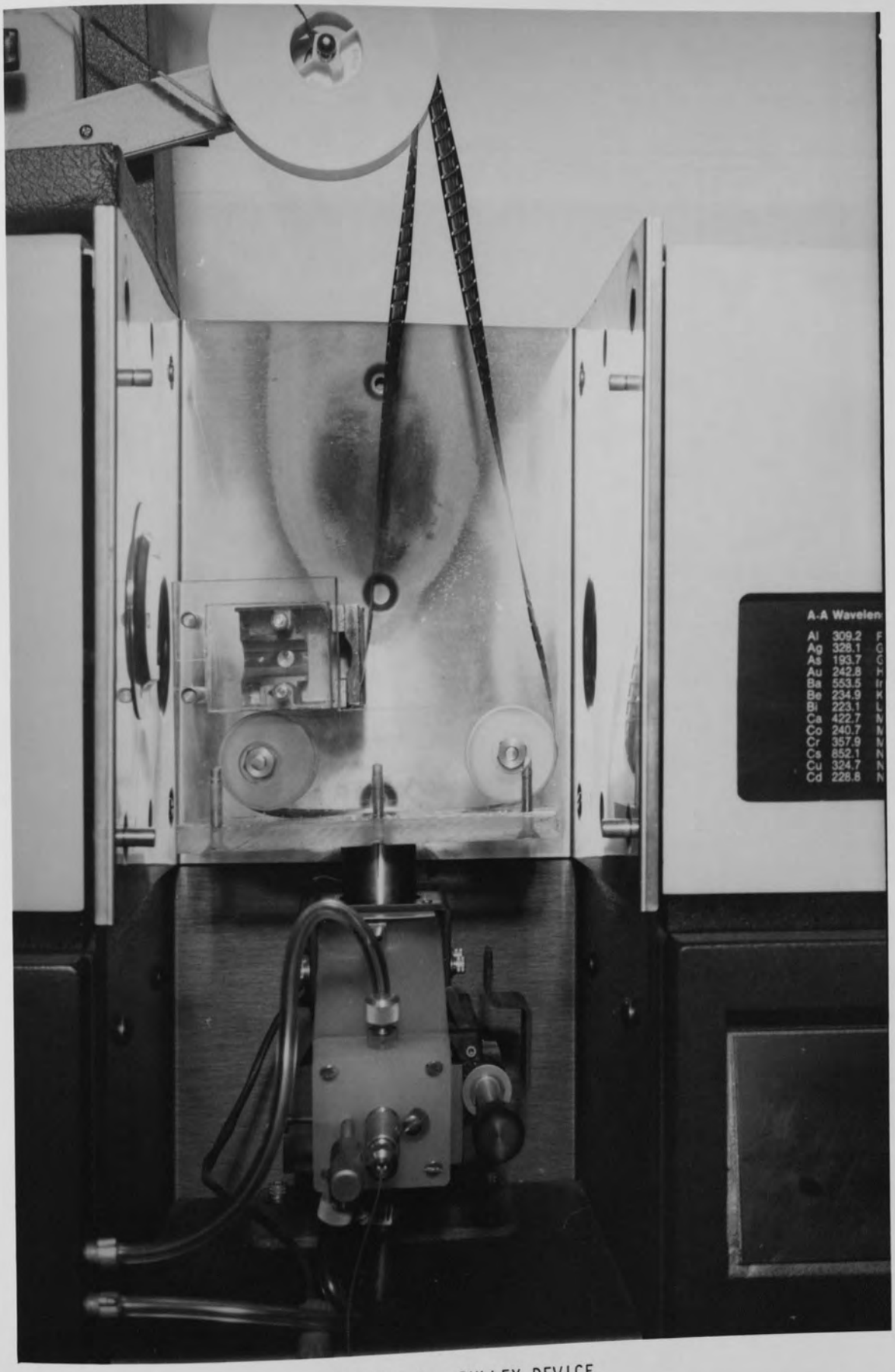

PLATE 5.5 PULLEY DEVICE

The projector was set at a speed of 12 frames per sec. and the change in the colour of the film was followed by the detection device of the instrument. This was converted into peak heights on the chart recorder as it passed through the light source. Figures 5.1 - 5.8 present typical responses produced by the A.A.S onto the chart recorder, using the nozzle reactor of $5.13 \times 10^{-3} m^3$ and at varying liquid flow rates. The results produced onto the chart recorder, gave true representations of the response to the tracer solution at the exit of the vessel.

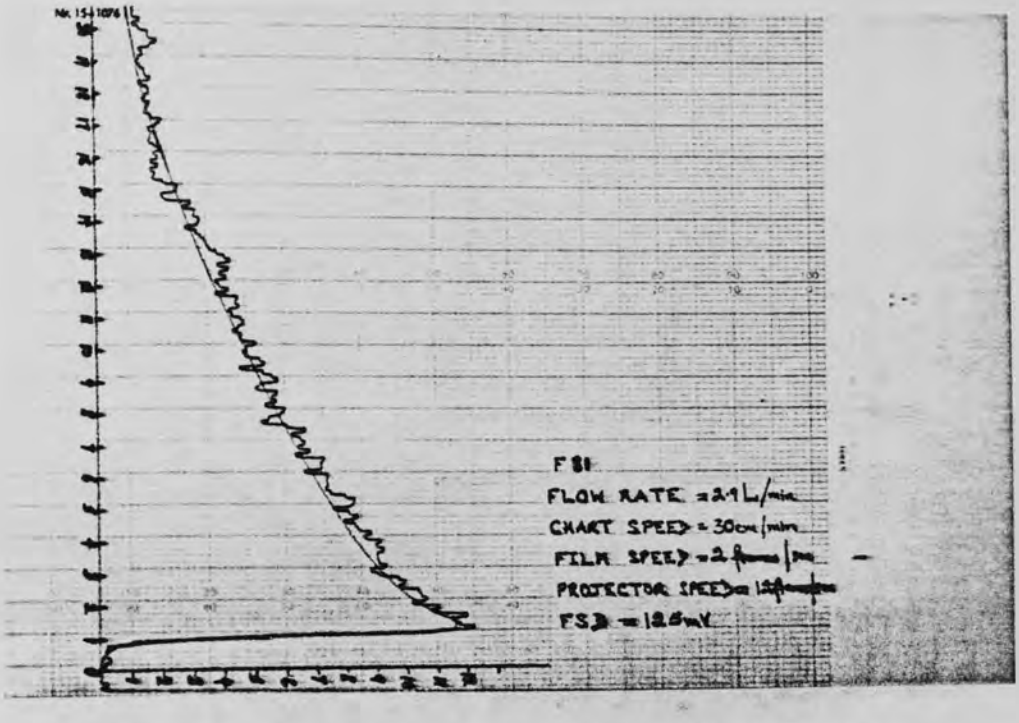

FIGURE 5.1 RTD RESPONSE FROM SPECTROPHOTOMETER AT LIQUID FLOW RATE = 2.9 L/min.

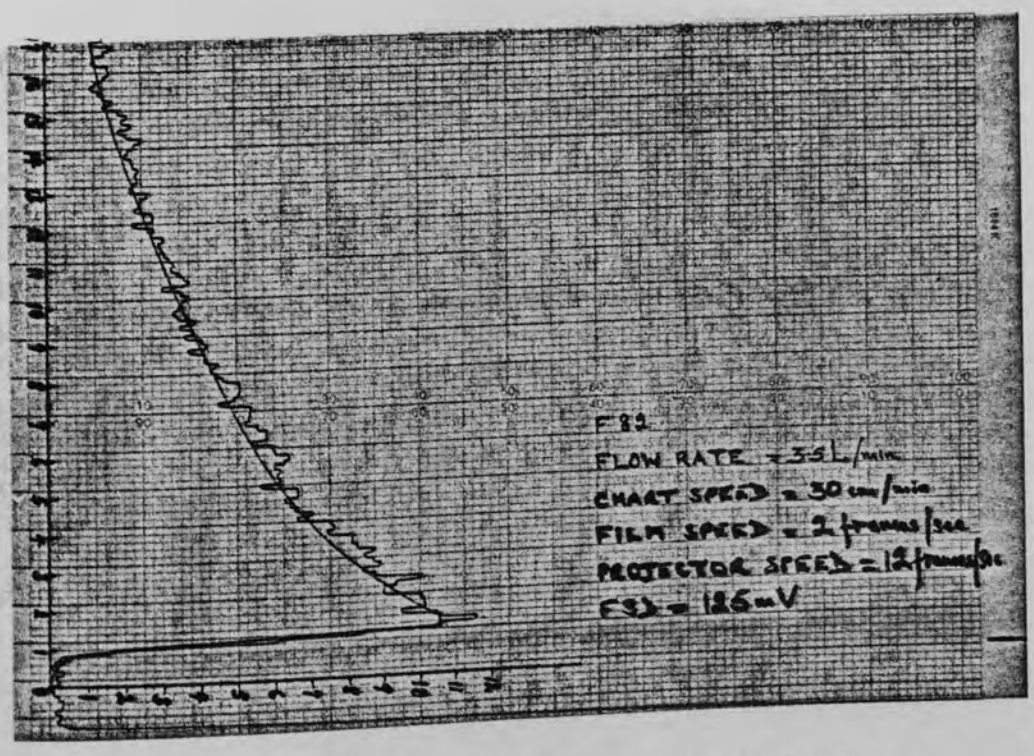

FIGURE 5.2 RTD RESPONSE FROM SPECTROPHOTOMETER AT LIQUID FLOW RATE = 3.5 L/min.

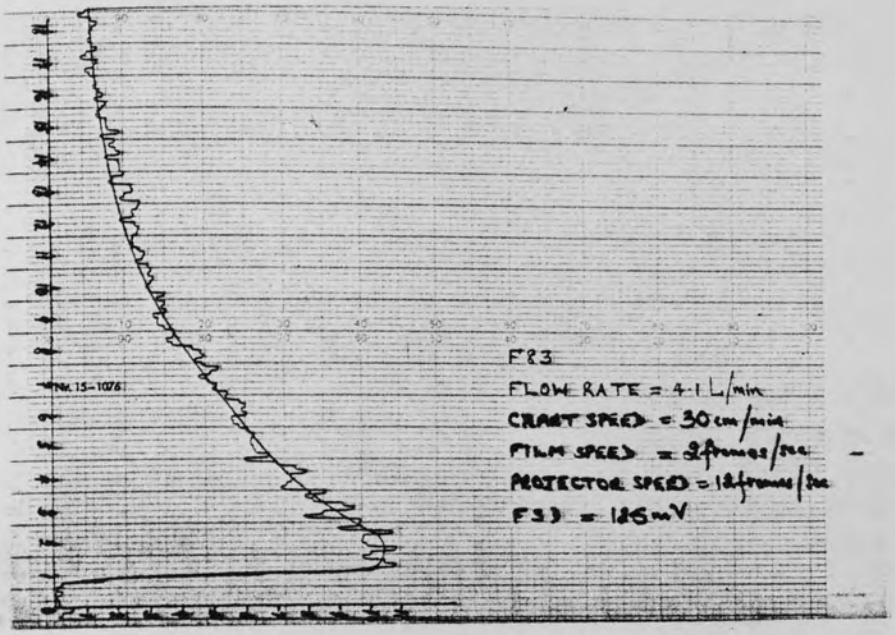

FIGURE 5.3 RTD RESPONSE FROM SPECTROPHOTOMETER AT LIQUID FLOW RATE = 4.1 L/min.

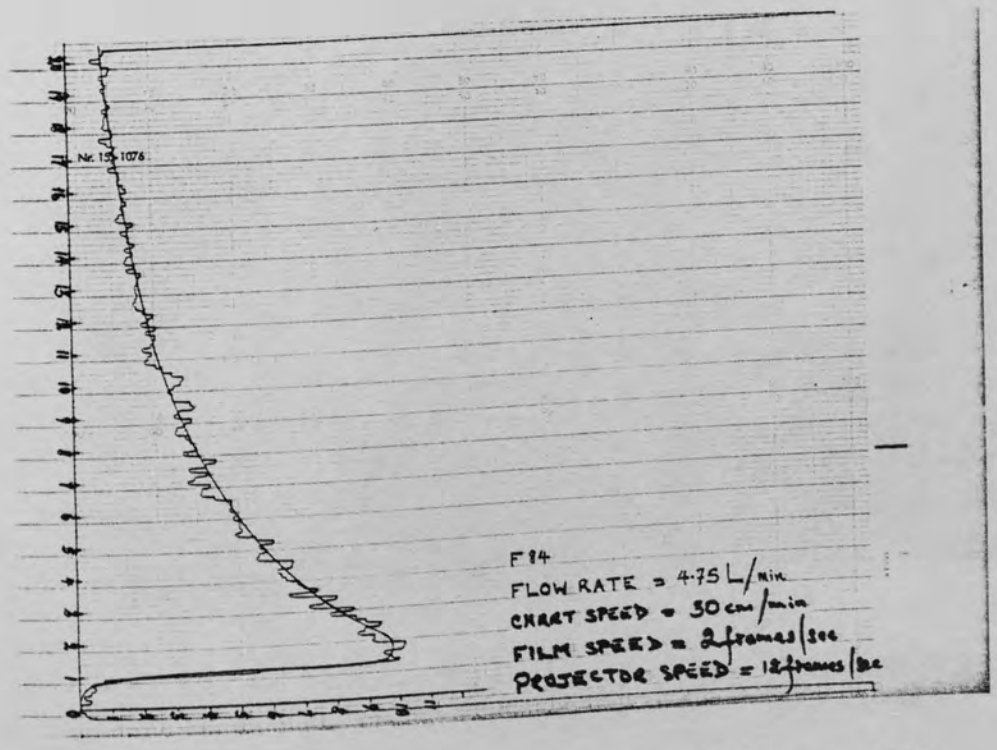

FIGURE 5.4 RTD RESPONSE FROM SPECTROPHOTOMETER AT LIQUID FLOW RATE = 4.75 L/min.

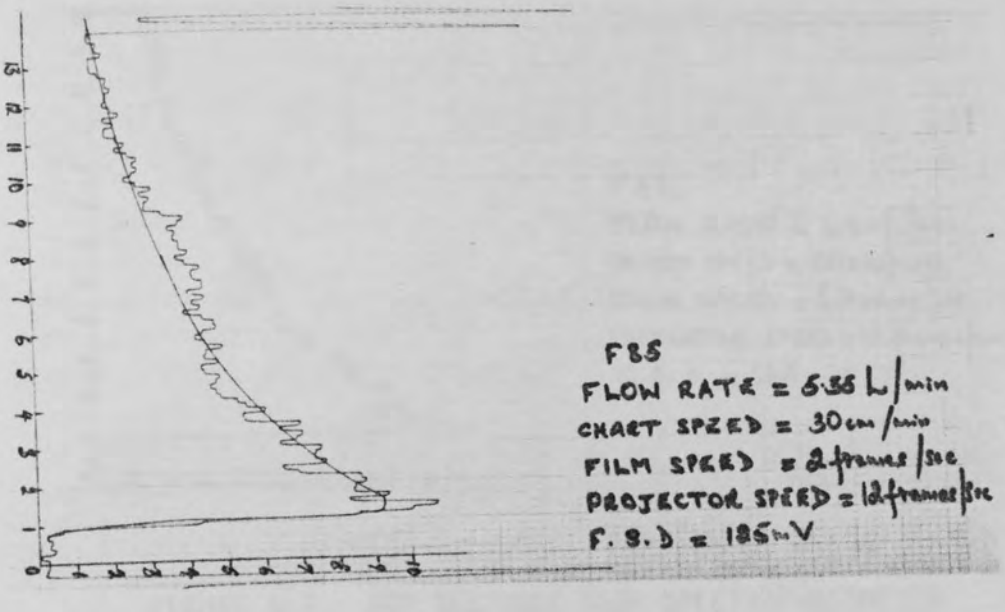

FIGURE 5.5 RTD RESPONSE FROM SPECTROPHOTOMETER AT LIQUID FLOW RATE = 5.35 L/min.

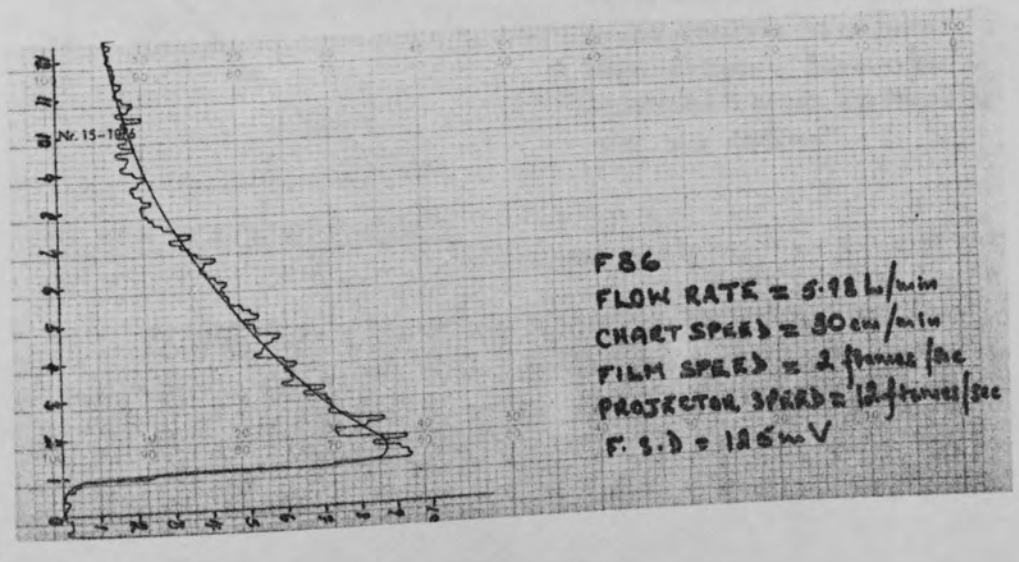

FIGURE 5.6 RTD RESPONSE FROM SPECTROPHOTOMETER AT LIQUID FLOW RATE = 5.98 L/min.

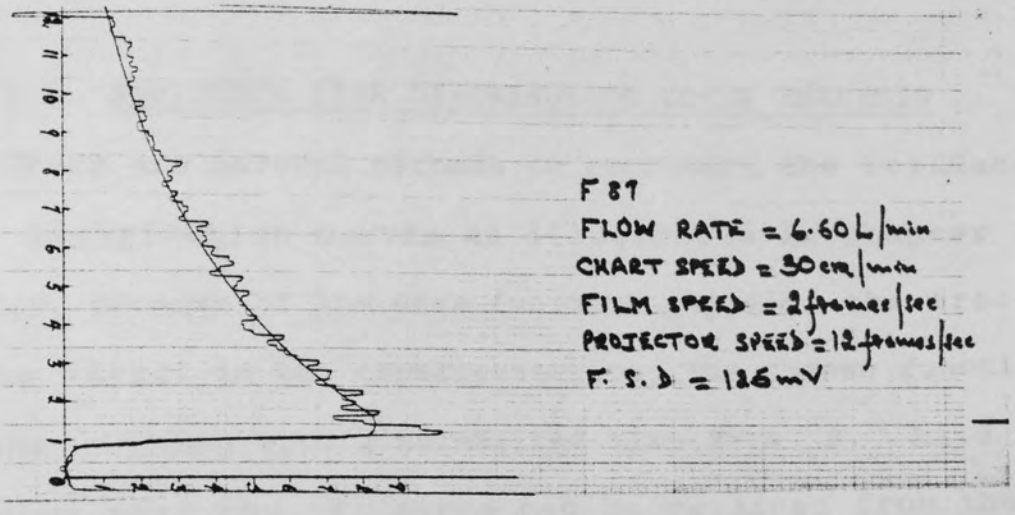

FIGURE 5.7 RTD RESPONSE FROM SPECTROPHOTOMETER AT LIQUID FLOW RATE = 6.60 L/min.

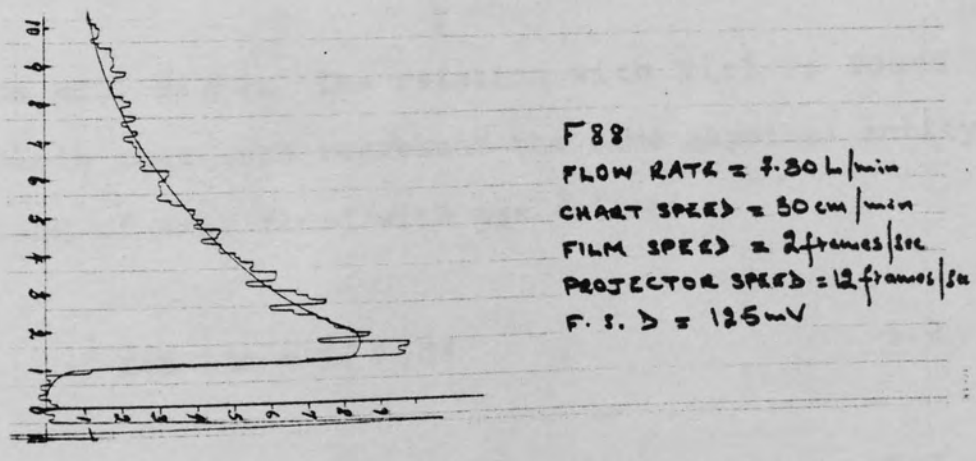

FIGURE 5.8 RTD RESPONSE FROM SPECTROPHOTOMETER AT LIQUID FLOW RATE = 7.30 L/min.

5.5 RESIDENCE TIME DISTRIBUTION CURVE ANALYSIS

There are several methods to represent the residence time distribution curves as illustrated in chapter 2. However, because of the wave function input of the tracer to the vessel in the experimentation, the chosen function was the 'E' form with a normalized time axis θ. Also it is known that the 'F' curve can be obtained from the E curve in accordance with the following expression:-

$$F(\theta) = \int_{\emptyset}^{\theta} E(\theta)d\theta \qquad 5.1$$

Generally, it is often convenient to use the dimensionless time of $\theta = \frac{t}{\bar{t}}$, and a corresponding version of the RTD, $E(\theta)$. The relation with E(t) is found from the basis that both represent the same physical entity, the fraction of exit fluid with age θ (146).

$$E(t)dt = E(\theta)d\theta \qquad 5.2$$

$$= E(\theta)\frac{dt}{\bar{t}} \qquad 5.3$$

and so:

$$E(\theta) = \bar{t}\,E(t) \qquad 5.4$$

$$\bar{t} = \frac{V_T}{Q_T} = \frac{\text{Volume of the vessel}}{\text{Liquid flow rate}}$$

From the speed of the chart recorder, projector and film and also the mean residence time $\bar{t}$, the dimensionless unit scale can be calculated.

For example, in Table 9.1 in Appendix B.

The speed of the chart recorder:	30 cm per min
Projector speed:	12 frames per sec.
Film speed:	8 frames per sec.
Liquid flow rate:	2.9 Litres per min.
Volume of the vessel:	0.55 Litre
Mean residence time:	11.3793 secs.

Therefore, 1 cm on the chart recorder output equals

$$\frac{12}{8} \times \frac{60}{30} \left(\frac{\text{frames}}{\text{sec}} \quad \frac{\text{sec}}{\text{frames}} \quad \frac{\text{sec}}{\text{cm}} \right)$$

$$= 3 \text{ secs real time}$$

when

$$\theta = \frac{t}{\bar{t}} = 1$$

therefore $t = 11.3793$ secs

Hence, at the distance $\frac{11.3793}{3} = 3.7931$ cm

from the starting point, θ is equal to 1. Using the rule "equal distance corresponds to equal time" any desired scale can be obtained and it is also known that

$$\int_{\emptyset}^{\infty} E(\theta)d\theta = 1 \qquad 5.5$$

Therefore, dividing the total area under the curve by the scale at which = 1 along the abscissa, the distance at $E(\theta) = 1$ can be obtained. In this example, the total area under the curve was calculated using the Simpson's $\frac{3}{8}$ Rule and it was found to be 96.7262 cm^2. Thus at the distance $\frac{96.7262}{3.7931}$ = 25.5ØØ6 cm from the ordinate origin, $E(\theta) = 1$. Hence each value of the ordinate was normalised into dimensionless concentration corresponding to the normalised dimensionless residence time. The result of this example in the form of $E(\theta)$ and $F(\theta)$ was tabulated in Table 5.6.

TABLE 5.6

TIME	DIMENSIONLESS	EXIT CONCENTRATION DIMENSIONLESS	
(S)	TIME (THETA)	E(THETA)	F(THETA)
0	.000	.000	.000
3	.264	.245	.032
6	.527	.337	.109
9	.791	.329	.197
12	1.055	.302	.280
15	1.318	.280	.357
18	1.582	.259	.428
21	1.845	.241	.494
24	2.109	.224	.555
27	2.373	.206	.612
30	2.636	.188	.664
33	2.900	.173	.712
36	3.164	.157	.756
39	3.427	.145	.796
42	3.691	.127	.832
45	3.955	.110	.863
48	4.218	.094	.890
51	4.482	.086	.914
54	4.745	.071	.935
57	5.009	.059	.952
60	5.273	.049	.966
63	5.536	.039	.978
66	5.800	.031	.987
69	6.064	.029	.995

CHAPTER SIX

RESULTS AND DISCUSSION

6.Ø PRESENTATION AND ANALYSIS OF EXPERIMENTAL RESULTS

6.1 FLOW VISUALIZATION IN NOZZLE REACTORS

6.2 RESIDENCE TIME DISTRIBUTION OF LIQUID IN CYLINDRICAL NOZZLE REACTORS

6.3 ANALYSIS OF THE RTD MODEL RESPONSE

6.4 LIQUID RTD IN CYLINDRICAL NOZZLE REACTORS

6.Ø PRESENTATION AND ANALYSIS OF EXPERIMENTAL RESULTS

6.1 FLOW VISUALIZATION IN NOZZLE REACTORS

The study of flow characteristics and analysis of the RTD of the liquid in cylindrical nozzle reactors of Ø.55 x $1Ø^{-3}m^3$, 1.52 x $1Ø^{-3}m^3$ and 5.13 x $1Ø^{-3}m^3$ respectively, were carried out by injecting an indicator of potassium permanganate solution and photographing the effluent by means of a high speed camera, as explained in Chapter 5.

However, flow visualization studies of liquid in the nozzle vessels were conducted with the use of an Ashai Pentax Spotmatic ES II camera, injecting the dye at the inlet, top and bottom ports of the reactors. Plates 6.1 - 6.6, show the flow patterns of the liquid at a low flow rate of 2.9 l/min. in 5.13 x $1Ø^{-3}m^3$ nozzle vessel. Plates 6.7 - 6.12, represent the flow patterns at a high flow rate of 13.Ø l/min. in the same vessel. The flow patterns are viewed from hydrodynamics of the liquid in the nozzle reactor.

At a steady liquid flow rate of 2.9 l/min., the indicator solution was introduced at an entry feed to the vessel. A low swirl of the solution around the cylindrical section of the reactor (Plate 6.1) was observed. The motion of the liquid was irrotational as it formed a fixed circular path in the vessel. After an elapse of time (Plate 6.2), a well defined air core was

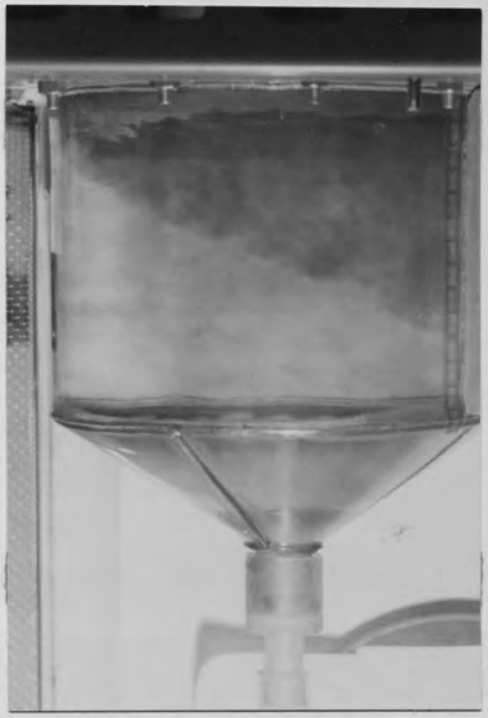

PLATE 6.1

Flow pattern of the tracer

2 seconds after entry

(Re = 5119)

PLATE 6.2

Flow pattern of the tracer

38 seconds after entry

(Re = 5119)

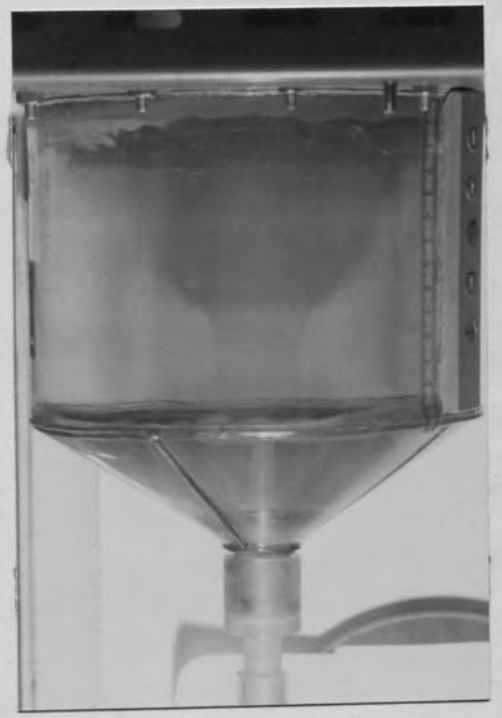

PLATE 6.3

Flow pattern of the tracer

71 seconds after entry

(Re = 5119)

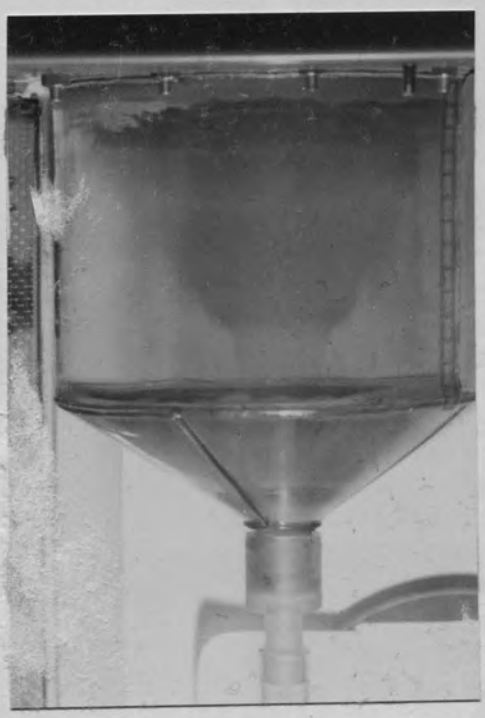

PLATE 6.4

Flow pattern of the tracer

112 seconds after entry

(Re =5119)

revealed along the axis of the vessel. The core was symmetrical at the axis and extended from the conical section to the top. Also, there was a depression of the dye solution at the top of the vessel which formed a hyperbolic shape. This form of shape was indicated by a free vortex motion of the liquid in the vessel.

With a steady flow of fresh liquid in the nozzle vessel, changes in flow patterns of the liquid were observed (Plates 6.3 - 6.4). A distinct depression of the tracer solution was present, as the dye diffused from the centre of the core to other regions in the vessel, resulting from the combined vortex that was established in the liquid. Plate 6.4 indicates a clear region at the wall with a prominent feature of the combined vortex. Brennan and Lehrer(125) had observed such a condition in their determinations of mixing time in an unbaffled vessel.

Further flow of the liquid at a constant rate, showed diffusion of the dye from the centre of the core, with the collapse of the combined vortex formation, to form clear regions along the walls of the vessel surrounding the air core (Plates 6.5 - 6.6). In these regions, it could be explained that the liquid remained clear, because the inward radial flow to transport the dye was small, whilst there were no shear forces to allow the turbulent diffusion of the dye. These clear regions had been observed by Bradley and Pulling (10) in their study

PLATE 6.5

Flow pattern of the tracer

2Ø2 seconds after entry

(Re = 5119)

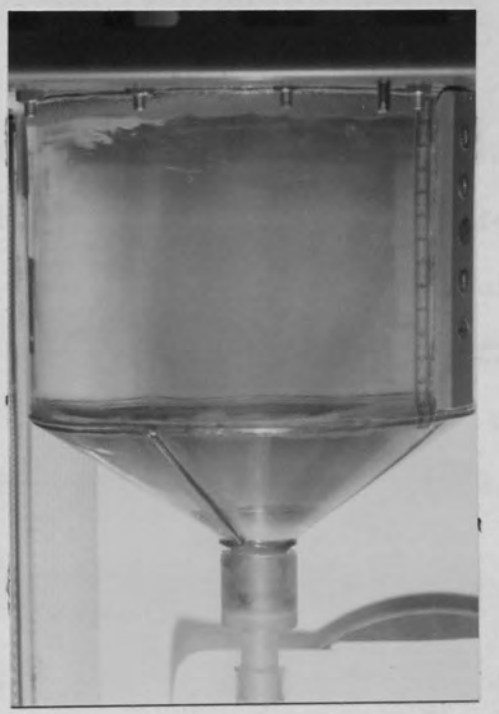

PLATE 6.6

Flow pattern of the tracer

22Ø seconds after entry

(Re = 5119)

of 1.5 in. and 3 in. respectively liquid cyclones.

At a high liquid rate of 13.1 l/min., with the dye injected at an entry feed to the same vessel, different flow patterns were observed (Plates 6.7 - 6.12). A rapid swirl of the dye solution in the bulk liquid vessel was noted within a second (Plate 6.7), followed by simultaneous diffusion of the tracer solution to the centre of the vessel. Plate 6.8 showed an annulus of the dye solution along the axis of the vessel. This could be termed as a solid body rotation of the air core symmetrical along the axis of the vessel. With the constant flow of liquid, a rapid diffusion of the dye solution with different flow patterns was noted (Plates 6.9 - 6.10), until after a period of time, there existed clear regions (Plates 6.11 - 6.12) around the walls of the vessel.

Further experiments were carried out, by injecting the tracer solution at the top and bottom ports into the wall of the vessel, and at varying liquid flow rate in $0.55 \times 10^{-3} m^3$ nozzle vessel. It was observed that, coupled with the changes in the flow patterns as already discussed, tracer injection at the bottom port showed a distinct reversal of the dye solution from the point of injection to the top of the vessel. After this phenomenon, a clear zone surrounding the core was observed, which indicated the region of short circuit flow. This secondary phenomenon, had been noted by Nuttal (20) and ascertained by Binnie (19), Bradley and Pulling (10).

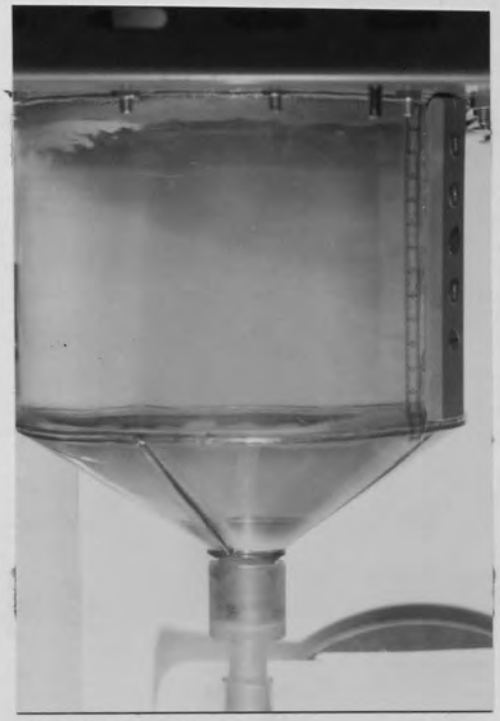

PLATE 6.7

Flow pattern of the tracer

1 second after entry

(Re = 23124)

PLATE 6.8

Flow pattern of the tracer

14 seconds after entry

(Re = 23124)

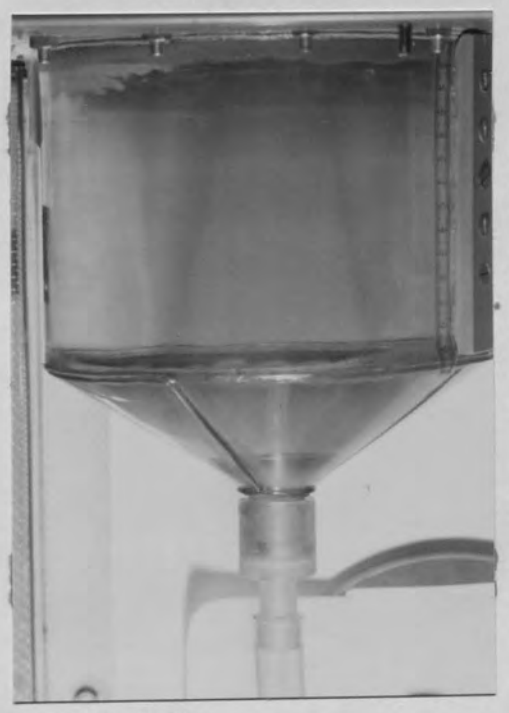

PLATE 6.9

Flow pattern of the tracer

28 seconds after entry

(Re = 23124)

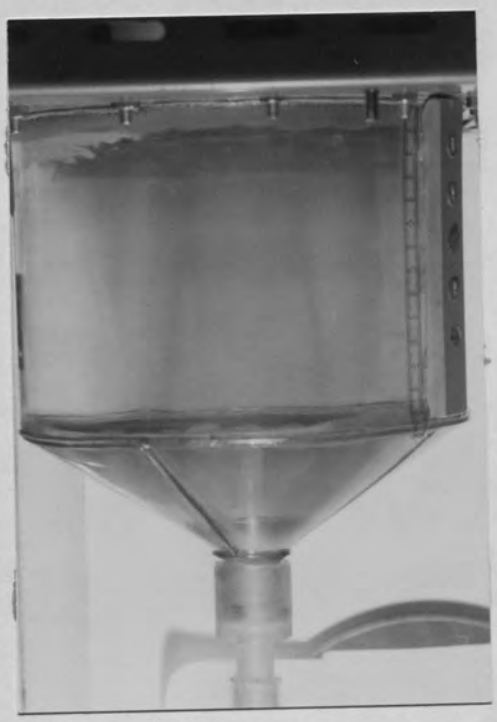

PLATE 6.1Ø

Flow pattern of the tracer

36 seconds after entry

(Re = 23124)

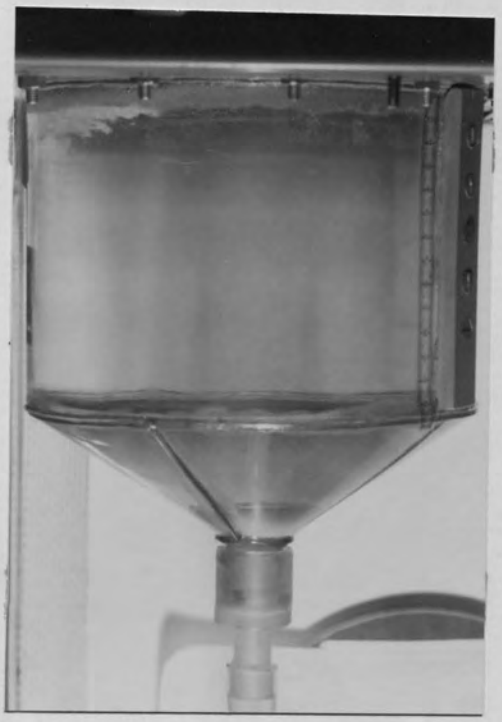

PLATE 6.11

Flow pattern of the tracer

51 seconds after entry

(Re = 23124)

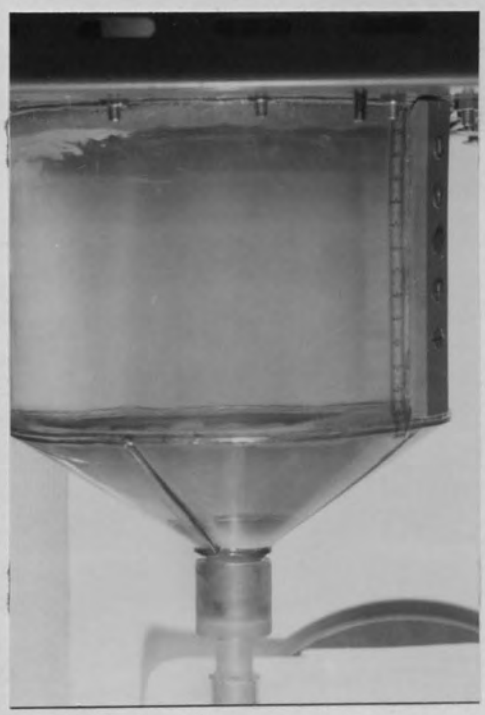

PLATE 6.12

Flow pattern of the tracer

65 seconds after entry

(Re = 23124)

However, it can be inferred that in all the fluid flow studies; the visual observation of the flow patterns in cylindrical nozzle vessels has given us necessary information as to their characteristic behaviour. It is hoped, that the analysis of the residence time distribution will further furnish us on their performance as chemical reactors. A video recording of the flow patterns is deposited in the Department of Chemical Engineering.

6.2 RESIDENCE TIME DISTRIBUTION OF LIQUID IN CYLINDRICAL NOZZLE REACTORS

The residence time distribution experiments were carried out in three geometrically cylindrical nozzle vessels. Tap water was used as the liquid flowing in the reactors and potassium permanganate as the tracer solution. Experiments were carried out for varying liquid rate, and the tracer solution for a series of experiment was introduced at the inlet, top and bottom ports of the nozzle vessels. The experimental data were obtained by means of an Atomic Absorption Spectrophotometer instrument, a suitable sodium lamp, a film projector and a chart recorder.

The real time component from the data was converted into a dimensionless form, and the concentration component was converted into the 'E - function'. The conversion of the experimental data is described in Chapter 5. The converted data were used in the computer program, and simulation exercises were carried out, until the model response gave a close enough fit to the experimental response. The programs for the normalisation of the experimental data and the model for the RTD are illustrated in Appendix C.

The parameters obtained for the interconnected zones and streams of the RTD model, the variance between the experimental and model response data are summarised in

Tables 6.1 - 6.13. The actual tabulation of the experimental data and model response data is also shown in Appendix B. Finally the graphs of the model and experimental response data are shown in Figures 6.1 - 6.54.

6.3 ANALYSIS OF THE RTD MODEL RESPONSE

Table 6.Ø illustrates the graphs of the RTD model, and Figures 6.1 - 6.54 represent the graphs of Ø.55 x $1Ø^{-3}m^3$ nozzle vessels respectively.

TABLE 6.Ø: FIGURES FOR RTD MODEL RESPONSE

TRACER INJECTION	RTD MODEL FIG. CODE	EXPERIMENTAL RUN CODE	NOZZLE VESSEL SIZE: $1Ø^{-3}M^3$
At Inlet	6.1- 6.9	F91- F99	Ø.55
" "	6.1Ø-6.18	F31- F39	1.52
" "	6.19-6.34	F81- F816	5.13
"the top	6.35-6.45	F11-F111	Ø.55
" "Bottom	6.46-6.54	F21- F29	Ø.55

EXPERIMENTAL DATA	A	B	J	K	M	N	L	STANDARD DEVIATION
RES91	.670	.330	.901	.052	.001	.000	0	.0017
RES92	.580	.420	.720	.057	.001	.000	0	.0019
RES93	.580	.420	.840	.054	.001	.000	0	.0013
RES94	.640	.360	.150	.044	.001	.000	0	.0028
RES95	.630	.370	.100	.035	.001	.000	0	.0037

TABLE 6.1 : MODEL RESULTS - USING COLOURED FILM - CODE F9

EXPERIMENTAL DATA	A	B	J	K	M	N	L	STANDARD DEVIATION
RES96	.640	.360	.200	.010	.001	.000	0	.0023
RES97	.640	.360	.300	.020	.001	.000	0	.0041
RES98	.450	.550	.350	.020	.001	.000	0	.0012
RES99	.550	.450	.200	.020	.001	.000	0	.0017

TABLE 6.2 : MODEL RESULTS - USING COLOURED FILM - CODE F9

EXPERIMENTAL DATA	A	B	J	K	M	N	L	STANDARD DEVIATION
RES31	.560	.440	.010	.350	.010	.000	0	.0033
RES32	.550	.450	.010	.270	.010	.000	0	.0093
RES33	.560	.440	.010	.200	.010	.000	0	.0071
RES34	.260	.740	.058	.010	.020	.000	0	.0059
RES35	.260	.740	.062	.010	.060	.000	0	.0130

TABLE 6.3 : MODEL RESULTS - USING COLOURED FILM - CODE F3

EXPERIMENTAL DATA	A	B	J	K	M	N	L	STANDARD DEVIATION
RES36	.260	.740	.060	.010	.010	.000	0	.0059
RES37	.260	.740	.065	.010	.010	.000	0	.0071
RES38	.260	.740	.060	.010	.016	.000	0	.0106
RES39	.260	.740	.086	.010	.017	.000	0	.0039

TABLE 6.4 : MODEL RESULTS - USING COLOURED FILM - CODE F3

EXPERIMENTAL DATA	A	B	J	K	M	N	L	STANDARD DEVIATION
RES81	.740	.260	.600	.055	.001	.000	0	.0196
RES82	.700	.300	.059	.045	.001	.000	0	.0261
RES83	.700	.300	.056	.050	.001	.000	0	.0270
RES84	.690	.310	.600	.050	.001	.000	0	.0031
RES85	.590	.410	.063	.035	.001	.000	0	.0063

TABLE 6.5 : MODEL RESULTS - USING COLOURED FILM - CODE F8

EXPERIMENTAL DATA	A	B	J	K	M	N	L	STANDARD DEVIATION
RES86	.590	.410	.060	.025	.001	.000	0	.0072
RES87	.590	.410	.057	.030	.001	.000	0	.0078
RES88	.370	.630	.045	.044	.001	.000	0	.0039
RES89	.360	.640	.041	.044	.001	.000	0	.0102

TABLE 6.6 : MODEL RESULTS - USING COLOURED FILM - CODE F8

EXPERIMENTAL DATA	A	B	J	K	M	N	L	STANDARD DEVIATION
RES810	.365	.635	.055	.030	.001	.000	0	.0131
RES811	.350	.650	.040	.050	.001	.000	0	.0206
RES812	.380	.620	.040	.035	.001	.000	0	.0048
RES813	.380	.620	.050	.030	.001	.000	0	.0046
RES814	.380	.620	.052	.030	.001	.000	0	.0059

TABLE 6.7 : MODEL RESULTS - USING COLOURED FILM - CODE F8

EXPERIMENTAL DATA	A	B	J	K	M	N	L	STANDARD DEVIATION
RES815	.390	.610	.034	.025	.001	.000	0	.0109
RES816	.380	.620	.050	.020	.001	.000	0	.0047

TABLE 6.8 : MODEL RESULTS - USING COLOURED FILM - CODE F8

EXPERIMENTAL DATA	A	B	J	K	M	N	L	STANDARD DEVIATION
RES11	.560	.440	.840	.080	.050	.000	0	.0144
RES12	.550	.450	.400	.085	.010	.000	0	.0270
RES13	.560	.440	.500	.079	.025	.000	0	.0206
RES14	.250	.750	.480	.080	.030	.000	0	.0042
RES15	.250	.750	.440	.040	.044	.000	0	.0074

TABLE 6.9 : MODEL RESULTS - USING COLOURED FILM - CODE F1

EXPERIMENTAL DATA	A	B	J	K	M	N	L	STANDARD DEVIATION
RES16	.260	.740	.400	.044	.040	.000	0	.0018
RES17	.720	.280	.630	.044	.300	.000	0	.0115
RES18	.850	.150	.910	.035	.030	.000	0	.0047
RES19	.010	.990	.150	.060	.060	.000	0	.0028

TABLE 6.10 : MODEL RESULTS - USING COLOURED FILM - CODE F1

EXPERIMENTAL DATA	A	B	J	K	M	N	L	STANDARD DEVIATION
RES110	.890	.110	.930	.045	.010	.000	0	.0093
RES111	.910	.090	.925	.050	.010	.000	0	.0041

TABLE 6.11 : MODEL RESULTS - USING COLOURED FILM - CODE F1

EXPERIMENTAL DATA	A	B	J	K	M	N	L	STANDARD DEVIATION
RES21	.560	.440	.010	.270	.010	.000	0	.0027
RES22	.560	.440	.150	.059	.010	.000	0	.0025
RES23	.560	.440	.100	.069	.010	.000	0	.0025
RES24	.260	.740	.480	.010	.010	.000	0	.0027
RES25	.260	.740	.450	.034	.010	.000	0	.0019

TABLE 6.12 : MODEL RESULTS - USING COLOURED FILM - CODE F2

EXPERIMENTAL DATA	A	B	J	K	M	N	L	STANDARD DEVIATION
RES26	.260	.740	.360	.050	.010	.000	0	.0015
RES27	.270	.730	.490	.047	.010	.000	0	.0063
RES28	.260	.740	.350	.045	.010	.000	0	.0020
RES29	.260	.740	.500	.050	.010	.000	0	.0020

TABLE 6.13 : MODEL RESULTS - USING COLOURED FILM - CODE F2

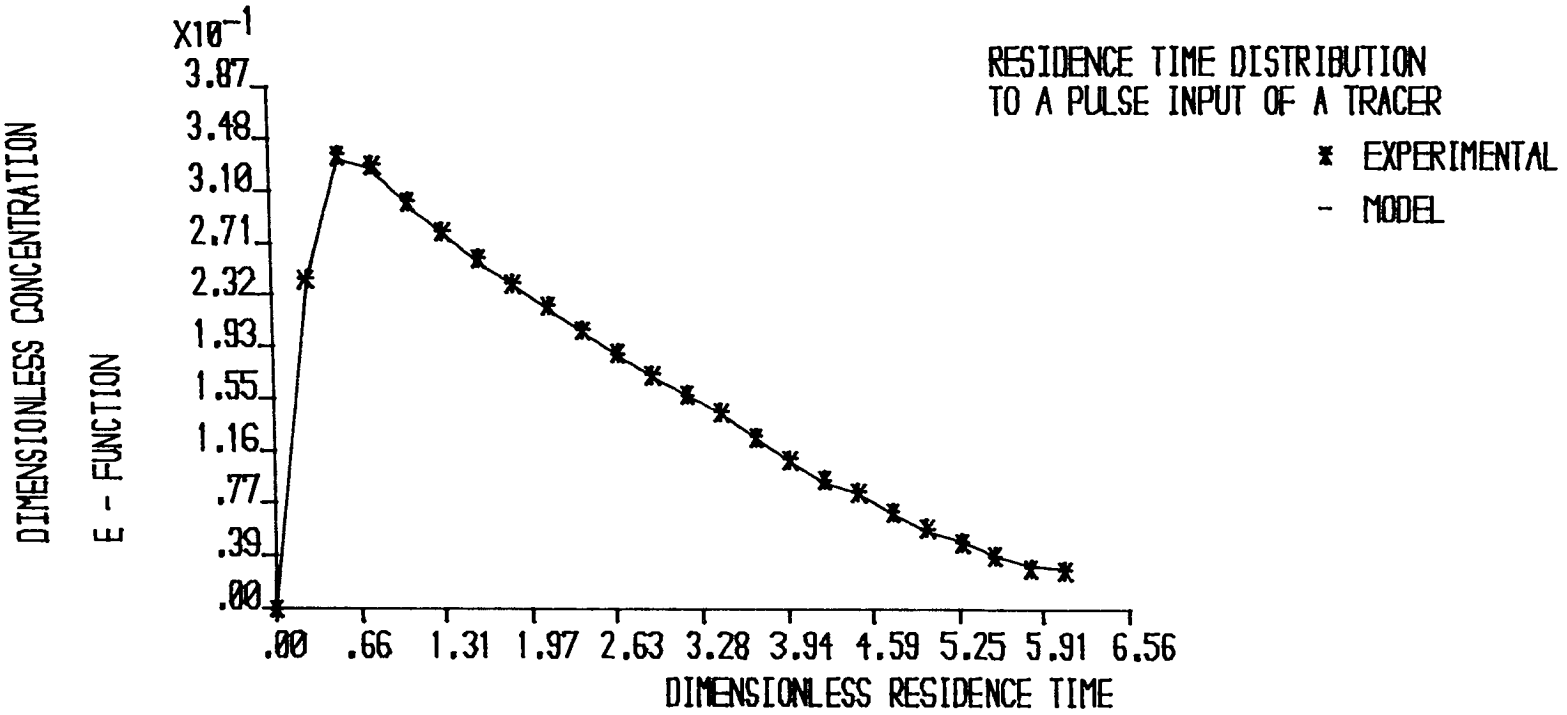

FIGURE 6.1 :RESIDENCE TIME DISTRIBUTION - RUN CODE F91

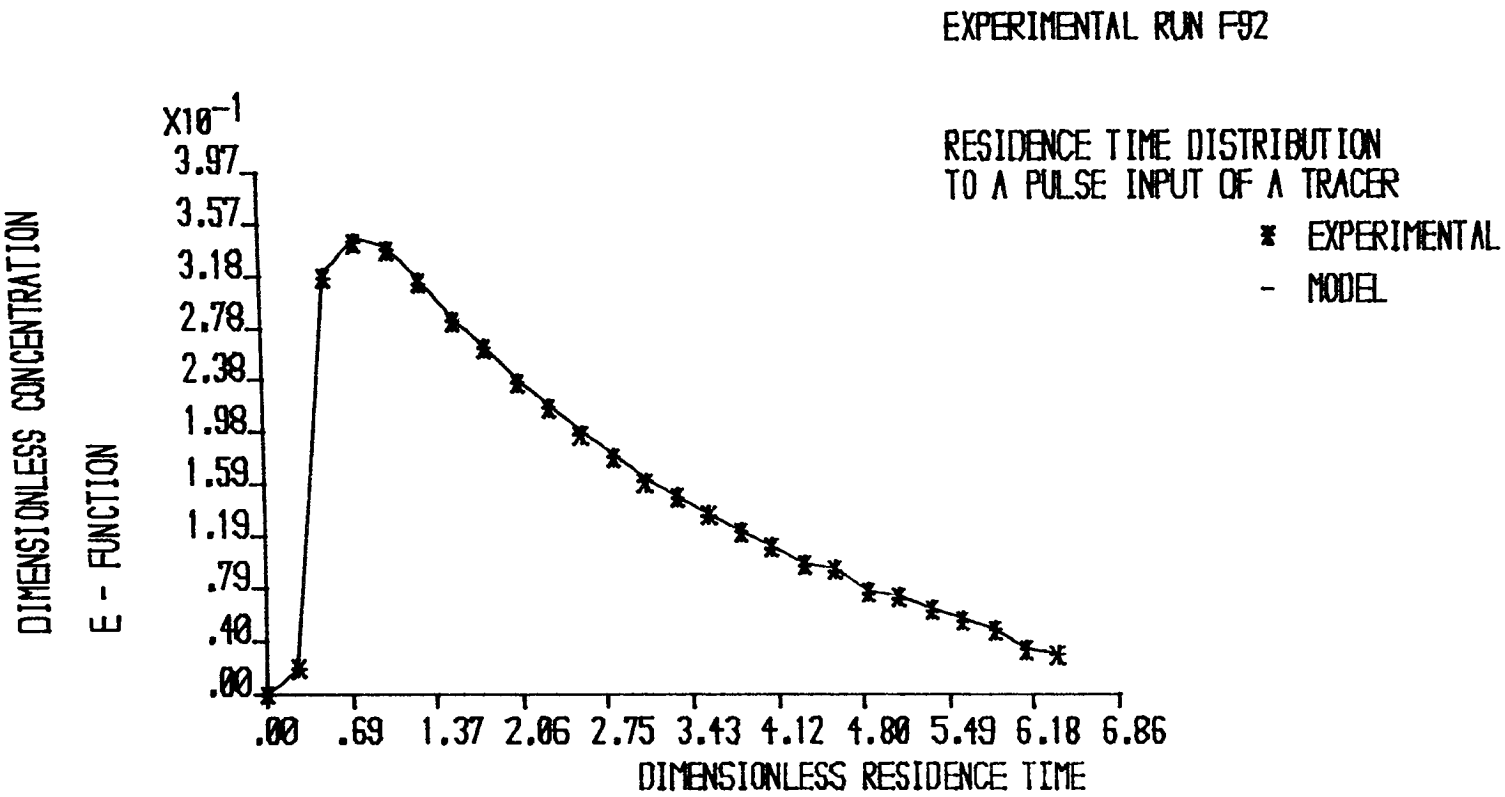

FIGURE 6.2 :RESIDENCE TIME DISTRIBUTION - RUN CODE F92

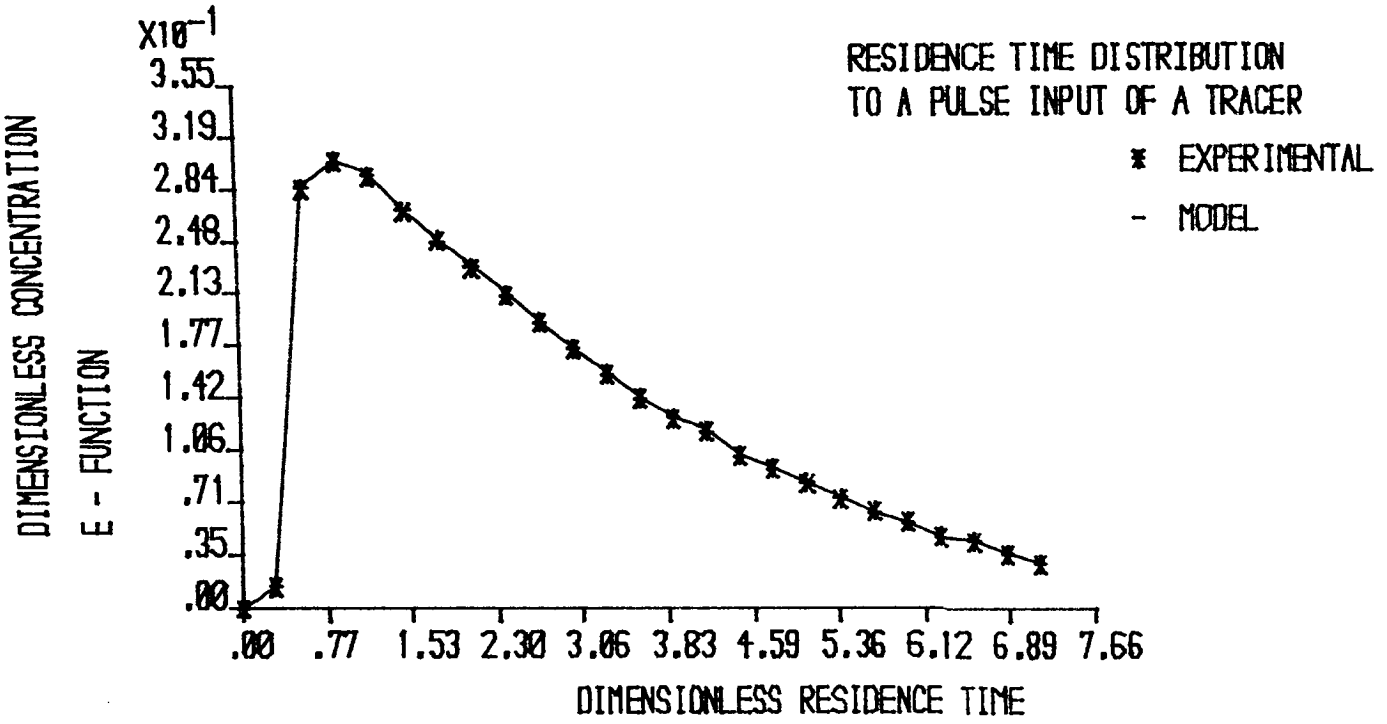

FIGURE 6.3 :RESIDENCE TIME DISTRIBUTION - RUN CODE F93

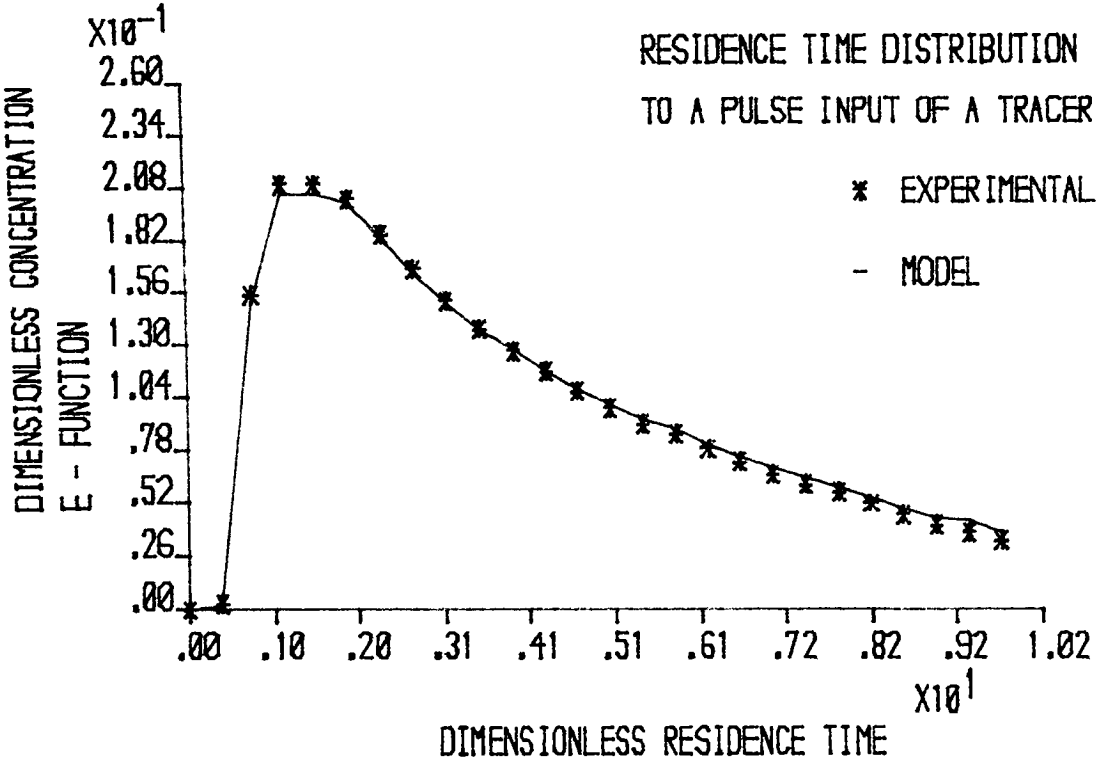

FIGURE 6.4 :RESIDENCE TIME DISTRIBUTION - RUN CODE F94

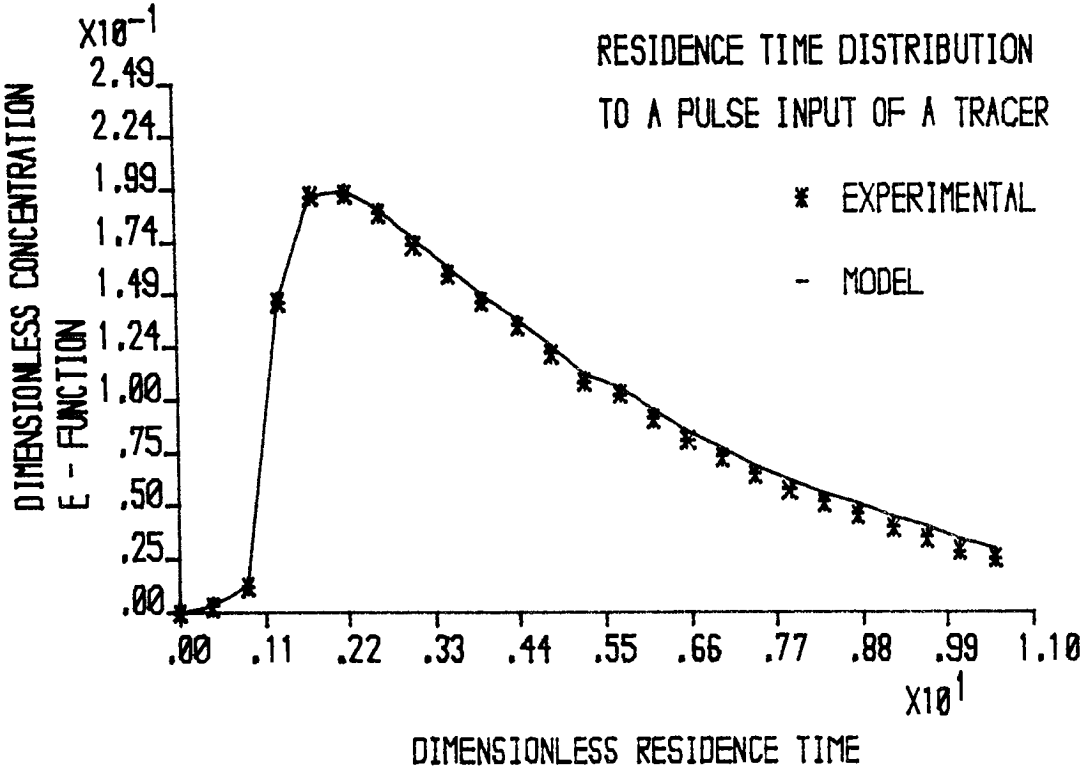

FIGURE 6.5 :RESIDENCE TIME DISTRIBUTION - RUN CODE F95

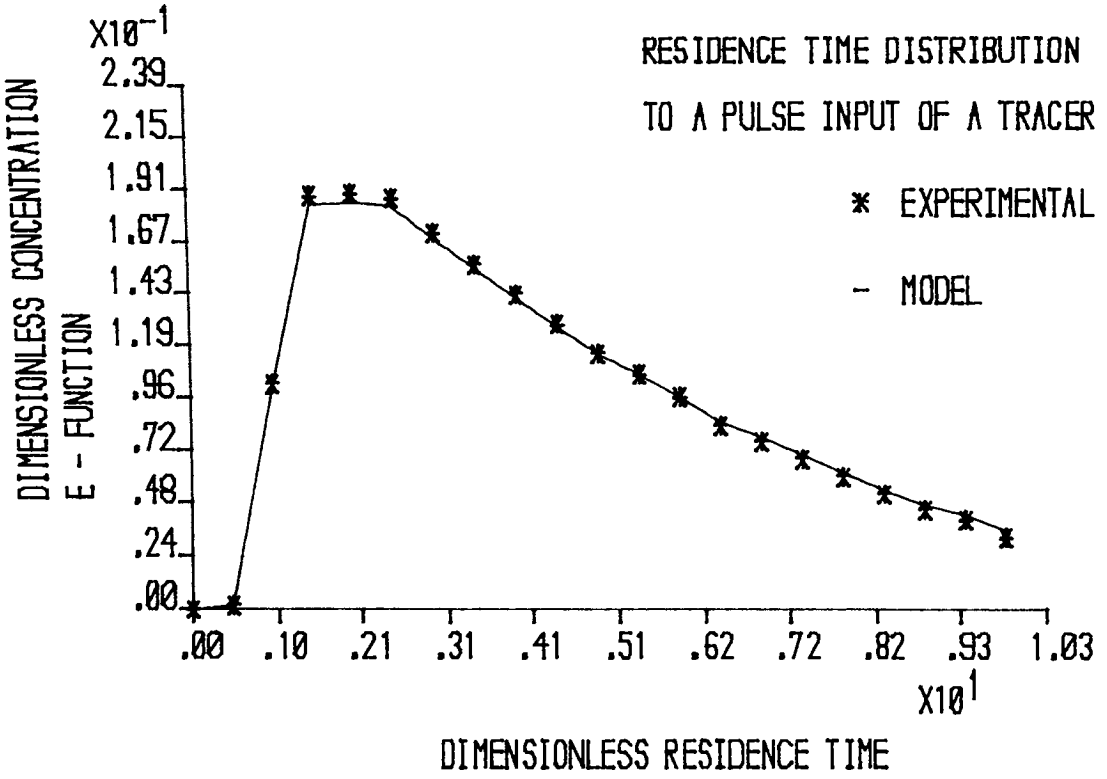

FIGURE 6.6 :RESIDENCE TIME DISTRIBUTION - RUN CODE F96

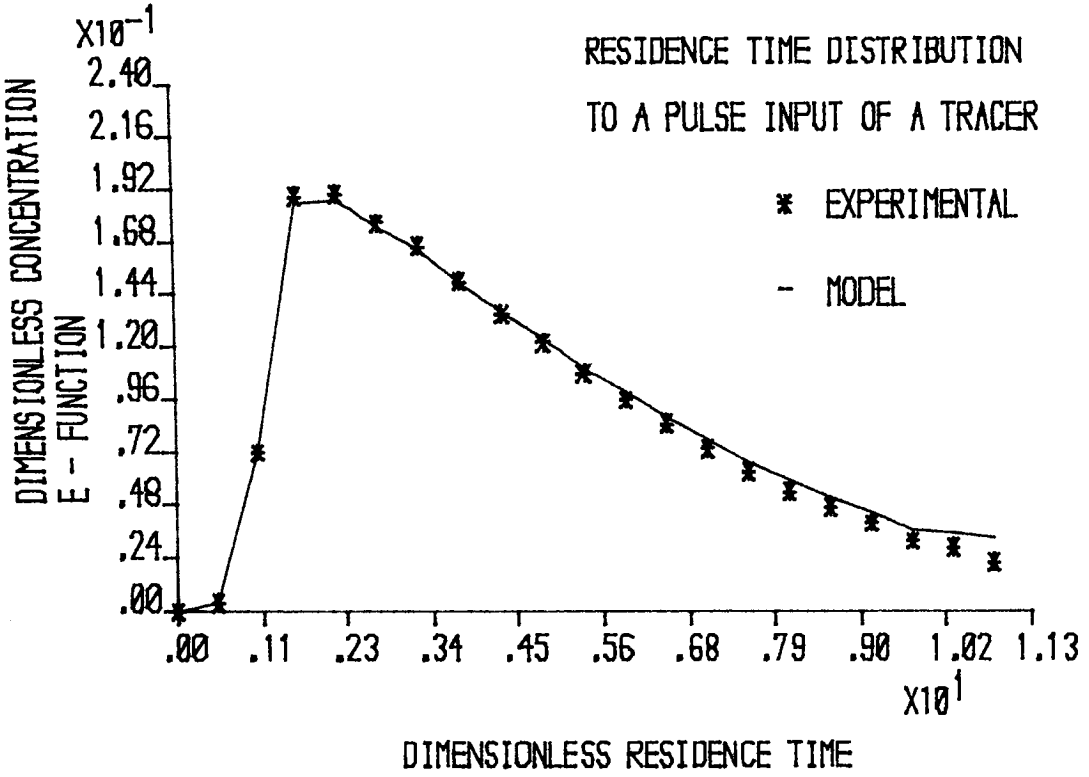

FIGURE 6.7 :RESIDENCE TIME DISTRIBUTION - RUN CODE F97

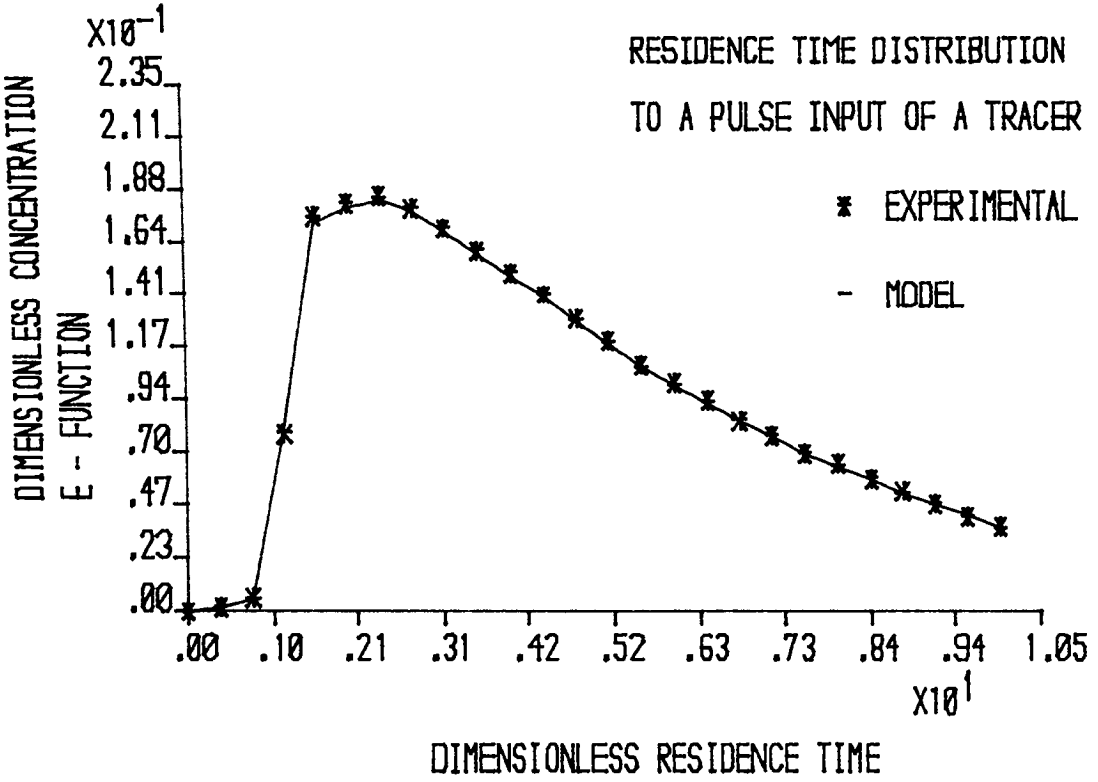

FIGURE 6.8 :RESIDENCE TIME DISTRIBUTION - RUN CODE F98

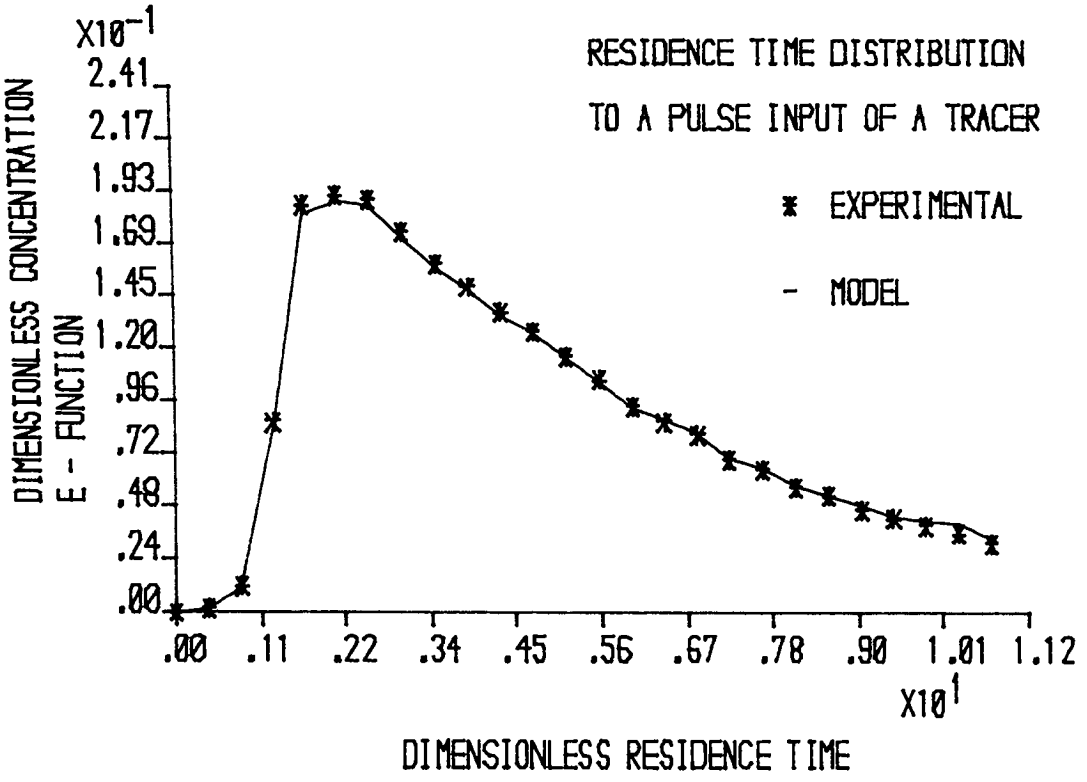

FIGURE 6.9 :RESIDENCE TIME DISTRIBUTION - RUN CODE F99

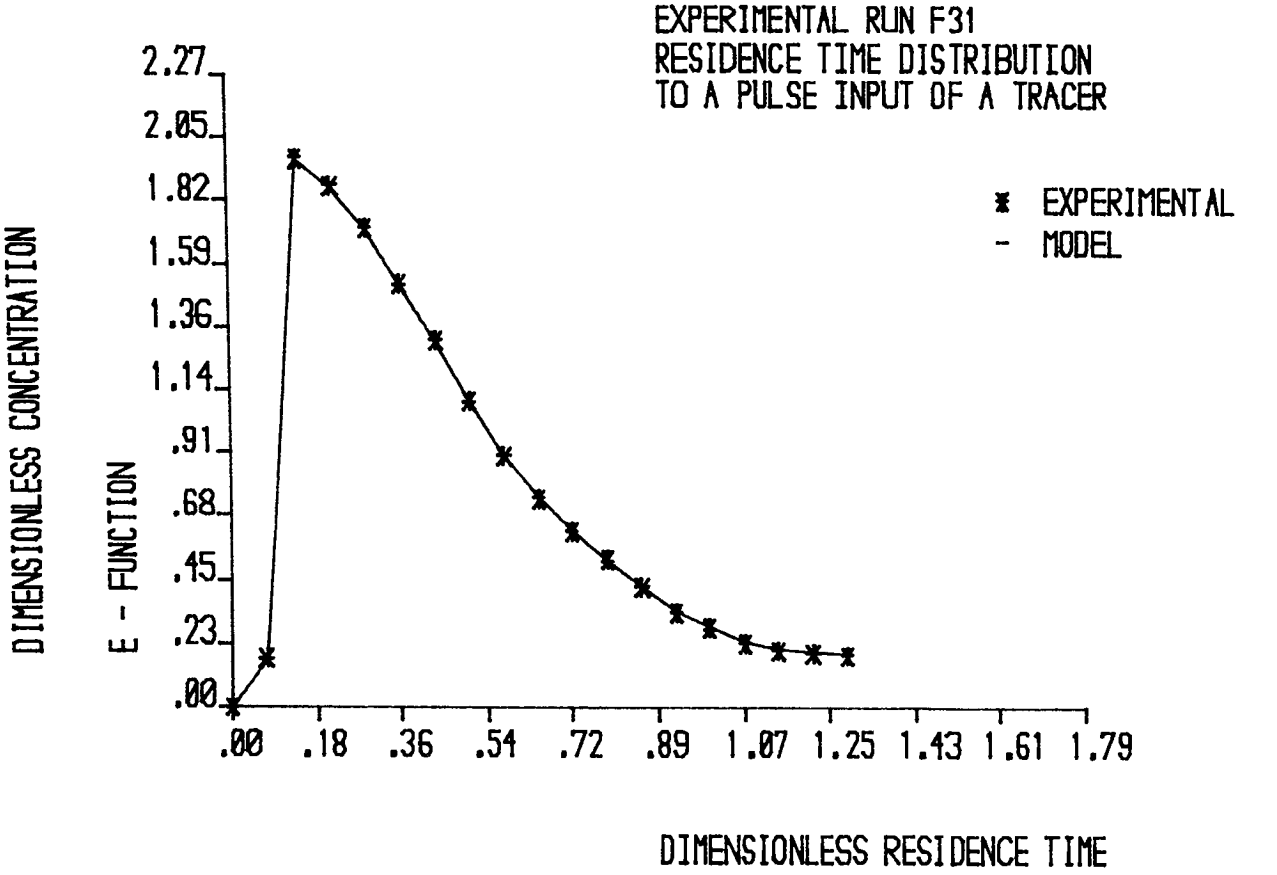

FIGURE 6.10 :RESIDENCE TIME DISTRIBUTION - RUN CODE F31

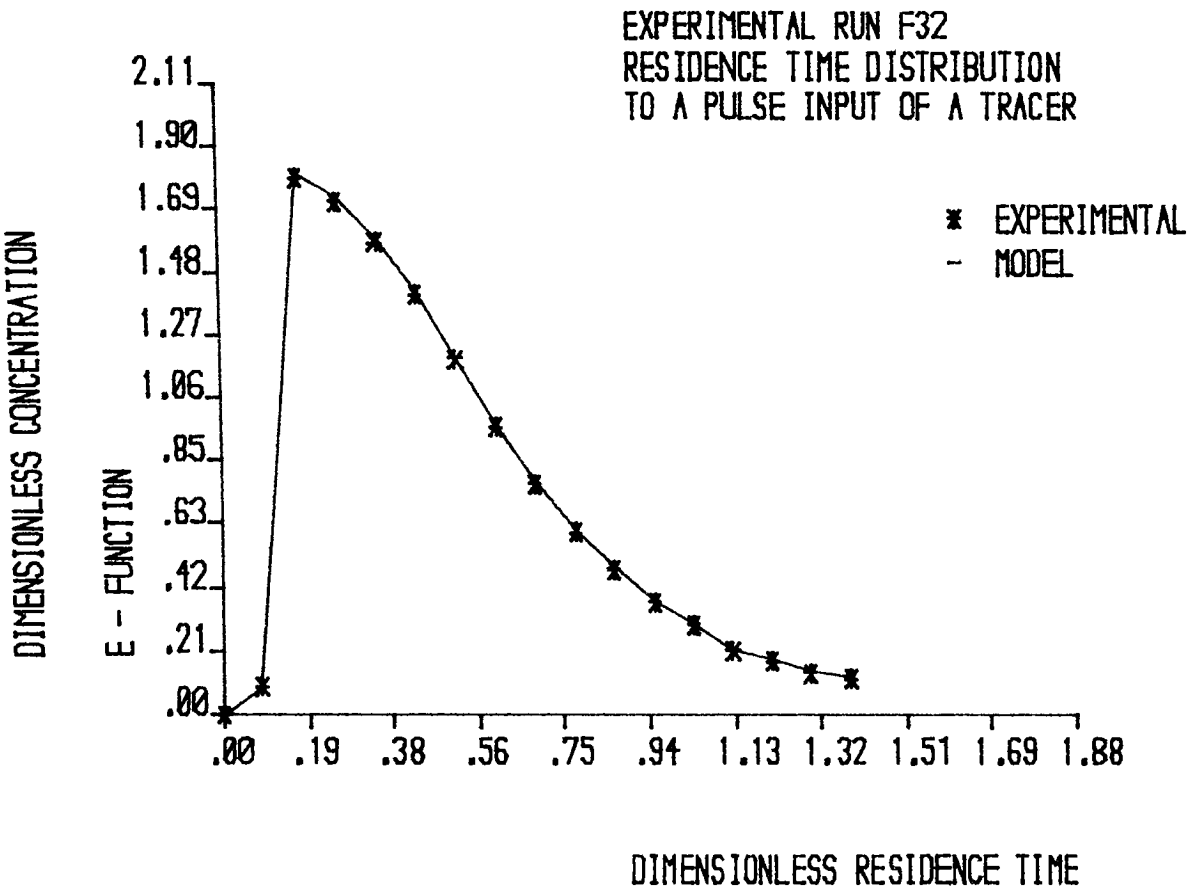

FIGURE 6.11 :RESIDENCE TIME DISTRIBUTION - RUN CODE F32

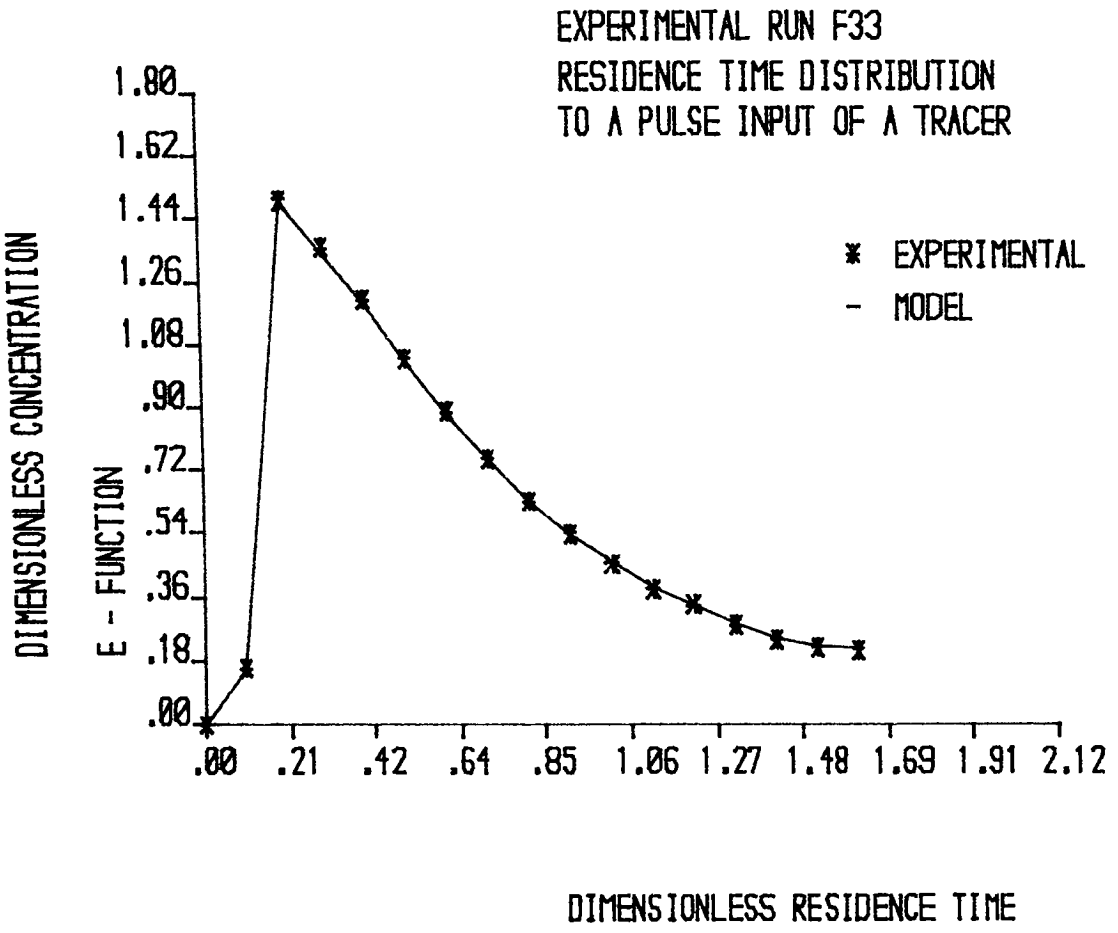

FIGURE 6.12 :RESIDENCE TIME DISTRIBUTION - RUN CODE F33

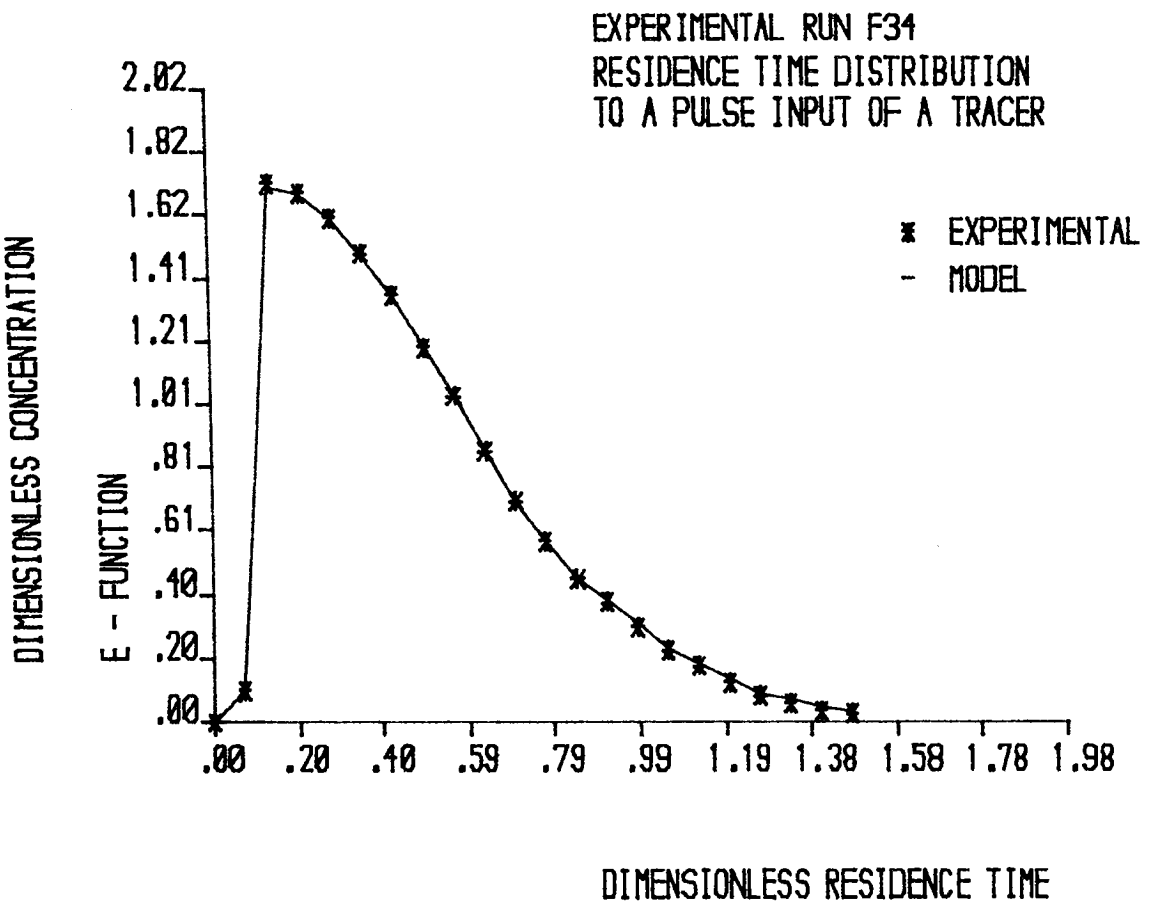

FIGURE 6.13 :RESIDENCE TIME DISTRIBUTION - RUN CODE F34

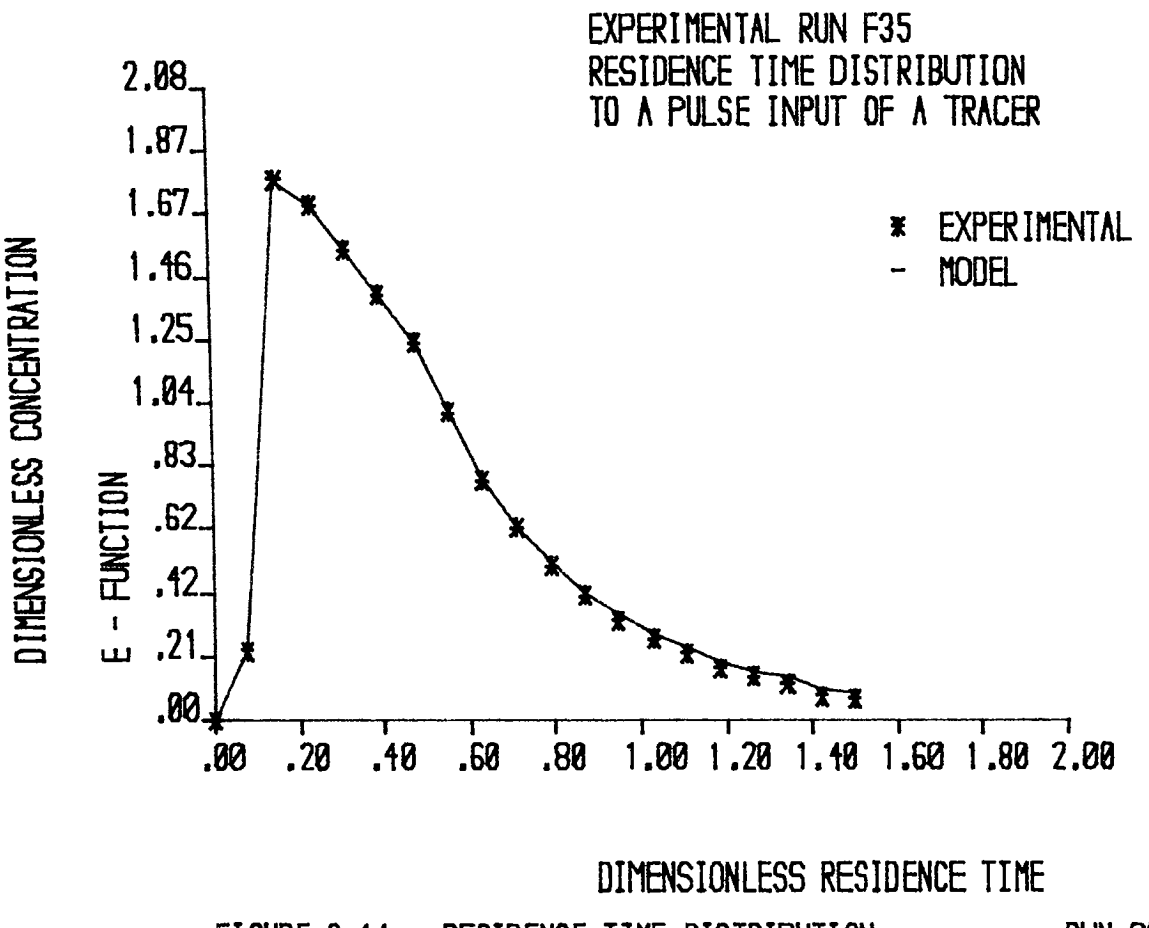

FIGURE 6.14 :RESIDENCE TIME DISTRIBUTION - RUN CODE F35

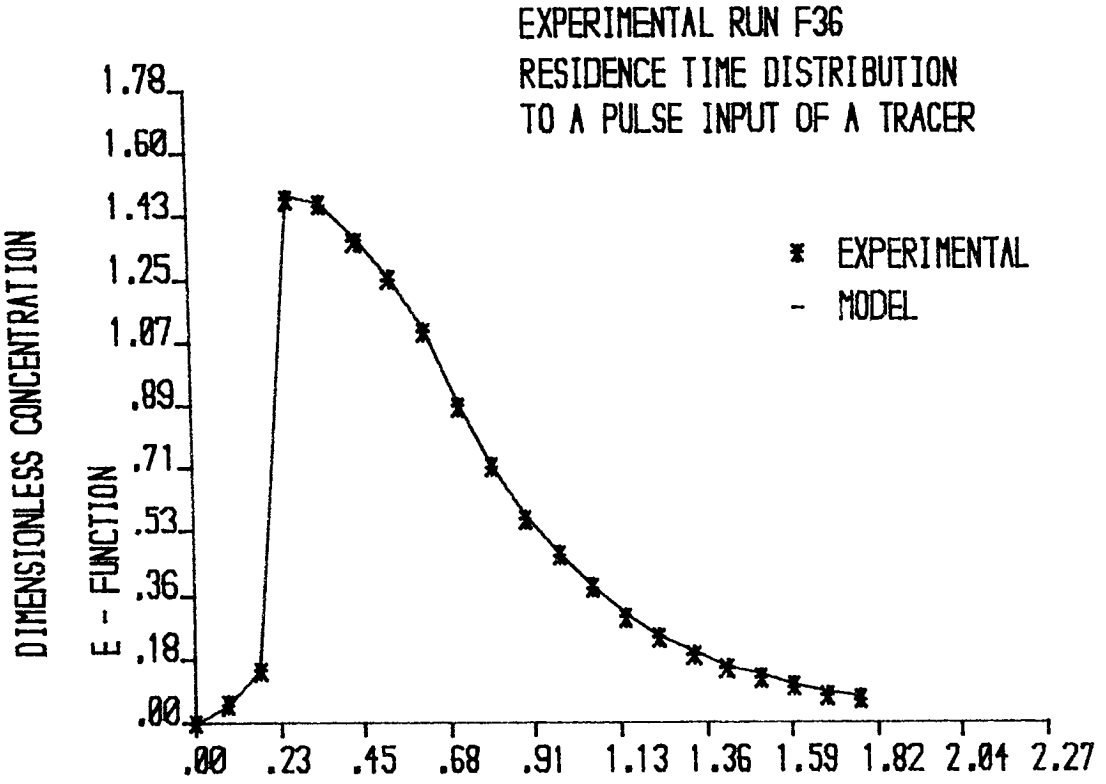

FIGURE 6.15 :RESIDENCE TIME DISTRIBUTION - RUN CODE F36

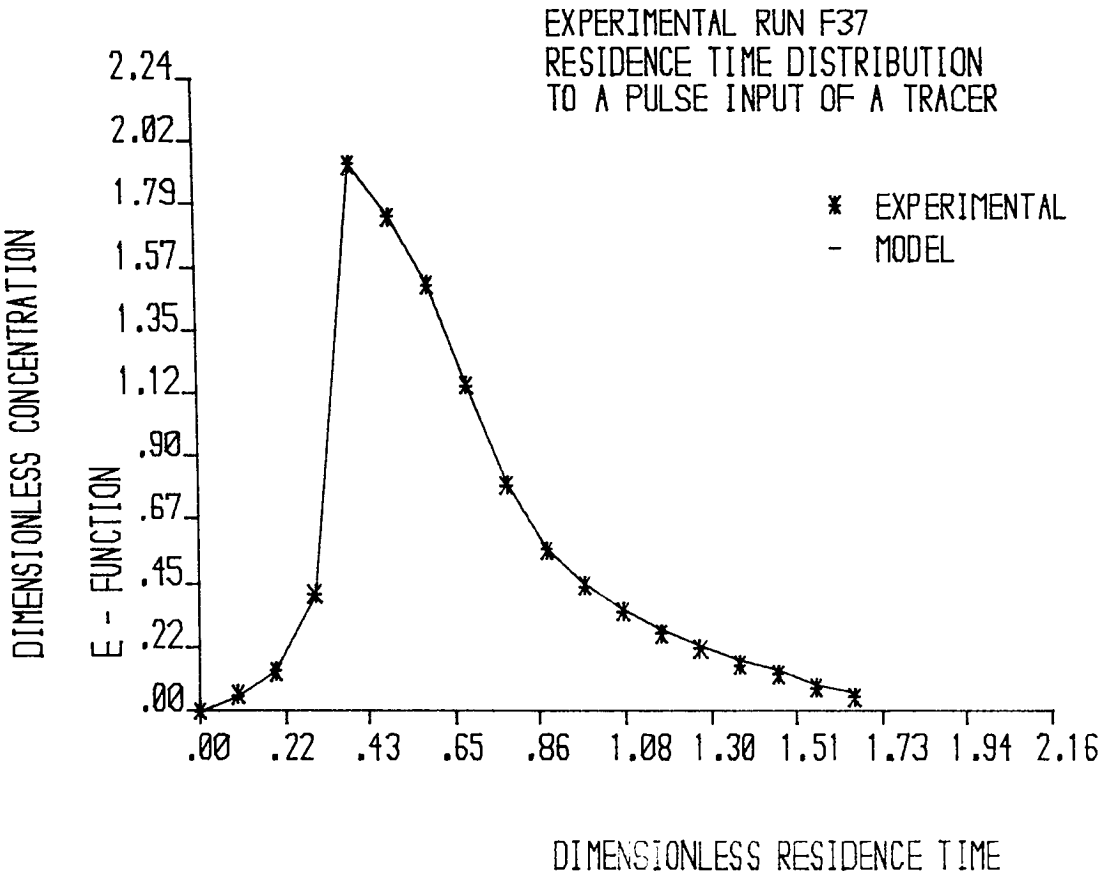

FIGURE 6.16 :RESIDENCE TIME DISTRIBUTION - RUN CODE F37

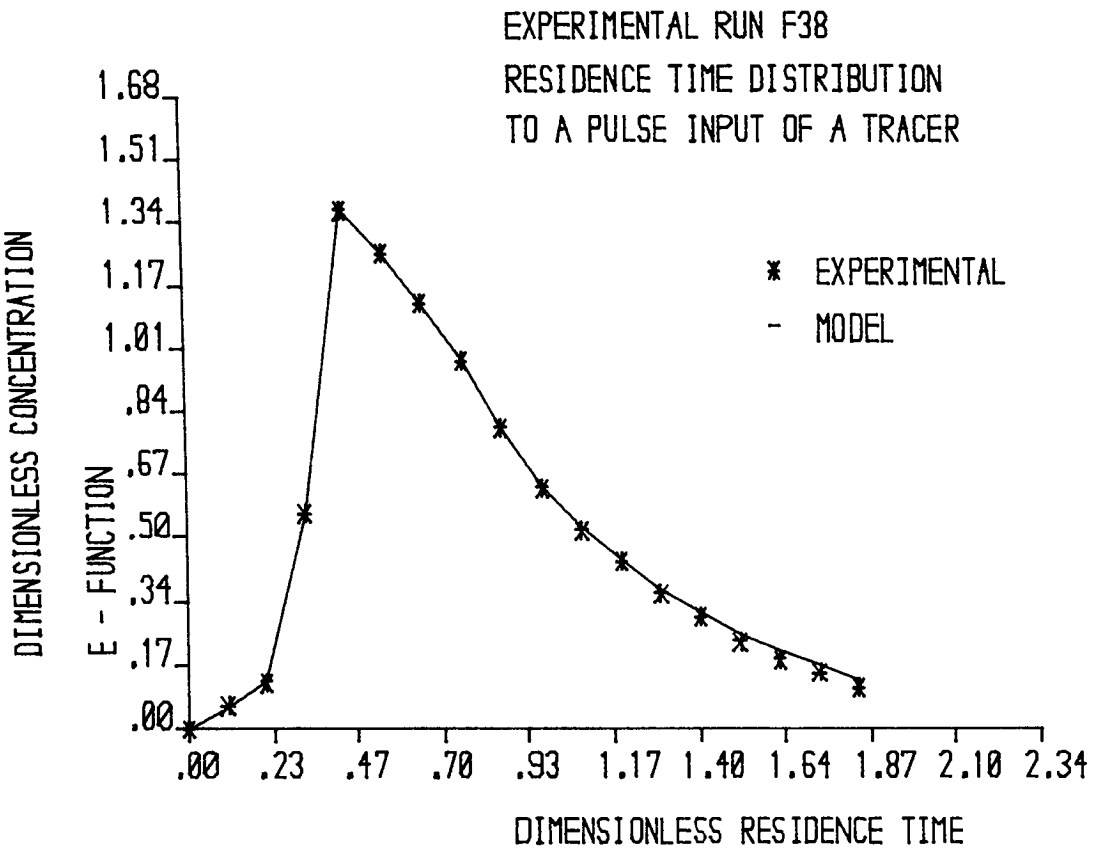

FIGURE 6.17 :RESIDENCE TIME DISTRIBUTION - RUN CODE F38

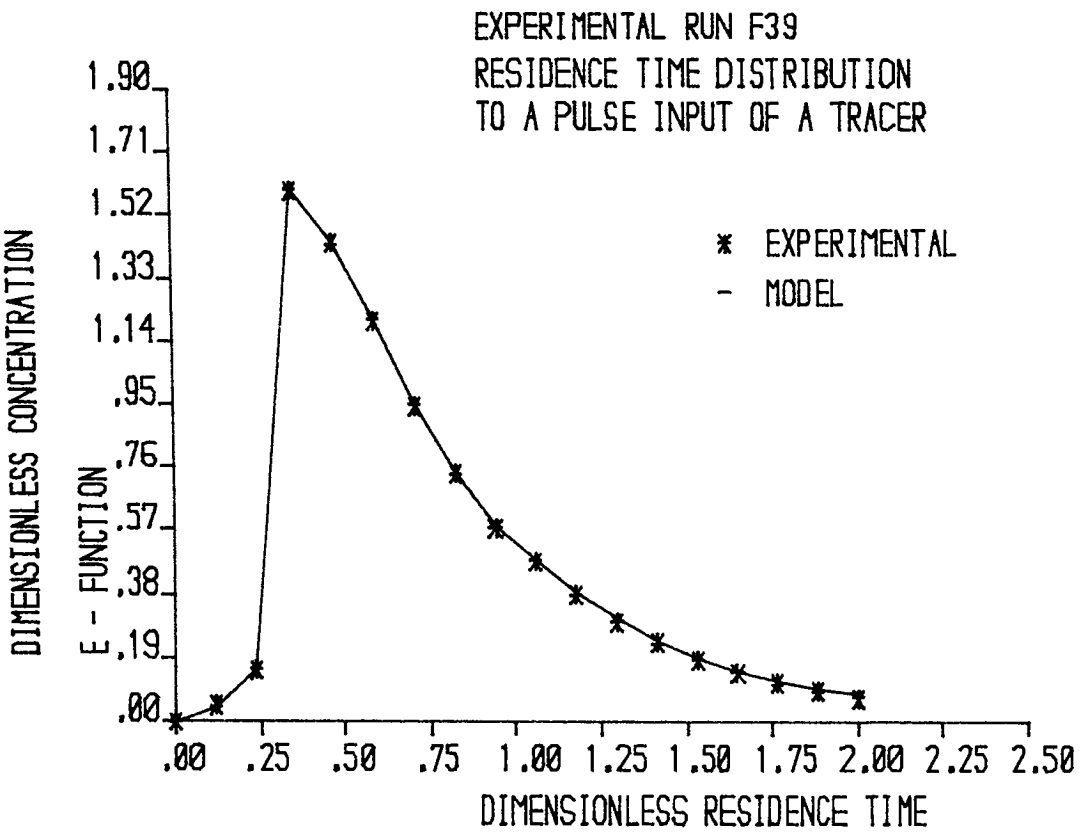

FIGURE 6.18 :RESIDENCE TIME DISTRIBUTION - RUN CODE F39

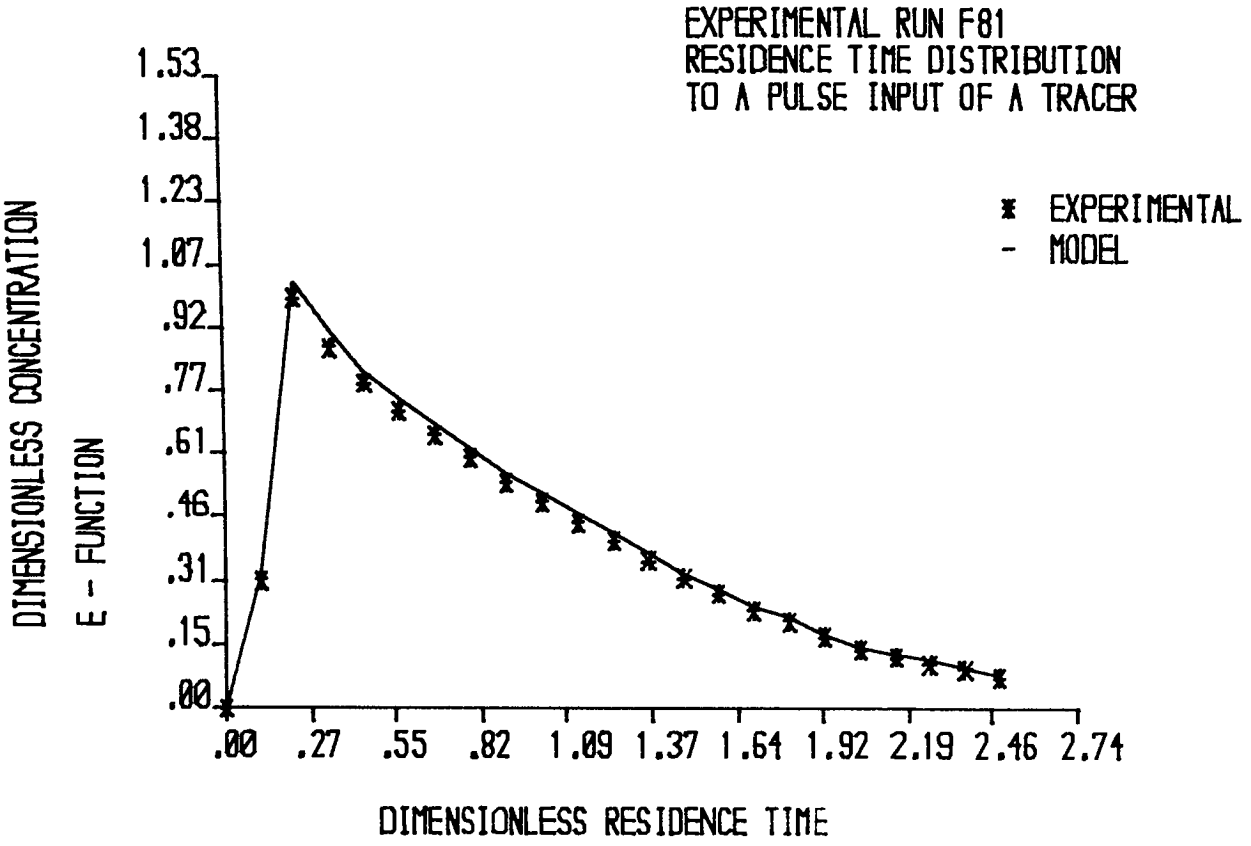

FIGURE 6.19 :RESIDENCE TIME DISTRIBUTION - RUN CODE F81

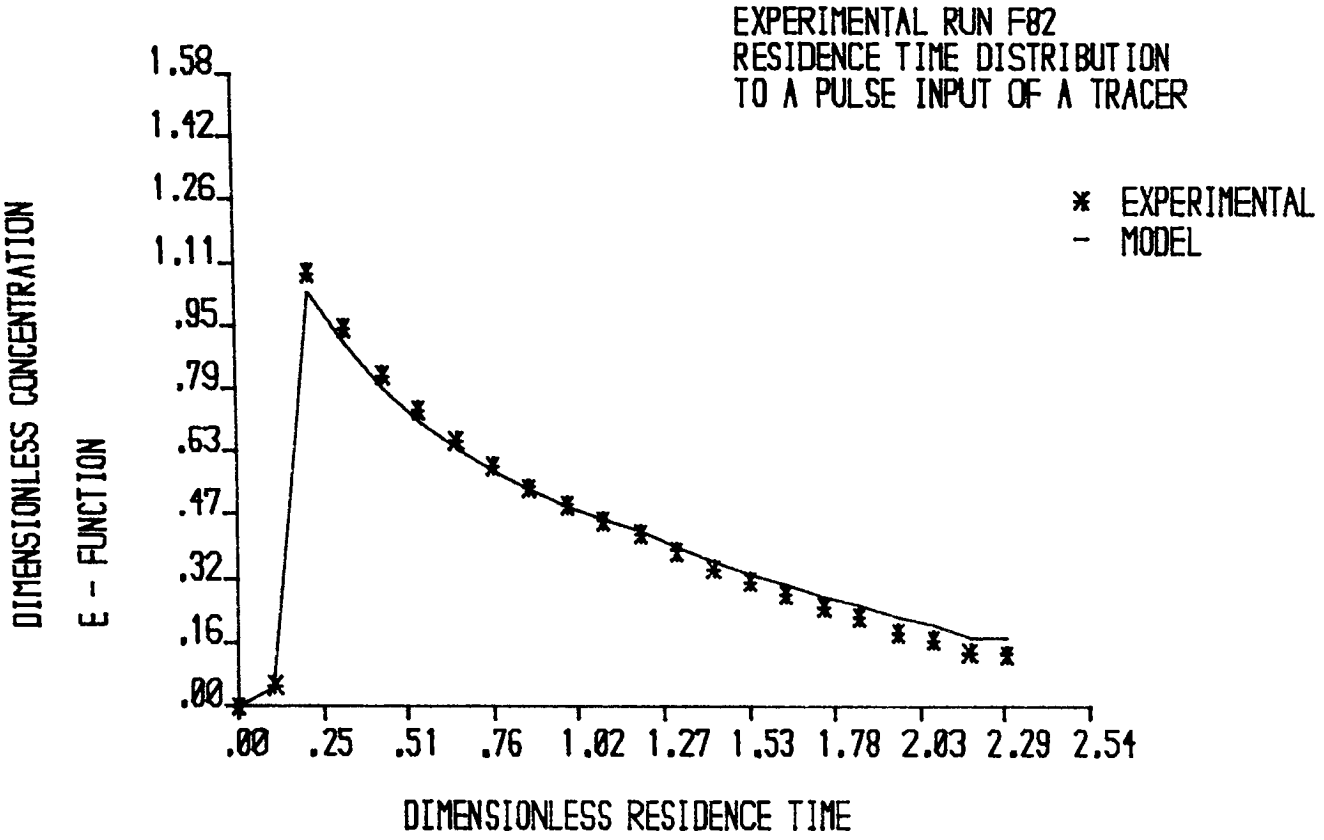

FIGURE 6.20 :RESIDENCE TIME DISTRIBUTION - RUN CODE F82

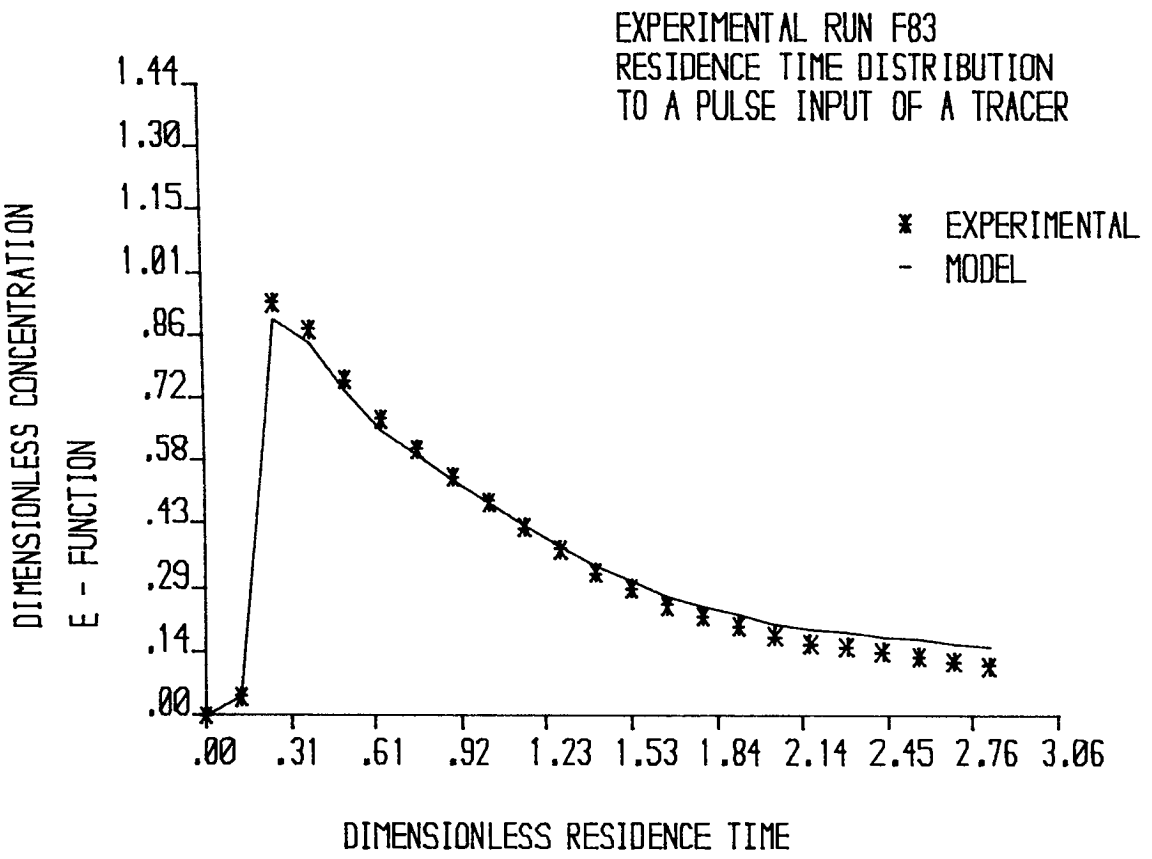

FIGURE 6.21 :RESIDENCE TIME DISTRIBUTION - RUN CODE F83

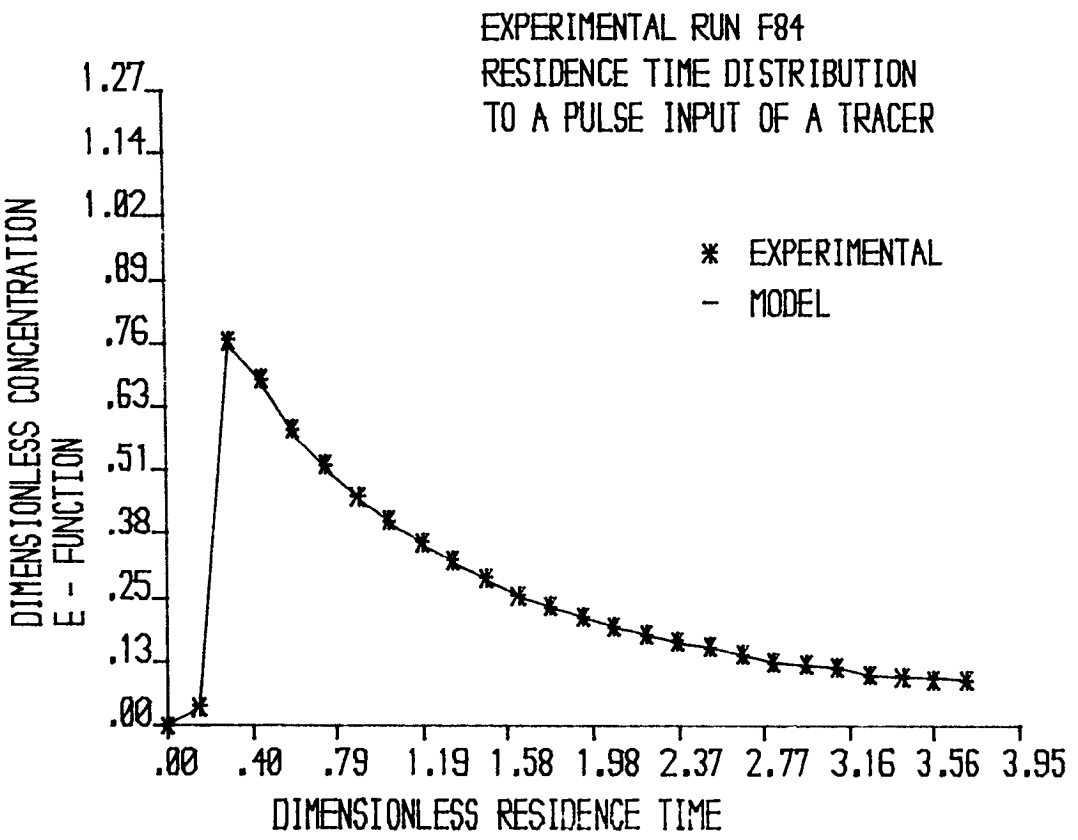

FIGURE 6.22 :RESIDENCE TIME DISTRIBUTION - RUN CODE F84

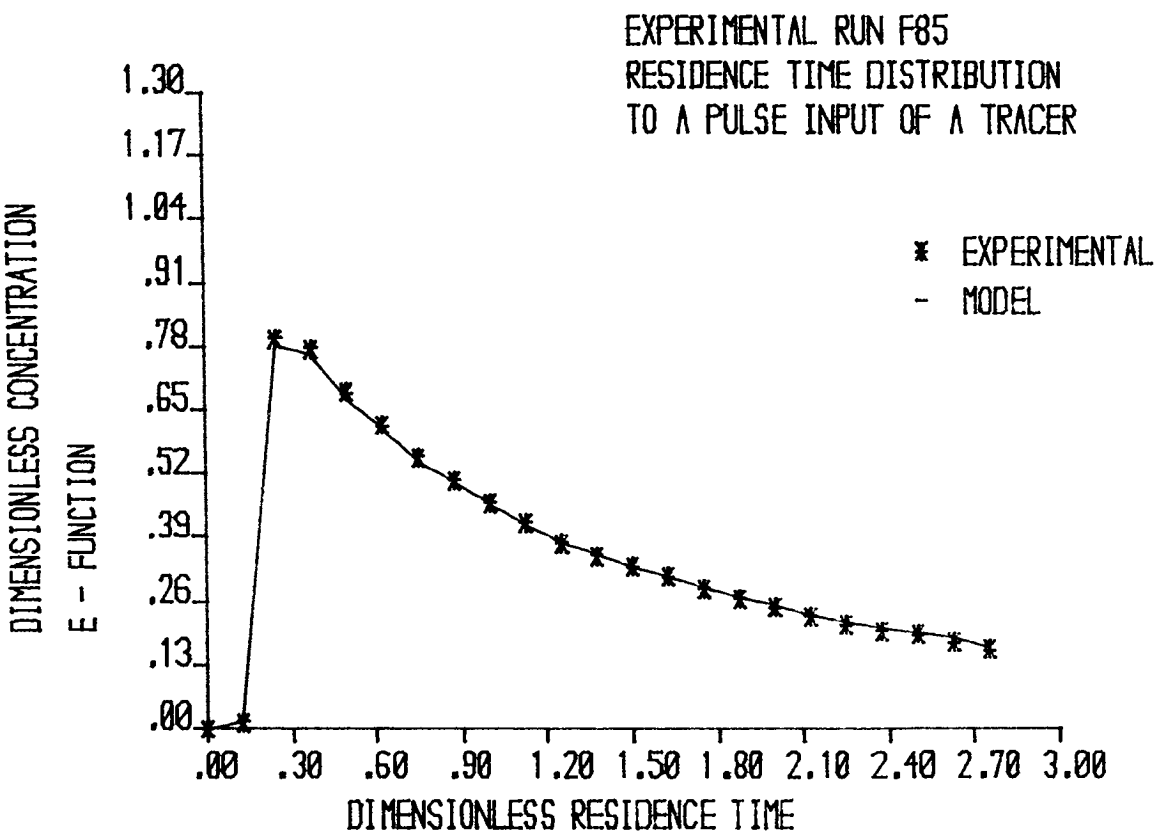

FIGURE 6.23 :RESIDENCE TIME DISTRIBUTION - RUN CODE F85

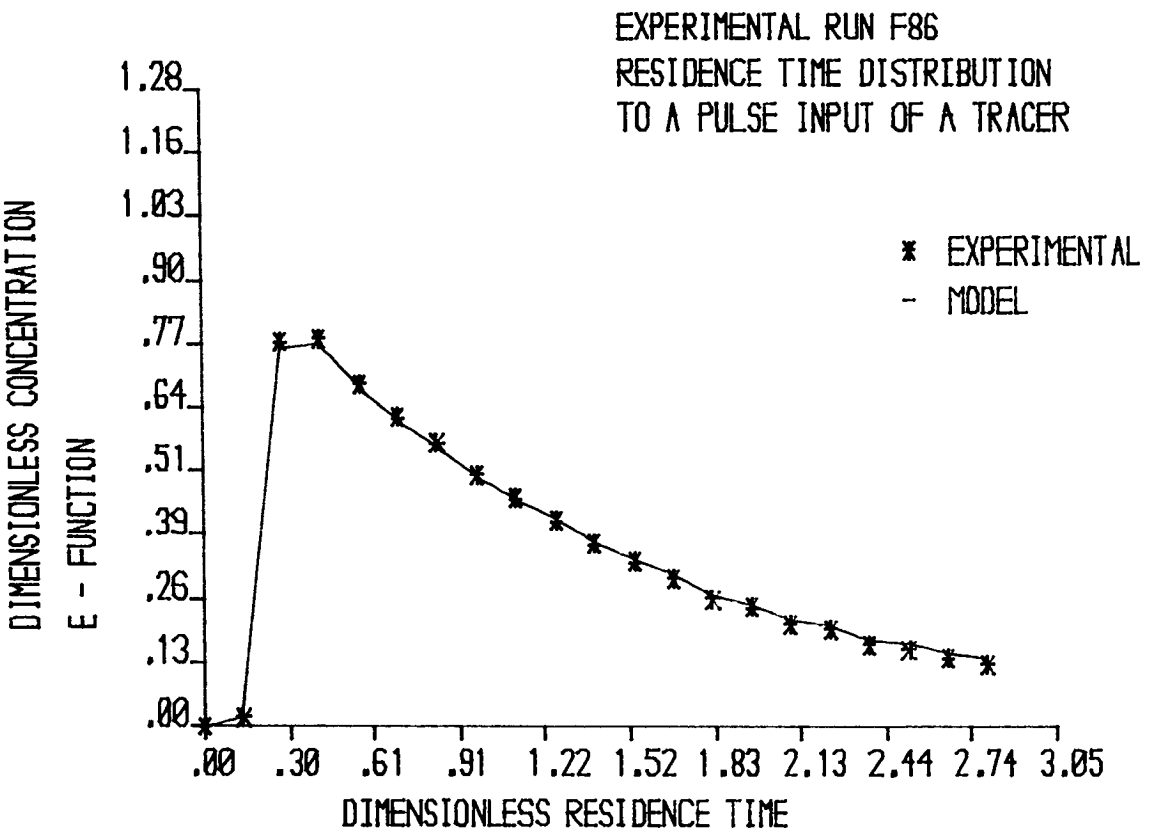

FIGURE 6.24 :RESIDENCE TIME DISTRIBUTION - RUN CODE F86

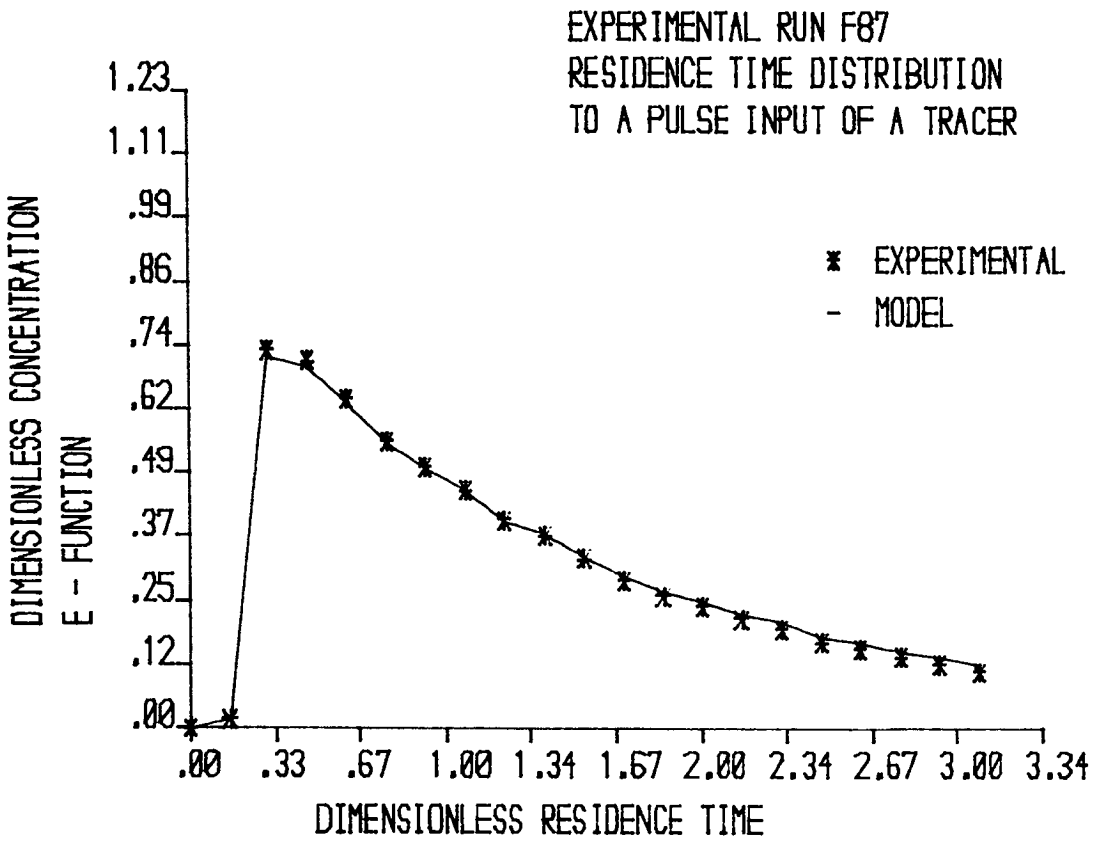

FIGURE 6.25 :RESIDENCE TIME DISTRIBUTION - RUN CODE F87

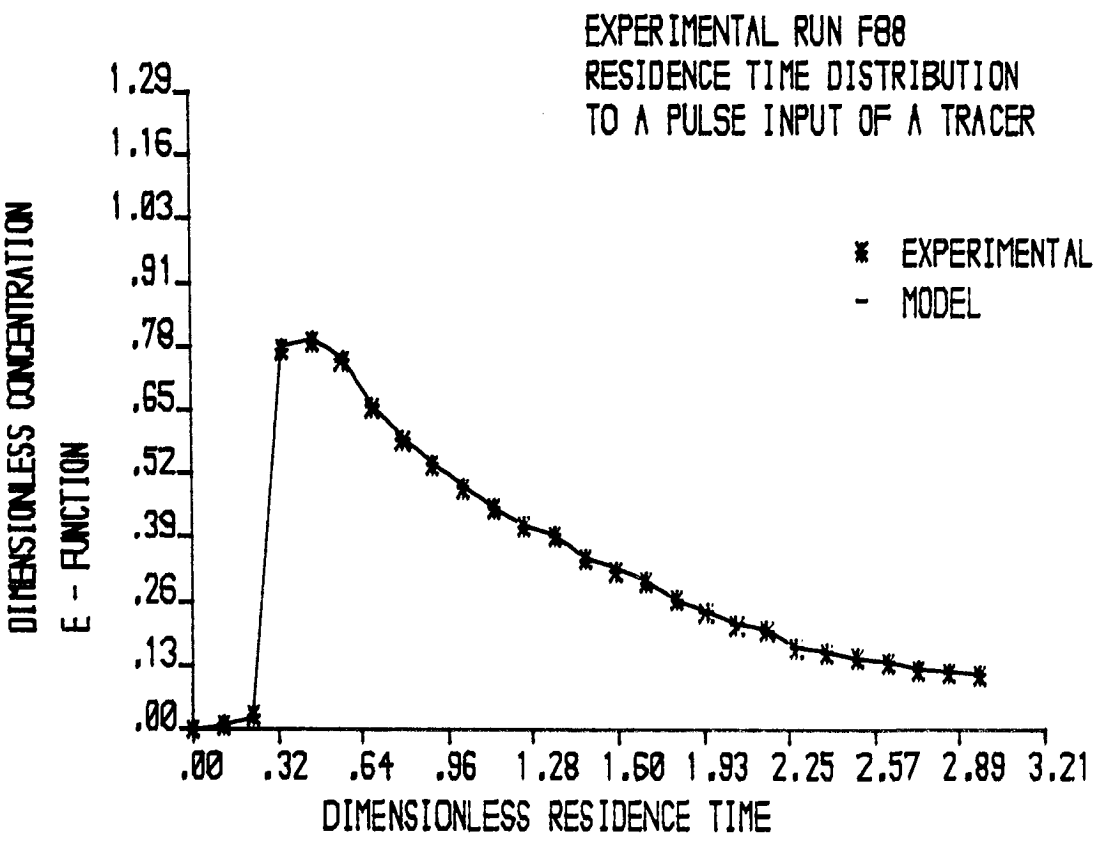

FIGURE 6.26 :RESIDENCE TIME DISTRIBUTION - RUN CODE F88

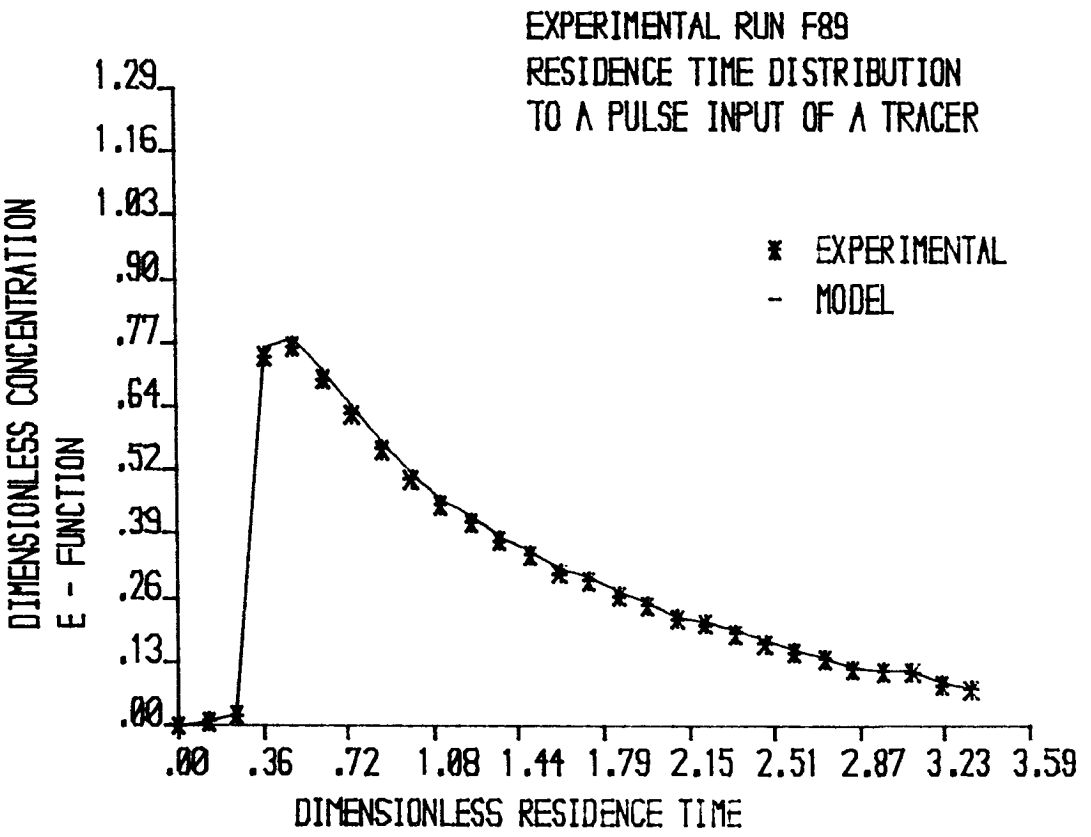

FIGURE 6.27 :RESIDENCE TIME DISTRIBUTION - RUN CODE F89

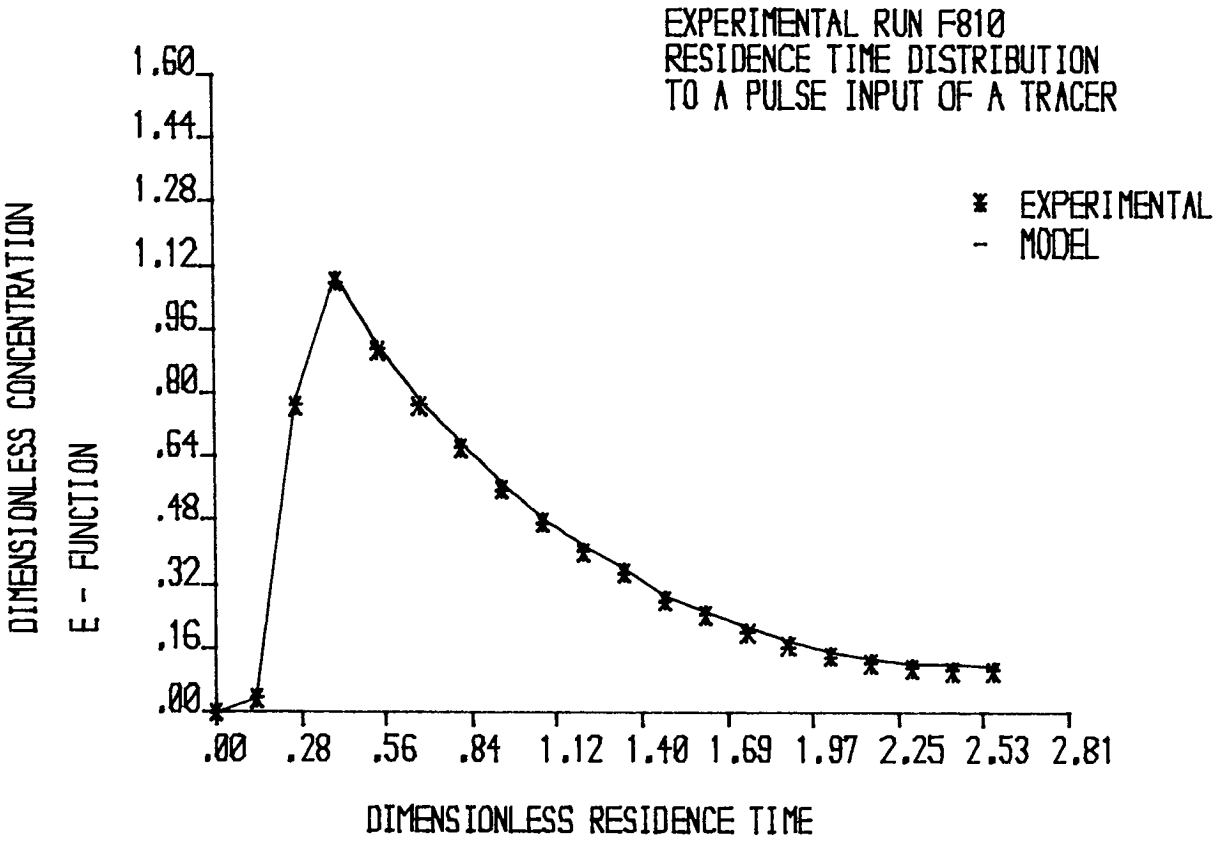

FIGURE 6.28 :RESIDENCE TIME DISTRIBUTION - RUN CODE F810

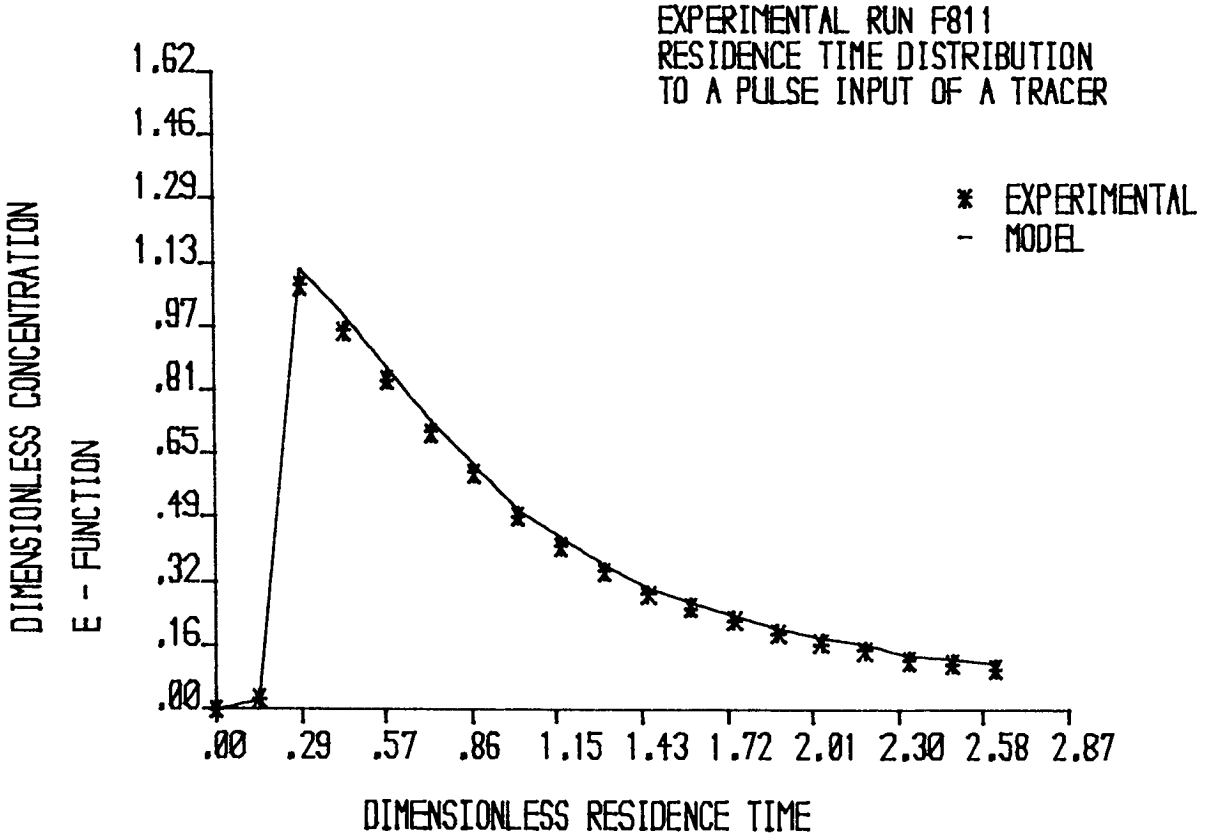

FIGURE 6.29 :RESIDENCE TIME DISTRIBUTION - RUN CODE F811

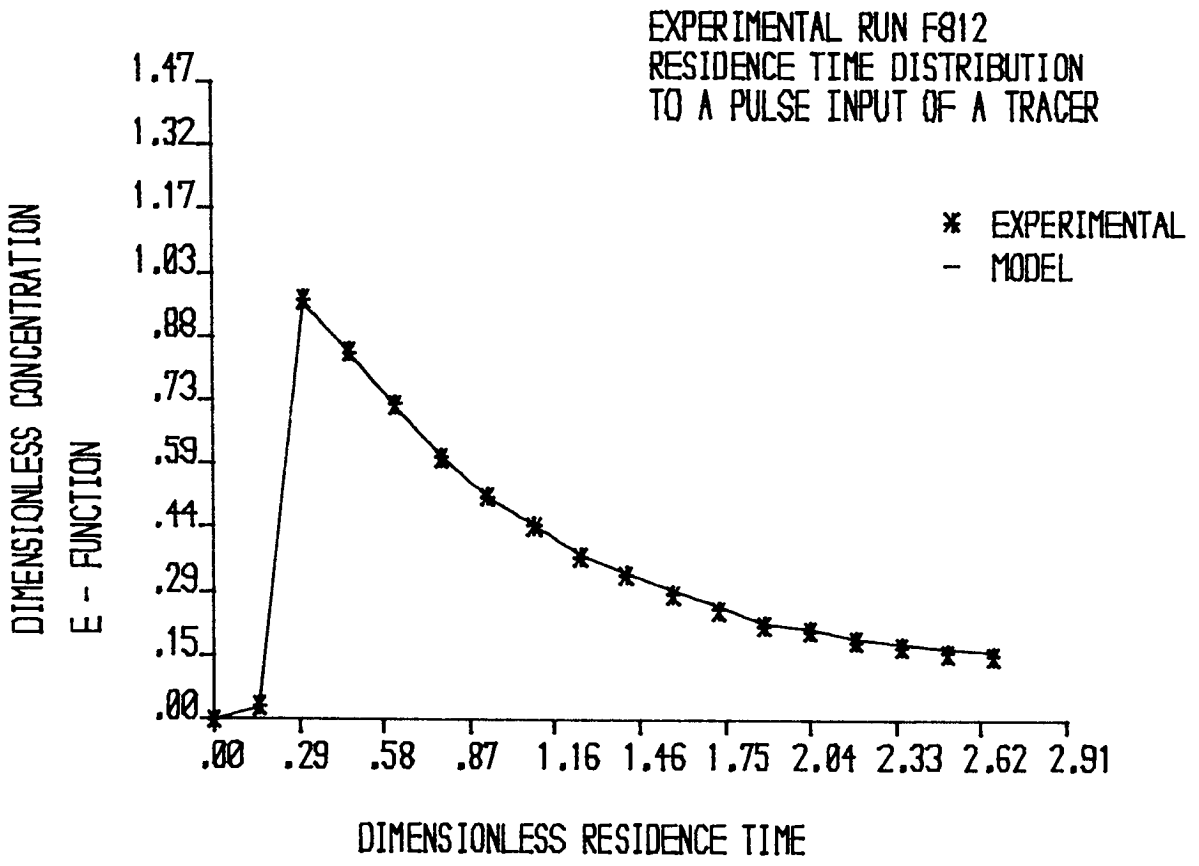

FIGURE 6.30 :RESIDENCE TIME DISTRIBUTION - RUN CODE F812

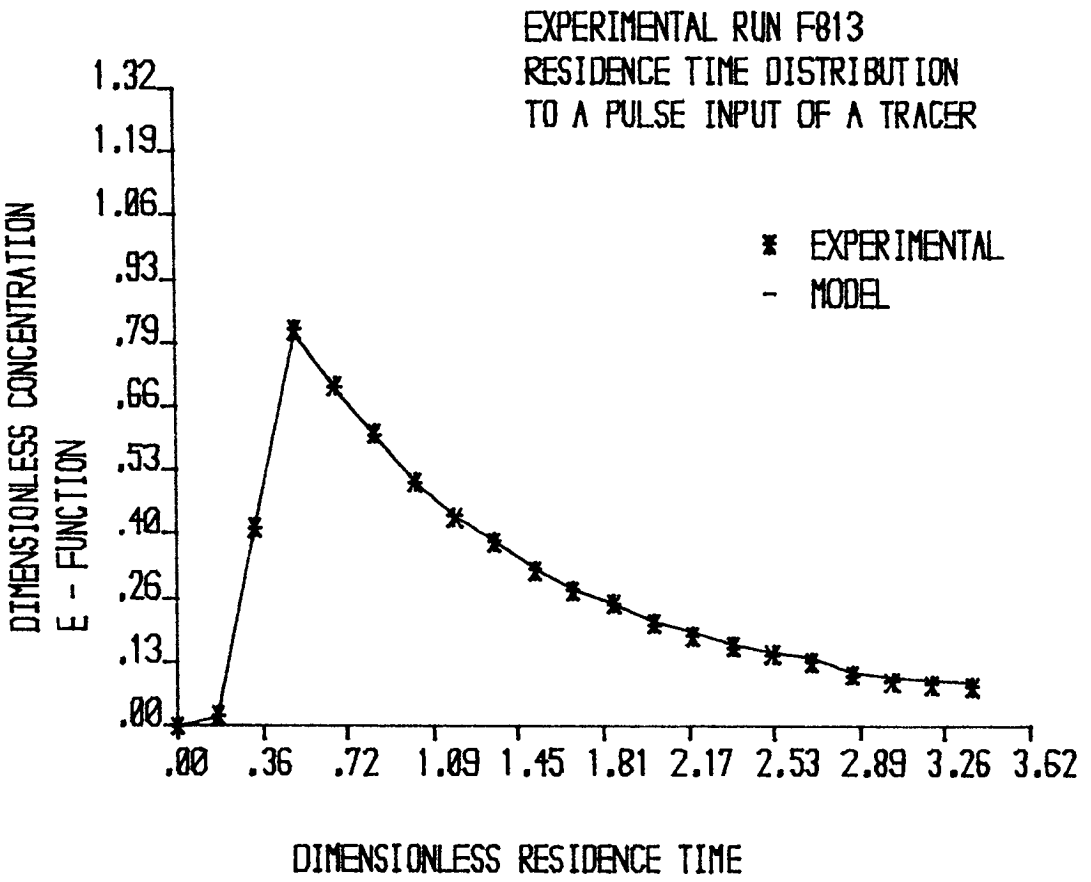

FIGURE 6.31 :RESIDENCE TIME DISTRIBUTION - RUN CODE F813

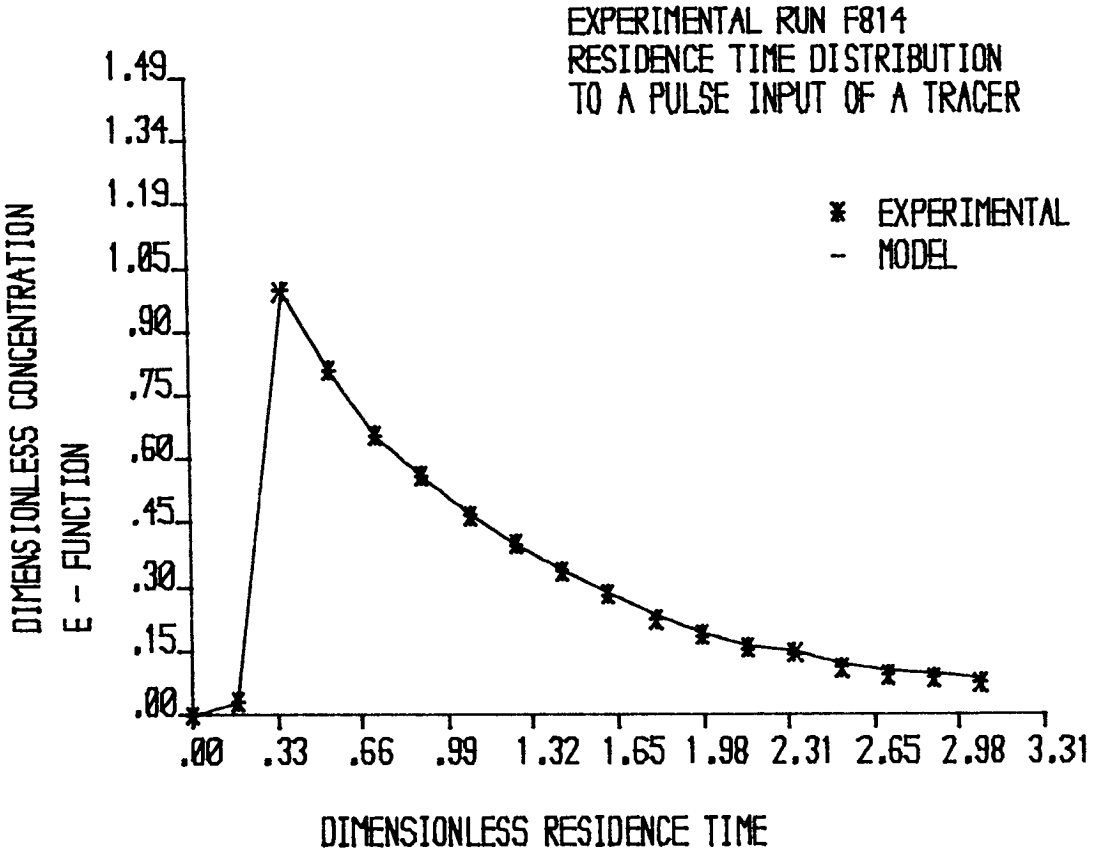

FIGURE 6.32 ;RESIDENCE TIME DISTRIBUTION - RUN CODE F814

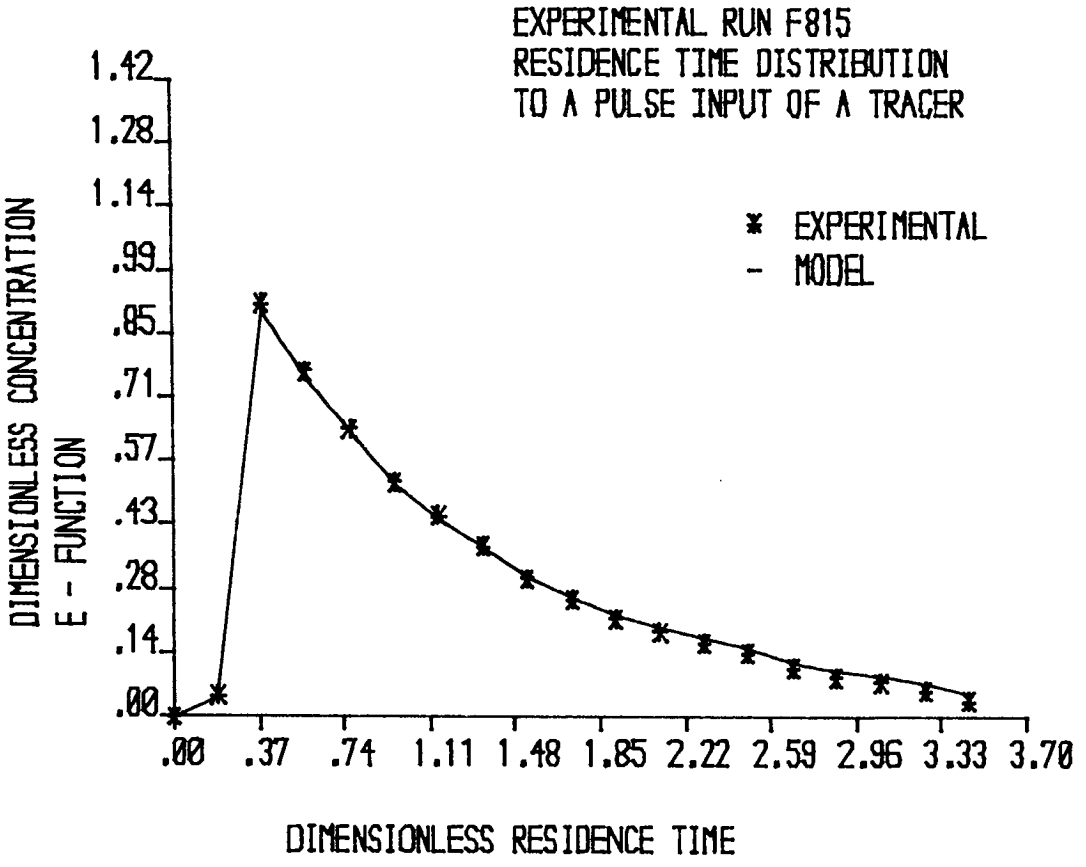

FIGURE 6.33 :RESIDENCE TIME DISTRIBUTION - RUN CODE F815

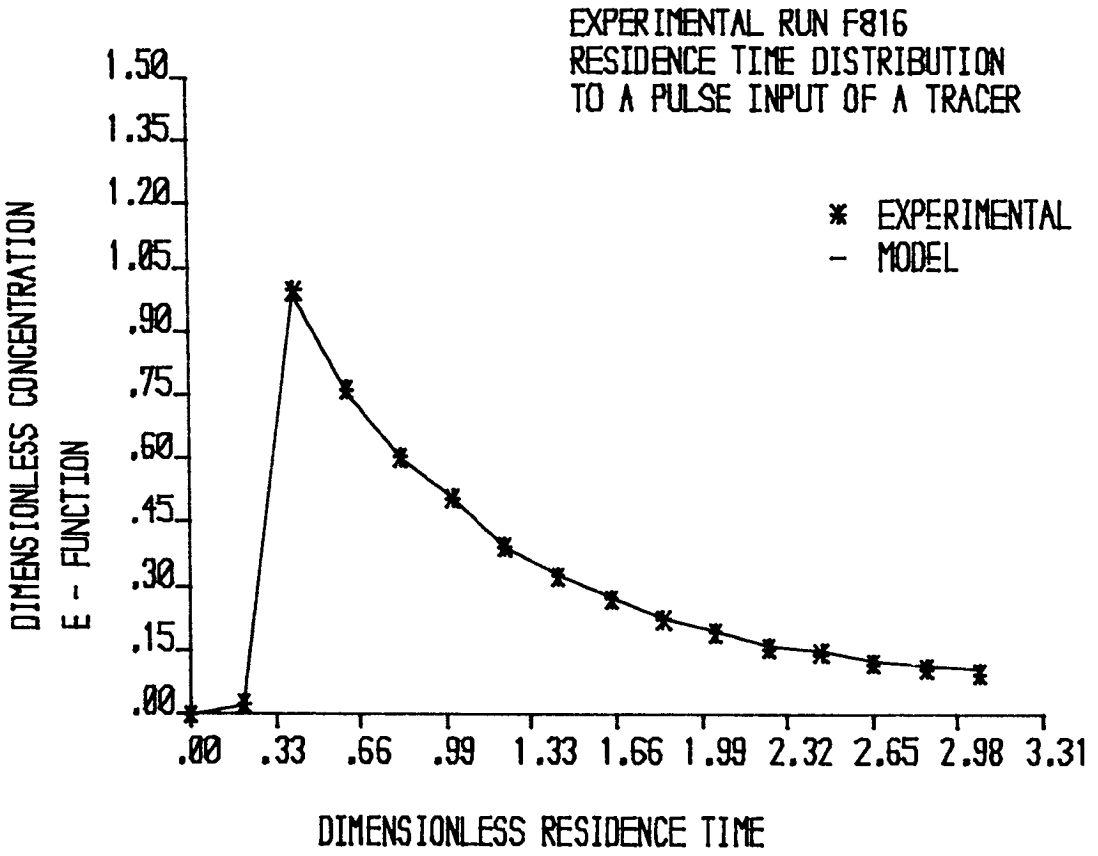

FIGURE 6.34 :RESIDENCE TIME DISTRIBUTION - RUN CODE F816

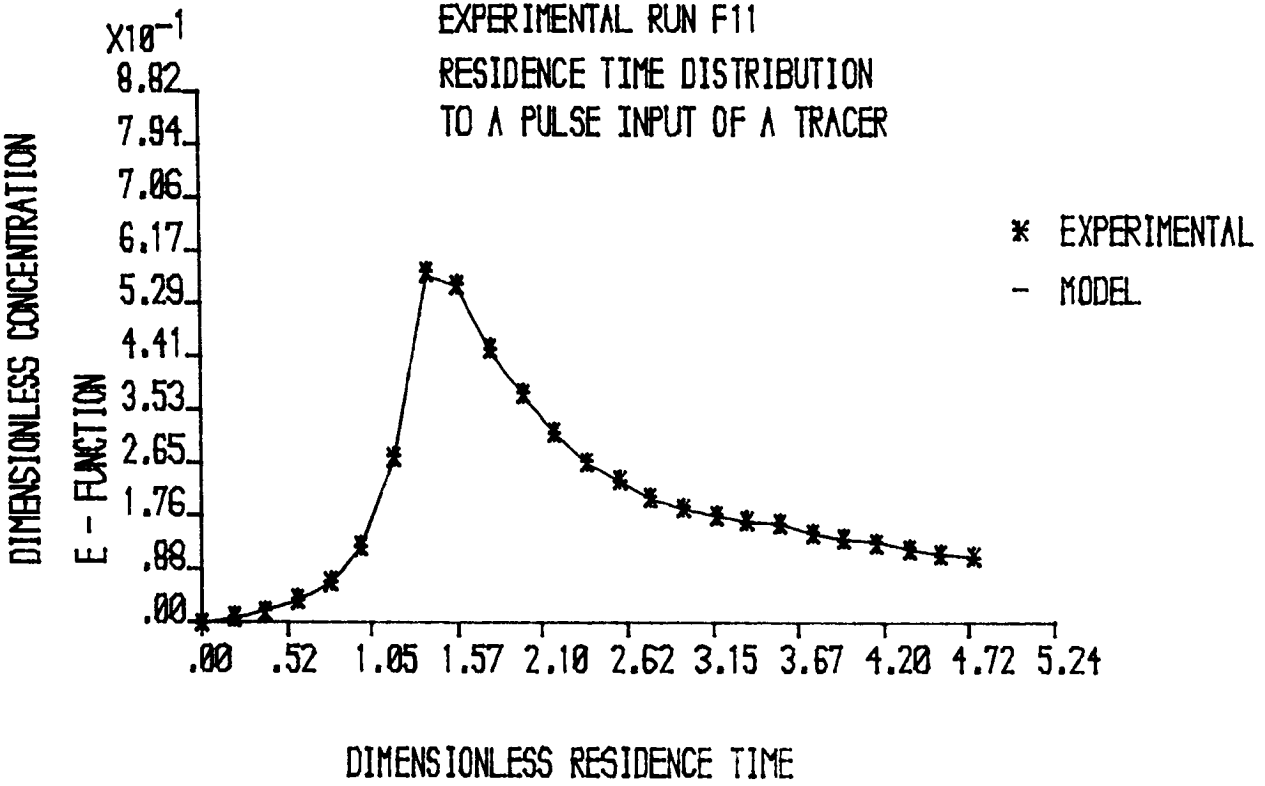

FIGURE 6.35 :RESIDENCE TIME DISTRIBUTION - RUN CODE F11

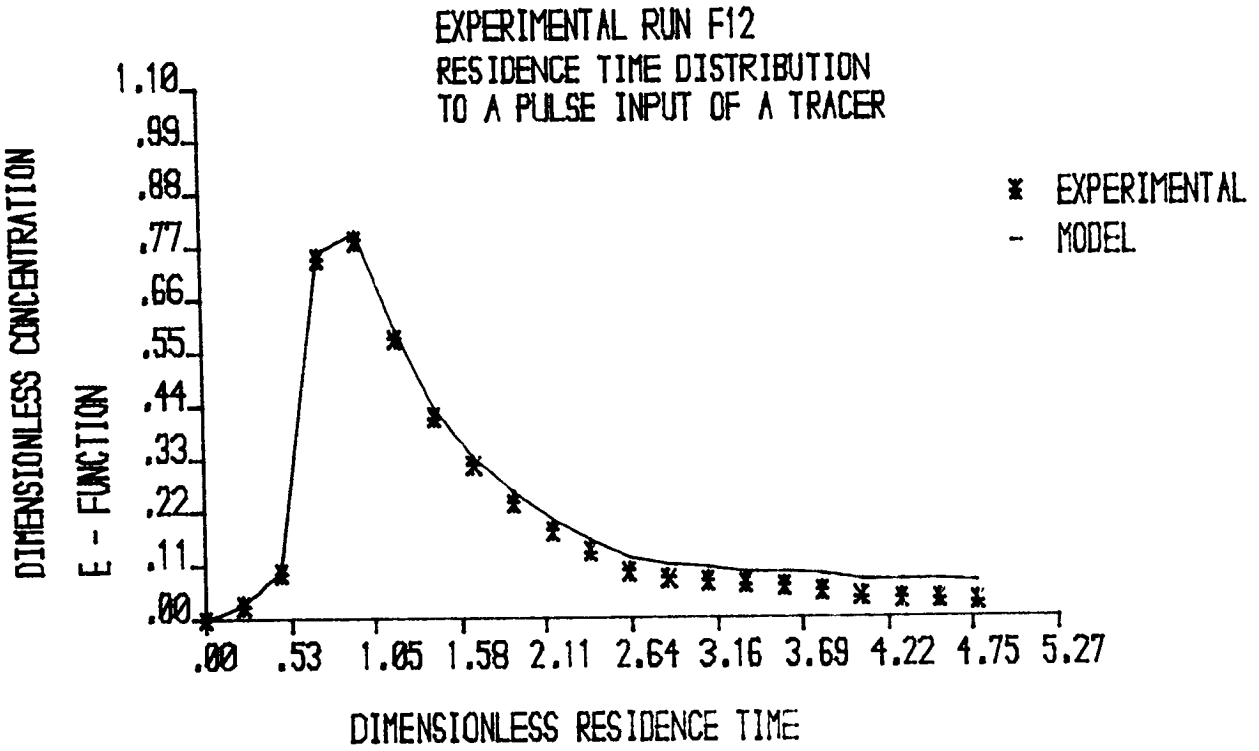

FIGURE 6.36 :RESIDENCE TIME DISTRIBUTION - RUN CODE F12

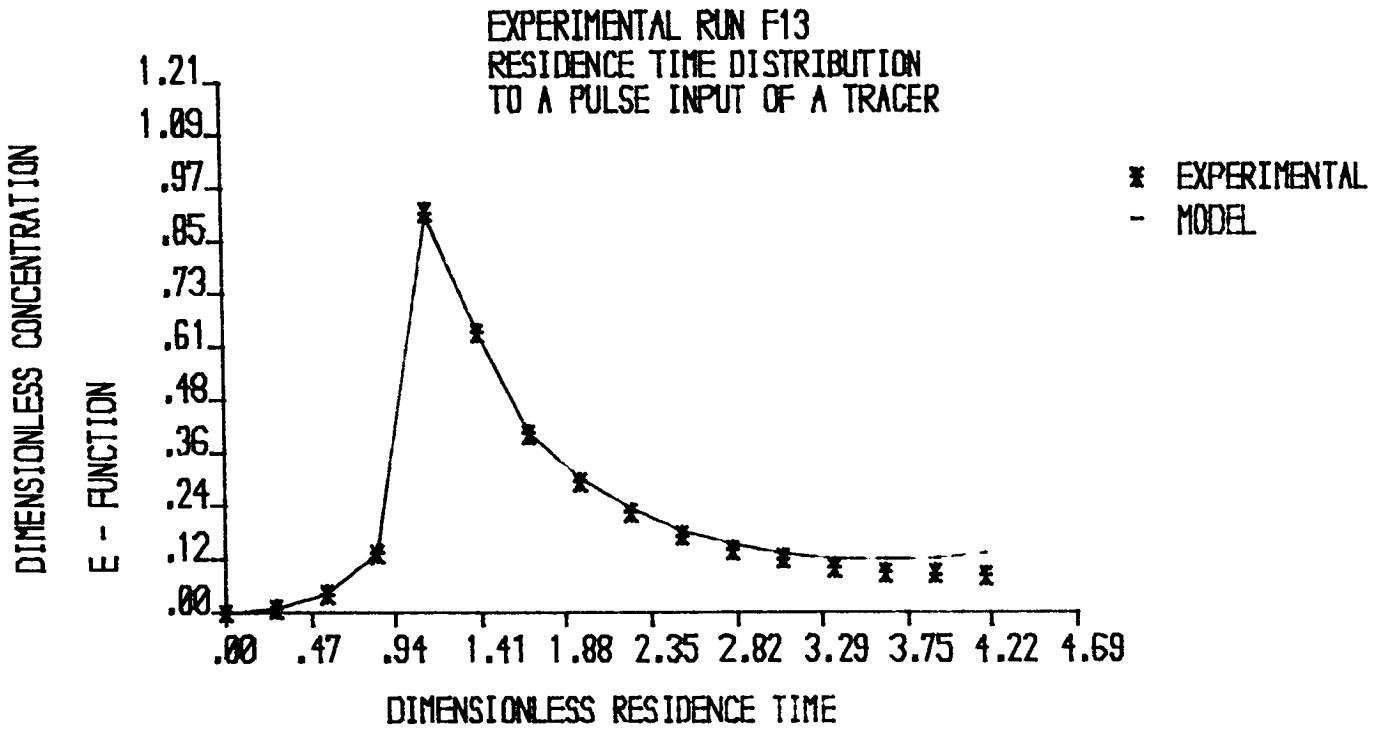

FIGURE 6.37 :RESIDENCE TIME DISTRIBUTION - RUN CODE F13

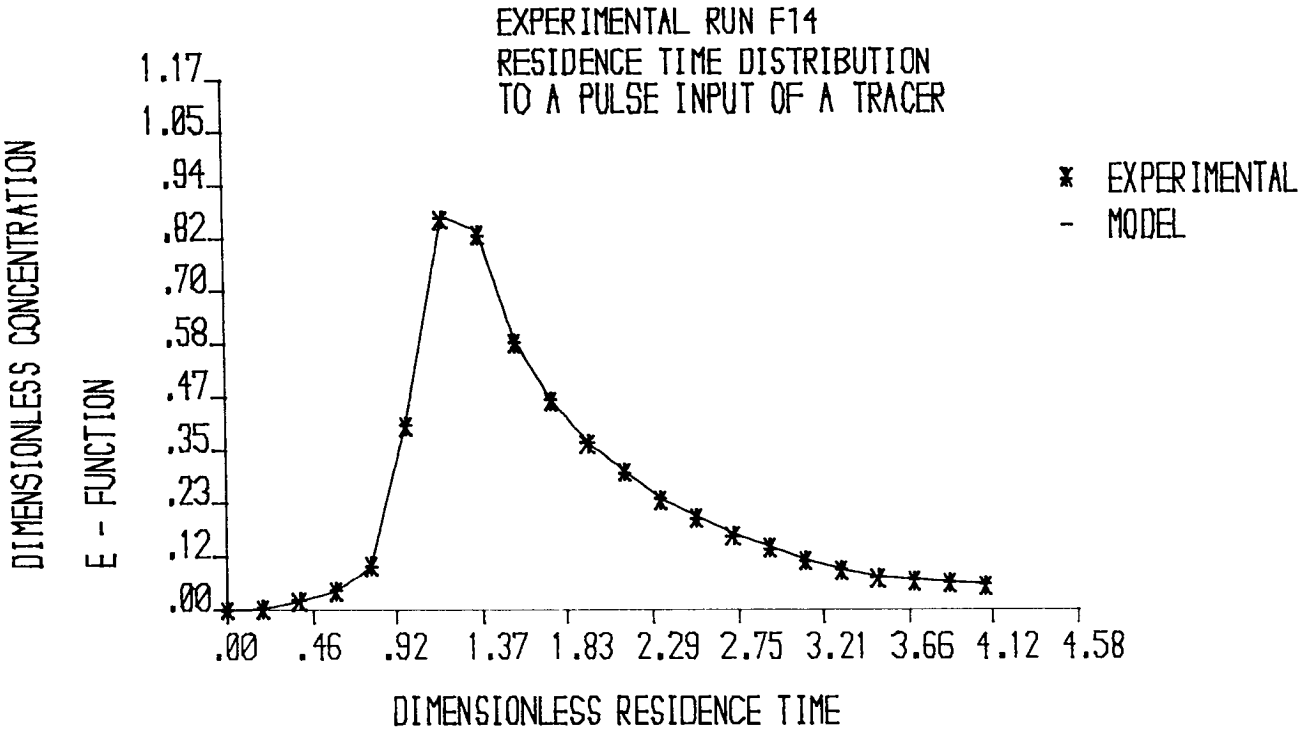

FIGURE 6.38 :RESIDENCE TIME DISTRIBUTION - RUN CODE F14

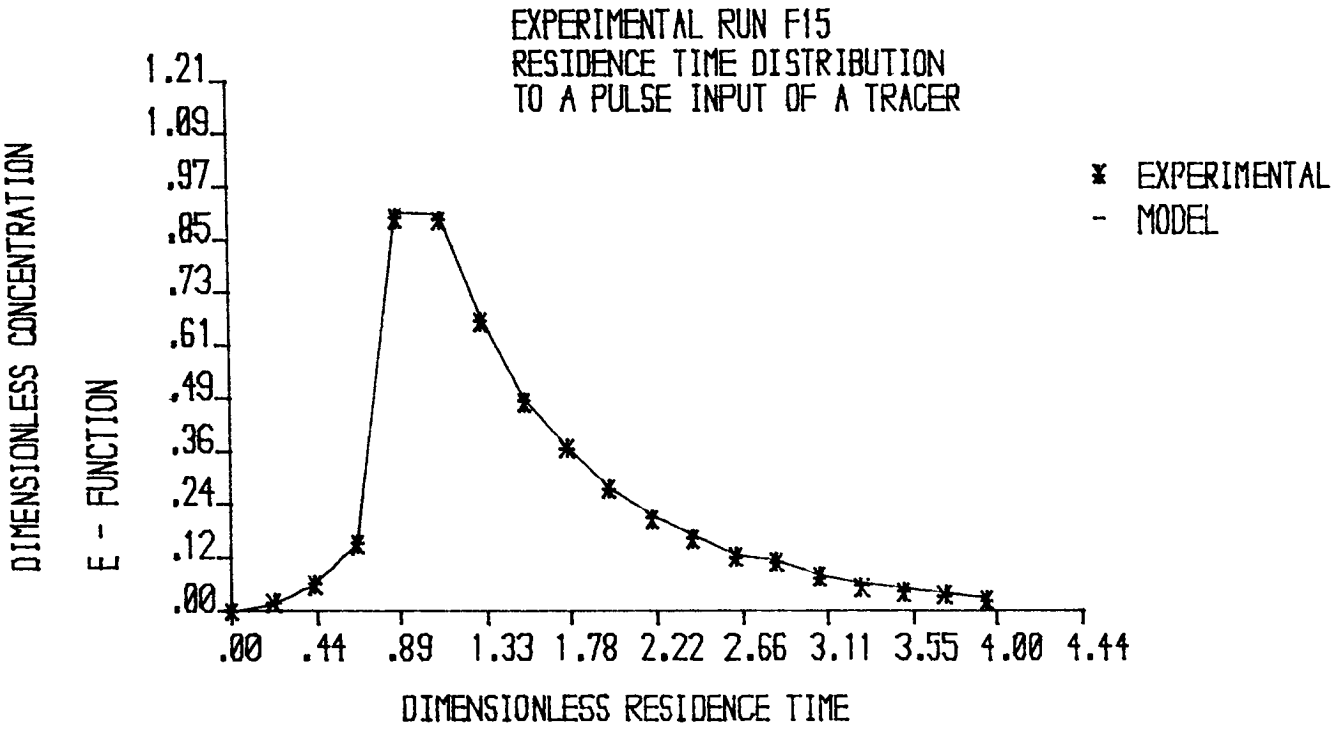

FIGURE 6.39 :RESIDENCE TIME DISTRIBUTION - RUN CODE F15

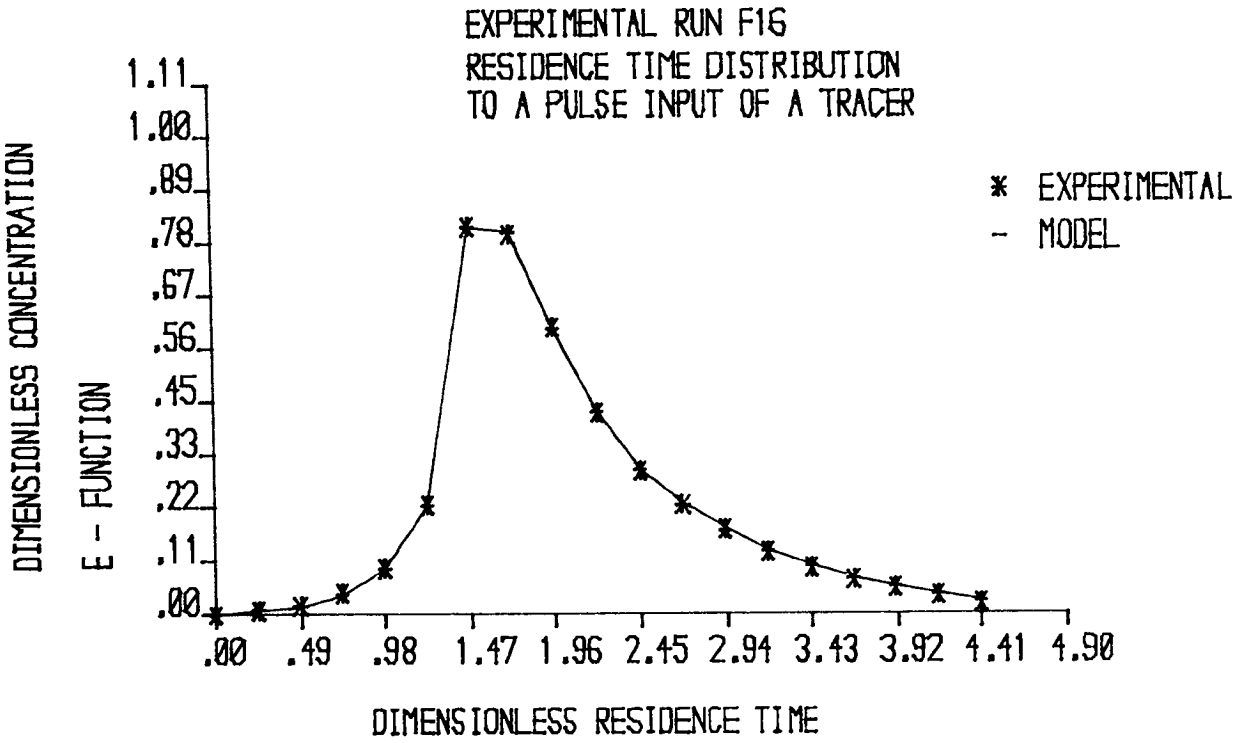

FIGURE 6.40 :RESIDENCE TIME DISTRIBUTION - RUN CODE F16

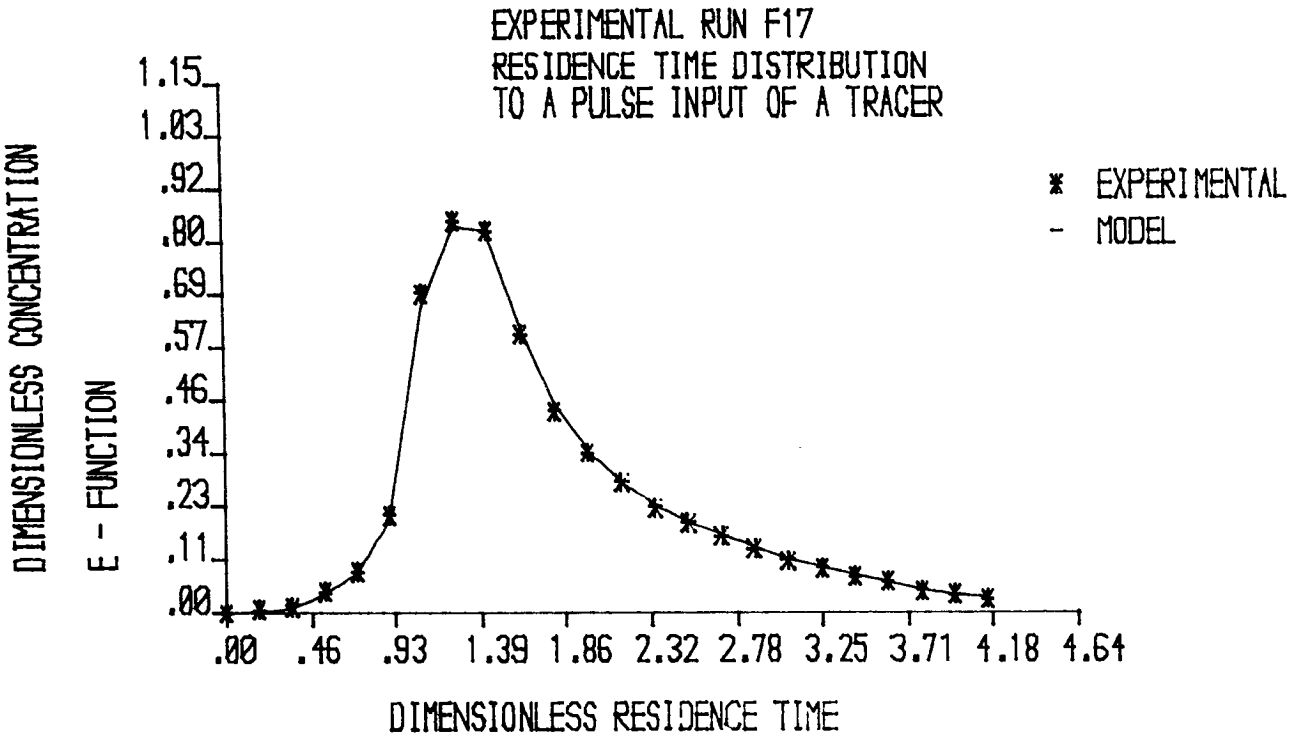

FIGURE 6.41 :RESIDENCE TIME DISTRIBUTION - RUN CODE F17

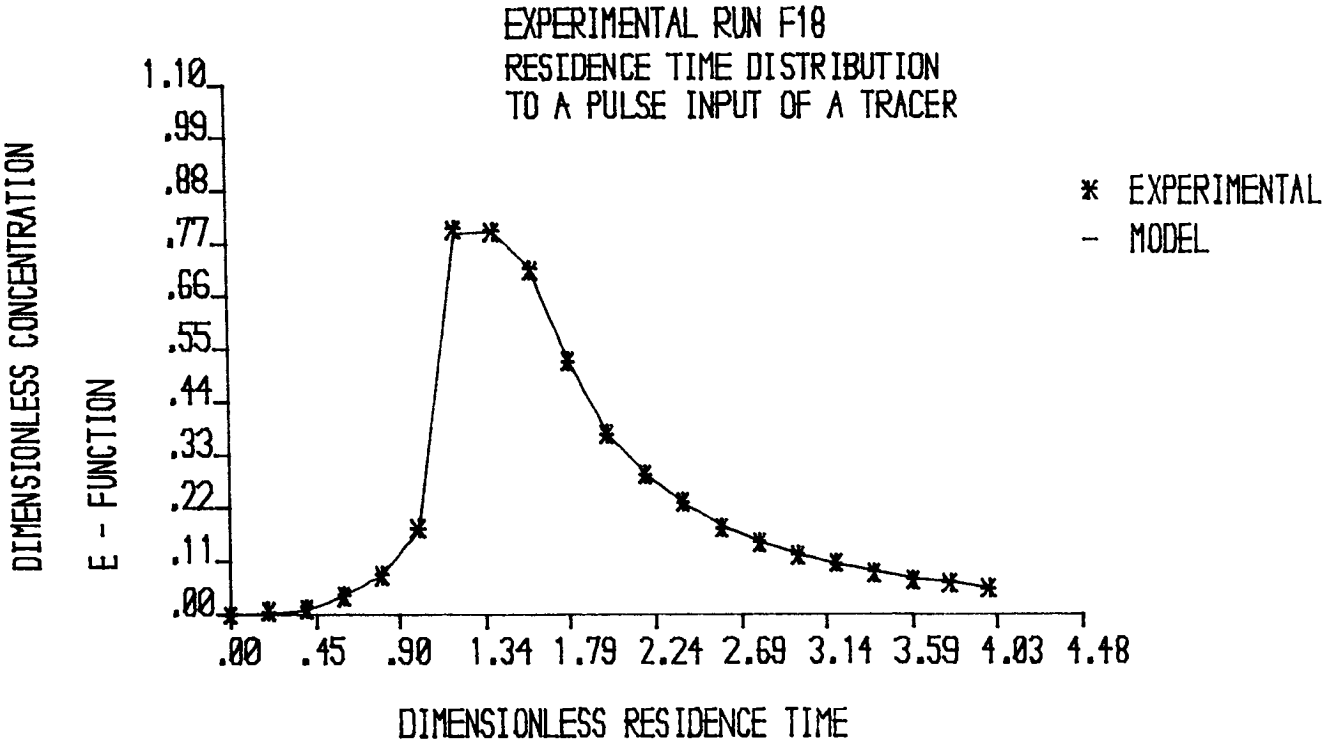

FIGURE 6.42 :RESIDENCE TIME DISTRIBUTION - RUN CODE F18

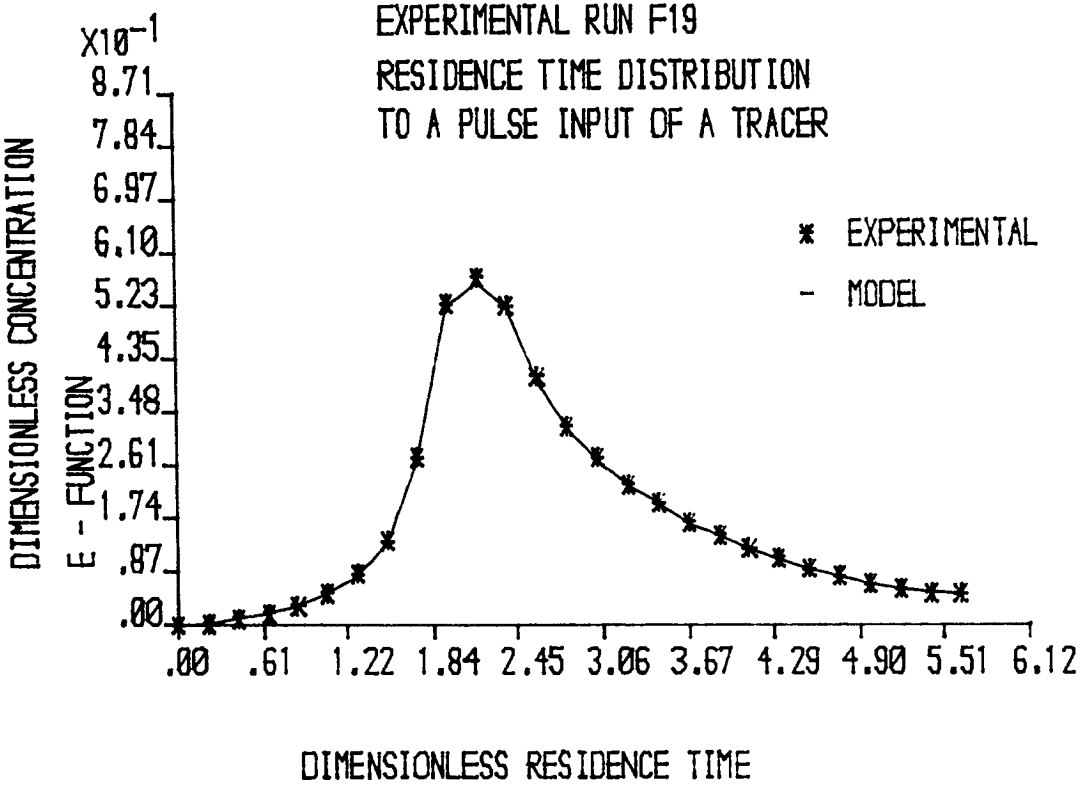

FIGURE 6.43 :RESIDENCE TIME DISTRIBUTION - RUN CODE F19

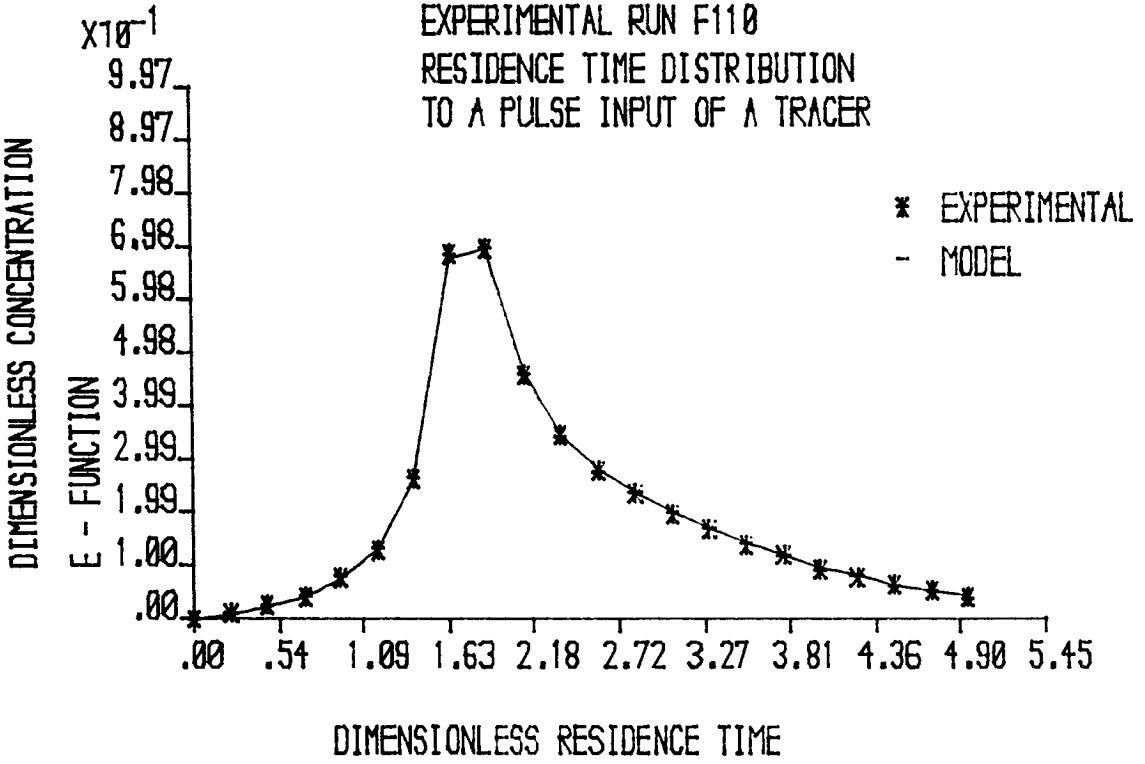

FIGURE 6.44 :RESIDENCE TIME DISTRIBUTION - RUN CODE F110

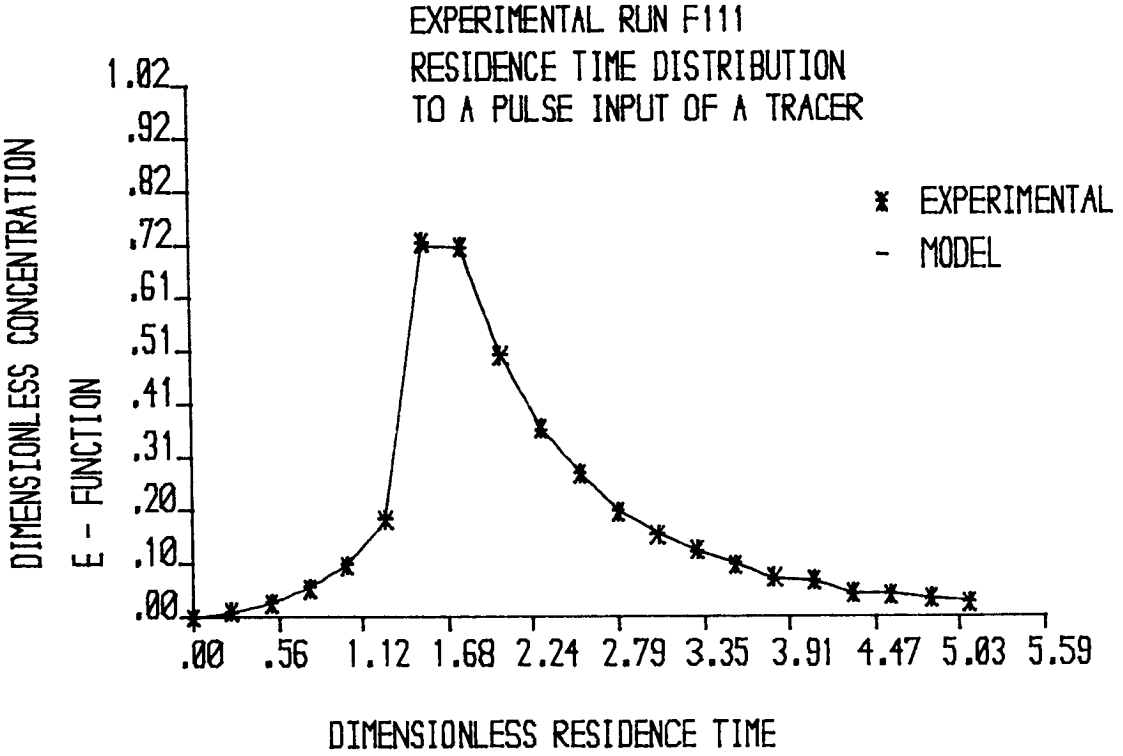

FIGURE 6.45 :RESIDENCE TIME DISTRIBUTION - RUN CODE F111

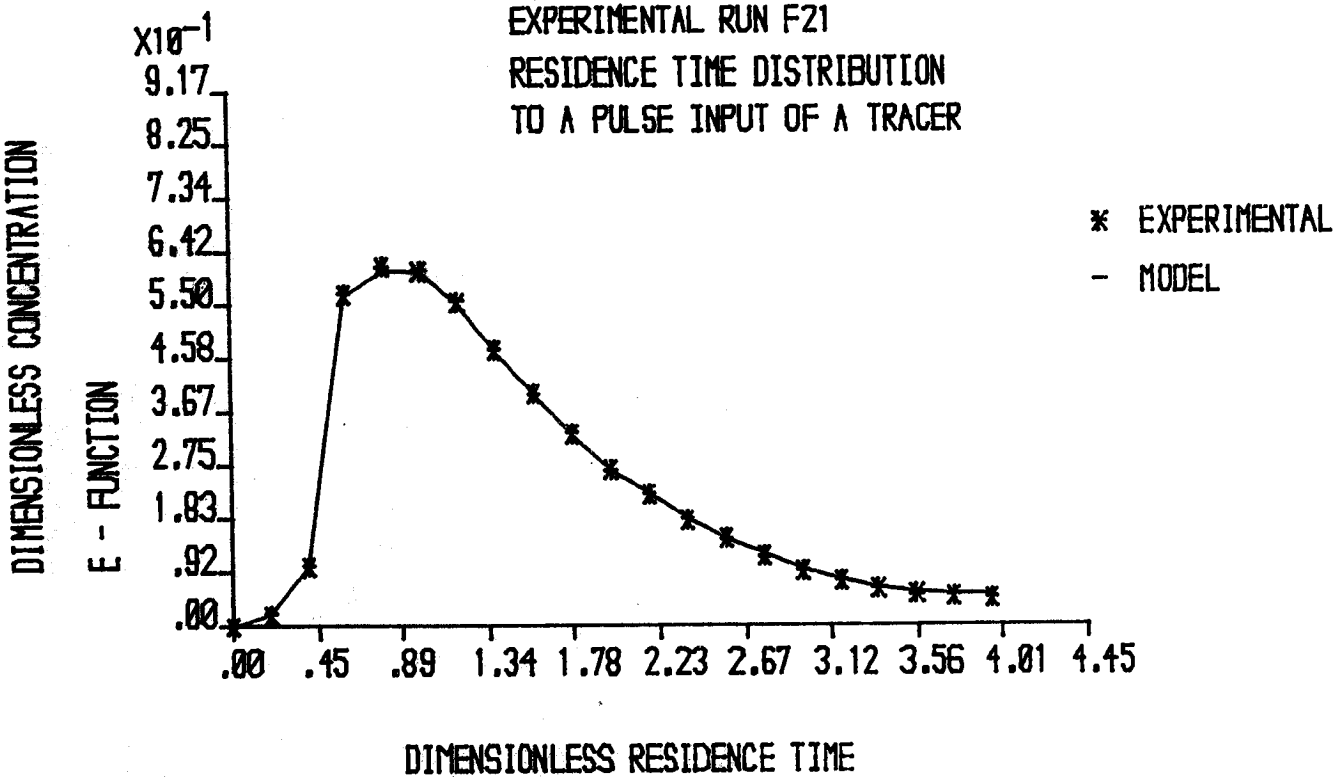

FIGURE 6.46 :RESIDENCE TIME DISTRIBUTION - RUN CODE F21

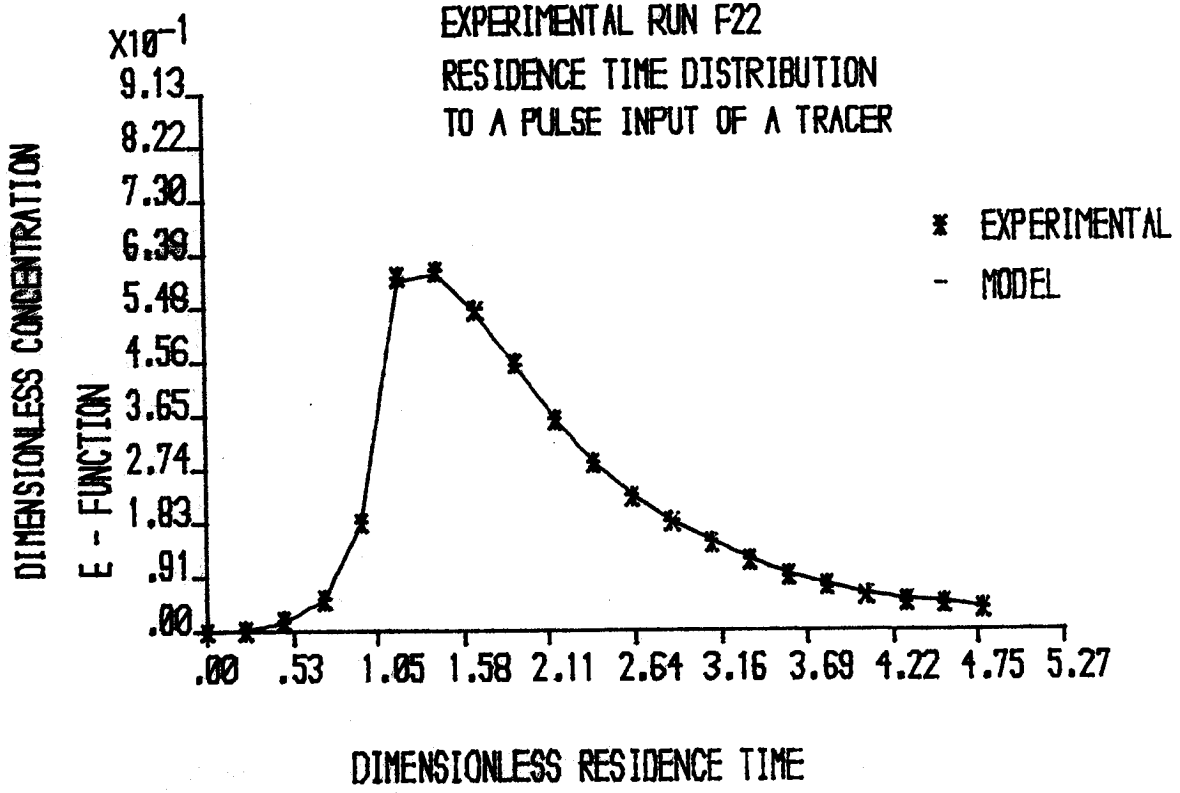

FIGURE 6.47 :RESIDENCE TIME DISTRIBUTION - RUN CODE F22

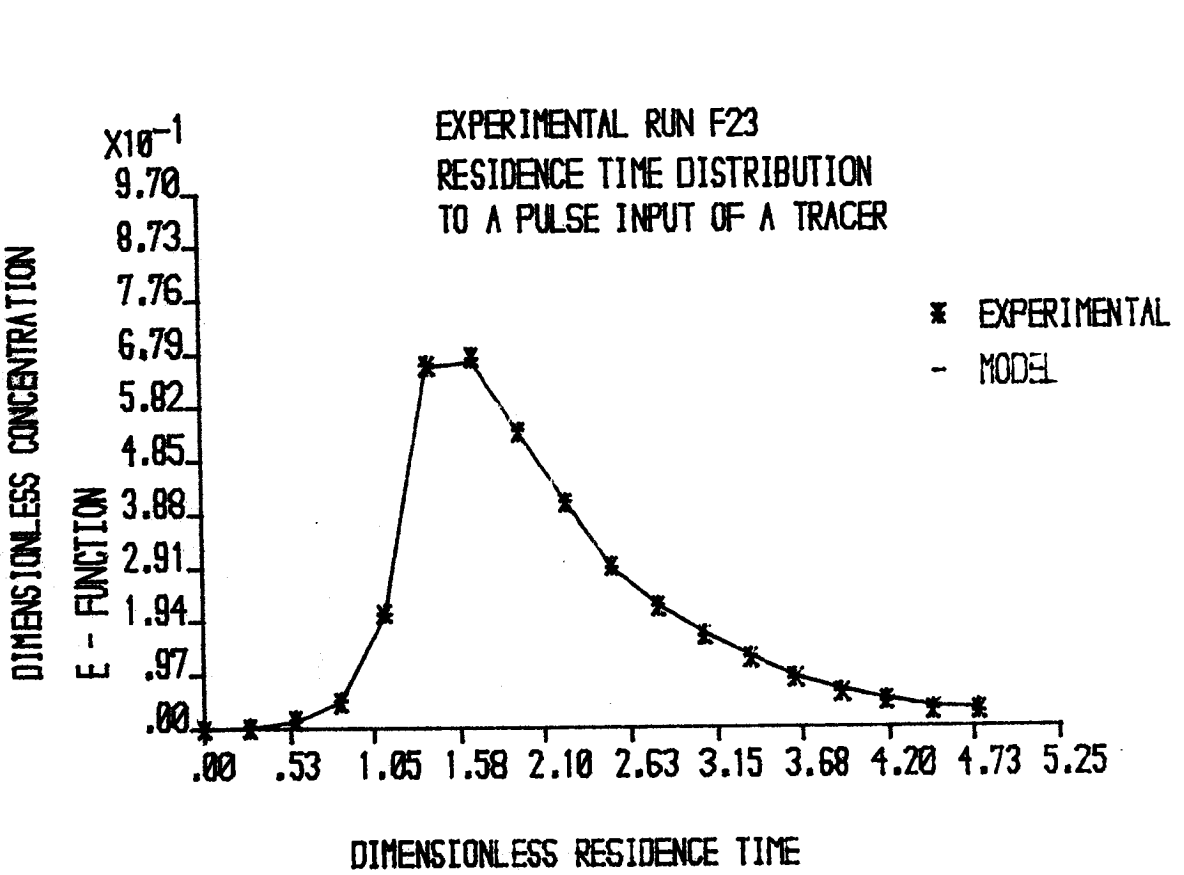

FIGURE 6.48 :RESIDENCE TIME DISTRIBUTION - RUN CODE F23

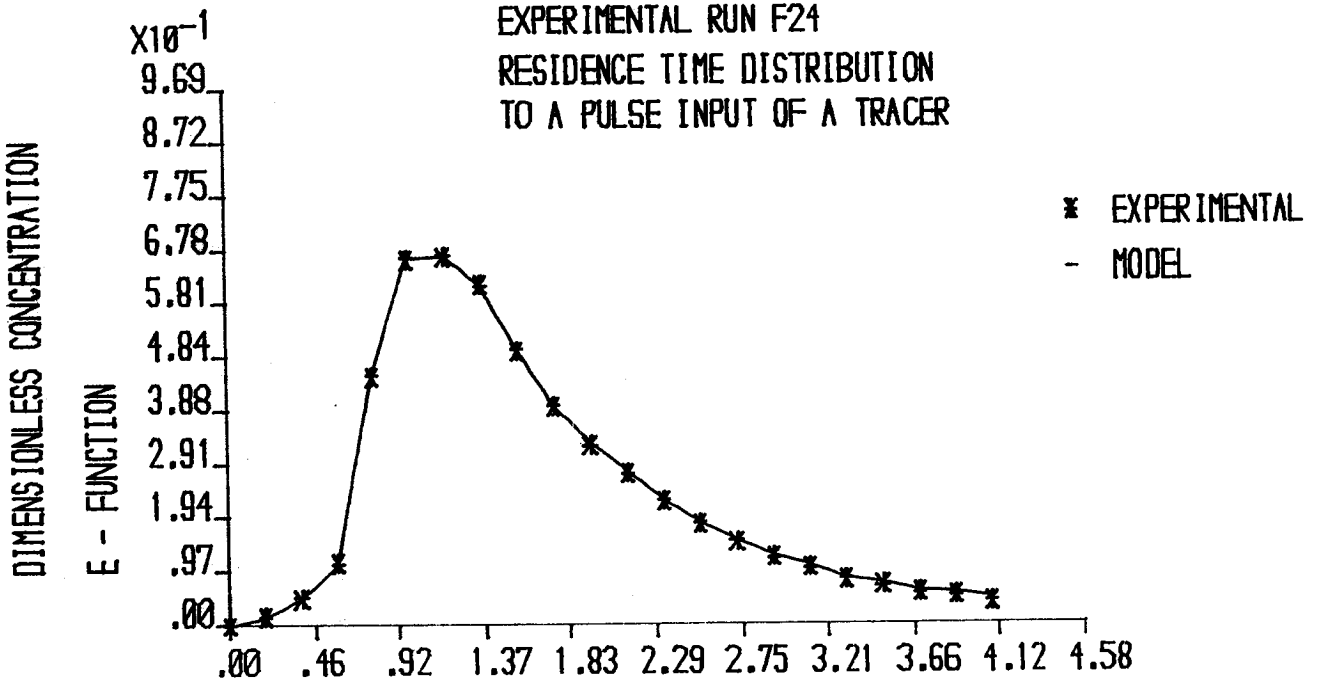

FIGURE 6.49 :RESIDENCE TIME DISTRIBUTION - RUN CODE F24

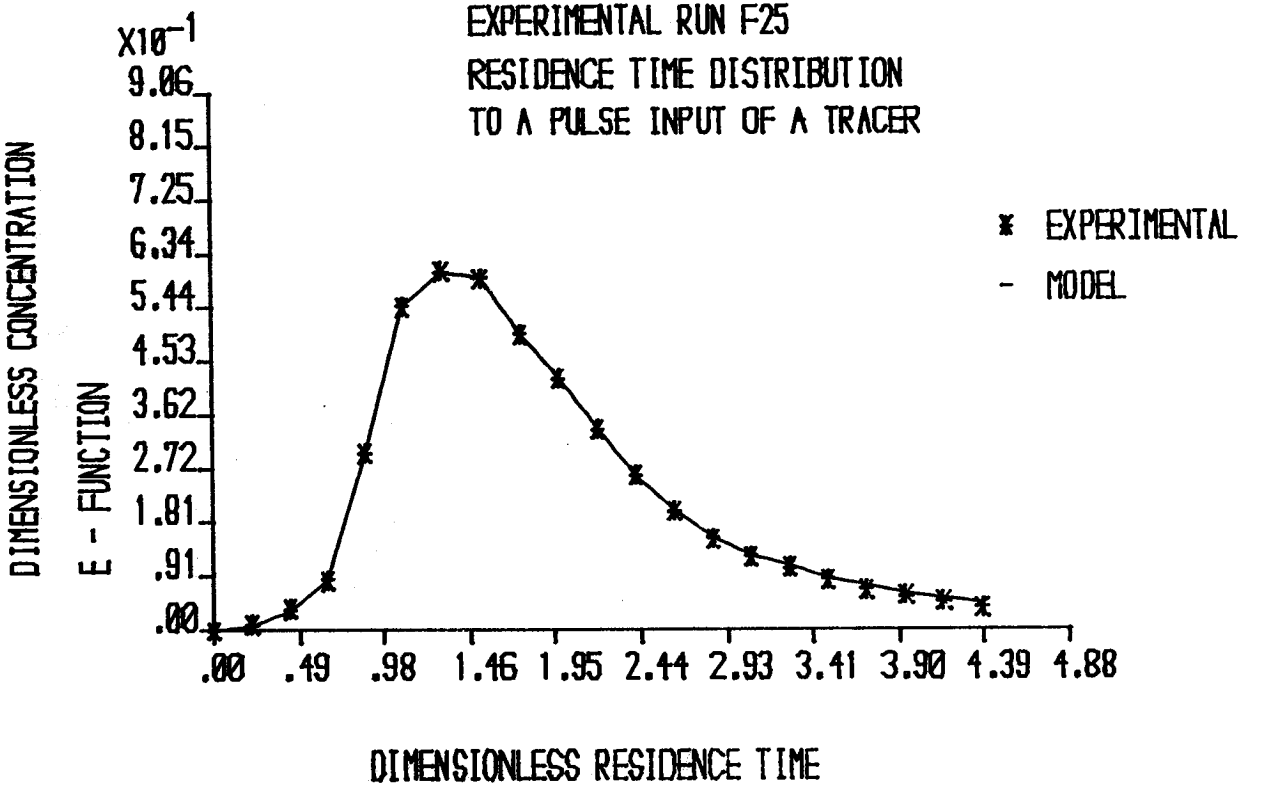

FIGURE 6.50 :RESIDENCE TIME DISTRIBUTION - RUN CODE F25

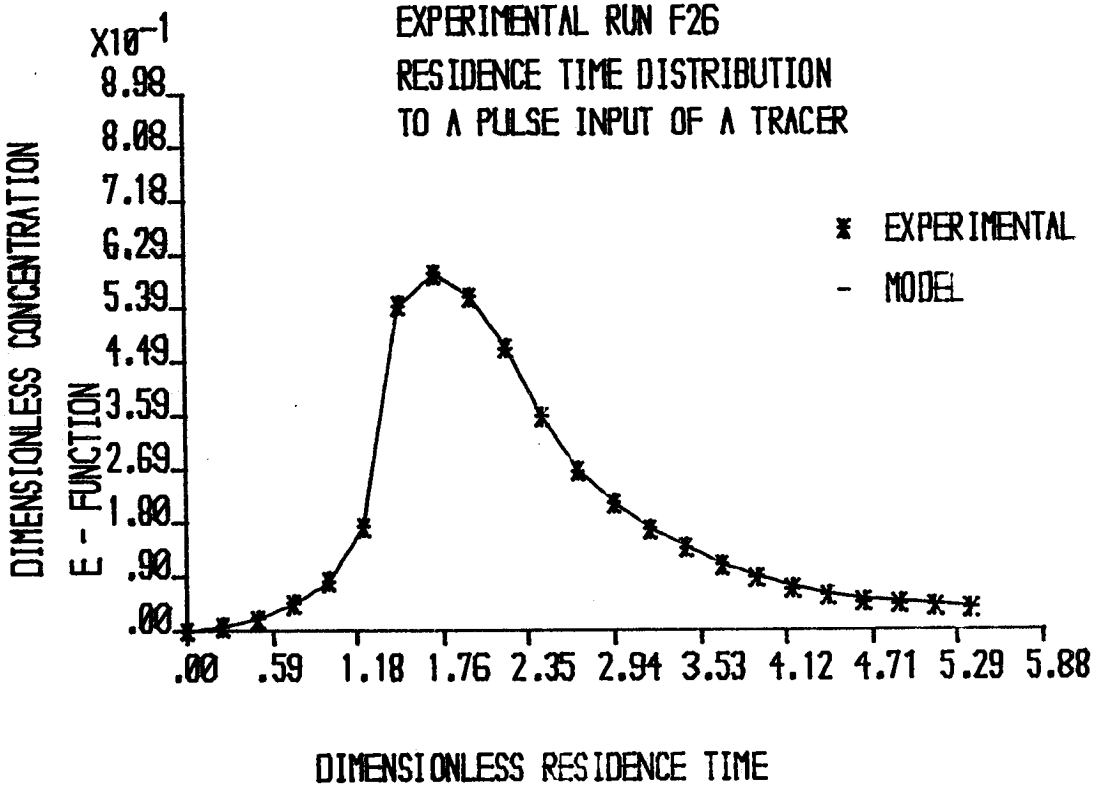

FIGURE 6.51 :RESIDENCE TIME DISTRIBUTION - RUN CODE F26

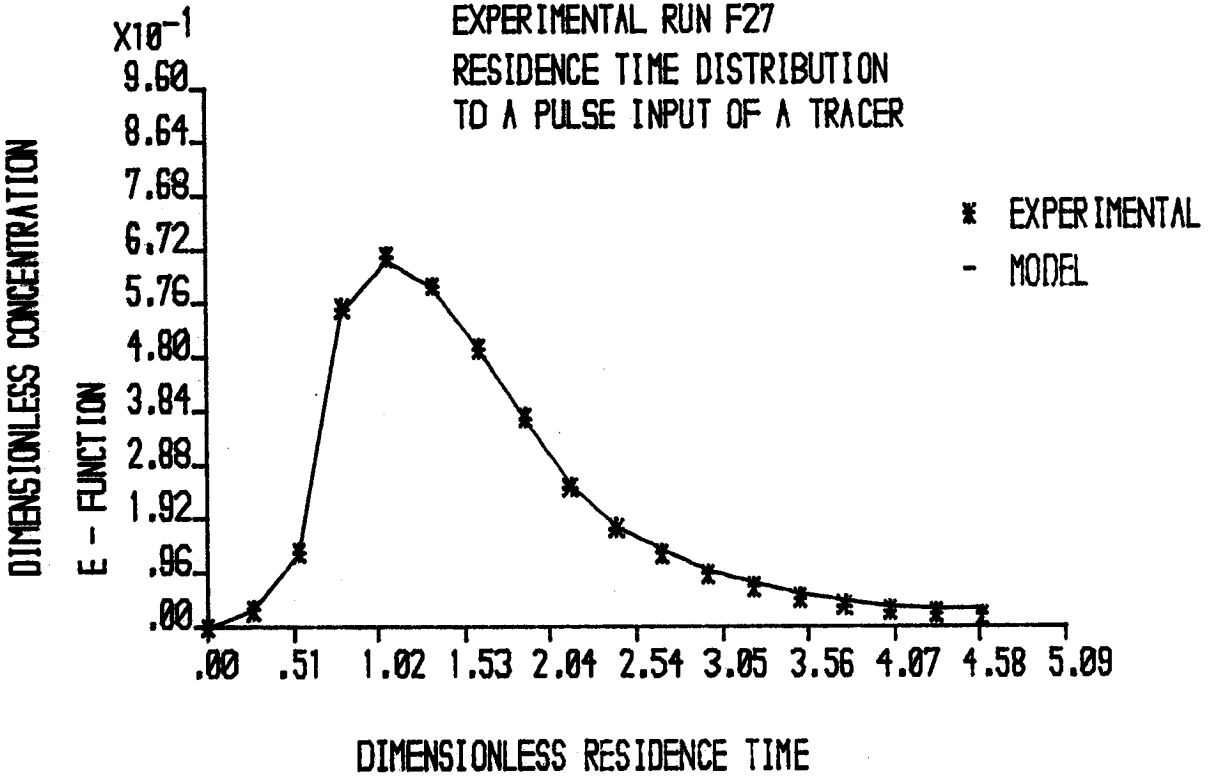

FIGURE 6.52 :RESIDENCE TIME DISTRIBUTION - RUN CODE F27

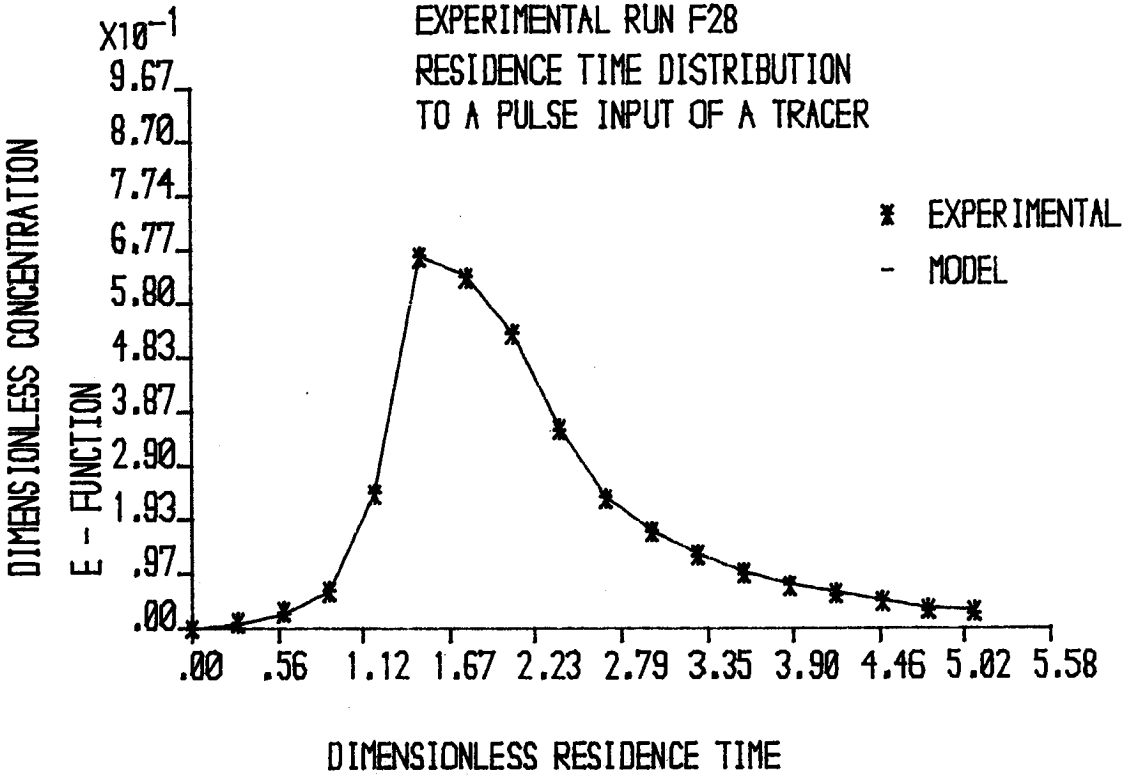

FIGURE 6.53 :RESIDENCE TIME DISTRIBUTION - RUN CODE F28

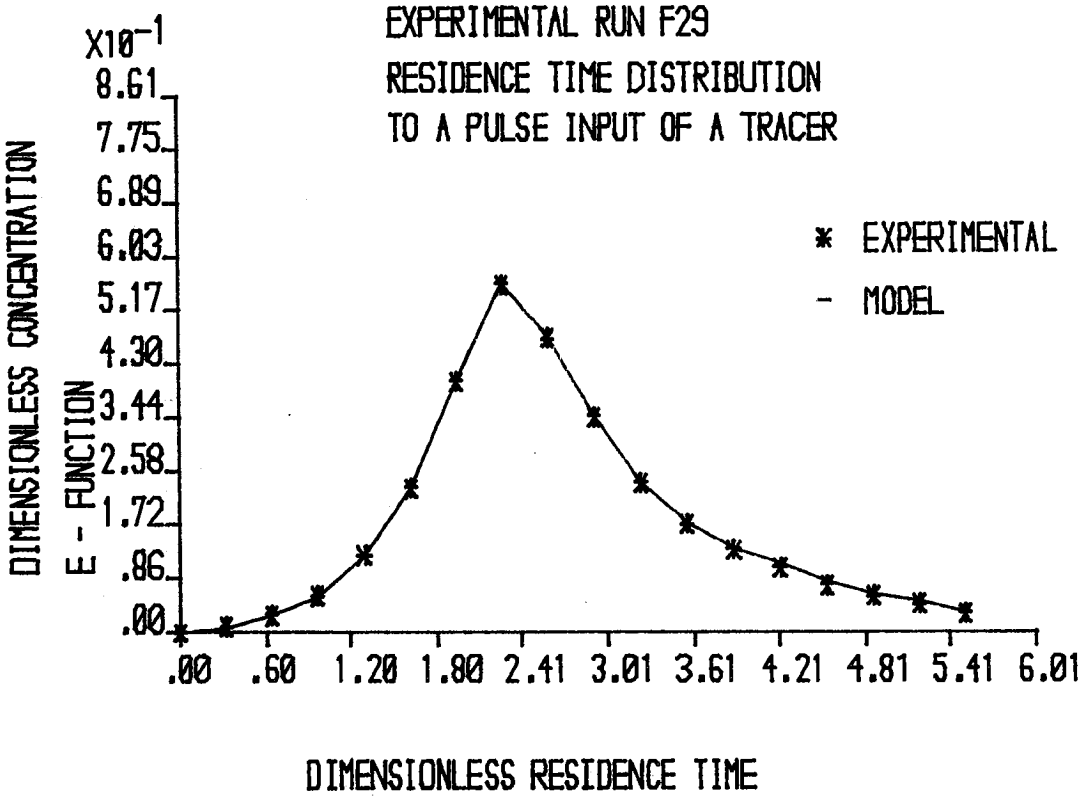

FIGURE 6.54 :RESIDENCE TIME DISTRIBUTION - RUN CODE F29

6.4 LIQUID RTD IN CYLINDRICAL NOZZLE REACTROS

The degree of mixing is generally related to the spread and the peak of the ' E - function ' curves. It is postulated, that the smaller the degree of mixing, the narrower and sharper the E - curves thus become (142). Hence, from the tracer information and the RTD model, interpretation is made as to whether the nozzle reactors show (i) considerable by - passing of the fluid, (ii) large dead space, or (iii) gross channelling of the fluid. These phenomena have been shown to be gross detrimental to the performance of industrial reactors (142,146,147).

The graphs of the model and experimental data, shown in Figures 6.1 to 6.54 and the variance between the model and experimental response profiles shown in Tables 6.1 to 6.13, illustrate that there is a good agreement between the model and experimental response curves. These Tables 6.1 to 6.13 further show that N = Ø, L = Ø, and thus A + B = 1.Ø. Hence the liquid particles irrespective of the feed flow rate reside mainly in streams A and B. There is no flow in stream C.

Tables 6.1 and 6.2 represent the RTD model parameters in Ø.55 x $1Ø^{-3}m^3$ nozzle reactor. These show a slight fluctuation in the fraction of the feed liquid rates along path A (Figure 4.1). There are high volume fractions in the plug flow zone J, at low feed rates in the nozzle reactor. This is 1Ø% at RES 95 and then increased to 2Ø% at RES 99. Alternately, the fraction of the volume in

CSTR zone K, shows a relative decrease in value, with corresponding increase in the feed flow rate. The fraction of the total feed rate along path B indicates a negligible change, independent of the liquid flow rate, and is Ø.1% of the volume of the nozzle vessel residing in the plug zone M. These results imply that at low feed flow rates, the intensity of mixing is reduced, suggesting that the flow of liquid is representing plug flow, as shown by high values in J. However, the increase in the length of the tail of the curves at high feed rates suggests the intense mixing activity in the vessel. However, this also signifies dead spaces in the nozzel vessel, and time delays indicate the active plug flow zone in the vessel (Figures 6.1 - 6.9).

Tables 6.3 and 6.4 show the RTD model parameters in $1.52 \times 1Ø^{-3} m^3$ nozzle vessel. The values of A vary slightly and then greatly decrease and after, remain constant with increase in the feed flow rates. This is accompanied by corresponding increase in B, until it remains constant. The varying model parameters are J and M, which are the volume fractions of the plug flow zones and thus affect the intensity of mixing in the vessel, and is shown by the narrow shapes in the RTD response curves (Figures 6.1Ø - 6.18). However, at higher feed flow rates, the intensity of mixing increases as indicated by the high values in the CSTR, zone A1, (1-J-K-M-N), and as evident by the long tail in the response profiles.

Tables 6.5 to 6.8 represent the RTD parameters in 5.13 x $1Ø^{-3}m^3$ nozzle vessel. In this, A decreases with simultaneous increase in B as the feed flow rates increase. Also, M remains constant at Ø.1% of the nozzle volume. However, the only other changes are J and K in path A. The trend in the value of J is erratic, at first; it increases, then decreases sharply, followed by a sudden increase and then finally decreases. K shows a slight change as the feed flow rates increase. Also, the trend in the value of the CSTR A1, (1-J-K-M-N), increases. These changing values in the model parameters can be elucidated by a decrease in the mixing intensity at low feed liquid rates with narrow distribution around the peak of the RTD profiles (Figures 6.19 -6.34), and prominent time delays as the values of B indicate in the plug flow zone M.

Tables 6.9 to 6.11 represent tracer injection at the top wall of Ø.55 x $1Ø^{-3}m^3$ nozzle vessel. In this case, the RTD profiles show a shift to the right. In contrast to the previous profiles, which indicate the shift of the RTD curves, greatly to the left; the values of A decrease slightly, then increased. Alternately, B increase slightly and then greatly decreased, except RES 19, which shows a sharp reduction in A with a high value of B. Also, the RTD model parameters, J, K, M show some conflicting changes in values, with the CSTR zone A1, (1-J-K-M-N) fluctuating between high and low values with

respect to the increase in the feed flow rates. The narrow shape in the curves around the peak at low feed rates shows a reduction in the intensity of mixing in the nozzle vessel. However, the long tails with the spread in the RTD profiles indicated the intensity of the nozzle liquid (Figures 6.35 - 6.45).

Tables 6.12 and 6.13 represent tracer injection at the bottom wall of $\emptyset.55 \times 1\emptyset^{-3} m^3$ vessel. This case shows a distinct reversal of the feed liquid flow in the nozzle vessel, as evident by the visual observation. The values of A decrease with increase in B at high feed rates. Also, the percentage in the volume of the plug flow zone M is 1%. The values of J increase and K decrease as the feed rates increase. However, such high values of B in the plug flow zone M, account for the reversal of the liquid flow and recirculation in the nozzle vessel (Figures 6.46 - 6.54).

CHAPTER SEVEN

FAST REACTION STUDIES IN NOZZLE REACTORS

7.1 MATHEMATICAL MODEL FOR FAST REACTION STUDIES

7.1.1 DERIVATION OF THE MATHEMATICAL MODEL FOR THE REACTION KINETICS

7.1.2 YIELD OF THE PRODUCT

7.2 DESCRIPTION OF EXPERIMENTAL APPARATUS

7.3 EXPERIMENTAL PROCEDURE

7.4 CALCULATION OF THE EXCESS SULPHURIC ACID FROM STOICHIOMETRY

7.5 DISCUSSION OF RESULTS

7.5.1 FLOW VISUALIZATION STUDIES INVOLVING AQUEOUS SULPHURIC ACID AND SODIUM CARBONATE SOLUTIONS IN $\emptyset.55 \times 10^{-3}$ M^3 NOZZLE VESSEL

7.5.2 RESULTS OF THE PROPOSED RTD MODEL

7.6 COMPARISONS WITH OTHER EXPERIMENTAL TECHNIQUES

7.1 MATHEMATICAL MODEL FOR FAST REACTION KINETICS

From the residence time distribution of the tracer when subjected to pulse injection into the nozzle vessel, showed that the behaviour of flow pattern was divided into two streams as shown in the Figure 7.1.
Stream A consists of a C.S.T.R. A1, a plug flow A2 and a C.S.T.R. A3. Stream B consists of plug flow B1 only.

The reaction mechanism between sodium carbonate in the presence of excess sulphuric acid is:

$$CO_3^{2-} + 2H_2SO_4 \text{ -----> } 2HSO_4 + H^+ + HCO_3^- \quad \text{(Instantaneous)} \quad 7.1$$

$$H^+ + HCO_3^- \text{ -----> } H_2O + CO_2 \quad 7.2$$

The reaction in 7.1 is fast and in the presence of excess acid, the reaction is assumed to be a first order reaction with respect to the limiting reactant concentration (Na_2CO_3). Sharma and Danckwerts (148) studied the catalysis by Bronsted bases of the reaction between carbon dioxide and water and suggested that carbon dioxide will undergo a pseudo first order reaction with a rate constant of about Ø.6 sec^{-1}.

ASSUMPTIONS USED IN THE MODEL :-
FIRST ORDER REACTION WITH RESPECT TO:
LIMITING REACTANT CONCENTRATION
NO CHANGE IN VOLUME (I.E. CONSTANT DENSITY)
ISOTHERMAL CONDITION (I.E. CONSTANT TEMPERATURE)
REACTION RATE CONSTANT :0.6 (SEC)-1
NO ACCUMULATION
STEADY STATE OPERATION

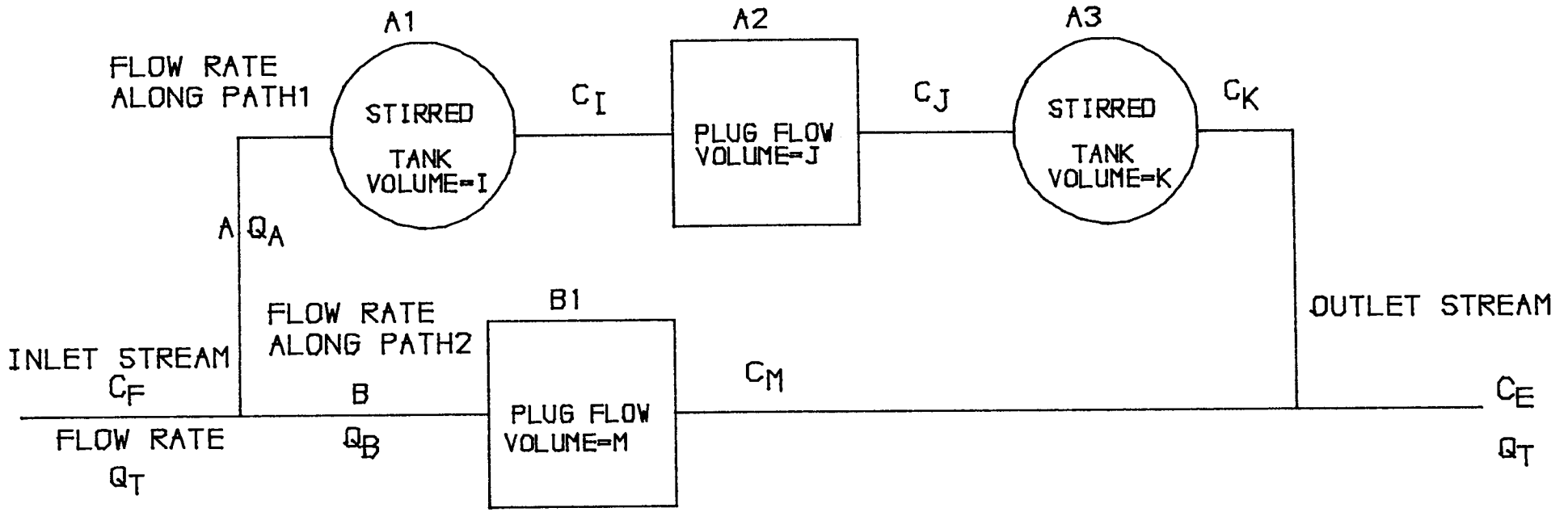

FIGURE 7.1 PROPOSED NOZZLE REACTOR MODEL

FOR FAST REACTION KINETICS

The parameters from the RTD simulation were used in the design calculation, and the nozzle reactor was assummed to be a closed system. Other assumptions used were:-

Isothermal condition (i.e. constant temperature)

No change in volume (i.e. constant density)

No accumulation

Steady state operation.

7.1.1 DERIVATION OF THE MATHEMATICAL MODEL FOR THE REACTION KINETICS

Material Balances:

Input = Output + Disappearance by reaction + Accumulation

7.3

Volume of the nozzle reactor = V_T

Total feed rate = Q_T

Mean residence time $\bar{t} = \frac{V_T}{Q_T}$

From the flow network using the RTD parameters,

A , B : the ratio of the flow in streams A and B.

I fraction by volume in C.S.T.R. A1

J " " " " Plug Flow A2

K " " " " C.S.T.R. A3

M " " " " Plug Flow B1

q_A , q_B - the flow rates in streams A and B respectively.

In stream A

C.S.T.R. A1

Volume of C.S.T.R. A1 $V_I = I \times V_T$ 7.4

Flow rate along C.S.T.R. $q_A = A \times Q_T$ 7.5

Mean residence time in C.S.T.R. A1

$$t_I = \frac{V_I}{q_A} \quad 7.6$$

Disappearance by chemical reaction

$$(-r) = kC \quad 7.7$$

From equ. 7.3

$$q_A C_F = q_A C_I + (-r)V_I \quad 7.8$$

substituting equ. 7.7 in equ. 7.8

$$q_A C_F = q_A C_I + kC_I V_I \quad 7.9$$

$$C_F = C_I + kt_I C_I \quad 7.10$$

Therefore $$C_I = \frac{C_F}{1 + kt_I} \quad 7.11$$

Hence, the exit concentration C_I from C.S.T.R. A1 forms an input concentration to plug flow A2.

Plug flow A2

Volume of plug flow A2 $V_J = J \times V_T$ 7.12

Flow rate along plug flow A2 = q_A

Mean residence time $$t_J = \frac{V_J}{q_A} \quad 7.13$$

hence the design equation for plug flow A2 with C_I as input concentration and C_J as output concentration is:

$$\frac{V_J}{q_A} = -\int_{C_I}^{C_J} \frac{dC}{(-r)} \qquad 7.14$$

substituting equ. 7.7 in equ. 7.14

$$\frac{V_J}{q_A} = -\int_{C_I}^{C_J} \frac{dC}{kC} \qquad 7.15$$

Integrating equ. 7.15 and re-arranging

$$kt_J = -\{\ln C\}_{C_I}^{C_J} \qquad 7.16$$

$$= -\{\ln C_J - \ln C_I\} \qquad 7.17$$

$$-kt_J = \ln \frac{C_J}{C_I} \qquad 7.18$$

$$\text{hence} \quad C_J = C_I \exp(-kt_J) \qquad 7.19$$

substituting equ. 7.11 in equ. 7.19

Therefore

$$C_J = \frac{C_F}{1 + kt_I} \exp(-kt_J) \qquad 7.20$$

Hence:

The exit concentration C_j from plug flow A2 forms an input concentration to C.S.T.R. A3

C.S.T.R. A3

Volume of C.S.T.R. A3 $V_K = K \times V_T$ 7.21

Flow rate along C.S.T.R. A3 = q_A

Mean residence time $t_K = \frac{V_K}{q_A}$ 7.22

Material Balance

$$q_A C_J = q_A C_K + (-r) V_K \quad 7.23$$

$$q_A C_J = q_A C_K + kV_K C_K \quad 7.24$$

Dividing equ. 7.24 by q_A and substituting equ. 7.22 in equ. 7.24

$$C_J = C_K + kt_K C_K \quad 7.25$$

Therefore

$$C_K = \frac{C_J}{1 + kt_K} \quad 7.26$$

Hence, substituting equ. 7.2Ø in equ. 7.26

$$C_K = \frac{C_F}{(1 + kt_I)(1 + kt_K)} \exp(-kt_J) \quad 7.27$$

Hence $C_{E1} = C_K$, the exit concentration from stream A

In Stream B

Plug Flow B1

Volume of plug flow B1 $V_M = M \times V_T$ 7.28

Flow rate along plug flow B1 $q_B = B \times Q_T$

7.29

Mean residence time $t_M = \frac{V_M}{q_B}$ 7.30

Hence the design equation for plug flow B1 with feed concentration C_F and exit concentration C_M

$$\frac{V_M}{q_B} = -\int_{C_F}^{C_M} \frac{dC}{(-r)} \qquad 7.31$$

substituting equs. 7.7 and 7.30 in equ. 7.31

$$t_M = -\int_{C_F}^{C_M} \frac{dC}{kC} \qquad 7.32$$

Integrating equ. 7.32 and re -arranging

$$-kt_M = \{\ln C\}_{C_F}^{C_M} \qquad 7.33$$

$$-kt_M = \ln \frac{C_M}{C_F} \qquad 7.34$$

Hence $C_M = C_F \exp(-kt_M)$ 7.35

$C_{E2} = C_M$, the exit concentration from stream B.

Material Balance at the outlet stream

$$q_A C_K + q_B C_M = (q_A + q_B) C_E \qquad 7.36$$

i.e.

$$q_A C_{E1} + q_B C_{E2} = (q_A + q_B) C_E \qquad 7.37$$

where C_E is the exit concentration from the model network.

Hence, the fractional conversion of the limiting reactant converted into product is:

$$X = \frac{C_F - C_E}{C_F} \qquad 7.38$$

or

$$X = 1 - \frac{C_E}{C_F}$$

7.1.2 YIELD OF THE PRODUCT

Denbigh (149) proposed the yield when two reactants A and B mix to form the desired product. In the case where one of the reactants is in excess (H_2SO_4), then the yield of the product C, is calculated relative to the limiting reactant sodium carbonate solution.

Using the stoichiometry : $\alpha A + \beta B = \gamma C + \delta D$ 7.39

Denbigh proposed that the overall yield is

$$\Phi = \frac{\alpha}{\gamma} \left(\frac{C}{A_t}\right) \qquad 7.40$$

(where $\frac{\alpha}{\gamma}$ is the stoichiometric factor)

where (C) is the amount of C formed over the duration of reaction and A_t is the total amount introduced into the system. Hence from the reaction between excess sulphuric acid and sodium carbonate,

$$Na_2CO_3 + 2H_2SO_4 = 2NaHSO_4 + H_2O + CO_2$$

The yield of the product

$$= \frac{1}{2} \frac{C}{A} \qquad 7.41$$

The concentration of the product was obtained by back-titrating it with standardized sodium hydroxide solution.

However, as some unreacted reactant was not recovered during the reaction, the yield was calculated using equ.7.41.

7.2 DESCRIPTION OF EXPERIMENTAL APPARATUS

The experimental apparatus for investigating fast reactions is illustrated in Figure 7.2. The pipe lines were constructed from Polyvinylchloride (PVC) and were connected from the two feed tanks to two Polypropylene Beresford pumps of capacity of 34 x 10^{-3} m^3/ min. and two pressure gauges. The flow rates from the pumps were controlled by two 19.05 mm diameter angle seat valves and metered by two metric type 18S rotameters with stanless steel floats. Two 3 way QVF glass valves were installed in each feed line to divert the flow back to the feed tanks, and a 24 S rotameter metered the effluent. Finally, a water - jet pump was connected via 6.35 mm valve and a flat optical pyrex glass to the top of the reactor.

7.3 EXPERIMENTAL PROCEDURE

Before the start of an experiment, 2 mls of phenolpthalein (1 % solution in propan-2 ol) were added to aqueous solutions of sodium carbonate and sulphuric acid stock tanks respectively. For each experiment, sulphuric acid solution was prepared in large excess concentration in comparison to sodium carbonate solution, and was conducted at an isothermal room condition. The carbonate solution coloured violet - red

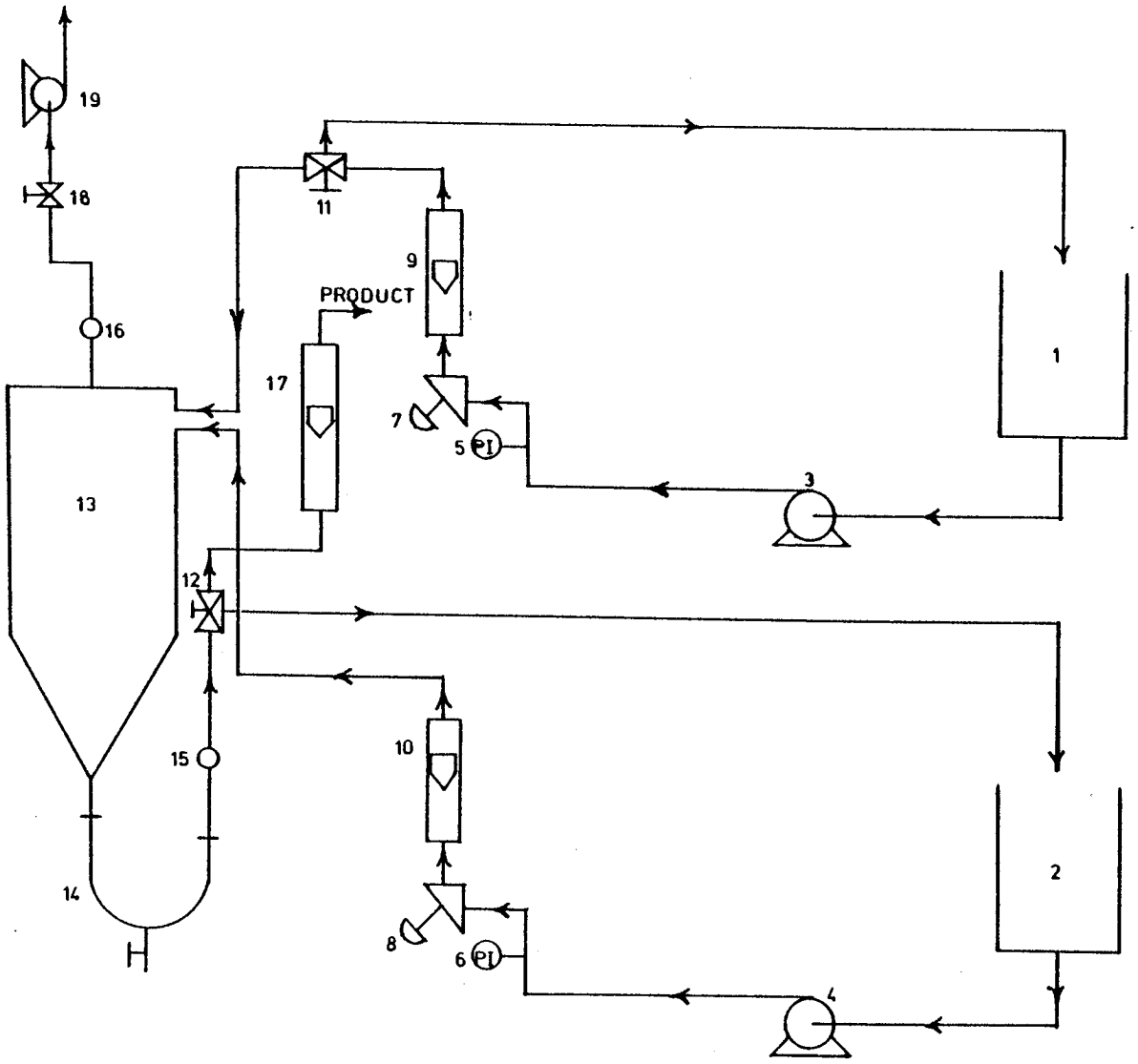

KEY

1,2	20-LITRE GLASS HOLDING TANKS
3,4	POLYPROPYLENE SIZE PV41 BERESFORD PUMPS
5,6	PRESSURE GAUGES
7,8	3/4 INCH DIAMETER ANGLE-SEAT VALVES
9,10	ROTAMETERS WITH STAINLESS STEEL FLOATS SIZE METRIC 18
11,12	3/4 INCH DIAMETER THREE-WAY Q·V·F GLASS VALVES
13	CYLINDRICAL NOZZLE REACTOR
14	1/2 INCH DIAMETER GLASS U-TUBE
15,16	2/5 INCH DIAMETER OPTICAL PYREX GLASS
17	ROTAMETER WITH STAINLESS STEEL FLOAT SIZE METRIC 24
18	1/4 INCH GLOBE VALVE
19	WATER-JET PUMP

FIGURE 7.2 FLOW DIAGRAM OF THE EXPERIMENTAL APPARATUS

and the acid solution remained unchanged by the tracer addition.

At the start of the experiment, the pumps were switched on and the coloured solution of sodium carbonate was pumped into the nozzle reactor. A 3 way QVF glass valve was used to divert the solution from the outlet orifice of the vessel to the feed, ensuring that homogeneity was attained in the feed tank. Another 3 way QVF glass valve in the acid line was also used to divert the flow of acid to the feed tank before entry to the nozzle reactor. The water tap connected to the jet pump was opened to create a vacuum at the top of the vessel.

After a steady state was maintained, the sodium carbonate solution was diverted to the outlet, metered by a 24 S rotameter. At the same time, sulphuric acid solution was introduced to the nozzle reactor. The neutralization reaction was instantaneous and irreversible, with reaction approaching completion within a residence time of a few seconds. The coloured solution in the vessel was decolourized with subsequent effervescence of carbon dioxide gas. A water jet vacuum pump was employed to expel most of the gas concentrated at the centre of the air - core. Although, some product solution was entrained at the top of the vessel, it was assumed negligible in comparison to the product from the outlet orifice.

The product solution was metered by a calibrated 24 S rotameter and a sample was collected in a measuring cylinder for a period of time. The solution was then transferred to a 5ØØ ml glass bottle and a Corning pH 119 meter, at room temperature was used to determine its acidity. The solution was then back - titrated with a standardized solution of sodium hydroxide. The amount of the excess acid used in the neutralization reaction was determined from stoichiometry. The yield of the product was determined analytically, based upon the limiting reactant solution. The fractional conversion of the limiting reactant was established from the proposed model of the RTD studies. Tables 7.1 - 7.6 show results of the neutralization experiments for varying feed molar concentrations and flow rates, using Ø.55 x $1Ø^{-3}$ m^3 and 5.13 x $1Ø^{-3}$ m^3 nozzle reactors respectively.

7.4 CALCULATION OF THE EXCESS SULPHURIC ACID FROM STOICHIOMETRY

Reaction involving excess sulphuric acid and sodium carbonate.

$$Na_2CO_3 + 2H_2SO_4 \text{ -----> } 2NaHSO_4 + H^+ + HCO_3^-$$

$$H^+ + HCO_3^- \text{ -----> } H_2O + CO_2$$

Titration of sodium bisulphate with standardized solution of sodium hydroxide.

$$NaHSO_4 + NaOH \text{ ----> } Na_2SO_4 + H_2O$$

From Stoichiometry:

$$2NaOH + H_2SO_4 = Na_2SO_4 + H_2O$$

i.e 80 gms of NaOH react with 98.08 gms of H_2SO_4

i.e 1000 mls of 1 M NaOH = 49.04 gms of H_2SO_4

or 1000 mls of 0.1 M NaOH = 4.904 gms of H_2SO_4

Hence :

$$\Theta \text{ mls of X M NaOH} = \frac{\Theta \cdot X \cdot 4.9\emptyset4}{1\emptyset\emptyset \cdot \emptyset.1}$$

gms of H_2SO_4

Thus,

If Y mls of product samples = $\frac{\Theta \cdot X \cdot 4.9\emptyset4}{1\emptyset\emptyset}$

gms of H_2SO_4

Therefore ,

$q \times 1\emptyset^{-3}$ m^3/s of " " = $\frac{\Theta \cdot X \cdot \emptyset.\emptyset49\emptyset4 \cdot q}{Y}$

Kg/s of H_2SO_4

X = Ø.1Ø7 and Ø.1Ø84 M NaOH respectively when titrated with Ø.1 M standard hydrochloric acid.

7.5 DISCUSSION OF RESULTS

7.5.1 FLOW VISUALIZATION STUDIES INVOLVING AQUEOUS SULPHURIC ACID AND SODIUM CARBONATE SOLUTIONS IN $\emptyset.55 \times 1\emptyset^{-3}$ M^{-3} NOZZLE VESSEL.

Experimental studies involving fast neutralization reaction between aqueous solutions of sodium carbonate (Na_2CO_3) and sulphuric acid (H_2SO_4) have been conducted in $\emptyset.55 \times 1\emptyset^{-3} m^3$ and $5.13 \times 1\emptyset^{-3} m^3$ nozzle vessels respectively. Table 7.Ø represents fast neutralization reaction at varying flow rates in $\emptyset.55 \times 1\emptyset^{-3} m^3$ nozzle reactor. Plates 7.1 - 7.3 represent each stage of the flow characteristics photographed by an Ashaii Pentax Spotmatic II camera, which reveal stages of the decolourization of the Na_2CO_3 solution by H_2SO_4 solution. Photographs taken during the neutralization reaction are analysed to determine the reaction time between Na_2CO_3 and H_2SO_4 solutions.

At a low flow rate of 4.65 l/min. of the reactants, Plates 7.1 - 7.8 illustrate the various changes in the flow characteristics in the nozzle vessel. Firstly, Plate 7.1 identifies the initial stage in the vessel with complete colourization of Na_2CO_3 by a tracer of phenolpthalein. With steady flow rates of the reactants, Plates 7.2 - 7.8 represent the changes in the flow

7.Ø FAST NEUTRALIZATION REACTION IN Ø.55 x 1Ø$^{-3}$ m^3 NOZZLE REACTOR

PLATE NUMBER	REACTANTS FLOW RATE L/MIN.	REACTION TIME t sec	MEAN RESIDENCE TIME $\bar{t}$ sec	$t/\bar{t}$
7.1	4.65	Ø.Ø	7.Ø97	Ø.ØØØ
7.2	"	1.4	"	1.197
7.3	"	9.8	"	1.381
7.4	"	1Ø.2	"	1.437
7.5	"	11.4	"	1.6Ø6
7.6	"	12.6	"	1.775
7.7	"	14.Ø	"	1.973
7.8	"	15.8	"	2.226
7.9	1Ø.5	Ø.Ø	3.143	Ø.ØØØ
7.1Ø	"	1.6	"	Ø.5Ø9
7.11	"	2.8	"	Ø.891
7.12	"	5.2	"	1.654
7.13	"	6.8	"	2.164

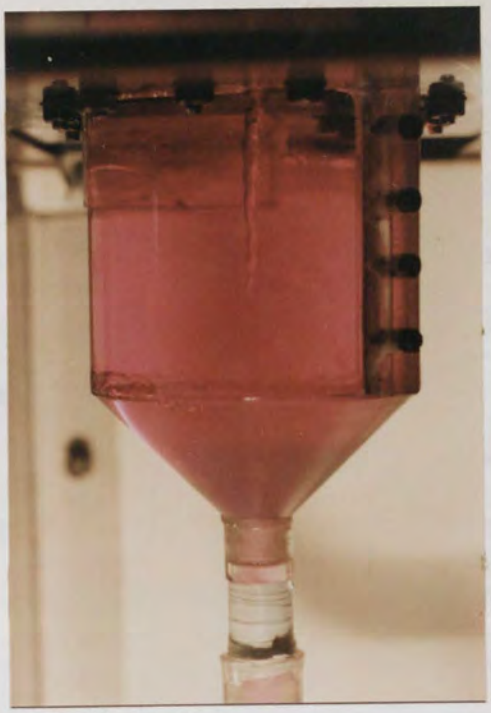

PLATE 7.1

Instantaneous reaction

Ø.Ø sec. before entry

of sulphuric acid solution

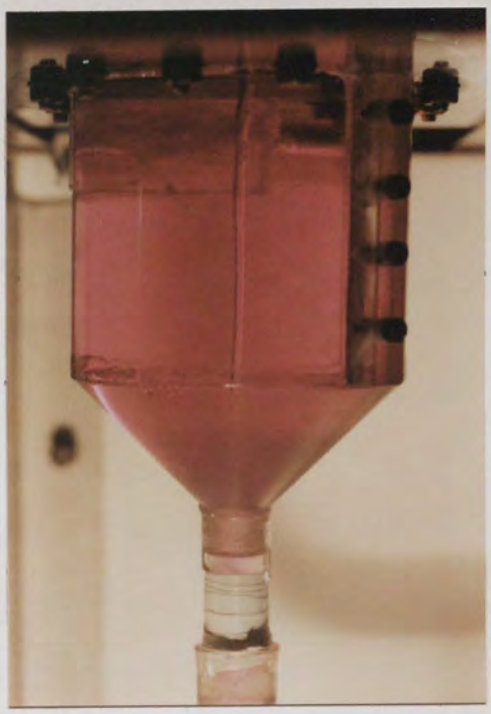

PLATE 7.2

Instantaneous reaction

1.4 secs. after entry

(Re = 82Ø7)

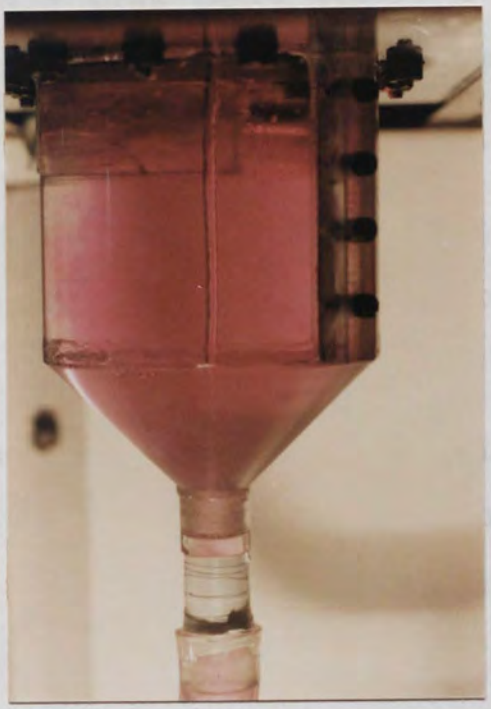

PLATE 7.3

Instantaneous reaction

9.8 secs. after entry

(Re = 82Ø7)

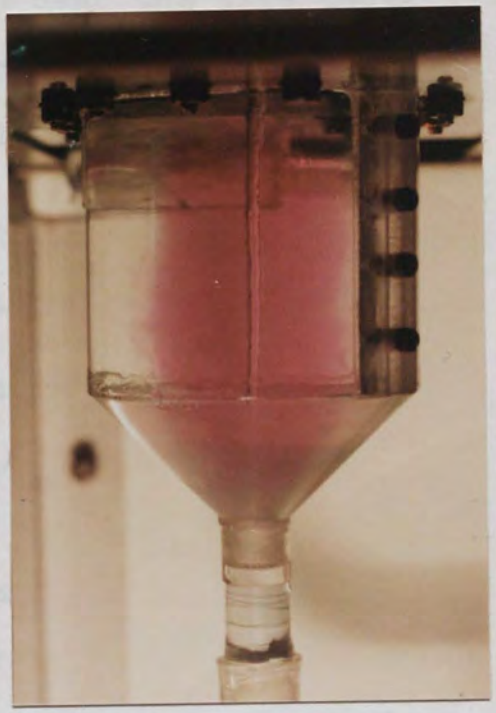

PLATE 7.4

Instantaneous reaction

1Ø.2 secs. after entry

(Re = 82Ø7)

characteristics after the sudden entry of H_2SO_4. In this case, the reaction is instantaneous with complete decolourization of Na_2CO_3 solution by H_2SO_4 solution after 18 seconds.

The hydrodynamics of the fast reaction in the system can be illustrated by the tangential flow of H_2SO_4, which upon entry into the nozzle vessel is converted into radial motion by the action of the centrifugal force which results in the subsequent decolourization of Na_2CO_3 solution around the walls of the vessel (Plates 7.3 - 7.8), before finally reaching the air - core at the centre of the vessel. The photographs on these plates further indicate that there occurs a region near the axis containing H_2SO_4 which has spent more than an average length of time in the nozzle vessel at $\frac{t}{\bar{t}} > 1.0$. As neutralization reaction progresses, photographs on Plates 7.5 - 7.8 illustrate annular regions containing the reactants which have been in the vessel for a period greater than $1.606\bar{t}$. It was noted that Place et al. (18) have earlier realized in a flow of this kind that there existed an upward flow near the cylindrical walls and through a narrow tube enveloping the axis, and a reverse flow, through an annular region between these, which as such represented two zones where the mean velocity is zero.

At higher reactants flow rate of 10.5 l/min. with the coloured Na_2CO_3 already in the system (Plate 7.9), the

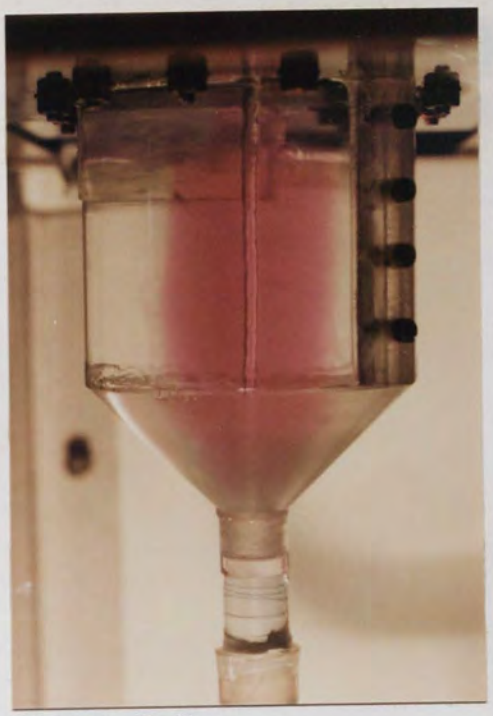

PLATE 7.5

Instantaneous reaction

11.4 secs. after entry

(Re = 82Ø7)

PLATE 7.6

Instantaneous reaction

12.6 secs. after entry

(Re = 82Ø7)

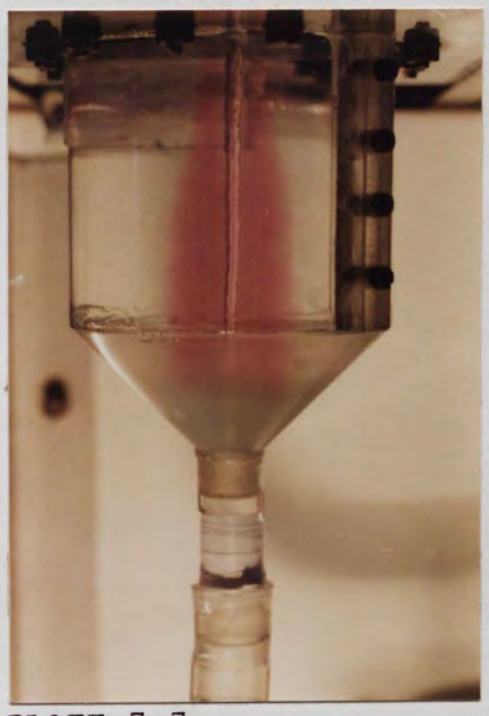

PLATE 7.7

Instantaneous reaction

14.Ø secs. after entry

(Re = 82Ø7)

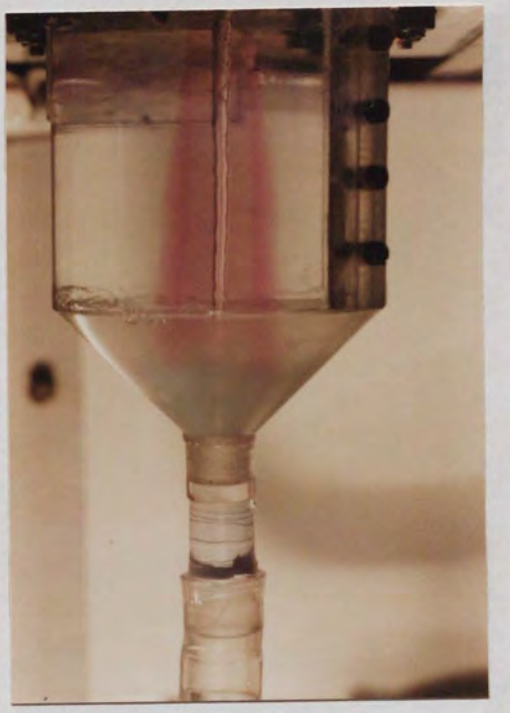

PLATE 7.8

Instantaneous reaction

15.8 secs. after entry

(Re = 82Ø7)

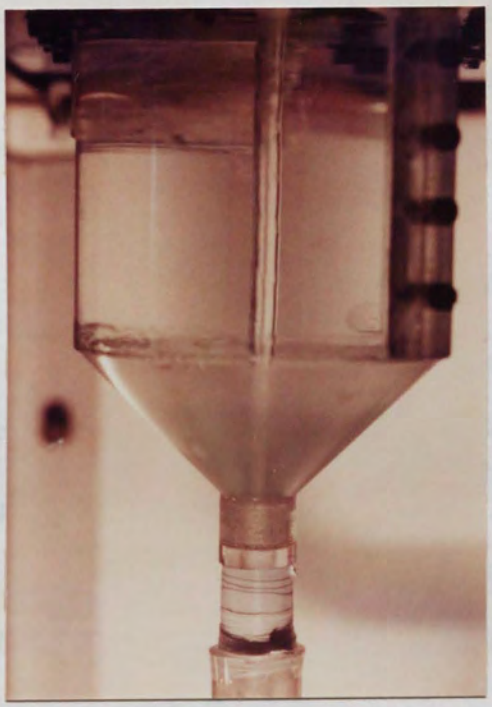

PLATE 7.13

Instantaneous reaction

6.8 secs. after entry (Re = 17472)

neutralization reaction with H_2SO_4 progresses at a faster rate, with clear regions visible at $Ø.5Ø9\bar{t}$ less than the mean residence time of the reactants in the vessel (Plate 7.1Ø). The tangential flow of the feeds, which upon entry is immediately transformed into radial flow by the action of the centrifugal force with faster diffusion of the tracer from the centre surrounding the air - core, to other regions in the vessel. However, in this case, an annular region is formed at a faster rate more than $Ø.891\bar{t}$ (Plate 7.11), and is fully established at $1.654\bar{t}$ (Plate 7.12). The reaction is seen to achieve complete decolourization of Na_2CO_3 at $2.164\bar{t}$ (Plate 7.13).

7.5.2 RESULTS OF THE PROPOSED RTD MODEL

Tables 7.1 - 7.6 show the results of the neutralization reaction in $Ø.55 \times 1Ø^{-3} m^3$ and $5.13 \times 1Ø^{-3} m^3$ nozzle reactors respectively. Tables 7.1 - 7.3 represent the results with varying molar feed concentrations and flow rates in $Ø.55 \times 1Ø^{-3} m^3$ nozzle vessel. The developed model of the RTD incorporating design equations for the CSTR and plug flow is used to evaluate the conversion of the limiting reactant feed (Na_2CO_3); the yield of the product is being determined volumetrically. The results indicate that for varying molar ratios of the reactants, and at increased flow rates; the yield of the product per mole of the limiting reactant increases with increase in the feeds rates. The amount of the excess acid that reacts in the

vessel also increases, although a slight reduction in conversion is obtained with the pH values being more acidic with increased flow rates of the feeds.

Tables 7.4 - 7.6 represent the results of 5.13 x $10^{-3} m^3$ nozzle reactor. In this case, the yield of the product changes slightly with respect to the feed rates; the amount of the acid used in the system is found from stoichiometry to increase, but the conversion decreases sharply with increases in the flow rates of the reactants. The noticeable reduction in conversion, accounts for the phenomena that occur in the system, such as some dead regions, recirculation with reversal of flow of the product in the vessel before the final exit from the outlet.

TABLE 7.1

REACTOR VOLUME = $\emptyset.55 \times 10^{-3}\ m^3$

$C_{Ao}(Na_2CO_3) = \emptyset.025M = 2.6498$ Kg mole/m^3

$C_{Bo}(H_2SO_4) = \emptyset.25M = 24.52$ Kg mole/m^3

H_2SO_4 Flow Rate $10^{-3}\ m^3/s$	Na_2CO_3 Flow Rate $10^{-3}\ m^3/s$	Product $10^{-3}\ m^3/s$	Product sample back titrated with Ø.1Ø7M Sodium Hydroxide		pH	Amount of Acid reacted in the vessel 10^{-3} Kg/s	Fractional Conversion X	Yield of product Kg mole/m^3 per Kg mole/m^3 Na_2CO_3
			Y mls of product	Average Titre (Θ) mls				
Ø.Ø275	Ø.Ø258	Ø.Ø373	15.Ø	12.15	1.17	Ø.1585	Ø.676	1.964
Ø.Ø383	Ø.Ø367	Ø.Ø6ØØ	15.Ø	19.65	Ø.98	Ø.4124	Ø.618	3.175
Ø.Ø5ØØ	Ø.Ø5ØØ	Ø.Ø947	15.Ø	33.12	Ø.78	1.Ø972	Ø.624	5.352
Ø.Ø55Ø	Ø.Ø55Ø	Ø.1Ø83	1Ø.Ø	19.78	Ø.73	1.1241	Ø.6Ø9	4.795
Ø.Ø6Ø8	Ø.Ø6ØØ	Ø.12ØØ	15.Ø	35.55	Ø.74	1.4923	Ø.443	5.745
Ø.Ø692	Ø.Ø667	Ø.1333	1Ø.Ø	24.82	Ø.75	1.7361	Ø.426	6.Ø16
Ø.Ø733	Ø.Ø75Ø	Ø.1398	1Ø.Ø	25.88	Ø.75	1.8985	-	-
Ø.Ø8Ø8	Ø.Ø8Ø8	Ø.16ØØ	1Ø.Ø	26.Ø4	Ø.76	2.1862	-	-
Ø.Ø867	Ø.Ø867	Ø.172Ø	1Ø.Ø	26.48	Ø.73	2.3899	-	-

TABLE 7.2

REACTOR VOLUME = Ø.55 x 10^{-3} m^3

$C_{Ao}(Na_2CO_3)$ = Ø.Ø375M = 2.6498 Kg mole/m^3 ?

$C_{Bo}(H_2SO_4)$ = Ø.25M = 24.52 Kg mole/m^3

H_2SO_4 Flow Rate 10^{-3} m^3/s	Na_2CO_3 Flow Rate 10^{-3} m^3/s	Product 10^{-3} m^3/s	Product sample back titrated with Ø.1Ø84M Sodium Hydroxide: Y mls of product	Average Titre Θ mls	pH	Amount of Acid reacted in the vessel 10^{-3} Kg/s	Fractional Conversion X	Yield of product Kg mole/m^3 per Kg mole/m^3 Na_2CO_3
Ø.Ø267	Ø.Ø258	Ø.Ø453	1Ø.Ø	12.99	1.35	Ø.3128	Ø.677	2.127
Ø.Ø342	Ø.Ø325	Ø.Ø64Ø	1Ø.Ø	15.9Ø	1.27	Ø.54Ø9	Ø.585	2.6Ø4
Ø.Ø392	Ø.Ø433	Ø.Ø82Ø	1Ø.Ø	16.4Ø	1.22	Ø.7149	Ø.611	2.685
Ø.Ø475	Ø.Ø517	Ø.Ø98Ø	1Ø.Ø	18.69	1.Ø8	Ø.9737	Ø.55Ø	3.Ø6Ø
Ø.Ø525	Ø.Ø567	Ø.1Ø67	1Ø.Ø	18.69	Ø.96	1.Ø6Ø1	Ø.617	3.Ø6Ø
Ø.Ø633	Ø.Ø658	Ø.13Ø7	1Ø.Ø	18.4Ø	Ø.94	1.2784	Ø.51Ø	3.Ø1Ø
Ø.Ø75Ø	Ø.Ø75Ø	Ø.15Ø7	1Ø.Ø	17.91	Ø.92	1.4348	-	-
Ø.Ø783	Ø.Ø783	Ø.164Ø	1Ø.Ø	18.89	Ø.91	1.6469	-	-

TABLE 7.3

REACTOR VOLUME = Ø.55 x 10^{-3} m^3

$C_{Ao}(Na_2CO_3)$ = Ø.Ø5M = 5.2995 Kg mole/m^3

$C_{Bo}(H_2SO_4)$ = Ø.25M = 24.52 Kg mole/m^3

H_2SO_4 Flow Rate 10^{-3} m^3/s	Na_2CO_3 Flow Rate 10^{-3} m^3/s	Product Flow Rate 10^{-3} m^3/s	Product sample back titrated with Ø.1Ø84M Sodium Hydroxide: Y mls of product	Average Titre Θ mls	pH	Amount of Acid reacted in the vessel 10^{-3} Kg/s	Fractional Conversion X	Yield of product Kg mole/m^3 per Kg mole/m^3 Na_2CO_3
Ø.Ø25Ø	Ø.Ø233	Ø.Ø44Ø	25.Ø	34.817	3.4Ø	Ø.3257	Ø.678	1.71Ø
Ø.Ø367	Ø.Ø358	Ø.Ø682	25.Ø	42.417	3.39	Ø.6151	Ø.584	2.Ø83
Ø.Ø45Ø	Ø.Ø467	Ø.Ø9Ø7	25.Ø	41.55Ø	3.42	Ø.8Ø13	Ø.584	2.Ø41
Ø.Ø492	Ø.Ø517	Ø.Ø98Ø	25.Ø	41.867	3.32	Ø.8724	Ø.6ØØ	2.Ø56
Ø.Ø55Ø	Ø.Ø583	Ø.112Ø	25.Ø	39.8ØØ	3.28	Ø.9479	Ø.6Ø6	1.955
Ø.Ø658	Ø.Ø7ØØ	Ø.1377	25.Ø	42.633	3.26	1.2483	Ø.5Ø5	2.Ø94
Ø.Ø783	Ø.Ø8ØØ	Ø.1613	25.Ø	43.517	3.31	1.4925	-	-

TABLE 7.4

REACTOR VOLUME = 5.13 x 10^{-3} m^3

$C_{Ao}(Na_2CO_3)$ = Ø.Ø25M= 2.6498 Kg mole/m^3

$C_{Bo}(H_2SO_4)$ = Ø.25M = 24.52 Kg mole/m^3

H_2SO_4 Flow Rate 10^{-3} m^3/s	Na_2CO_3 Flow Rate 10^{-3} m^3/s	Product Flow Rate 10^{-3} m^3/s	Product sample back titrated with Ø.1Ø84M Sodium Hydroxide: Y mls of product	Average Titre (Θ) mls	pH	Amount of Acid reacted in the vessel 10^{-3} Kg/s	Fractional Conversion X	Yield of product Kg mole/m^3 per Kg mole/m^3 Na_2CO_3
Ø.Ø267	Ø.Ø225	Ø.Ø438	25.Ø	18.6Ø	1.5Ø	Ø.1732	Ø.795	1.826
Ø.Ø375	Ø.Ø367	Ø.Ø683	25.Ø	16.9Ø	1.43	Ø.2454	Ø.738	1.661
Ø.Ø5ØØ	Ø.Ø5ØØ	Ø.Ø9ØØ	25.Ø	1Ø.18	1.62	Ø.1948	Ø.62Ø	Ø.999
Ø.Ø6Ø8	Ø.Ø667	Ø.1267	25.Ø	6.33	1.82	Ø.17Ø5	Ø.394	Ø.621
Ø.Ø75Ø	Ø.Ø758	Ø.1597	25.Ø	11.52	1.55	Ø.3692	Ø.37Ø	1.133
Ø.Ø867	Ø.Ø892	Ø.1787	25.Ø	2Ø.15	1.31	Ø.7657	Ø.397	1.98Ø
Ø.1Ø17	Ø.1Ø17	Ø.196Ø	25.Ø	25.88	1.18	1.Ø786	Ø.4Ø2	3.542
Ø.1192	Ø.1167	Ø.2267	25.Ø	16.15	1.38	Ø.7785	-	-
Ø.1292	Ø.125Ø	Ø.2387	25.Ø	29.93	1.18	1.5191	-	-

TABLE 7.5

REACTOR VOLUME = 5.13 x 10^{-3} m^3

$C_{Ao}(Na_2CO_3)$ =Ø.Ø375M= 3.9746 Kg mole/m^3

$C_{Bo}(H_2SO_4)$ = Ø.25M = 24.52 Kg mole/m^3

H_2SO_4 Flow Rate 10^{-3} m^3/s	Na_2CO_3 Flow Rate 10^{-3} m^3/s	Product Flow Rate 10^{-3} m^3/s	Product sample back titrated with Ø.1Ø84M Sodium Hydroxide: Y mls of product	Average Titre Θ mls	pH	Amount of Acid reacted in the vessel 10^{-3} Kg/s	Fractional Conversion X	Yield of product Kg mole/m^3 per Kg mole/m^3 Na_2CO_3
Ø.Ø3ØØ	Ø.Ø275	Ø.Ø493	25.Ø	5.63	2.Ø2	Ø.Ø59Ø	Ø.7Ø3	Ø.369
Ø.Ø367	Ø.Ø35Ø	Ø.Ø677	25.Ø	1Ø.97	1.77	Ø.1579	Ø.74Ø	Ø.719
Ø.Ø467	Ø.Ø483	Ø.Ø96Ø	25.Ø	9.96	1.79	Ø.2Ø33	Ø.623	Ø.652
Ø.Ø6ØØ	Ø.Ø6ØØ	Ø.1173	25.Ø	17.7Ø	1.61	Ø.4415	Ø.395	1.158
Ø.Ø7Ø8	Ø.Ø725	Ø.14ØØ	25.Ø	2Ø.1Ø	1.53	Ø.5984	Ø.386	1.317
Ø.Ø917	Ø.Ø892	Ø.1893	25.Ø	14.39	1.6Ø	Ø.5792	Ø.396	Ø.942
Ø.1Ø83	Ø.1Ø67	Ø.2Ø93	25.Ø	3Ø.Ø4	1.35	1.3369	Ø.393	1.968
Ø.1175	Ø.1167	Ø.2373	25.Ø	15.68	1.5Ø	Ø.7912	-	-

TABLE 7.6

REACTOR VOLUME = 5.13 x 10^{-3} m^3

$C_{Ao}(Na_2CO_3)$ = Ø.Ø5M = 5.2995 Kg mole/m^3

$C_{Bo}(H_2SO_4)$ = Ø.25M = 24.52 Kg mole/m^3

H_2SO_4 Flow Rate 10^{-3} m^3/s	Na_2CO_3 Flow Rate 10^{-3} m^3/s	Product 10^{-3} m^3/s	Product sample back titrated with Ø.1Ø84M Sodium Hydroxide		pH	Amount of Acid reacted in the vessel 10^{-3} Kg/s	Fractional Conversion X	Yield of product Kg mole/m^3 per Kg mole/m^3 Na_2CO_3
			Y mls of product	Average Titre Θ mls				
Ø.Ø275	Ø.Ø275	Ø.Ø393	25.Ø	8.96	1.9Ø	Ø.Ø749	Ø.751	Ø.441
Ø.Ø342	Ø.Ø35Ø	Ø.Ø527	25.Ø	11.14	1.84	Ø.1248	Ø.741	Ø.547
Ø.Ø483	Ø.Ø45Ø	Ø.Ø897	25.Ø	15.47	1.67	Ø.2951	Ø.621	Ø.76Ø
Ø.Ø542	Ø.Ø542	Ø.1Ø53	25.Ø	6.47	1.98	Ø.1449	Ø.617	Ø.318
Ø.Ø658	Ø.Ø667	Ø.128Ø	25.Ø	7.68	1.96	Ø.2Ø9Ø	Ø.383	Ø.377
Ø.Ø8Ø8	Ø.Ø8ØØ	Ø.16ØØ	25.Ø	15.58	1.65	Ø.53Ø1	Ø.398	Ø.766
Ø.1Ø25	Ø.1Ø17	Ø.1947	25.Ø	17.32	1.6Ø	Ø.7171	Ø.4Ø3	Ø.851
Ø.1192	Ø.1183	Ø.2373	25.Ø	14.Ø2	1.64	Ø.7Ø74	-	-

7.6 COMPARISONS WITH OTHER EXPERIMENTAL TECHNIQUES

From the studies and model formulations as reported in the literature (Chapter two); to the author's knowledge, no study as described in this thesis has been undertaken to determine the RTD in novel cylindrical nozzle vessels. The only study pertaining to a similar geometrically shape vessels (128), involved the use of a step input of a tracer into the system with the effluent concentration determined by a conductivity bridge meter. In this case, a tank in series model with a delay was formulated to simulate the cumulative RTD profiles. However, RTD studies in other related flow systems have been well documented.

Clegg and Coates (111) have developed a flow model for a jet stirred cylindrical vessel, and was based upon their observations from a flow visualization studies. They employed a cylindrical vessel of 29.21 mm internal diameter and 30.48 mm high, and with an inlet and outlet nozzles offset from the axis. A pulse reponse technique was applied and from observation of simple entrainment and back flow theory; they correlated their results by means of a tank in series model.

Sinclair and Mc Naughton (131) on the other hand studied the RTD in jet stirred cylindrical vessels with length to diameter ratios of 1:1, 2:1, 3:1 respectively, with axial inlet and outlet nozzles. In their investigation they used an absorptiometer to record the effluent

and proposed a model similar to Cholette and Cloutier's 4C model (148). They elucidated that the jet region could be identified with a perfectly mixed section as the size of eddies relative to the size of the jet region increases and the backflow region with a pure plug flow.

Moeller and Dealy (112) investigated backmixing in a cylindrical confined jet and the RTDs were determined by monitoring the concentration in the outlet stream of a tracer which was injected into the primary jet by a conductivity probe. In their study, they formulated a mixed model comprising of a plug flow tube and a CSTR. They concluded from their work that the recirculation eddy was more effective in the mixing process for lower values of Craya - Curtet number. As such, an increase in the recirculation rate in the eddy resulted in a corresponding increase in the amount of the dead space in the confined jet, which in turn caused the mixedness of the fluid in the system to increase.

Lastly, Bradley and Pulling (10) have limited their research to the study of flow characteristics in hydraulic cyclones and the phenomena as observed in this thesis, namely the existence of reverse flow, a stationary annular layer and clear regions along the walls were confirmed.

CHAPTER EIGHT

CHEMISTRY OF SULPHONATION
NEUTRALIZATION REACTION INVOLVING
DODECYLBENZENE SULPHONIC ACID
AND
AQUEOUS SOLUTION OF SODIUM CARBONATE

8.1 INTRODUCTION

Soaps which have been used for domestic and industrial purposes for many centuries are primarily the salts of fatty acids, derived from natural oils and fats, and are thus produced by saponification with alkalis, usually sodium hydroxide. As the price and availability of natural oils and fats varies unpredictably, coupled with the formation of undesirable scum which is often produced when used in hard water; an increasing need for an alternative source such as synthetic detergents was sought.

Detergents or synthetic surfactants have now been considered and used as alternatives to soap, as they are cheap and are readily available from petrochemical raw materials. The primary actions of a detergent are mainly,

(i) to detach the dirt from the surface to be cleaned and either,

(ii) to disperse or dissolve the dirt in the wash liquor such that the cleaned substrate can be separated from the wash liquor without the dirt being redeposited on it. The major activity to the above requirements is the nature of the interfaces between the substrate, the dirt and the wash liquor. As such, a formulated detergent system acts by modifying the properties of these interfaces, thus altering the energy of the interactions between the dirt and the substrate.

To achieve this, the detergent formulation must contain materials that are adsorbed at these interfaces, i.e. it must contain surface active molecules. These are termed surfactants and can be represented by a general formula RX, where R is a hydrophobic tail group and X is a hydrophilic head group, such as COO^-. However, depending on the nature of R and X, such molecules may be either water - soluble or oil - soluble and the balance between the hydrophobic and hydrophilic groups largely determines the detergent properties (150).

The oil - soluble grouping is provided by a long and straight chain hydrocarbon of adequate length to achieve the required oil solubility, i.e. from C_8 to C_{18}. On the other hand, the water - soluble group can be provided by a variety of groups, e.g. sulphate, sulphonate, carboxylate and hydroxyl groups. The first three are capable of undergoing ionization in aqueous solutions to give an oil - soluble anion, whilst the metallic cations remain in the aqueous phase. These are termed anionic detergents, and sodium dodecylbenzene sulphonates are in this class of detergents.

8.2 MECHANISM OF REACTION

The principal aromatic chemicals used in the synthesis of anionic surfactants are benzene (C_6H_6) and phenol (C_6H_5OH). The former is often used since it can readily be converted to alkylbenzenes which are intermediates converted by sulphonation to alkylbenzene sulphonic acids. Monoalkyl benzenes in which the side chain contains about C_{10}- C_{15} are commonly referred to as detergent alkylates. However, two types of detergent alkylates have been employed as raw materials for the production of anionic surfactants by further processing to alkyl arlysulphonates. The older, branched - chain type which has ceased is referred to as 'hard detergent alkylate'. This branch gives persistent foam which is caused by the lack of biodegradation of its alkylbenzene sulphonate derivative (ABS) in sewage, disposal systems, rivers and streams.

An alternative to ABS, are alkylbenzene sulphonates produced from the recent biodegradable "linear detergent alkylates" (LAB or soft detergent alkylates) and as such are biologically soft. An olefin such as propylene is polymerized from the catalytic cracking process, composed of about 30 - 50% propylene mixed with 50 - 70% propane and other light hydrocarbons (151).

$$\underset{\text{Propylene}}{C_3H_6} \xrightarrow[\text{catalyst}]{\text{Polymerized}} \underset{\substack{\text{Dedecene}\\(\text{Propylene}\\\text{tetramer})}}{C_{12}H_{24}} \text{ and } \underset{\substack{\text{Pentadecene}\\(\text{Propylene}\\\text{pentamer})}}{C_{15}H_{30}} \qquad 8.1$$

The alkylation process is the addition of benzene across the double bond of the olefin (tetramer or tetrapentamer) in the presence of aluminium chloride ($AlCl_3$) or hydrogen fluoride (HF) as catalyst.

$$C_{12}H_{24} \text{ or } C_{15}H_{30} + \underset{\text{Benzene}}{C_6H_6} \xrightarrow{AlCl_3 \text{ or } HF} \underset{\substack{\text{Tetramer - type}\\ \text{Dodecylbenzene}}}{C_{12}H_{25}.C_6H_5} \text{ or } \underset{\substack{\text{Pentamer - type}\\ \text{Pentadecylbenzene}}}{C_{15}H_{31}.C_6H_5}$$

8.2

Alkylbenzenes are sulphonated with oleum (usually 20% SO_3), 100% sulphuric acid or anhydrous sulphur trioxide to give a greater than 95% yield of the sulphonate.

$$\underset{\text{Dodecylbenzene}}{C_{12}H_{25}.C_6H_5} + H_2SO_4 \longrightarrow \underset{\substack{\text{Dodecylbenzene}\\ \text{sulphonic acid}\\ \text{(Dobane JN)}}}{C_{12}H_{25}.C_6H_4.SO_3H} + H_2O$$

8.3

The sulphonic acid is usually neutralized with aqueous alkali to give a slurry containing 40 - 55% of sodium dodecylbenzene sulphonate and 5 - 6% of sodium sulphate (Na_2SO_4), the mixture being suitable for processing into the majority of finished detergent products.

$$C_{12}H_{25}\cdot C_6H_4SO_3H + NaOH \longrightarrow C_{12}H_{25}\cdot C_6H_4SO_3Na + H_2O$$

Sodium dodecylbenzene sulphonate

8.4

However, Na_2CO_3 is a common ingredient of soaps and detergent powders. Sometimes, it is used in relatively small quantities for pH adjustment, sometimes in larger amounts to give a desired alkalinity to the product and at other times, is used as a filler.

The reaction mechanism involving aqueous solution of Na_2CO_3 and dodecylbezene sulphonic acid (Dobane JN) is:

$$2C_{12}H_{25}\cdot C_6H_4SO_3H + Na_2CO_3 \xrightarrow{Fast} 2C_{12}H_{25}\cdot C_6H_4SO_3Na + H_2O + CO_2\uparrow \qquad 8.5$$

8.3 EXPERIMENTAL PROGRAMME

Dodecylbenzene sulphonic acid (Dobane JN) used in the investigation of neutralization reaction with aqueous sodium carbonate was obtained from Unilever Research. The principal compositions are:

(i) 97% (w/w) Linear alkylate

(ii) 2% (w/w) Inorganic and organic matter

(iii) 1% (w/w) Sulphuric acid.

The pH of Dobane JN was determined experimentally, using Rotovisco, RV 12, Haake viscometer.

pH = 1.34

Dobane JN was calibrated via an 18S rotameter with a stainless steel float along its process line. This assures that the actual flow rate of Dobane JN entering the nozzle vessel can correctly be ascertained.

The supplied Dobane JN is hygroscopic and highly acidic darkbrown viscous liquid. As such, its viscosity was determined experimentally and is 167Ø.7Ø mPa.s (16.7Ø7 poise). Since the PV 41 Beresford pump in the feed line was unable to cope with its viscous state, an organic solvent 111 Trichloroethane was employed to adjust its viscosity to a reasonable state for it to be pumped. The graphs of the viscosity are shown in Appendix D.

8.3.1 REACTION PROCEDURE

Linear alkylbenzene sulphonic acid (Dobane JN) supplied by Unilever with a viscosity of 167Ø.7 mPa.s (16.7Ø7 poise) and a pH value of 1.34, was first diluted with 97%

(w/w) 111 Trichloroethane to reduce its viscosity to the permissible level for the Polypropylene PV 41 Beresford pump in the feed line. The stock tanks were filled with Dobane JN and Ø.5 M sodium carbonate solution. Before the neutralization reaction of Dobane JN with Na_2CO_3 in the nozzle vessel; the carbonate solution was pumped into the nozzle reactor. A 3 way QVF glass valve was used to divert the solution from the outlet orifice of the vessel back to the stock tank. The Dobane JN in the second stock tank was stirred with a paddle stirrer and another 3 way QVF glass valve in the feed line was employed to divert the flow of Dobane JN to the feed tank before entry to the nozzle vessel. The process of recycling the reactants to their respective stock tanks was to ensure that homogeneity was attained. The water tap connected to the jet pump was opened to create a vacuum at the top of the vessel.

After a steady state was maintained, the sodium carbonate solution was diverted to the outlet. At the same instance, Dobane JN was introduced to the vessel. The neutralization reaction was very rapid as the dark viscous liquid reacted with Na_2CO_3 in the nozzle vessel to form a product of sodium dodecylbenzene sulphonate (ABS), which is a creamy - white slurry. A water jet vacuum pump was employed to expel most of the carbon dioxide bubbles that were formed at the centre of the air - core. Although, some product was entrained along with the foam

formed at the top of the vessel, it was assumed negligible in comparison to the product collected from the outlet orifice. The ABS was collected in a bucket, then transferred to a 500 ml glass bottle. A Corning pH 119 meter at room temperature was used to determine its alkalinity. Further experiments were carried out for varying flow rates of the reactants and at an increased viscosity of Dobane JN. Analytical test was then performed on each product sample to determine the percentage of the anionic detergent present in the product.

Before the start of analytical test, the milky product for each run was centrifuged in a CU 5000 basket centrifuge at 1500 r.p.m. for 15 minutes. Sedimentation of the product with a clear liquid at the top was attained after this period. 10 gms of each product sample was weighed and Hyamine test was conducted to evaluate the percentage of the anionic detergent present in the product. Photographs of the representative samples are shown in Plates 8.1 - 8.3.

8.4 CHEMICAL ANALYSIS

The product samples obtained at different reaction parameters and conditions were analysed to determine the percentages of the active detergent and sodium sulphate present in the product.

The method adopted for analysis of the active detergent was obtained from Unilever Research Laboratory and from Heinerth (152). That of sodium sulphate

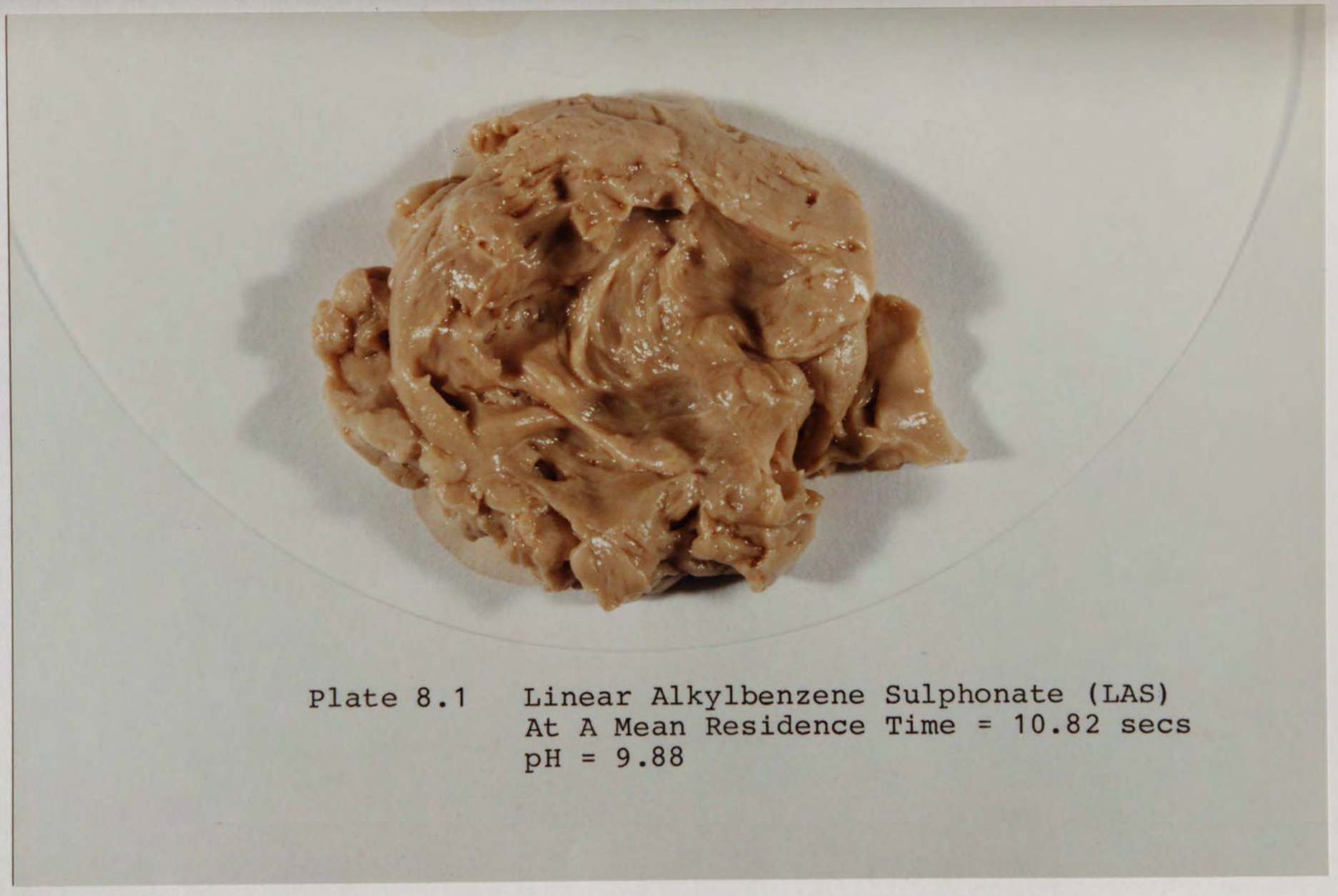

Plate 8.1 Linear Alkylbenzene Sulphonate (LAS)
At A Mean Residence Time = 10.82 secs
pH = 9.88

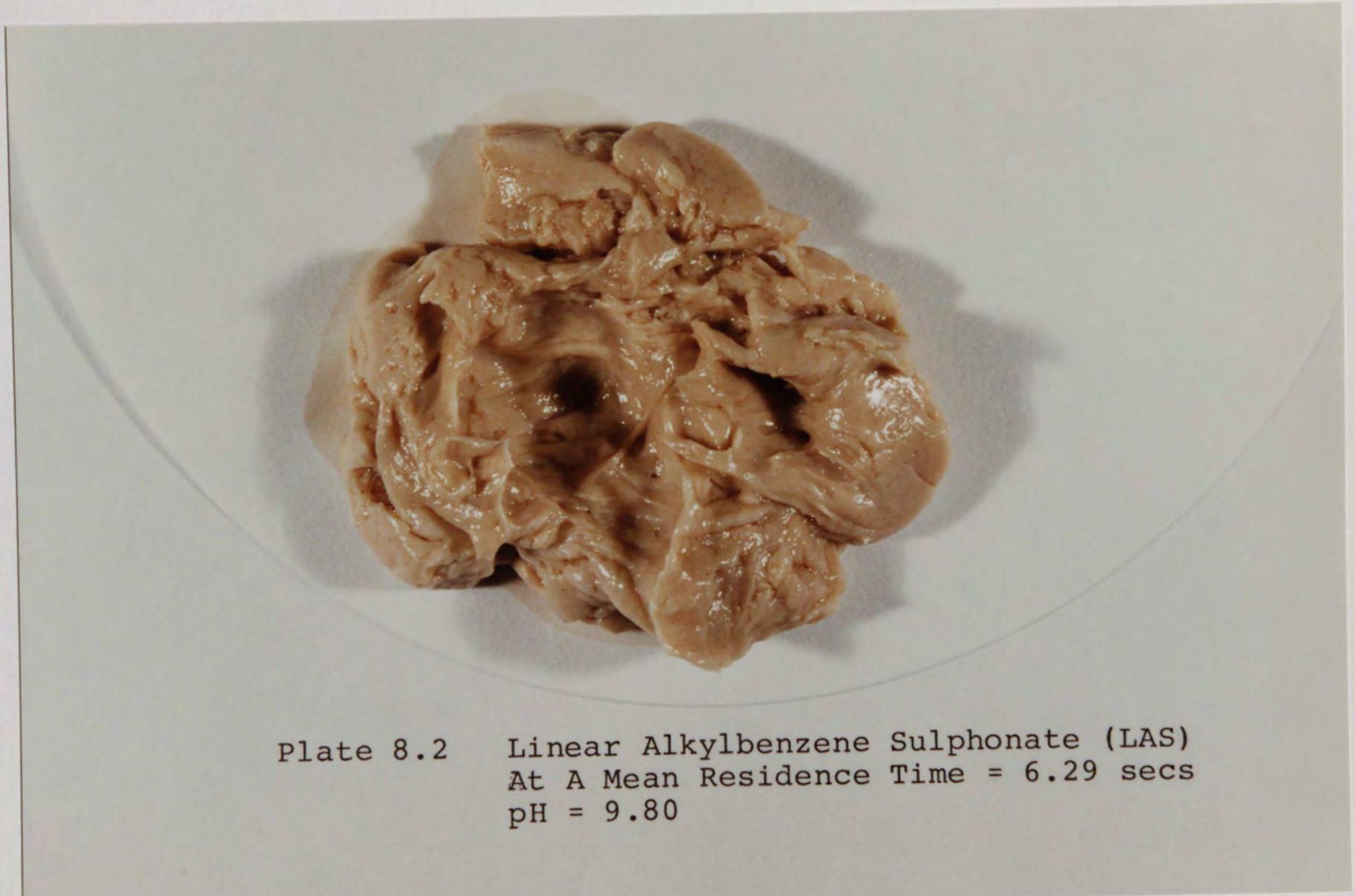

Plate 8.2 Linear Alkylbenzene Sulphonate (LAS)
At A Mean Residence Time = 6.29 secs
pH = 9.80

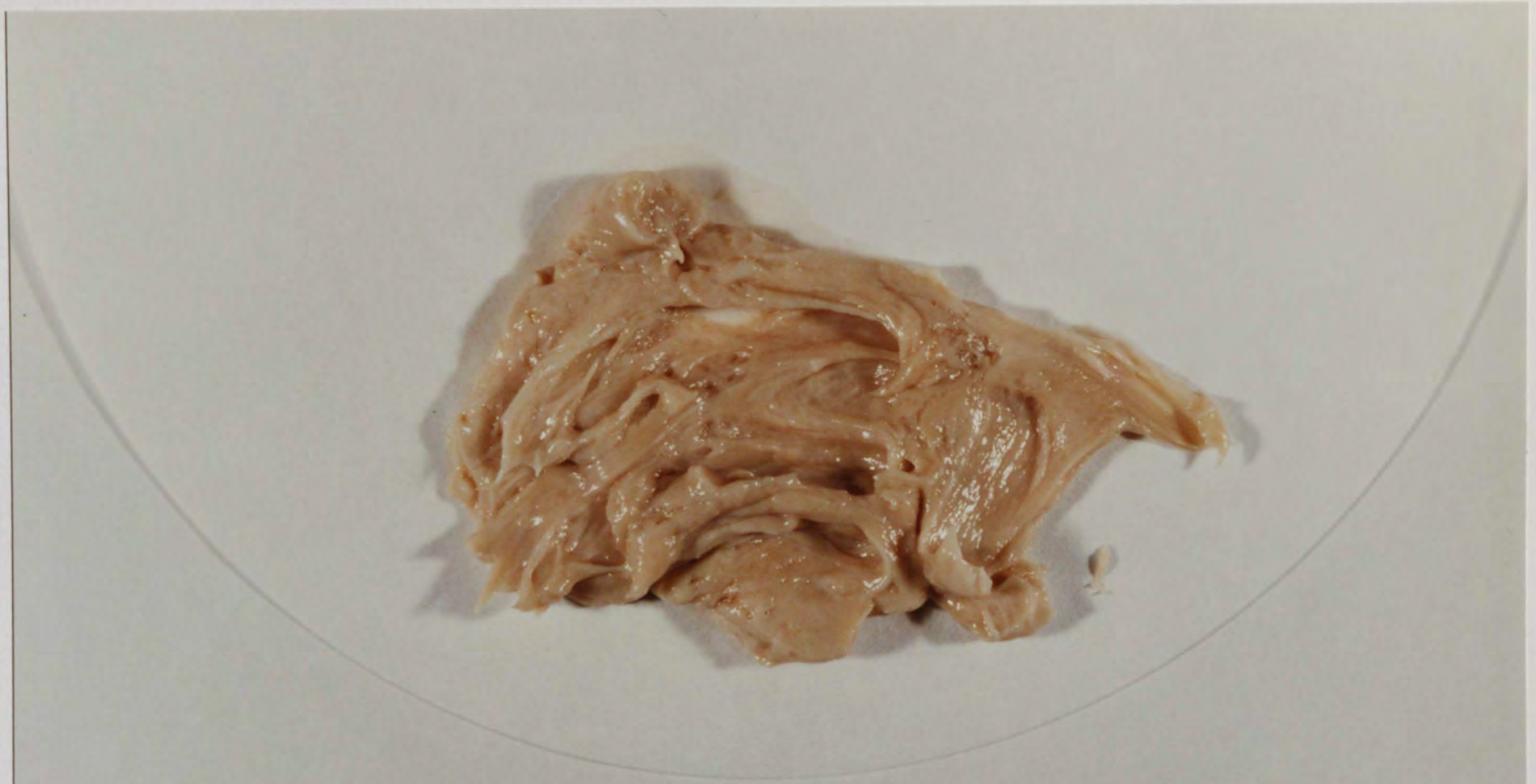

Plate 8.3 Linear Alkylbenzene Sulphonate (LAS)
At A Mean Residence Time = 3.25 secs
pH = 9.44

determination was obtained from Grant (153) and from Milwidsky and Gabriel (154).

8.4.1 DETERMINATION OF THE ACTIVE DETERGENT

An aqueous solution of the sample is titrated with a standard cationic active solution (Hyamine 1622) in a two phase water - chloroform system using a mixture of a cationic dye (dimidium bromide) and an anionic dye (disulphone blue V) as indicator. The anionic surfactant forms a salt with cationic dye which dissolves in the chloroform layer and colours it red - pink. The end point is attained when the Hyamine cation displaces the dimidium cation from the chloroform soluble salt and the pink colour leaves the chloroform layer as the dye passes to the aqueous phase. The pink colour is completely discharged from the chloroform layer which is then a faint greyish - blue. Hyamine added in excess forms a salt with the anionic dye disulphine blue V which dissolves in the chloroform layer and colours it blue.

Hyamine 1622 solution (Ø.ØØ4 M) and mixed indicator stock solution are supplied by BDH Chemicals. Acid indicator solution is prepared from the mixed indicator stock solution. 2ØØ mls of distilled water and 2Ø mls mixed indicator stock solution are mixed in a 5ØØ ml graduated flask. After adding 2Ø mls 5 N sulphuric acid, the mixture is diluted with distilled water to 5ØØ ml. This is then stored in an amber bottle.

THE PROCEDURE IS AS FOLLOWS:-

Approximately 10 gms of sample are weighed and placed in a 250 ml beaker. The sample is then dissolved in 150 mls of distilled water by warming in a water bath. The dissolved sample is then transferred to a 1000 ml standard volumetric flask (SVF) and diluted. Any foam occurring in the neck of the SVF is destroyed by adding few drops of ethanol. The solution is diluted up to the level with distilled water and mixed thoroughly. 10 mls of the titrand solution is transferred to a 100 ml measuring cylinder with a stopper. After adding 10 mls of the acid indicator solution and 15 mls of chloroform, the mixture is then titrated with 0.004 M Hyamine 1622 (titrant) solution until a faint greyish blue colour is formed in the chloroform phase. The titration is performed by shaking the titration vessel vigorously each time after adding 0.5 ml of the titrant.

The calculation to determine the percentage of active detergent is as follows:-

Let:

Weight (gm) of the sample	W
Molarity of Hyamine 1622 solution	M
Volume (ml) of Hyamine 1622 consumed	V
Molecular weight of anionic - active matter	MW

Then: Anionic Active Detergent (wt %) =

$$\frac{V \cdot M \cdot MW \cdot 100}{1000 \cdot W}$$

$$= \frac{V \cdot M \cdot MW}{10 \cdot W} \text{ wt \%}$$

where the values of M and MW and W are Ø.ØØ4, 348 and 1Ø respectively.

$$\% \text{ AD} = Ø.Ø1392 \cdot V$$

8.4.2 DETERMINATION OF SODIUM SULPHATE

A 25 ml of the titrand solution is added to 1ØØ mls of dry acetone in a 25Ø ml conical flask. An electrode of a pH meter is placed into the solution. Dilute acetic acid solution is then added to reduce the pH to a range of 4.1 to 4.3 (this range is selected to prevent hydrolysis of organic sulphates), taking care not to exceed these limits. 2 mls of a Ø.1 w/v % solution of dithizone in acetone is added. This acidified solution is then titrated with Ø.ØØ2 N (Ø.ØØ1 M) lead nitrate solution, until the green colour of the dithizone changes to the first permanent orange - red colour of lead dithizonate.

The calculation to determine the percentage of Na_2SO_4 is as follows: -

$$\% \text{ inorganic sulphate} = \frac{v \cdot (E + 48)}{125}$$

where v = volume of Ø.Ø2 N (Ø.Ø1 M) lead nitrate solution used (ml).

E = equivalent weight of the cation,

Na = 23 NH_4 = 17 e.t.c.

From the analytical results, the fractional conversion of Dobane JN to sodium dodecylbenzene sulphonate (ABS) is calculated as follows :-

$$X = \frac{\frac{\%\ AD}{348}}{\frac{\%\ AD}{348} + \frac{\%\ Na_2SO_4}{142}}$$

where 348 = Molecular weight of sodium dodecylbenzene sulphonate (ABS)

142 = Molecular weight of sodium sulphate (Na_2SO_4).

8.5 DISCUSSION OF RESULTS

8.5.1 NEUTRALIZATION REACTION

The results of the reaction between Dodecylbenzene sulphonic acid (Dobane JN) and aqueous Na_2CO_3 are shown in Tables 8.1 - 8.3 . Plates 8.1 - 8.3 reveal the textures of the product, sodium dodecylbenzene sulphonate (ABS) after being centrifuged at different mean residence times and pH values. The results are for different viscosity of Dobanic acid and at varying feed rates of the reactants. The experiments are conducted at room temperature.

It has been noted that the three main steps of the manufacture of sodium dodecylbenzene sulphonate (ABS), namely the alkylation, sulphonation and neutralization are exothermic. The neutralization reaction between Dobane JN and Na_2CO_3 in the nozzle reactor is no exception, with the result that the reaction temperature increased several degrees above the room condition. However, this does not require cooling of the reactor. The products obtained are alkaline, milky - white slurry with an average pH value of 9.Ø5, 9.67, and 8.81 respectively. It has been cited that a similar sulphonic acid with 2Ø - 5Ø% sodium hydroxide (NaOH) solution at 51.7^{o}C yields a pH value of 8.Ø (155). The only inert material in the final product is Na_2SO_4.

Quantitative analyses to determine the percentages of both the active detergent matter and Na_2SO_4 have been carried out as detailed in sections 8.4.1 and 8.4.2

TABLE 8.1

REACTOR VOLUME = Ø.55 x $1Ø^{-3}M^3$
DODECYLBENZENE SULPHONIC ACID
(DOBANE JN) = 97.Ø% (w/w)
Na_2CO_3 = Ø.5 M

VISCOSITY OF DOBANIC ACID WITH 111 TRICHOLOROETHANE = 366.27 mPa.s (cp)
pH OF DOBANIC ACID WITH 111 TRICHOLOROETHANE = Ø.81

SAMPLE NUMBER	DOBANIC ACID JN FLOW RATE	Na_2CO_3 $1Ø^{-3}M^3$	PRODUCT LAS pH	MEAN RESIDENCE TIME $\bar{t}$ secs	% AD	% Na_2SO_4	X
1	Ø.ØØ32	Ø.Ø433	9.71	11.828	45.38	-	-
2	Ø.ØØ76	Ø.Ø6ØØ	9.66	8.2Ø9	48.13	-	-
3	Ø.Ø112	Ø.Ø8Ø8	9.47	5.978	49.28	-	-
4	Ø.Ø15Ø	Ø.Ø967	9.23	4.924	48.65	-	-
5	Ø.Ø2Ø3	Ø.115Ø	7.93	4.Ø65	44.61	-	-
6	Ø.Ø25Ø	Ø.135Ø	8.28	3.438	49.31	-	-

Av = 9.Ø5

TABLE 8.2

REACTOR VOLUME = Ø.55 x $1Ø^{-3}M^3$
DODECYLBENZENE SULPHONIC ACID
(DOBANE JN) = 97.Ø% (w/w)
Na_2CO_3 = Ø.5 M

VISCOSITY OF DOBANIC ACID WITH 111 TRICHOLOROETHANE = 417.68 mPa.s (cp)
pH OF DOBANIC ACID WITH 111 TRICHOLOROETHANE = Ø.75

SAMPLE NUMBER	DOBANIC ACID JN FLOW RATE	Na_2CO_3 $1Ø^{-3}M^3$	PRODUCT LAS pH	MEAN RESIDENCE TIME $\bar{t}$ secs	% AD	% Na_2SO_4	X
1	Ø.ØØ5Ø	Ø.Ø458	9.88	1Ø.827	5Ø.67	Ø.261	98.78
2	Ø.ØØ63	Ø.Ø575	9.61	8.621	48.54	Ø.166	99.15
3	Ø.ØØ98	Ø.Ø775	9.8Ø	6.3ØØ	49.56	Ø.187	99.1Ø
4	Ø.Ø143	Ø.Ø917	9.57	5.189	48.65	Ø.258	98.73
5	Ø.Ø183	Ø.1217	9.69	3.929	49.9Ø	Ø.176	99.1Ø
6	Ø.Ø273	Ø.1417	9.44	3.254	49.53	Ø.125	99.37

Av = 9.67

TABLE 8.3

REACTOR VOLUME = Ø.55 x $1Ø^{-3}M^3$
DODECYLBENZENE SULPHONIC ACID
(DOBANE JN) = 97.Ø% (w/w)
Na_2CO_3 = Ø.5 M

VISCOSITY OF DOBANIC ACID WITH 111 TRICHOLOROETHANE = 591.17 mPa.s (cp)
pH OF DOBANIC ACID WITH 111 TRICHOLOROETHANE = Ø.75

SAMPLE NUMBER	DOBANIC ACID JN FLOW RATE	Na_2CO_3 $1Ø^{-3}M^3$	PRODUCT LAS pH	MEAN RESIDENCE TIME $\bar{t}$ secs	% AD	% Na_2SO_4	X
1	Ø.ØØ43	Ø.Ø392	9.72	12.644	49.38	Ø.135	99.3Ø
2	Ø.ØØ68	Ø.Ø5ØØ	8.76	9.683	48.77	Ø.148	99.29
3	Ø.Ø1Ø3	Ø.Ø675	9.25	7.Ø69	49.14	Ø.17Ø	99.16
4	Ø.Ø135	Ø.Ø758	9.26	6.159	53.28	Ø.1Ø7	99.48
5	Ø.Ø18Ø	Ø.Ø933	9.12	4.942	52.2Ø	Ø.1Ø9	99.47
6	Ø.Ø213	Ø.1125	7.75	4.111	44.68	Ø.115	99.38
7	Ø.Ø267	Ø.1342	7.8Ø	3.418	44.44	Ø.119	99.38

Av = 8.81

respectively. The only comparison of this work in relation to other studies, is that of Dykes (156) and Altiokka (157); who investigated the sulphation of α - olefins (hexadecene) and subsequently analysed the percentages of the active detergent matter and Na_2SO_4 in the same procedure as carried out in this study. The results show higher percentages in the product, active detergent matter in contrast to the results of Dykes and Altiokka. Correspondingly, the percentages of Na_2SO_4 are lower. These relatively low percentages of Na_2SO_4 in this work, suggest that substantial amount of Dobane JN has been converted into the product during the neutralization reaction as evident by the high percentages in the conversion (Tables 8.2 - 8.3). These show that the average values of conversion from Dobanic acid to the product ABS, at varying viscosity of the acid and reactants feed rates are 99.Ø4% and 99.35% respectively. It has been stated that the yields for the neutralization step in the sulphonation process are always 95% or greater (155).

In conclusion, the micromixing phenomena involving the fast reaction of Dobane JN with Na_2CO_3 and at varying viscosity of Dobanic acid and volumetric flow rates have been investigated in the nozzle reactor. High conversion of the segregated product sodium dodecylbenzene sulphonate (ABS) has been achieved and the pH value has been tested,

and found to conform within the range obtained for commercial use. The product, ABS has been tested to give a high percentage of the anionic active detergent.

CHAPTER NINE

CONCLUSIONS

AND

RECOMMENDATIONS FOR FURTHER WORK

9.1 CONCLUSIONS

(1). In this study, three geometrically similar nozzle reactors have been designed and constructed to investigate the possibility of such a reactor system for commercial use. The series of investigation conducted on these nozzle reactors appear to be unique.

(2). Flow visualization and residence time distribution studies involving tracer injections have been conducted on these nozzle reactors with a view to gain an insight to the fluid behaviour in such systems, and also to determine their performance as efficient mixers. The fluid flow characteristics in the nozzle reactors have been shown to validate the work of Binnie et al., Bradley and Pulling and many others as cited in Chapter two. An added feature in the flow visualization study, is the reversal of flow of the liquid when an inert tracer of potassium permanganate is injected at the top and bottom ports of the reactors.

(3). The experimental procedure using the high speed photographic technique for the RTD analysis appears to be sound. The analyses of the coloured film using an Atomic

Absorption Spectrophotometer give good and true representations of the fluid flow characteristics in the systems. These aspects of the investigations are unique.

(4). A generalized model consisting of a net work of CSTR's and plug flow reactors has been formulated to simulate the coloured tracer response of the effluent from the outlet orifice of the reactors. Simulation exercises have been carried out to determine the parameters of the model, employing the Harris 5ØØ computer in an interactive mode. A very good agreement has been shown between the model and experimental response data. Furthermore, the three geometrically similar nozzle reactors revealed that such systems can be represented as series of continuous stirred tanks with a plug flow between them, and a parallel stream of a plug flow.

(5). Micromixing studies, involving neutralization reaction of sulphuric acid (H_2SO_4) and sodium carbonate (Na_2CO_3) at varying molar feed concentrations and reactants volumetric flow rates have been conducted on Ø.55 x $1Ø^{-3}m^3$ and 5.13 x $1Ø^{-3}m^3$nozzle reactors respectively. Flow visualization investigations showing the decolourization of Na_2CO_3 when reacted with H_2SO_4 in the systems have been analysed by means of reaction times. The fractional conversion has been determined using the modified model which represents the behaviour of the

nozzle reactor with respect to the limiting reactant (Na_2CO_3). The yield of the product has been determined volumetrically, and this shows that the yield per mole of the limiting reactant increases with relative increase in the feed volumetric flow rates. Subsequently, the amount of the excess acid used in the system also increases; although a slight reduction in conversion is obtained, the pH values of the product being more acidic with increased flow rates of the reactants.

(6). Neutralization reaction between Dodecylbenzene sulphonic acid (Dobane JN) and Na_2CO_3 has been conducted at varying viscosity of Dobanic acid, when mixed with 111 Tricholoroethane and feed volumetric flow rates of the reactants. The product, sodium dodecylbenzene sulphonate (ABS) has been analyzed and shown to possess a high percentage of the anionic active detergent. Alternately, the percentage of an inert sodium sulphate (Na_2SO_4) in the product has been revealed to be low. Subsequently, a high conversion of Dobane JN to the product ABS has been achieved, irrespective of the viscosity or the reactants volumetric flow rates.

9.2 RECOMMENDATIONS FOR FURTHER WORK

(1). Accurate detection of the input tracer could be obtained by inserting a conductivity probe connected to a recorder at the entry port to the reactor. It could be assumed that such a probe would not in any circumstances disturb the flow patterns in the system. A square - wave generator based on a duplex syringe pump as used by Spencer and Lunt (158) in their stirred reactor or a motorized syringe could be considered for producing square - wave of an inert tracer to the system.

(2). Further designs could be implemented by varying the inlet orifices to the reactor and arranging the inlets in opposite directions in order to ascertain what effects such alterations would exert on the flow patterns and to the yield and conversion of commercial products.

(3). The mathematical model has been established to be valid for any continuous flow system and the program to simulate the effluent tracer has been demonstrated to be interactive on the Harris 500 computer. However, improvements could be employed to reduce the iteration required to obtain the model parameters. For such a program to be available for industrial use or run on micro computers, necessary modifications are envisaged.

(4). It has been shown in the design formulation of the reactor for neutralization betweeen H_2SO_4 and Na_2CO_3 that pseudo - first order reaction, based on the limiting reactant concentration was considered. It has been tested, however that if second order reaction with respect to the feed reactants has been considered to determine the fractional conversion of the reactants to the product, erroneous results would have been obtained for the conversions, since as detailed in Chapter two, fast reactions often yield very high values of the rate constants. However, detailed kinetics studies would be necessary in future and to incorporate this in a diffusion type model as reported by Toor et al. and Ou et al., with the use of the decay law employing the intensity of segregation as demonstrated in Chapter two, in predicting the necessary conversion. Such investigation would give unsatisfactory results to the deterministic approach as used in this study.

(5). The viscosity of Dobane JN as supplied by Unilever has been shown to be (167Ø.7Ø mPa.s) highly viscous and as such the Dobanic acid was incapable of being pumped by the Polypropylene Beresford PV41 pump. It was also noted during experimentations that the heat generated by the pump reduced the viscosity of Dobane JN. However, to use the Dobanic acid without addition of 111

Tricholoroethane, a more powerful pump should be installed.

(6). Stainless steel nozzle reactor can be employed to test very viscous system at very high temperature and pressure.

(7). Finally, the nozzle reactor can be employed for commercial use as the construction is simple and the overall cost is cheap.

APPENDICIES

APPENDIX

A DIMENSIONS OF THE CYLINDRICAL NOZZLE VESSELS

B RESIDENCE TIME DISTRIBUTION ANALYSIS:- EXPERIMENTAL AND MODEL RESPONSE

C PROGRAM LISTINGS FOR THE NORMALIZATION OF THE EXPERIMENTAL DATA AND RTD MODEL

D GRAPHS OF THE VISCOSITY OF DOBANIC ACID AND, WITH 111 TRICHOLOROETHANE

APPENDIX A

The size of a cylindrical nozzle reactor from its geometry comprises:-

(1) The volume of the right circular cylinder

(2) The volume of the frustum of right cones

(3) The volume of the orifice

Hence the total volume, V of the nozzle reactor is:-

$$V = \pi R^2 H_1 + \frac{L_1}{3}\pi \{ R^2 + RR_o + R_o^2 \} + \pi R_o^2 L$$

CYLINDRICAL NOZZLE REACTOR GEOMETRY

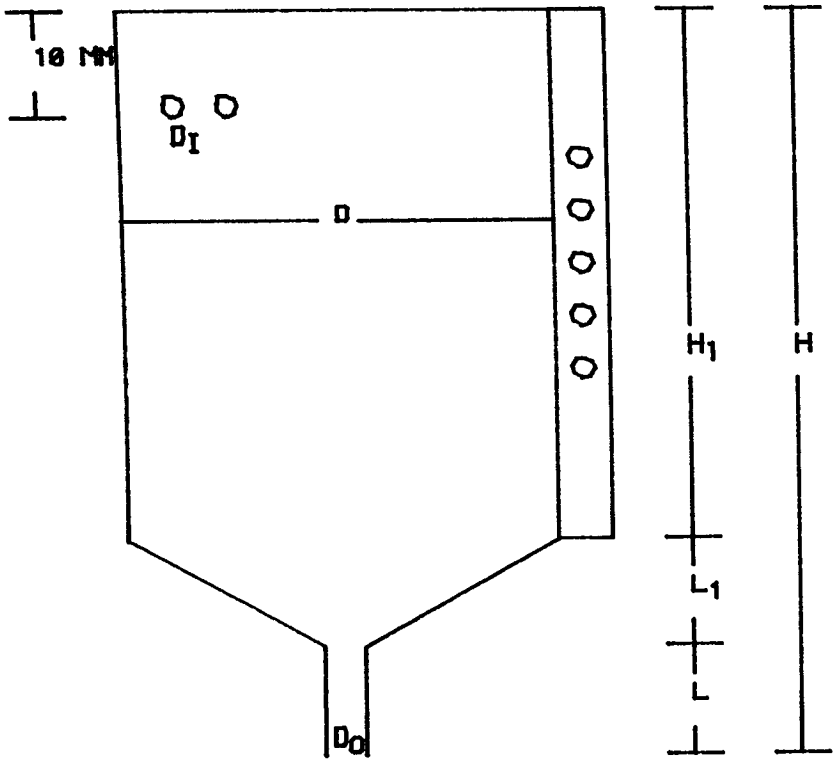

CYLINDRICAL NOZZLE REACTOR GEOMETRY

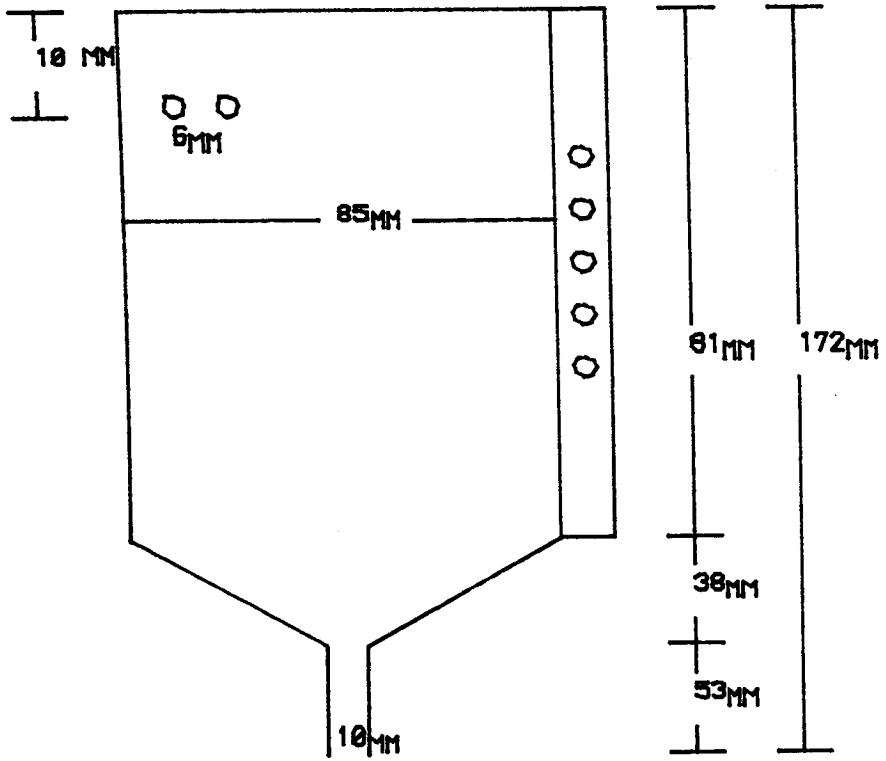

THE VOLUME OF THE CYLINDRICAL NOZZLE REACTOR 1 IS 0.55 LITRE

CYLINDRICAL NOZZLE REACTOR GEOMETRY

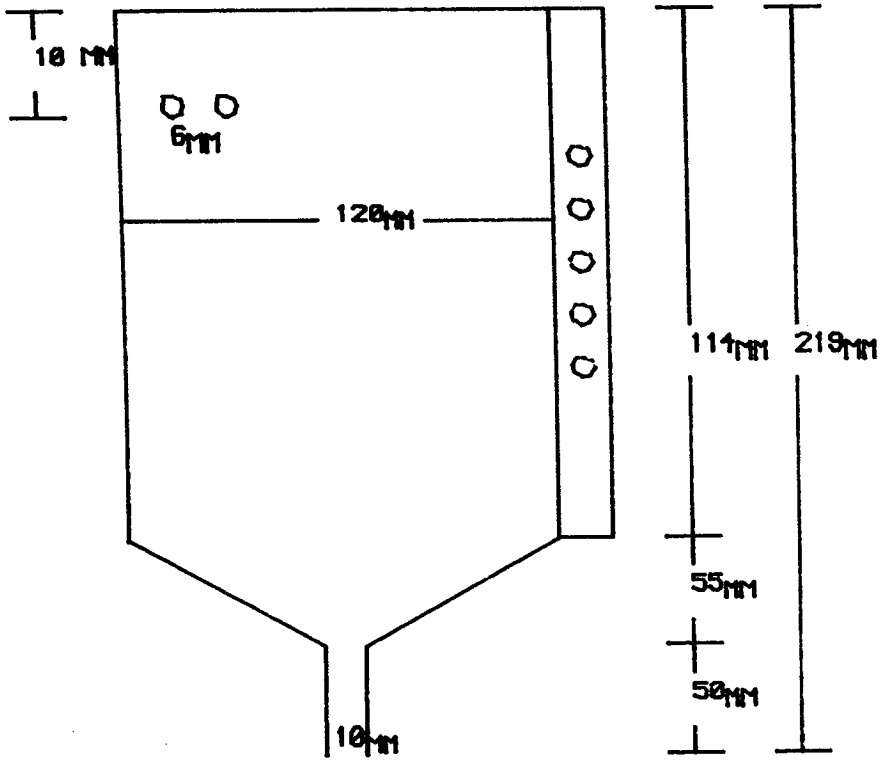

THE VOLUME OF THE CYLINDRICAL NOZZLE REACTOR 2

IS 1.52 LITRE

CYLINDRICAL NOZZLE REACTOR GEOMETRY

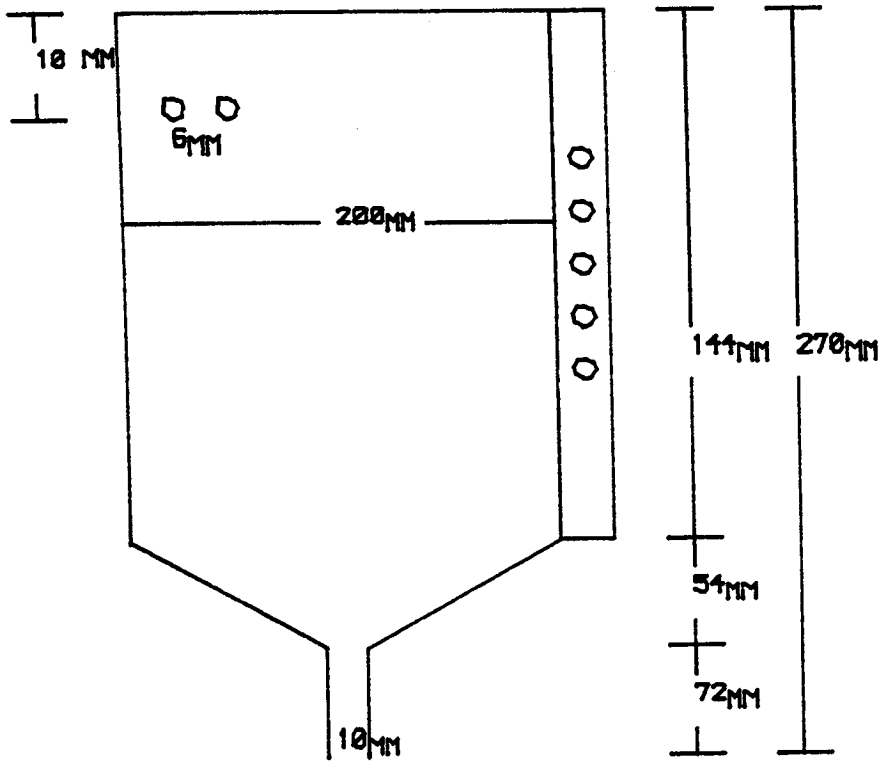

THE VOLUME OF THE CYLINDRICAL NOZZLE REACTOR 3 IS 5.13 LITRE

APPENDIX B

RESIDENCE TIME DISTRIBUTION ANALYSIS:-

EXPERIMENTAL AND MODEL RESPONSE

TABLE T91 : RUN1

TIME (S)	DIMENSIONLESS TIME (THETA)	EXIT CONCENTRATION DIMENSIONLESS	
		EXPERIMENTAL	MODEL
0	.000	.000	.000
3	.264	.245	.243
6	.527	.337	.334
9	.791	.329	.326
12	1.055	.302	.299
15	1.318	.280	.278
18	1.582	.259	.257
21	1.845	.241	.239
24	2.109	.224	.222
27	2.373	.206	.204
30	2.636	.188	.186
33	2.900	.173	.172
36	3.164	.157	.156
39	3.427	.145	.144
42	3.691	.127	.126
45	3.955	.110	.109
48	4.218	.094	.093
51	4.482	.086	.085
54	4.745	.071	.070
57	5.009	.059	.058
60	5.273	.049	.049
63	5.536	.039	.039
66	5.800	.031	.031
69	6.064	.029	.029

TABLE T92 : RUN2

TIME (S)	DIMENSIONLESS TIME (THETA)	EXIT CONCENTRATION DIMENSIONLESS	
		EXPERIMENTAL	MODEL
0	.000	.000	.000
2	.255	.019	.019
4	.509	.316	.319
7	.764	.344	.347
9	1.018	.338	.341
12	1.273	.312	.315
14	1.527	.283	.286
16	1.782	.262	.265
19	2.036	.236	.238
21	2.291	.217	.219
24	2.545	.198	.198
26	2.800	.179	.181
28	3.055	.160	.162
31	3.309	.148	.149
33	3.564	.135	.136
36	3.818	.122	.123
38	4.073	.110	.111
40	4.327	.097	.098
43	4.582	.093	.094
45	4.836	.076	.077
48	5.091	.072	.073
50	5.345	.063	.064
52	5.600	.055	.056
55	5.855	.049	.049
57	6.109	.034	.034
60	6.364	.030	.030

TABLE T53 : RUN3

TIME (S)	DIMENSIONLESS TIME (THETA)	EXIT CONCENTRATION DIMENSIONLESS	
		EXPERIMENTAL	MODEL
0	.000	.000	.000
2	.298	.015	.015
4	.596	.285	.287
7	.895	.303	.305
9	1.193	.294	.296
12	1.491	.270	.272
14	1.789	.249	.251
16	2.087	.231	.233
19	2.385	.212	.214
21	2.684	.193	.194
24	2.982	.175	.176
26	3.280	.158	.159
28	3.578	.141	.142
31	3.876	.128	.129
33	4.175	.119	.120
36	4.473	.102	.103
38	4.771	.093	.094
40	5.069	.084	.085
43	5.367	.074	.075
45	5.665	.065	.065
48	5.964	.058	.058
50	6.262	.048	.048
52	6.560	.045	.045
55	6.858	.037	.037
57	7.156	.030	.030

TABLE T9+ : RUN+

TIME (S)	DIMENSIONLESS TIME (THETA)	EXIT CONCENTRATION DIMENSIONLESS	
		EXPERIMENTAL	MODEL
0	.000	.000	.000
2	.389	.003	.003
5	.777	.155	.151
8	1.166	.210	.206
10	1.555	.210	.206
13	1.943	.203	.200
16	2.332	.185	.183
18	2.720	.168	.166
21	3.109	.152	.151
24	3.498	.138	.138
27	3.886	.127	.127
29	4.275	.117	.117
32	4.664	.107	.108
35	5.052	.099	.100
37	5.441	.091	.093
40	5.830	.086	.088
43	6.218	.079	.081
45	6.607	.072	.074
48	6.995	.066	.069
51	7.384	.061	.064
54	7.773	.057	.060
56	8.161	.052	.055
59	8.550	.047	.050
62	8.939	.041	.045
64	9.327	.038	.043
67	9.716	.034	.037

TABLE T95 : RUN5

TIME (S)	DIMENSIONLESS TIME (THETA)	EXIT CONCENTRATION DIMENSIONLESS	
		EXPERIMENTAL	MODEL
0	.000	.000	.000
2	.438	.003	.004
5	.875	.012	.013
8	1.313	.146	.147
10	1.751	.196	.197
13	2.189	.197	.199
16	2.626	.188	.190
18	3.064	.173	.176
21	3.502	.159	.162
24	3.940	.146	.149
27	4.377	.135	.138
29	4.815	.122	.126
32	5.253	.108	.112
35	5.690	.102	.106
37	6.128	.091	.095
40	6.566	.081	.085
43	7.004	.073	.077
45	7.441	.065	.069
48	7.879	.058	.062
51	8.317	.052	.056
54	8.755	.046	.051
56	9.192	.040	.045
59	9.630	.035	.040
62	10.068	.029	.034
64	10.505	.025	.030

TABLE T96 : RUN6

TIME (S)	DIMENSIONLESS TIME (THETA)	EXIT CONCENTRATION DIMENSIONLESS	
		EXPERIMENTAL	MODEL
0	.000	.000	.000
2	.489	.002	.002
5	.979	.102	.100
8	1.468	.188	.184
10	1.957	.189	.185
13	2.446	.187	.183
16	2.936	.171	.168
18	3.425	.157	.155
21	3.914	.143	.141
24	4.403	.129	.128
27	4.893	.116	.115
29	5.382	.106	.106
32	5.871	.096	.096
35	6.361	.083	.084
37	6.850	.076	.077
40	7.339	.068	.069
43	7.828	.060	.061
45	8.318	.052	.054
48	8.807	.045	.047
51	9.296	.040	.042
54	9.785	.032	.035

TABLE T97 : RUN7

TIME (S)	DIMENSIONLESS TIME (THETA)	EXIT CONCENTRATION DIMENSIONLESS	
		EXPERIMENTAL	MODEL
0	.000	.000	.000
2	.540	.004	.005
5	1.080	.072	.072
8	1.620	.189	.186
10	2.160	.190	.188
13	2.700	.177	.175
16	3.240	.166	.165
18	3.780	.150	.150
21	4.320	.135	.136
24	4.860	.122	.123
27	5.400	.108	.110
29	5.940	.096	.099
32	6.480	.085	.088
35	7.020	.074	.078
37	7.560	.063	.067
40	8.100	.054	.059
43	8.640	.047	.052
45	9.180	.040	.045
48	9.720	.032	.037
51	10.260	.029	.035
54	10.800	.022	.033

TABLE T9B : RUN8

TIME (S)	DIMENSIONLESS TIME (THETA)	EXIT CONCENTRATION DIMENSIONLESS	
		EXPERIMENTAL	MODEL
0	.000	.000	.000
1	.398	.002	.002
3	.796	.006	.006
5	1.193	.079	.078
7	1.593	.176	.174
9	1.991	.182	.180
10	2.389	.185	.183
12	2.787	.180	.178
14	3.185	.171	.169
16	3.584	.161	.159
18	3.982	.151	.149
19	4.380	.141	.140
21	4.778	.130	.129
23	5.176	.120	.119
25	5.575	.109	.108
27	5.973	.101	.100
28	6.371	.093	.092
30	6.769	.085	.084
32	7.167	.078	.077
34	7.565	.070	.069
36	7.964	.065	.064
37	8.362	.059	.058
39	8.760	.053	.052
41	9.158	.048	.047
43	9.556	.042	.042
45	9.955	.037	.037

TABLE T99 : RUN9

TIME (S)	DIMENSIONLESS TIME (THETA)	EXIT CONCENTRATION DIMENSIONLESS	
		EXPERIMENTAL	MODEL
0	.000	.000	.000
1	.428	.002	.002
3	.857	.012	.012
5	1.285	.087	.086
7	1.713	.186	.183
8	2.141	.191	.188
10	2.570	.189	.186
12	2.998	.174	.171
14	3.426	.159	.157
16	3.854	.149	.147
17	4.283	.137	.135
19	4.711	.128	.127
21	5.139	.117	.116
23	5.567	.106	.105
24	5.996	.094	.093
26	6.424	.087	.087
28	6.852	.081	.081
30	7.280	.070	.070
32	7.709	.065	.065
33	8.137	.057	.057
35	8.565	.053	.053
37	8.994	.047	.048
39	9.422	.043	.044
40	9.850	.040	.041
42	10.278	.036	.040
44	10.707	.032	.033

TABLE T31 : RUN1

TIME (S)	DIMENSIONLESS TIME (THETA)	EXIT CONCENTRATION DIMENSIONLESS	
		EXPERIMENTAL	MODEL
0	.000	.000	.000
2	.072	.175	.175
4	.143	1.974	1.967
6	.215	1.876	1.870
9	.286	1.721	1.716
11	.358	1.520	1.516
13	.429	1.314	1.311
15	.501	1.093	1.091
18	.572	.902	.901
20	.644	.747	.746
22	.715	.629	.629
24	.787	.526	.527
27	.859	.433	.434
29	.930	.340	.342
31	1.002	.283	.285
33	1.073	.232	.234
36	1.145	.208	.209
38	1.216	.196	.199
40	1.288	.186	.189

TABLE T32 : RUN2

TIME (S)	DIMENSIONLESS TIME (THETA)	EXIT CONCENTRATION DIMENSIONLESS	
		EXPERIMENTAL	MODEL
0	.000	.000	.000
2	.086	.093	.094
4	.173	1.798	1.814
6	.259	1.718	1.733
9	.345	1.578	1.592
11	.432	1.401	1.414
13	.518	1.191	1.202
15	.604	.957	.966
18	.691	.771	.779
20	.777	.607	.614
22	.863	.486	.492
24	.950	.374	.379
27	1.036	.299	.304
29	1.123	.215	.219
31	1.209	.177	.181
33	1.295	.140	.143
36	1.382	.121	.124

TABLE T33 : RUN3

TIME (S)	DIMENSIONLESS TIME (THETA)	EXIT CONCENTRATION DIMENSIONLESS	
		EXPERIMENTAL	MODEL
0	.000	.000	.000
2	.101	.160	.159
4	.202	1.498	1.482
6	.303	1.358	1.344
9	.405	1.207	1.196
11	.506	1.039	1.030
13	.607	.887	.880
15	.708	.755	.750
18	.809	.631	.628
20	.910	.539	.537
22	1.012	.455	.454
24	1.113	.384	.384
27	1.214	.336	.337
29	1.315	.280	.282
31	1.418	.240	.243
33	1.517	.220	.223
36	1.618	.212	.215

TABLE T34 : RUN4

TIME (S)	DIMENSIONLESS TIME (THETA)	EXIT CONCENTRATION DIMENSIONLESS	
		EXPERIMENTAL	MODEL
0	.000	.000	.000
1	.070	.101	.101
2	.141	1.721	1.712
4	.211	1.691	1.683
5	.281	1.610	1.603
6	.352	1.493	1.487
8	.422	1.362	1.357
9	.492	1.194	1.191
10	.562	1.038	1.036
12	.633	.860	.859
13	.703	.698	.699
14	.773	.577	.579
16	.844	.456	.459
17	.914	.380	.384
18	.984	.304	.309
20	1.055	.228	.234
21	1.125	.177	.183
22	1.195	.127	.134
24	1.266	.081	.088
25	1.336	.061	.069
27	1.406	.040	.049
28	1.477	.025	.034

TABLE T35 : RUN5

TIME (S)	DIMENSIONLESS TIME (THETA)	EXIT CONCENTRATION DIMENSIONLESS	
		EXPERIMENTAL	MODEL
0	.000	.000	.000
1	.079	.228	.228
2	.158	1.782	1.778
4	.238	1.696	1.694
5	.317	1.549	1.549
6	.396	1.397	1.398
8	.475	1.240	1.243
9	.554	1.012	1.017
10	.634	.785	.792
12	.713	.628	.637
13	.792	.506	.517
14	.871	.405	.417
16	.950	.329	.343
17	1.030	.268	.283
18	1.109	.223	.239
20	1.188	.172	.190
21	1.267	.142	.161
22	1.346	.121	.141
24	1.425	.081	.102
25	1.505	.071	.093

TABLE T36 : RUN6

TIME (S)	DIMENSIONLESS TIME (THETA)	EXIT CONCENTRATION DIMENSIONLESS	
		EXPERIMENTAL	MODEL
0	.000	.000	.000
1	.089	.051	.051
2	.177	.148	.149
4	.266	1.476	1.483
5	.354	1.459	1.467
6	.443	1.357	1.364
8	.531	1.247	1.254
9	.620	1.103	1.110
10	.708	.891	.897
12	.797	.717	.723
13	.885	.573	.578
14	.974	.467	.472
16	1.062	.378	.383
17	1.151	.297	.302
18	1.239	.238	.243
20	1.328	.191	.196
21	1.416	.153	.158
22	1.505	.127	.132
24	1.593	.102	.107
25	1.682	.076	.082
27	1.770	.064	.070

TABLE T37 : RUN7

TIME (S)	DIMENSIONLESS TIME (THETA)	EXIT CONCENTRATION DIMENSIONLESS	
		EXPERIMENTAL	MODEL
0	.000	.000	.000
1	.098	.055	.055
2	.195	.142	.143
4	.293	.411	.413
5	.391	1.938	1.943
6	.488	1.752	1.757
8	.586	1.505	1.510
9	.684	1.149	1.154
10	.782	.794	.798
12	.879	.569	.573
13	.977	.438	.442
14	1.075	.350	.356
16	1.172	.274	.281
17	1.270	.219	.228
18	1.368	.184	.174
20	1.465	.131	.142
21	1.563	.082	.093
22	1.661	.049	.061

TABLE T3B : RUN8

TIME (S)	DIMENSIONLESS TIME (THETA)	EXIT CONCENTRATION DIMENSIONLESS	
		EXPERIMENTAL	MODEL
0	.000	.000	.000
1	.108	.063	.063
2	.216	.126	.127
4	.324	.567	.567
5	.432	1.377	1.377
6	.540	1.259	1.259
8	.648	1.125	1.126
9	.756	.974	.976
10	.864	.797	.799
12	.973	.638	.641
13	1.081	.525	.531
14	1.189	.441	.449
16	1.297	.357	.369
17	1.405	.294	.309
18	1.513	.231	.248
20	1.621	.185	.203
21	1.729	.147	.166
22	1.837	.109	.129

TABLE T39 : RUN9

TIME (S)	DIMENSIONLESS TIME (THETA)	EXIT CONCENTRATION DIMENSIONLESS	
		EXPERIMENTAL	MODEL
0	.000	.000	.000
1	.118	.046	.046
2	.236	.157	.158
4	.353	1.595	1.597
5	.471	1.434	1.436
6	.589	1.202	1.204
8	.707	.948	.951
9	.825	.740	.743
10	.943	.578	.581
12	1.060	.481	.485
13	1.178	.379	.383
14	1.296	.301	.305
16	1.414	.236	.240
17	1.532	.185	.190
18	1.650	.148	.153
20	1.767	.116	.121
21	1.885	.092	.098
22	2.003	.074	.080

TABLE TB1 : RUN1

TIME (S)	DIMENSIONLESS TIME (THETA)	EXIT CONCENTRATION DIMENSIONLESS	
		EXPERIMENTAL	MODEL
0	.000	.000	.000
12	.113	.308	.320
24	.226	.995	1.034
36	.339	.876	.911
48	.452	.786	.817
60	.565	.720	.748
72	.678	.663	.689
84	.791	.606	.630
96	.904	.545	.566
108	1.018	.497	.517
120	1.131	.450	.468
132	1.244	.403	.419
144	1.357	.355	.369
156	1.470	.313	.325
168	1.583	.275	.286
180	1.696	.237	.246
192	1.809	.213	.221
204	1.922	.171	.178
216	2.035	.142	.148
228	2.148	.123	.128
240	2.261	.109	.113
252	2.374	.095	.099
264	2.487	.076	.079

TABLE TB2 : RUN2

TIME (S)	DIMENSIONLESS TIME (THETA)	EXIT CONCENTRATION DIMENSIONLESS	
		EXPERIMENTAL	MODEL
0	.000	.000	.000
9	.109	.051	.050
19	.218	1.081	1.038
28	.327	.942	.905
38	.437	.823	.792
48	.546	.736	.708
57	.655	.659	.638
67	.764	.597	.583
76	.873	.545	.537
86	.982	.499	.497
96	1.092	.463	.466
105	1.201	.427	.434
115	1.310	.386	.397
124	1.419	.340	.355
134	1.528	.309	.328
144	1.637	.278	.300
153	1.747	.247	.272
163	1.856	.221	.250
172	1.965	.185	.217
182	2.074	.165	.200
192	2.183	.134	.172
201	2.292	.129	.169

TABLE TB3 : RUN3

TIME (S)	DIMENSIONLESS TIME (THETA)	EXIT CONCENTRATION DIMENSIONLESS	
		EXPERIMENTAL	MODEL
0	.000	.000	.000
9	.128	.045	.045
19	.256	.941	.906
28	.384	.879	.847
38	.512	.762	.735
48	.639	.672	.649
57	.767	.605	.590
67	.895	.538	.530
76	1.023	.484	.482
86	1.151	.426	.429
96	1.279	.377	.385
105	1.407	.323	.336
115	1.535	.287	.303
124	1.662	.251	.271
134	1.790	.224	.248
144	1.918	.202	.228
153	2.046	.179	.208
163	2.174	.161	.193
172	2.302	.156	.190
182	2.430	.143	.180
192	2.558	.134	.173
201	2.685	.121	.162
211	2.813	.113	.155

TABLE TB4 : RUN4

TIME (S)	DIMENSIONLESS TIME (THETA)	EXIT CONCENTRATION DIMENSIONLESS	
		EXPERIMENTAL	MODEL
0	.000	.000	.000
9	.148	.039	.039
19	.296	.770	.763
28	.444	.691	.685
38	.593	.592	.587
48	.741	.521	.516
57	.889	.458	.454
67	1.037	.410	.406
76	1.185	.367	.364
86	1.333	.332	.329
96	1.481	.296	.293
105	1.630	.260	.258
115	1.778	.237	.235
124	1.926	.217	.215
134	2.074	.197	.195
144	2.222	.182	.180
153	2.370	.170	.168
163	2.519	.158	.157
172	2.667	.142	.141
182	2.815	.126	.125
192	2.963	.122	.121
201	3.111	.118	.117
211	3.259	.103	.102
220	3.407	.099	.098
230	3.556	.095	.094
240	3.704	.091	.090

TABLE TB5 : RUN5

TIME (S)	DIMENSIONLESS TIME (THETA)	EXIT CONCENTRATION DIMENSIONLESS	
		EXPERIMENTAL	MODEL
0	.000	.000	.000
7	.125	.013	.013
14	.250	.798	.785
21	.375	.776	.763
28	.501	.687	.676
36	.626	.620	.611
43	.751	.554	.547
50	.876	.509	.503
57	1.001	.461	.457
64	1.126	.421	.418
72	1.251	.381	.379
79	1.377	.355	.354
86	1.502	.332	.332
93	1.627	.310	.311
100	1.752	.288	.290
108	1.877	.266	.268
115	2.002	.248	.251
122	2.127	.230	.234
129	2.253	.213	.217
136	2.378	.199	.204
144	2.503	.191	.196
151	2.628	.177	.183
158	2.753	.160	.166

TABLE TB6 : RUN6

TIME (S)	DIMENSIONLESS TIME (THETA)	EXIT CONCENTRATION DIMENSIONLESS	
		EXPERIMENTAL	MODEL
0	.000	.000	.000
7	.140	.018	.018
14	.280	.775	.764
21	.420	.784	.774
28	.560	.692	.685
36	.699	.623	.617
43	.839	.572	.588
50	.979	.507	.505
57	1.119	.461	.460
64	1.259	.415	.416
72	1.399	.369	.371
79	1.539	.332	.335
86	1.679	.300	.304
93	1.818	.258	.264
100	1.958	.240	.246
108	2.098	.208	.216
115	2.238	.198	.206
122	2.378	.166	.175
129	2.518	.157	.187
136	2.658	.138	.149
144	2.798	.125	.136

TABLE TB7 : RUN7

TIME (S)	DIMENSIONLESS TIME (THETA)	EXIT CONCENTRATION DIMENSIONLESS	
		EXPERIMENTAL	MODEL
0	.000	.000	.000
7	.154	.018	.018
14	.309	.735	.722
21	.463	.712	.700
28	.618	.641	.632
36	.772	.558	.552
43	.928	.508	.504
50	1.081	.463	.460
57	1.235	.405	.404
64	1.389	.374	.375
72	1.544	.330	.332
79	1.698	.289	.293
86	1.853	.258	.263
93	2.007	.240	.246
100	2.161	.214	.221
108	2.316	.196	.204
115	2.470	.169	.178
122	2.625	.156	.165
129	2.779	.138	.148
136	2.933	.125	.136
144	3.088	.111	.123

TABLE TB8 : RUN8

TIME (S)	DIMENSIONLESS TIME (THETA)	EXIT CONCENTRATION DIMENSIONLESS	
		EXPERIMENTAL	MODEL
0	.000	.000	.000
4	.114	.009	.009
9	.228	.028	.028
14	.342	.772	.779
19	.455	.706	.793
24	.569	.748	.755
28	.683	.655	.661
33	.797	.589	.595
38	.911	.538	.543
43	1.025	.491	.496
48	1.138	.449	.453
52	1.252	.412	.416
57	1.366	.393	.397
62	1.480	.346	.349
67	1.594	.323	.326
72	1.708	.299	.302
76	1.821	.262	.264
81	1.935	.239	.241
86	2.049	.215	.217
91	2.163	.201	.203
96	2.277	.168	.170
100	2.391	.159	.160
105	2.504	.145	.146
110	2.618	.136	.137
115	2.732	.122	.123
120	2.846	.117	.118
124	2.960	.112	.113

TABLE TB9 : RUN9

TIME (S)	DIMENSIONLESS TIME (THETA)	EXIT CONCENTRATION DIMENSIONLESS	
		EXPERIMENTAL	MODEL
0	.000	.000	.000
4	.124	.009	.009
9	.247	.023	.024
14	.371	.749	.769
19	.495	.768	.789
24	.618	.702	.721
28	.742	.632	.649
33	.866	.562	.577
38	.989	.501	.514
43	1.113	.449	.461
48	1.237	.412	.423
52	1.360	.374	.384
57	1.484	.346	.355
62	1.608	.309	.317
67	1.731	.295	.303
72	1.855	.262	.269
76	1.979	.243	.250
81	2.102	.215	.221
86	2.226	.206	.212
91	2.350	.187	.192
96	2.473	.168	.172
100	2.597	.150	.154
105	2.721	.136	.140
110	2.844	.117	.120
115	2.968	.112	.115
120	3.092	.108	.111
124	3.215	.084	.086
129	3.339	.075	.077

TABLE TB10 : RUN10

TIME (S)	DIMENSIONLESS TIME (THETA)	EXIT CONCENTRATION DIMENSIONLESS	
		EXPERIMENTAL	MODEL
0	.000	.000	.000
4	.135	.035	.036
9	.269	.771	.785
14	.404	1.079	1.099
19	.539	.911	.929
24	.674	.771	.787
28	.808	.666	.681
33	.943	.561	.575
38	1.078	.477	.490
43	1.213	.406	.418
48	1.347	.350	.362
52	1.482	.280	.291
57	1.617	.245	.256
62	1.752	.203	.213
67	1.886	.168	.178
72	2.021	.140	.150
78	2.158	.128	.136
81	2.291	.112	.123
86	2.425	.107	.118
91	2.560	.105	.116

TABLE TB11 : RUN11

TIME (S)	DIMENSIONLESS TIME (THETA)	EXIT CONCENTRATION DIMENSIONLESS	
		EXPERIMENTAL	MODEL
0	.000	.000	.000
4	.145	.026	.027
9	.291	1.078	1.118
14	.436	.963	.999
19	.582	.835	.866
24	.727	.706	.732
28	.873	.603	.626
33	1.018	.488	.508
38	1.164	.417	.435
43	1.309	.353	.369
48	1.455	.295	.309
52	1.600	.257	.270
57	1.746	.225	.238
62	1.891	.193	.205
67	2.037	.167	.178
72	2.182	.154	.165
76	2.328	.128	.138
81	2.473	.116	.126
86	2.619	.103	.113

TABLE TB12 : RUN12

TIME (S)	DIMENSIONLESS TIME (THETA)	EXIT CONCENTRATION DIMENSIONLESS	
		EXPERIMENTAL	MODEL
0	.000	.000	.000
4	.157	.030	.030
9	.313	.966	.962
14	.470	.845	.841
19	.626	.725	.723
24	.783	.604	.603
28	.939	.513	.514
33	1.096	.447	.449
38	1.253	.374	.377
43	1.409	.332	.335
48	1.566	.290	.294
52	1.722	.254	.259
57	1.879	.217	.222
62	2.035	.205	.211
67	2.192	.181	.188
72	2.349	.169	.176
76	2.505	.157	.164
81	2.662	.151	.159

TABLE TB13 : RUN13

TIME (S)	DIMENSIONLESS TIME (THETA)	EXIT CONCENTRATION DIMENSIONLESS	
		EXPERIMENTAL	MODEL
0	.000	.000	.000
4	.168	.023	.023
9	.337	.411	.407
14	.505	.822	.814
19	.674	.705	.699
24	.842	.605	.601
28	1.011	.505	.503
33	1.179	.434	.433
38	1.347	.382	.382
43	1.516	.323	.324
48	1.684	.282	.284
52	1.853	.252	.254
57	2.021	.211	.214
62	2.189	.188	.192
67	2.358	.164	.168
72	2.526	.147	.152
76	2.695	.135	.140
81	2.863	.106	.112
86	3.032	.094	.100
91	3.200	.088	.095
96	3.368	.082	.089

TABLE TB14 : RUN14

TIME (S)	DIMENSIONLESS TIME (THETA)	EXIT CONCENTRATION DIMENSIONLESS	
		EXPERIMENTAL	MODEL
0	.000	.000	.000
4	.180	.031	.031
9	.360	.993	.987
14	.539	.807	.803
19	.719	.652	.650
24	.899	.559	.559
28	1.079	.466	.467
33	1.259	.397	.399
38	1.438	.335	.338
43	1.618	.279	.283
48	1.798	.224	.229
52	1.978	.186	.192
57	2.158	.155	.162
62	2.337	.143	.150
67	2.517	.112	.120
72	2.697	.093	.102
76	2.877	.087	.096
81	3.057	.075	.085

TABLE T815 : RUN15

TIME (S)	DIMENSIONLESS TIME (THETA)	EXIT CONCENTRATION DIMENSIONLESS	
		EXPERIMENTAL	MODEL
0	.000	.000	.000
4	.192	.047	.047
9	.384	.919	.900
14	.575	.771	.757
19	.767	.640	.630
24	.959	.522	.516
28	1.151	.445	.442
33	1.343	.379	.378
38	1.535	.308	.310
43	1.726	.261	.265
48	1.918	.219	.225
52	2.110	.190	.198
57	2.302	.166	.175
62	2.494	.142	.152
67	2.685	.107	.119
72	2.877	.089	.102
76	3.069	.077	.091
81	3.261	.059	.074
86	3.453	.036	.052

TABLE TB16 : RUN16

TIME (S)	DIMENSIONLESS TIME (THETA)	EXIT CONCENTRATION DIMENSIONLESS	
		EXPERIMENTAL	MODEL
0	.000	.000	.000
4	.204	.024	.024
9	.409	.996	.988
14	.613	.761	.756
19	.817	.604	.601
24	1.021	.507	.506
28	1.228	.392	.392
33	1.430	.326	.327
38	1.634	.272	.274
43	1.839	.223	.226
48	2.043	.193	.197
52	2.247	.157	.162
57	2.451	.145	.150
62	2.656	.121	.127
67	2.860	.109	.115
72	3.064	.097	.104

TABLE T11 : RUN1

TIME (S)	DIMENSIONLESS TIME (THETA)	EXIT CONCENTRATION DIMENSIONLESS	
		EXPERIMENTAL	MODEL
0	.000	.000	.000
2	.198	.010	.010
4	.395	.020	.020
6	.593	.039	.039
9	.791	.069	.068
11	.989	.128	.127
13	1.186	.276	.274
15	1.384	.582	.577
18	1.582	.562	.557
20	1.780	.454	.450
22	1.977	.381	.378
24	2.175	.316	.313
27	2.373	.268	.266
29	2.570	.237	.235
31	2.768	.209	.207
33	2.966	.193	.191
36	3.164	.180	.178
38	3.361	.170	.169
40	3.559	.164	.163
42	3.757	.150	.149
45	3.955	.140	.139
47	4.152	.134	.133
49	4.350	.124	.123
51	4.548	.114	.113
54	4.745	.110	.109

TABLE T12 : RUN2

TIME (S)	DIMENSIONLESS TIME (THETA)	EXIT CONCENTRATION DIMENSIONLESS	
		EXPERIMENTAL	MODEL
0	.000	.000	.000
2	.239	.028	.030
4	.477	.096	.100
6	.716	.744	.758
9	.955	.783	.799
11	1.193	.579	.597
13	1.432	.414	.433
15	1.670	.317	.337
18	1.909	.240	.261
20	2.148	.182	.205
22	2.386	.138	.161
24	2.625	.099	.124
27	2.864	.083	.109
29	3.102	.077	.103
31	3.341	.069	.096
33	3.580	.066	.096
36	3.818	.055	.088
38	4.057	.044	.080
40	4.295	.041	.079
42	4.534	.039	.079
45	4.773	.033	.074

TABLE T13 : RUN3

TIME (S)	DIMENSIONLESS TIME (THETA)	EXIT CONCENTRATION DIMENSIONLESS	
		EXPERIMENTAL	MODEL
0	.000	.000	.000
2	.280	.011	.012
4	.559	.043	.044
6	.839	.136	.137
9	1.118	.912	.909
11	1.398	.638	.639
13	1.677	.407	.411
15	1.957	.298	.304
18	2.236	.228	.236
20	2.516	.176	.185
22	2.795	.144	.154
24	3.075	.122	.132
27	3.355	.103	.121
29	3.634	.092	.122
31	3.914	.087	.127
33	4.193	.084	.136

TABLE T14 : RUN4

TIME (S)	DIMENSIONLESS TIME (THETA)	EXIT CONCENTRATION DIMENSIONLESS	
		EXPERIMENTAL	MODEL
0	.000	.000	.000
1	.194	.005	.005
2	.389	.022	.022
4	.583	.043	.044
5	.777	.095	.096
6	.972	.406	.411
8	1.168	.861	.870
9	1.360	.826	.835
10	1.555	.590	.597
12	1.749	.460	.465
13	1.943	.366	.370
14	2.137	.303	.307
16	2.332	.244	.247
17	2.526	.203	.206
18	2.720	.163	.166
20	2.915	.135	.137
21	3.109	.108	.110
22	3.303	.087	.089
24	3.498	.070	.072
25	3.692	.065	.067
27	3.886	.060	.062
28	4.081	.054	.056

TABLE T15 : RUN5

TIME (S)	DIMENSIONLESS TIME (THETA)	EXIT CONCENTRATION DIMENSIONLESS	
		EXPERIMENTAL	MODEL
0	.000	.000	.000
1	.219	.019	.020
2	.438	.062	.063
4	.657	.154	.157
5	.875	.901	.914
6	1.094	.894	.908
8	1.313	.663	.674
9	1.532	.478	.487
10	1.751	.370	.378
12	1.970	.278	.285
13	2.189	.213	.219
14	2.407	.167	.173
16	2.626	.123	.129
17	2.845	.111	.117
18	3.064	.077	.082
20	3.283	.056	.061
21	3.502	.046	.051
22	3.721	.037	.042
24	3.940	.025	.030

TABLE T16 : RUN6

TIME (S)	DIMENSIONLESS TIME (THETA)	EXIT CONCENTRATION DIMENSIONLESS	
		EXPERIMENTAL	MODEL
0	.000	.000	.000
1	.245	.009	.009
2	.489	.017	.017
4	.734	.043	.043
5	.979	.097	.098
6	1.223	.229	.230
8	1.468	.814	.815
9	1.712	.800	.802
10	1.957	.600	.602
12	2.202	.423	.425
13	2.446	.300	.302
14	2.691	.229	.231
16	2.936	.177	.179
17	3.180	.131	.133
18	3.425	.100	.102
20	3.670	.074	.076
21	3.914	.057	.059
22	4.159	.040	.042
24	4.403	.026	.028

TABLE T17 : RUN7

TIME (S)	DIMENSIONLESS TIME (THETA)	EXIT CONCENTRATION DIMENSIONLESS	
		EXPERIMENTAL	MODEL
0	.000	.000	.000
0	.180	.006	.006
1	.360	.015	.013
2	.540	.045	.042
3	.720	.090	.087
4	.900	.211	.205
5	1.080	.692	.661
6	1.260	.848	.839
7	1.440	.827	.828
8	1.620	.602	.620
9	1.800	.436	.453
9	1.980	.346	.354
10	2.160	.283	.286
11	2.340	.229	.233
12	2.520	.196	.198
13	2.700	.165	.169
14	2.880	.138	.140
15	3.060	.114	.115
16	3.240	.096	.097
17	3.420	.078	.080
18	3.600	.066	.068
18	3.780	.048	.051
19	3.960	.039	.040
20	4.140	.030	.031

TABLE T1B : RUN8

TIME (S)	DIMENSIONLESS TIME (THETA)	EXIT CONCENTRATION DIMENSIONLESS	
		EXPERIMENTAL	MODEL
0	.000	.000	.000
0	.199	.006	.006
1	.398	.014	.013
2	.597	.041	.040
3	.796	.083	.082
4	.995	.180	.178
5	1.195	.801	.793
6	1.394	.796	.796
7	1.593	.718	.720
8	1.792	.525	.529
9	1.991	.373	.375
9	2.190	.290	.291
10	2.389	.232	.233
11	2.588	.180	.181
12	2.787	.152	.153
13	2.986	.124	.124
14	3.185	.105	.106
15	3.385	.088	.089
16	3.584	.072	.072
17	3.783	.066	.066
18	3.982	.055	.055

TABLE T19 : RUN9

TIME (S)	DIMENSIONLESS TIME (THETA)	EXIT CONCENTRATION DIMENSIONLESS	
		EXPERIMENTAL	MODEL
0	.000	.000	.000
0	.216	.004	.004
1	.433	.011	.011
2	.649	.019	.019
3	.865	.032	.032
4	1.081	.053	.052
5	1.298	.084	.083
6	1.514	.137	.135
7	1.730	.274	.271
8	1.946	.527	.521
9	2.163	.571	.585
9	2.379	.523	.517
10	2.595	.409	.404
11	2.812	.327	.323
12	3.028	.274	.271
13	3.244	.232	.229
14	3.460	.200	.198
15	3.677	.169	.167
16	3.893	.148	.146
17	4.109	.126	.125
18	4.325	.110	.109
18	4.542	.093	.092
19	4.758	.080	.079
20	4.974	.067	.066
21	5.191	.059	.058
22	5.407	.053	.052
23	5.623	.051	.050

TABLE T110 : RUN10

TIME (S)	DIMENSIONLESS TIME (THETA)	EXIT CONCENTRATION DIMENSIONLESS	
		EXPERIMENTAL	MODEL
0	.000	.000	.000
0	.236	.011	.011
1	.471	.026	.026
2	.707	.042	.042
3	.943	.079	.078
4	1.178	.132	.132
5	1.414	.264	.262
6	1.649	.686	.681
7	1.885	.696	.697
8	2.121	.459	.464
9	2.356	.343	.345
9	2.592	.277	.278
10	2.828	.237	.238
11	3.063	.198	.199
12	3.299	.169	.170
13	3.535	.142	.143
14	3.770	.119	.120
15	4.006	.092	.093
16	4.241	.079	.080
17	4.477	.063	.064
18	4.713	.053	.053
18	4.948	.040	.041

TABLE T111 : RUN11

TIME (S)	DIMENSIONLESS TIME (THETA)	EXIT CONCENTRATION DIMENSIONLESS	
		EXPERIMENTAL	MODEL
0	.000	.000	.000
0	.254	.012	.012
1	.509	.029	.028
2	.763	.058	.058
3	1.018	.101	.100
4	1.272	.188	.186
5	1.527	.722	.715
6	1.781	.711	.710
7	2.036	.506	.509
8	2.290	.361	.363
9	2.545	.275	.275
9	2.799	.202	.203
10	3.053	.159	.160
11	3.308	.127	.127
12	3.562	.101	.102
13	3.817	.075	.075
14	4.071	.069	.069
15	4.326	.046	.046
16	4.580	.043	.043
17	4.835	.035	.035
18	5.089	.029	.029

TABLE T21 : RUN1

TIME (S)	DIMENSIONLESS TIME (THETA)	EXIT CONCENTRATION DIMENSIONLESS	
		EXPERIMENTAL	MODEL
0	.000	.000	.000
2	.198	.021	.021
4	.395	.103	.103
6	.593	.570	.566
9	.791	.617	.613
11	.989	.610	.606
13	1.188	.557	.553
15	1.384	.475	.472
18	1.582	.398	.396
20	1.780	.330	.329
22	1.977	.268	.267
24	2.175	.225	.225
27	2.373	.182	.182
29	2.570	.150	.150
31	2.768	.120	.121
33	2.966	.096	.097
36	3.164	.077	.078
38	3.361	.064	.065
40	3.559	.054	.055
42	3.757	.051	.054
45	3.955	.047	.053

TABLE T22 : RUN2

TIME (S)	DIMENSIONLESS TIME (THETA)	EXIT CONCENTRATION DIMENSIONLESS	
		EXPERIMENTAL	MODEL
0	.000	.000	.000
2	.239	.004	.004
4	.477	.018	.018
6	.716	.055	.055
9	.955	.185	.184
11	1.193	.600	.595
13	1.432	.613	.609
15	1.670	.547	.544
18	1.909	.453	.451
20	2.148	.360	.359
22	2.386	.286	.286
24	2.625	.229	.230
27	2.864	.185	.186
29	3.102	.151	.153
31	3.341	.120	.122
33	3.580	.092	.094
36	3.818	.074	.077
38	4.057	.059	.062
40	4.295	.048	.051
42	4.534	.044	.047
45	4.773	.037	.040

TABLE T23 : RUN3

TIME (S)	DIMENSIONLESS TIME (THETA)	EXIT CONCENTRATION DIMENSIONLESS	
		EXPERIMENTAL	MODEL
0	.000	.000	.000
2	.280	.004	.004
4	.559	.016	.016
6	.839	.050	.050
9	1.118	.210	.209
11	1.398	.660	.656
13	1.677	.870	.886
15	1.957	.540	.537
18	2.236	.410	.409
20	2.516	.292	.292
22	2.795	.220	.221
24	3.075	.168	.169
27	3.355	.128	.130
29	3.634	.090	.092
31	3.914	.064	.067
33	4.193	.048	.051
36	4.473	.032	.035
38	4.752	.030	.033

TABLE T24 : RUN4

TIME (S)	DIMENSIONLESS TIME (THETA)	EXIT CONCENTRATION DIMENSIONLESS	
		EXPERIMENTAL	MODEL
0	.000	.000	.000
1	.194	.016	.016
2	.389	.049	.050
4	.583	.112	.113
5	.777	.451	.451
6	.972	.663	.663
8	1.166	.669	.669
9	1.360	.614	.615
10	1.555	.498	.499
12	1.749	.396	.398
13	1.943	.325	.327
14	2.137	.274	.276
16	2.332	.224	.227
17	2.526	.183	.186
18	2.720	.150	.153
20	2.915	.122	.125
21	3.109	.102	.106
22	3.303	.081	.085
24	3.498	.071	.075
25	3.692	.057	.061
27	3.886	.051	.055
28	4.081	.041	.045

TABLE T25 : RUN5

TIME (S)	DIMENSIONLESS TIME (THETA)	EXIT CONCENTRATION DIMENSIONLESS	
		EXPERIMENTAL	MODEL
0	.000	.000	.000
1	.219	.010	.010
2	.438	.035	.035
4	.657	.086	.085
5	.875	.298	.295
6	1.094	.547	.541
8	1.313	.605	.598
9	1.532	.595	.588
10	1.751	.499	.494
12	1.970	.423	.419
13	2.189	.338	.335
14	2.407	.259	.257
16	2.626	.200	.199
17	2.845	.154	.154
18	3.064	.125	.126
20	3.283	.104	.105
21	3.502	.086	.087
22	3.721	.069	.071
24	3.940	.058	.060
25	4.158	.048	.050
27	4.377	.038	.040

TABLE T26 : RUN6

TIME (S)	DIMENSIONLESS TIME (THETA)	EXIT CONCENTRATION DIMENSIONLESS	
		EXPERIMENTAL	MODEL
0	.000	.000	.000
1	.245	.007	.007
2	.489	.020	.020
4	.734	.046	.046
5	.979	.083	.083
6	1.223	.175	.176
8	1.468	.544	.545
9	1.712	.597	.598
10	1.957	.560	.561
12	2.202	.472	.473
13	2.446	.359	.360
14	2.691	.267	.268
16	2.936	.212	.214
17	3.180	.170	.172
18	3.425	.138	.140
20	3.670	.111	.113
21	3.914	.088	.090
22	4.159	.070	.072
24	4.403	.059	.061
25	4.648	.048	.050
27	4.893	.044	.046
28	5.137	.041	.043
29	5.382	.037	.039

TABLE T27 : RUN7

TIME (S)	DIMENSIONLESS TIME (THETA)	EXIT CONCENTRATION DIMENSIONLESS	
		EXPERIMENTAL	MODEL
0	.000	.000	.000
1	.270	.031	.031
2	.540	.134	.133
4	.810	.567	.561
5	1.080	.660	.654
6	1.350	.608	.604
8	1.620	.495	.493
9	1.890	.371	.371
10	2.160	.247	.250
12	2.430	.175	.180
13	2.700	.132	.138
14	2.970	.095	.102
16	3.240	.072	.079
17	3.510	.052	.060
18	3.780	.037	.045
20	4.050	.029	.038
21	4.320	.025	.034
22	4.590	.021	.030

TABLE T2B : RUN8

TIME (S)	DIMENSIONLESS TIME (THETA)	EXIT CONCENTRATION DIMENSIONLESS	
		EXPERIMENTAL	MODEL
0	.000	.000	.000
1	.299	.010	.010
2	.597	.028	.028
4	.896	.069	.069
5	1.195	.244	.245
6	1.493	.666	.667
8	1.792	.630	.632
9	2.090	.528	.530
10	2.389	.356	.358
12	2.688	.234	.236
13	2.986	.173	.175
14	3.285	.130	.132
16	3.584	.098	.100
17	3.882	.077	.079
18	4.181	.061	.063
20	4.480	.049	.052
21	4.778	.033	.036
22	5.077	.028	.031

TABLE T29 : RUN9

TIME (S)	DIMENSIONLESS TIME (THETA)	EXIT CONCENTRATION DIMENSIONLESS	
		EXPERIMENTAL	MODEL
0	.000	.000	.000
1	.324	.010	.010
2	.649	.027	.027
4	.973	.058	.059
5	1.298	.125	.126
6	1.622	.232	.233
8	1.948	.405	.406
9	2.271	.560	.561
10	2.595	.473	.474
12	2.920	.348	.350
13	3.244	.241	.243
14	3.569	.174	.176
16	3.893	.135	.137
17	4.217	.106	.109
18	4.542	.077	.080
20	4.866	.058	.061
21	5.191	.046	.049
22	5.515	.031	.034

APPENDIX C

PROGRAM LISTINGS FOR THE NORMALIZATION OF THE EXPERIMENTAL DATA AND RTD MODEL

```
1 C       PROGRAMME TO CALCULATE THE RESIDENCE TIME DISTRIBUTION
2 C       IN A CONTINUOUS NOZZLE REACTOR
3         DIMENSION X(40),Y(40)
4         DIMENSION T(40),DT(40),DCONC(40)
5         REAL MRT,MT,JETA,JETV,JETRE,JETM
6         COMMON/COKE/N
7         INTEGER RUN,TIME(40)
8 C       VOLUME OF THE REACTOR V:LITRE
9 C       VOLUME FLOW RATE Q:LITRE/MIN
10 C      DENSITY OF FLUID RHO:KG/LITRE
11 C      INTERNAL DIAMETER OF REACTOR DR:MM
12 C      INTERNAL DIAMETER OF INLET TUBE DJ:MM
13 C      VISCOSITY OF FLUID VIS:KG/M.S
14 C      REYNOLDS NUMBER :RE
15        READ(7,-)RUN
16        READ(7,-)V,DR,DJ
17        READ(7,-)Q1,Q2,MT
18        Q=Q1+Q2
19        RHO=0.998
20        VIS=0.001
21        PIE=3.1416
22        RE1=(4*RHO*Q1)/(PIE*DJ*0.001*VIS*60.0)
23        RE2=(4*RHO*Q2)/(PIE*DJ*0.001*VIS*60.0)
24        RE=(4*RHO*Q)/(PIE*DR*0.001*VIS*60.0)
25        WRITE(6,1000)
26   1000 FORMAT(1H ,3X,'REYNOLDS NUMBERS'//,1H ,3X,
27       *'INLET NOZZLE 1',5X,'INLET NOZZLE 2',5X,'CYLINDRICAL REACTOR',
28       *//,1H ,60(1H*))
29        WRITE(6,1500)RE1,RE2,RE
30   1500 FORMAT(1H ,3(E10.4,15X))
31 C
32 C
33 C      READ RAW DATA IN CM.
34        READ(7,-)N
35        DO 10 I =1,N
36        READ(7,-)X(I),Y(I)
37     10 CONTINUE
38 C
39        WRITE(6,1550)V,Q
40   1550 FORMAT(1H ,///,3X,'VOLUME OF THE REACTOR','=',
41       *F10.4,3X,'L',1H ,///,3X,'VOLUME FLOW RATE','=',
42       *F10.4,3X,'L/MIN')
43 C      MEAN RESIDENCE TIME OF THE REACTOR SYSTEM
44        MRT=(V*60.0)/Q
45        WRITE(6,1600)MRT
46   1600 FORMAT(1H ,//3X,'MEAN RESIDENCE TIME:SEC',
47       *F10.4,3X,'SEC')
48 C      RECORDER CHART SPEED :CM/MIN
49 C      PROJECTOR SPEED :FRAMES/SEC
50 C      FILM SPEED :FRAMES/SEC
51        READ(7,-)CS,PS,FS
52        RT=(PS*60.0)/(FS*CS)
53 C      REAL TIME IN SECONDS :SEC/CM
54        DO 20 I=1,N
```

```
55          T(I)=X(I)*RT
56          DT(I)=T(I)/MRT
57          TIME(I)=T(I)
58        2Ø CONTINUE
59          WRITE(6,17ØØ)RT
60     17ØØ FORMAT(1H ,//,3X,'REAL TIME','=',F1Ø.4,3X,'SEC/CM')
61          CALL SIMPS(X,Y,H,AREA)
62          WRITE(6,2ØØØ)AREA
63     2ØØØ FORMAT(1H ,//,3X,'AREA UNDER CURVE','=',F1Ø.4,3X,'CM^2)
64 C        THE VALUE OF THE DIMENSIONLESS RESIDENCE TIME .DRT. IN CM.
65 C        AT WHICH T=MRT
66          DRT=MRT/RT
67          WRITE(6,18ØØ)DRT
68     18ØØ FORMAT(1H ,//3X,'RESIDENCE TIME IN CM.','=',F1Ø.4,3X,'CM.')
69 C        THE CORRESPONDING VALUE OFTHE DIMENSIONLESS CONCENTRATION
70 C        IN CM. AT WHICH DRT=1.Ø
71          DC=AREA/DRT
72          WRITE(6,25ØØ)DC
73     25ØØ FORMAT(1H ,//3X,'DIMENSIONLESS CONCENTRATION IN CM.',
74         *'=',F1Ø.4,3X,'CM')
75          DO 3Ø I=1,N
76          DCONC(I)=Y(I)/DC
77        3Ø CONTINUE
78          H1=DT(2)-DT(1)
79          CALL SIMPS1(DT,DCONC,H1,RESULT)
80          AMRT=RESULT
81          WRITE(6,27ØØ)AMRT
82     27ØØ FORMAT(1H ,//3X,'AREA UNDER THETA AND E(THETA) =',F1Ø.4)
83          WRITE(6,3ØØØ)
84     3ØØØ FORMAT(1H ,//,1ØX,'TIME',3X,'DIMENSIONLESS RESIDENCE TIME',
85         *4X,'DIMENSIONLESS CONCENTRATION',/1H ,7Ø(1HX*))
87          DO 4Ø I=1,N
88          WRITE(6,4ØØØ)I,TIME(I),DT(I),DCONC(I)
89     4ØØØ FORMAT(1H ,I2,6X,I3,8X,2(F1Ø.3,3ØX))
90        4Ø CONTINUE
91          CALL PLOT(DT,DCONC,RE,RUN)
92          STOP
93          END
94          SUBROUTINE SIMPS(A,B,H,AREA)
95          COMMON/COKE/N
96          DIMENSION A(4Ø),B(4Ø)
97          H=A(2)-A(1)
98          NPANEL=N-1
99          NHALF=NPANEL/2
100         NBEGIN=1
101         AREA=Ø.Ø
102         IF((NPANEL-2*NHALF) .EQ. Ø) GO TO 5Ø
103         AREA=(3.*H)/8*(B(1)+3*B(2)+3*B(3)+B(4))
104         NBEGIN=4
105       5Ø AREA=AREA+H/3*(B(NBEGIN+4*B(NBEGIN+1)+B(N))
106         NBEGIN=NBEGIN+2
107         IF(NBEGIN .EQ. N)RETURN
108         NEND=N-2
109         DO 6Ø I=NBEGIN,NEND,2
```

```
110         AREA=AREA+H/3*(2*B(I)+4*B(I+1))
111      60 CONTINUE
112         RETURN
113         END
114         SUBROUTINE SIMPS1(DT,DCONC,H1,RESULT)
115         COMMON/COKE/N
116         DIMENSION DT(40),DCONC(40)
117 C       CHECK TO SEE IF NO. OF PANELS IS EVEN
118 C       IS N-1
119         NPANEL=N-1
120         NHALF=NPANEL/2
121         NBEGIN=1
122         RESULT=0.0
123         IF((NPANEL-2*NHALF) .EQ. 0) GO TO 222
124 C       NO. OF PANELS IS ODD USE 3/8 RULE
125 C       ON FIRST THREE PANELS,1/3 RULE ON REST OF THEM
126         RESULT=3*H1/8*(DCONC(1)+3*DCONC(2)+3*DCONC(3)+DCONC(4))
127         NBEGIN=4
128 C       APPLY 1/3 RULE -ADD IN FIRST, SECOND,LAST VALUES
129    222  RESULT=RESULT+H1/3*(DCONC(NBEGIN)+4*DCONC(NBEGIN+1)+DCONC(N))
130         NBEGIN=NBEGIN+2
131         IF(NBEGIN .EQ. N)RETURN
132         NEND=N-2
133         DO 333 I=NBEGIN,NEND,2
134         RESULT=RESULT+H1/3*(2*DCONC(I)+4*DCONC(I+1))
135    333  CONTINUE
136         RETURN
137         END
138         SUBROUTINE PLOT(DT,DCONC,RE,RUN)
139         DIMENSION DT(40),DCONC(40)
140         INTEGER RUN
141         COMMON/COKE/N
142         CALL TEMPO(AY,DCONC)
143         AX=DT(N)
144         XX=AX+0.25
145         PP=0.30+AY
146         QQ=.39+AY
147         TT=0.59+XX
148         SS=0.39+XX
149         AA=AY-PP
150         BB=AY-QQ
151         CC=XX-TT
152         DD=XX-SS
153         YY=AY+0.5
154         ZZ=YY+0.1
155         ZZ1=YY-0.1
156         WW=YY-0.2
157         CALL GINO
158         CALL SOFCHA
159         CALL UNITS(0.70)
160         CALL SHIFT2(50.0,50.0)
161         CALL CHASIZ(3.0,5.0)
162         CALL AXIPOS(1,0.0,0.0,160.0,1)
163         CALL AXIPOS(1,0.0,0.0,120.0,2)
```

```
      CALL AXISCA(3,10,0.0,XX,1)
      CALL AXISCA(3,10,0.0,YY,2)
      CALL AXIDRA(1,1,1)
      CALL AXIDRA(-1,-1,2)
      CALL GRASYM(DT,DCONC,N,8,0)
      CALL GRAPOL(DT,DCONC,N)
      CALL GRAMOV(.5,AA)
      CALL CHAHOL('DIMENSIONLESS RESIDENCE TIME*.')
      CALL GRAMOV(.55,BB)
      CALL CHAHOL('REYNOLDS NUMBER=*.')
      CALL GRAMOV(2.0,BB)
      CALL CHAFLO(RE,10)
      CALL GRAMOV(CC,.2)
      CALL CHAANG(90.)
      CALL CHAHOL('DIMENSIONLESS CONCENTRATION*.')
      CALL CHAANG(0.)
      CALL GRAMOV(DD,.2)
      CALL CHAANG(90.)
      CALL CHAHOL('E - FUNCTION*.')
      CALL CHAANG(0.)
      CALL GRAMOV(1.5,ZZ)
      CALL CHAHOL('EXPERIMENTAL RUN F*.')
      CALL CHAINT(RUN,-3)
      CALL GRAMOV(1.5,WW)
      CALL CHAHOL('RESIDENCE TIME DISTRIBUTION*.')
      CALL GRAMOV(1.5,WW)
      CALL CHAHOL('TO A PULSE INPUT OF A TRACER*.')
      CALL DEVEND
      RETURN
      END
      SUBROUTINE TEMPO(AY,DCONC)
      DIMENSION DCONC(40)
      COMMON/COKE/N
      AY=DCONC(1)
      DO 90 I=1,N
      IF(DCONC(I) .GT. AY)AY=DCONC(I)
   90 CONTINUE
      WRITE(6,5000)AY
 5000 FORMAT(1H ,//,3X,'AY', '=',F10.4)
      RETURN
      END
EOF
EOT
```

```
C       MATHEMATICAL MODEL TO SIMULATE THE RESIDENCE TIME DISTRIBUTION
C       OF A RESPONSE CURVE TO A PULSE INPUT OF A TRACER
        DIMENSION U(100),YR(100),XE(100),YE(100)
        REAL A,B,J,K,M,N,L
        REAL K1,IT,MRT,P
        INTEGER D,TIME(100)
        COMMON/COKE1/K1
        COMMON/COKE2/XP(100)
        COMMON/COKE3/TR(100)
        COMMON/COKE4/WR(100)
        COMMON/COKE5/XEND,I
        WRITE(6,1000)
 1000 FORMAT(30X,'A',6X,'B',6X,'J',6X,'K',6X,'M',6X,'N',6X,'L')
        L2=0
        READ(7,-)IT,MRT
        READ(7,-)N1
        DO 20 J1=1,N1
        READ(7,-)J1,TIME(J1),XE(J1),YE(J1)
        L2=L2+1
   20 CONTINUE
        HT1=XE(2)-XE(1)
        HT2=IT/MRT
        P=HT2
        RATIO=HT1/HT2
        XP(1)=0.0
        DO 25 J2=2,N1
        XP(J2)=XP(J2-1)+HT2
        E=XP(J2)
   25 CONTIUE
   30 KKK=1
        DO 35 I1=1,L2
        U(I1)=0.0
        TR(I1)=0.0
        WR(I1)=0.0
        YR(I1)=0.0
   35 CONTINUE
        WRITE(1,1500)
 1500 FORMAT(1H1,'INPUT A,B,J,K,M,N,L')
        READ(1,-)A,B,J,K,M,N,L
        WRITE(6,2000)A,B,J,K,M,N,L
 2000 FORMAT(20X,7F8.3)
        WRITE(6,1110)HT1,E,L2
 1110 FORMAT(30X,'HT1=',F7.3,6X,'E=',F7.3,6X,'L2=',I4)
        IF(A .EQ. 0.0) GO TO 101
        WRITE(6,1120)HT2,RATIO,P
 1120 FORMAT(30X,'HT2=',F7.3,6X,'RATIO=',F7.3,6X,'P=',F7.3)
        CALL SUB1(L2,WR,YE,RATIO)
        DO 40 I1=1,L2
        TR(I1)=WR(I1)
   40 CONTINUE
        IF(ABS(J+K+M+N+L-1) .LT. 0.001) GO TO 55                    A1
C       CONTINUOUS STIRRED TANK REACTOR
        K1=A/(1-J-K-M-N-L)
        WRITE(6,2500)K1
```

```
55          CALL SUB2(E)
56       55 DO 5Ø I1=1,L2
57          U(I1)=WR(I1)
58       5Ø CONTINUE
59          IF(J .EQ. Ø.Ø) GO TO 8Ø
6Ø C        DELAY                                          A2
61          DO 6Ø I1=1,L2
62          TR(I1)=U(I1)
63       6Ø CONTINUE
64          D=J/(A*P)+Ø.5
65          WRITE(6,3ØØØ)D
66          CALL SUB3(D,L2,TR,WR)
67          DO 7Ø I1=1,L2
68          U(I1)=WR(I1)
69       7Ø CONTINUE
7Ø       8Ø IF(K .EQ. Ø.Ø) GO TO 1Ø1
71 C        C.S.T.R.                                       A3
72          DO 9Ø I1=1,L2
73          TR(I1)=U(I1)
74       9Ø CONTINUE
75          K1=A/K
76          WRITE(6,25ØØ)K1
77          CALL SUB2(E)
78          DO 1ØØ I1=1,L2
79          U(I1)=WR(I1)
8Ø      1ØØ CONTINUE
81      1Ø1 IF(B .EQ. Ø.Ø) GO TO 151
82 C        DELAY                                          B1
83          CALL SUB1(L2,WR,YE,RATIO)
84          DO 11Ø I1=1,L2
85          YR(I1)=WR(I1)
86          TR(I1)=WR(I1)
87      11Ø CONTINUE
88          IF(M .EQ. Ø.Ø) GO TO 131
89          D=M/(B*P)+Ø.5
9Ø          WRITE(6,3ØØØ)D
91          CALL SUB3(D,L2,TR,WR)
92          DO 12Ø I1=1,L2
93          YR(I1)=WR(I1)
94      12Ø CONTINUE
95      131 IF(N .EQ. Ø.Ø) GO TO 151
96 C        C.S.T.R.                                       B2
97       DO 13Ø I1=1,L2
98          TR(I1)=YR(I1)
99      13Ø CONTINUE
1ØØ         K1=B/N
1Ø1         WRITE(6,25ØØ)K1
1Ø2         CALL SUB2(E)
1Ø3         DO 14Ø I1=1,L2
1Ø4         YR(I1)=WR(I1)
1Ø5     14Ø CONTINUE
1Ø6     151 CALL SUB1(L2,WR,YE,RATIO)
1Ø7         DO 15Ø I1=1,L2
1Ø8         TR(I1)=WR(I1)
```

```
109    15Ø CONTINUE
11Ø         IF(ABS(1.-A-B) .LT. Ø.ØØ1) GO TO 157
111 C       DELAY                                                    C1
112         D=L/(P*(1.Ø-A-B))+Ø.5
113         WRITE(6,3ØØØ)D
114         CALL SUB3(D,L2,TR,WR)
115 C       CALCULATE RESPONSE
116    157  DO 16Ø I1=1,L2
117         WR(I1)=A*U(I1)+B*YR(I1)+(1.Ø-A-B)*WR(I1)
118         WRITE(6,35ØØ)TIME(I1),XE(I1),YE(I1),WR(I1)
119    16Ø  CONTINUE
12Ø   35ØØ FORMAT(1H ,2ØX,I3,3F1Ø.3)
121   3ØØØ FORMAT(1H ,2ØX,I6)
122   25ØØ FORMAT(1H ,2ØX,F1Ø.3)
123 C       SUM OF SQUARED ERRORS,VARIANCE AND STANDARD DEVIATION
124         S1=Ø.Ø
125         DO 17Ø L=1,L2
126         S1=S1+(YE(L)-WR(L))**2
127    17Ø  CONTINUE
128         S2=S1/(L2-2)
129         S3=SQRT(S2)
13Ø         WRITE(6,4ØØØ)S1,S2,S3
131   4ØØØ FORMAT(1H ,2ØX,'SUM OF SQUARED ERROR=',F1Ø.4/2ØX,
132        *'VARIANCE=',F1Ø.4/2ØX,'STANDARD DEVIATION=',F1Ø.4)
133         WRITE(1,2ØØ)
134    2ØØ  FORMAT(1H1,'DO YOU WANT MORE TRIAL?')
135         WRITE(1,2Ø1)
136    2Ø1  FORMAT(1H1,'INPUT 1 YES AND Ø FOR NO')
137         READ(1,-)KKK
138         IF(KKK .EQ. 1) GO TO 3Ø
139         STOP
14Ø         END
141         SUBROUTINE SUB1(L2,WR,YE,RATIO)
142         REAL YE(1ØØ),WR(1ØØ)
143         DO 9Ø I2=1,L2
144         WR(I2)=RATIO*YE(I2)
145      9Ø CONTINUE
146         RETURN
147         END
148         SUBROUTINE SUB2(E)
149         REAL XEND,TOL,X,W(2,7),Y(2)
15Ø         COMMON/COKE5/XEND,I
151         EXTERNAL FCN,OUT
152         N=1
153         I=1
154         IR=1
155         TOL=1Ø.Ø**(-4)
156         X=Ø.Ø
157         XEND=E
158         Y(1)=Ø.Ø
159         IFAIL=1
16Ø         CALL DØ2BBF(X,XEND,N,Y,TOL,IR,FCN,OUT,W,IFAIL)
161         IF(TOL .LT. Ø.Ø)WRITE(6,45ØØ)
162   45ØØ FORMAT(1H ,5X,'RANGE TOO SHORT FOR TOL')
```

```
163         IF(IFAIL .GT. Ø.Ø) WRITE(6,5ØØØ)IFAIL
164   5ØØØ FORMAT(1H ,5X,'IFAIL=',I1)
165         RETURN
166         END
167         SUBROUTINE FCN(T,Y,F)
168         REAL T,F(2),Y(2),K1
169         COMMON/COKE1/K1
170         COMMON/COKE3/TR(1ØØ)
171         COMMON/COKE5/XEND,I
172         F(1)=K1*(TR(I)-Y(1))
173         RETURN
174         END
175         SUBROUTINE OUT(X,Y)
176         REAL X,Y(2),XEND
177         COMMON/COKE4/WR(1ØØ)
178         COMMON/COKE2/XP(1ØØ)
179         COMMON/COKE5/XEND,I
180         WR(I)=Y(1)
181         I=I+1
182         X=XP(I)
183         RETURN
184         END
185         SUBROUTINE SUB3(D,L2,TR,WR)
186         REAL WR(1ØØ),TR(1ØØ)
187         IF(D .LT. 1) GO TO 5Ø
188         IF(D .GT. L2) GO TO 6Ø
189         DO 4Ø J2=1,L2
190         J2=L2+1-J2
191         IF(J2 .LT. D) GO TO 7Ø
192         U1=TR(J2-D)
193         GO TO 8Ø
194       7Ø U1=Ø.Ø
195       8Ø WR(J2)=U1
196       4Ø CONTINUE
197         GO TO 1Ø
198       5Ø DO 2Ø J2=1,L2
199         WR(J2)=TR(J2)
200       2Ø CONTINUE
201         GO TO 1Ø
202       6Ø DO 3Ø J2=1,L2
203         WR(J2)=Ø.Ø
204       3Ø CONTINUE
205       1Ø CONTINUE
206         RETURN
207         END
EOF..
EOT..
```

APPENDIX D

GRAPHS OF THE VISCOSITY OF DOBANIC ACID AND,

WITH 111 TRICHOLOROETHANE

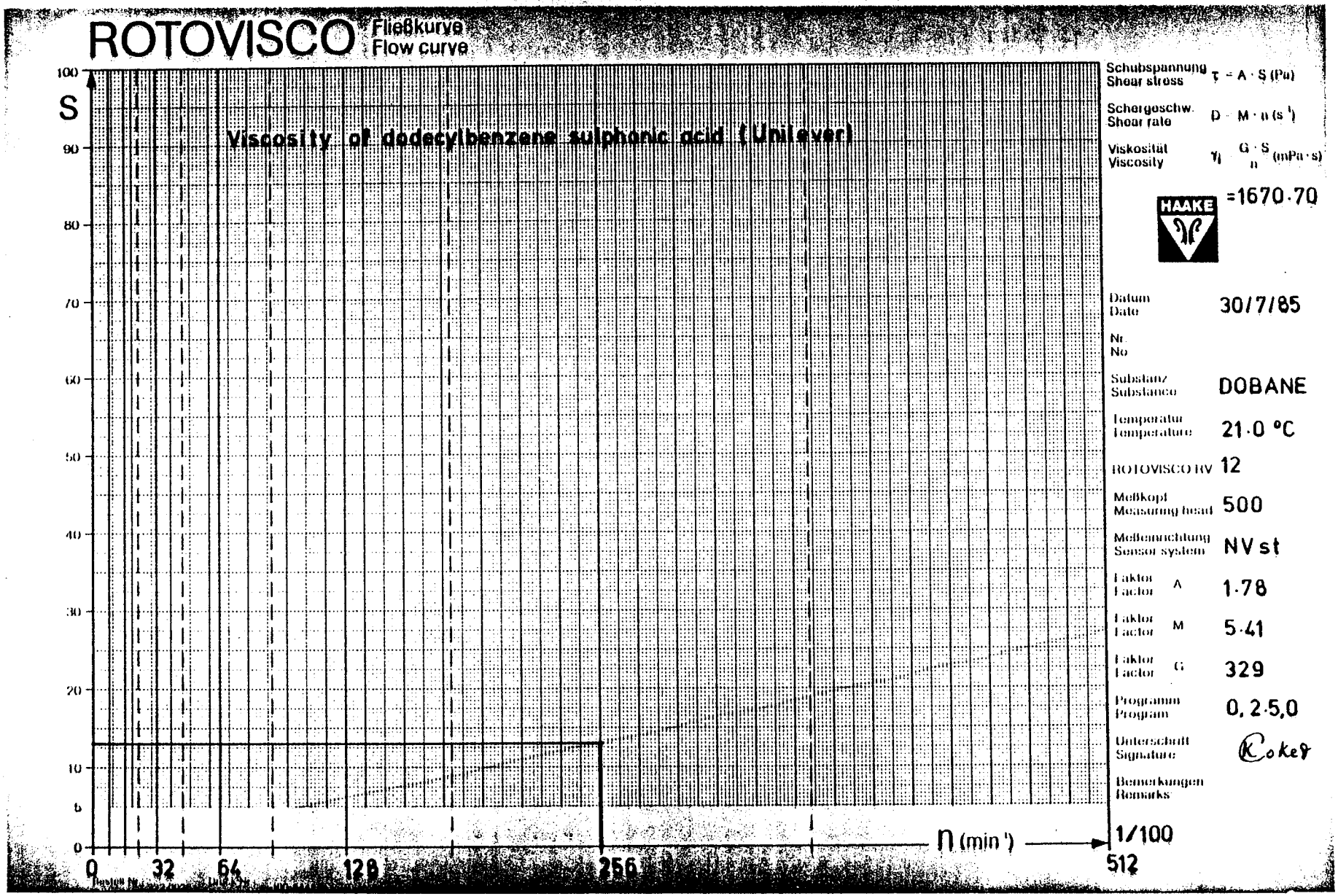
ROTOVISCO
Fließkurve
Flow curve
Viscosity of dodecylbenzene sulphonic acid (Unilever)
S
100
90
80
70
60
50
40
30
20
10
5
0
0
32
64
128
256
512
n (min⁻¹)
Schubspannung
Shear stress
τ = A · S (Pa)
Schergeschw.
Shear rate
D = M · n (s⁻¹)
Viskosität
Viscosity
η G · S / n (mPa · s)
HAAKE
=1670·70
Datum
Date
30/7/85
Nr.
No
Substanz
Substance
DOBANE
Temperatur
Temperature
21·0 °C
ROTOVISCO RV
12
Meßkopf
Measuring head
500
Meßeinrichtung
Sensor system
NV st
Faktor
Factor
A
1·78
Faktor
Factor
M
5·41
Faktor
Factor
G
329
Programm
Program
0, 2·5,0
Unterschrift
Signature
Coker
Bemerkungen
Remarks
1/100

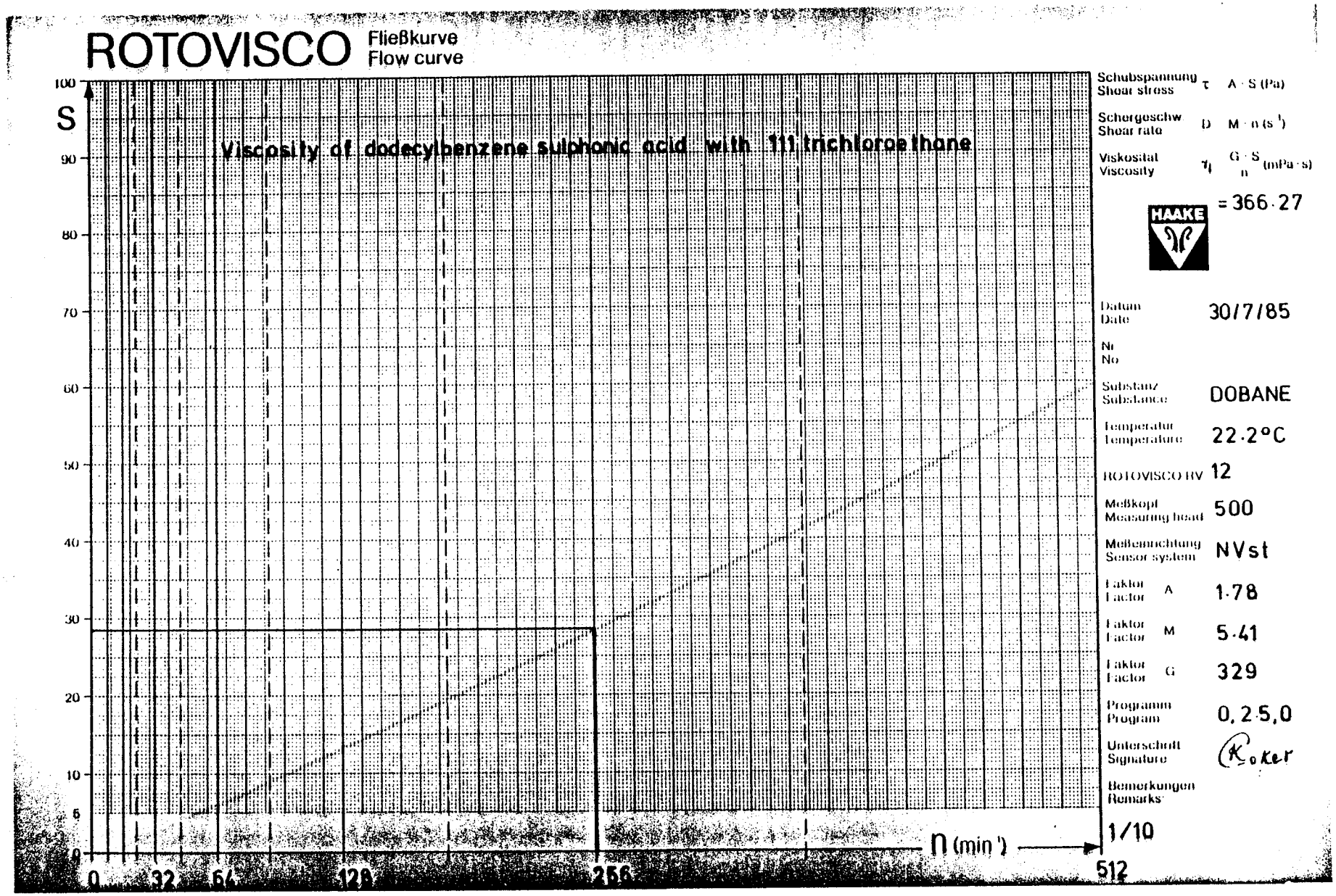
ROTOVISCO
Fließkurve
Flow curve
Viscosity of dodecylbenzene sulphonic acid with 111 trichloroethane
S
100
90
80
70
60
50
40
30
20
10
6
0
0
32
64
128
256
512
n (min⁻¹)
Schubspannung
Shear stress
τ
A · S (Pa)
Schergeschw
Shear rate
D
M · n (s⁻¹)
Viskosität
Viscosity
η
G · S / n (mPa · s)
= 366 · 27
HAAKE
Datum
Date
30/7/85
Nr
No
Substanz
Substance
DOBANE
Temperatur
Temperature
22.2°C
ROTOVISCO RV
12
Meßkopf
Measuring head
500
Meßeinrichtung
Sensor system
NVst
Faktor
Factor
A
1.78
Faktor
Factor
M
5.41
Faktor
Factor
G
329
Programm
Program
0, 2.5, 0
Unterschrift
Signature
Bemerkungen
Remarks
1/10

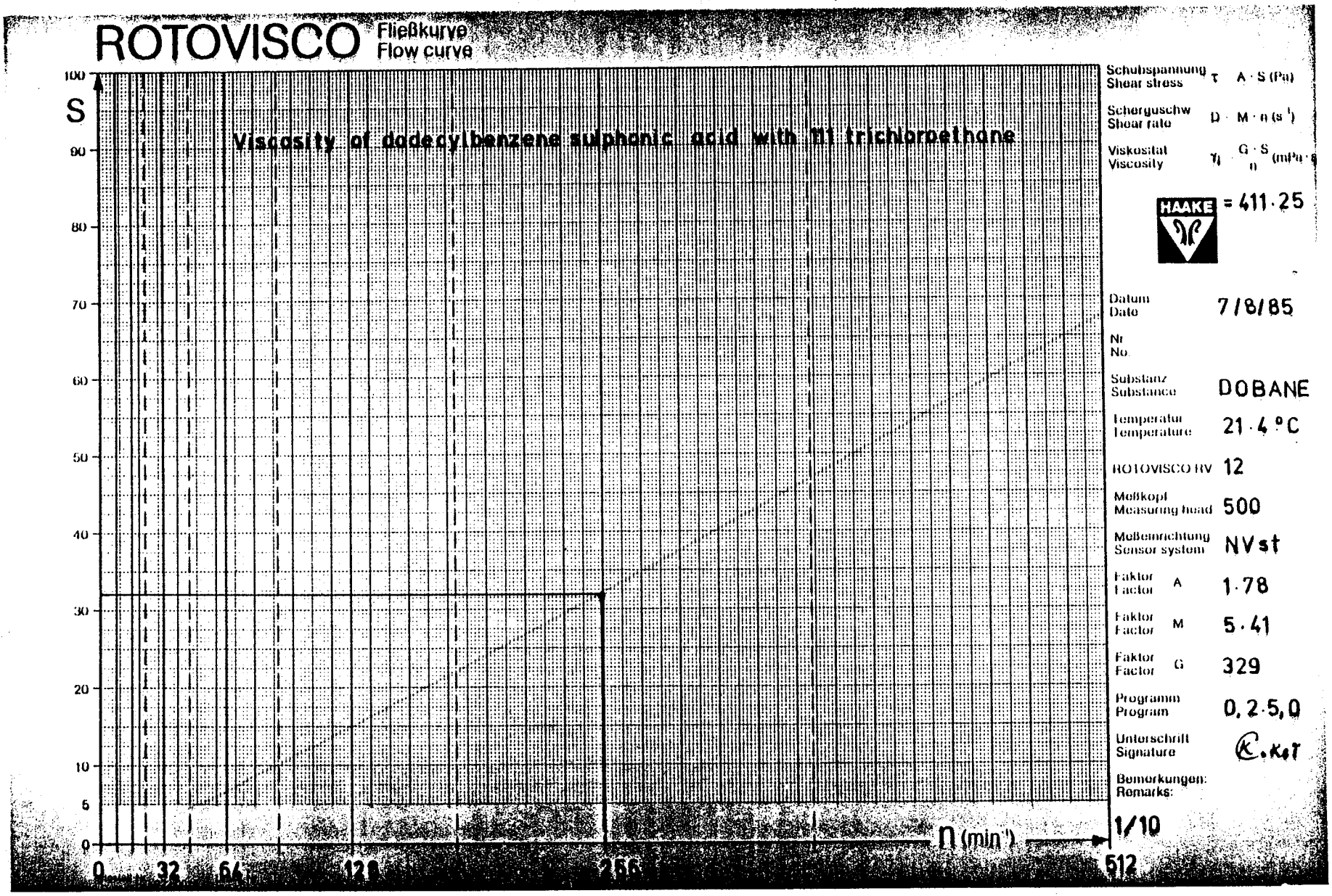
ROTOVISCO Fließkurve
Flow curve
Viscosity of dodecylbenzene sulphonic acid with 11 trichloroethane
S
100
90
80
70
60
50
40
30
20
10
5
0
n (min⁻¹)
0
32
64
128
256
512
Schubspannung Shear stress τ A · S (Pa)
Scherguschw Shear rate D · M · n (s⁻¹)
Viskosität Viscosity η G · S / n (mPa · s)
HAAKE = 411·25
Datum Date 7/8/85
Nr No
Substanz Substance DOBANE
Temperatur Temperature 21·4 °C
ROTOVISCO RV 12
Meßkopf Measuring head 500
Meßeinrichtung Sensor system NVst
Faktor Factor A 1·78
Faktor Factor M 5·41
Faktor Factor G 329
Programm Program 0, 2·5, 0
Unterschrift Signature
Bemerkungen: Remarks:
1/10

ROTOVISCO Fließkurve / Flow curve

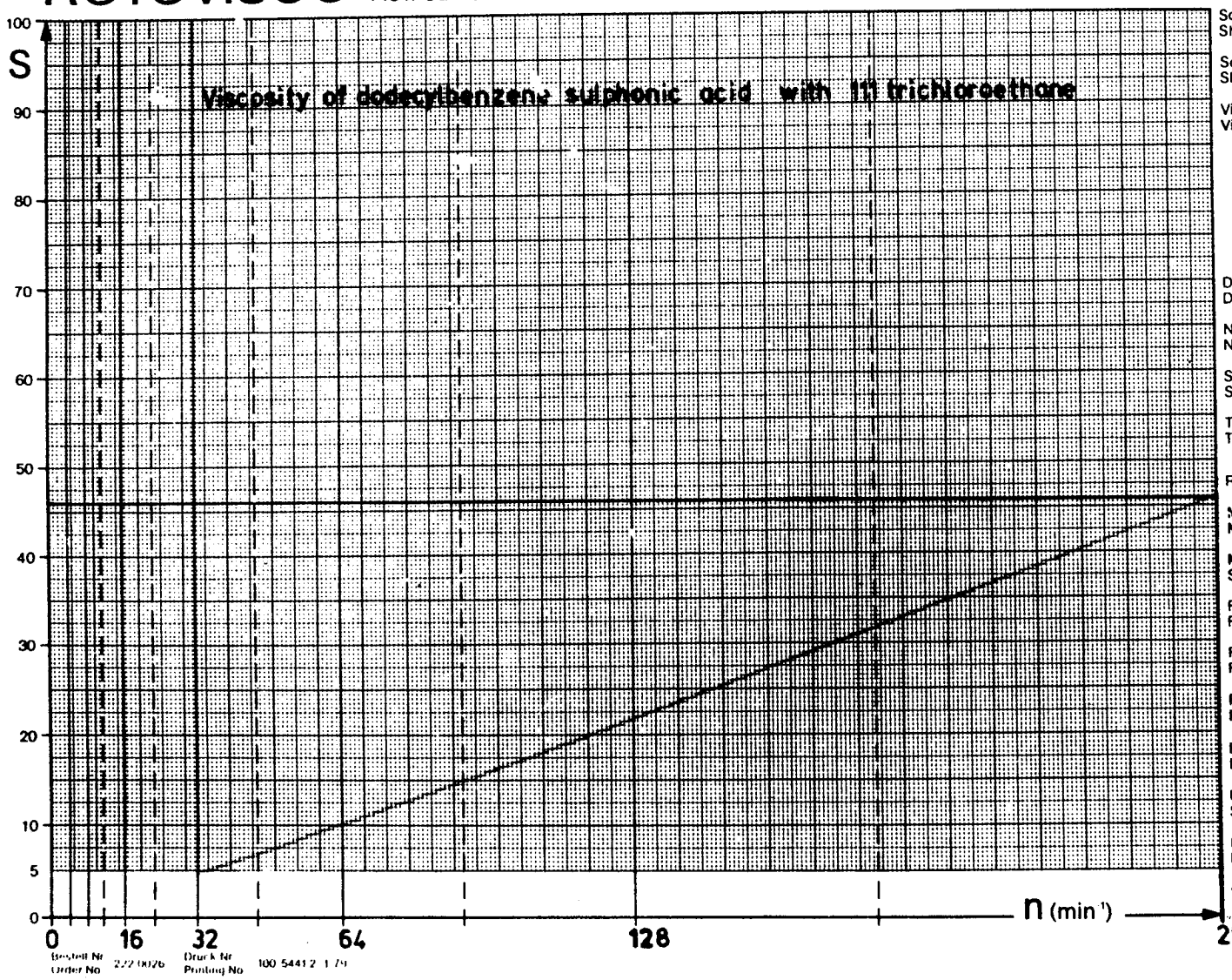

Schubspannung / Shear stress $\tau = A \cdot S$ (Pa)

Schergeschw. / Shear rate $D = M \cdot n$ (s^{-1})

Viskosität / Viscosity $\eta = \frac{G \cdot S}{n}$ (mPa·s)

HAAKE =591.17

Datum / Date 11/9/85

Nr. / No.

Substanz / Substance DOBANE

Temperatur / Temperature 21.6 °C

ROTOVISCO RV 12

Meßkopf / Measuring head 500

Meßeinrichtung / Sensor system NVst

Faktor / Factor A 1.78

Faktor / Factor M 5.41

Faktor / Factor G 329

Programm / Program 0,2.5,0

Unterschrift / Signature

Bemerkungen: / Remarks:

1/10

Bestell Nr / Order No 222 0026 Druck Nr / Printing No 100 5441 2 1 79

NOMENCLATURE

a	Radius of an inner cylindrical core	mm
a_{cr}	Critical radius of the bubble	mm
A_o	Area of orifice	m^2
A_s	Area of inlet swirl channel	m^2
C	Concentration	Kg mole.m^{-3}
d_i	Inlet orifice diameter	mm
d_o	Outlet orifice diameter	mm
D	Nozzle vessel diameter	mm
$E(t)$	Exit age distribution function	-
F_C	Centrifugal force	N
F_D	Drag force	N
F_R	Resultant force	N
$F(t)$	Cumulative exit age distribution	-
g	Gravitational acceleration	$m.s^{-2}$
k	Reaction rate constant	s^{-1}
P	Pressure	$N.m^{-2}$
Q_T	Volumetric flow rate	$m^3.s^{-1}$
R_{AC}	Radius of air - core	mm
R_I	Radius of inlet orifice	mm
R_o	Radius of outlet orifice	mm

t	Time	s
$\bar{t}$	Mean residence time	s
V	Volume of the gas bubble	m^3
V_T	Volume of the nozzle reactor	m^3
r, θ, z	Cylindrical co - ordinates	
V_r	Radial velocity component	$m.s^{-1}$
V_θ	Tangential velocity component	$m.s^{-1}$
V_z	Axial velocity component	$m.s^{-1}$
X	Fractional conversion	-

GREEK LETTERS

α	Age	
θ	Dimensionless mean residence time	$(\frac{t}{\bar{t}})$
λ	Life expectancy	
μ	Viscosity	$(kg.m^{-1}.s^{-1})$
π	Constant = 3.1416	
ρ	Density	$(kg.m^{-3})$
Ω	Circulation constant	$(m^2.s^{-1})$
ω	Angular velocity	$(rad.s^{-1})$
Φ	Over all yield	

DIMENSIONLESS GROUPS

Fr	Froude number	$\frac{V_I^2}{D_I g}$ or $\frac{N^2 D}{g}$
Re	Reynolds number	$\frac{\rho V_I D_I}{\mu}$
Θ	Dimensionless mixing time	$\frac{T_i V_i}{D_i}$

Subscripts:

ac	air - core
cr	critical
g	gas
i	Inlet orifice of the nozzle reactor
l	liquid
o	Outlet orifice of the nozzle reactor

REFERENCES

1. Uhl, V.W., and Gray, J.B., Mixing: Theory and Practice Vol. 1, Academic Press Inc (1966).
2. Brodkey, R.S., Chem. Eng. Commun., 8, 1 (1981).
3. Westerterp, K.R., van Swaaij, W.P.M., and Beenackers, A.A.C.M., Chemical Reactor Design and Operation. John Wiley and Sons (1984).
4. Charpentier, J.C., Trans. Inst. Chem. Engrs., 60, 131 (1982).
5. Beenackers, A.A.C.M., and van Swaaij, W.P.M., Chem. Reaction Eng. Proc. 6th Europ., 4th Int. Symp., Dechema,Frankfurt am Maim, p. VI - 260 (1976).
6. Goldstein, A.M., Chem. Eng. Sci., 28, 1021 (1973).
7. Dahlstrom, D.A., Chem. Eng. Prog. Symp. Ser., 50, 41 (1954).
8. Kelsall, D.F., Trans. Inst. Chem. Engrs., 30, 87 (1952).
9. Kelsall, D.F., Chem. Eng. Sci., 2, 254 (1953).
10. Bradley, D., and Pulling, D.J., Trans. Inst. Chem. Engrs., 37, 34 (1959).
11. Binnie, A.M., and Teare, J.D., Proc. Roy. Soc. A 235, 78 (1956).
12. Binnie, A.M., and Hookings, G.A., Proc. Roy. Soc. A 194, 398 (1948).

13. Binnie, A.M., and Harris, D.P., Quart. Journ. Mech. and Applied Math., 3, 89 (1950).

14. Binnie, A.M., Hookings, G.A., and Kamel, M.Y.M., Journ. Fluid Mech., 3, 261 (1957).

15. Long, R.R., Quart. Journ. Mech. and Applied Math., 9, 385 (1956).

16. Som, S.K., and Sen, S.N., Can Journ. Chem. Eng., 60, 153 (1982).

17. Harvey, J.F., and Hermandorfer, H.W., Trans. Soc. Naval Architects and Marine Engrs., 51, 61 (1943).

18. Place, G., Ridgway, K., and Danckwerts, P.V., Trans. Inst. Chem. Engrs., 37, 268 (1959).

19. Binnie, A.M., Quart. Journ. Mech. and Applied Math., 10, Pt. 3, 276 (1957).

20. Nuttal, J.B., Nature, 172, 582 (1953).

21. Gaunt, G.N., Trans. Inst. Chem. Engrs., 61, 271 (1983).

22. Burggraf, O.R., Stewartson, K., and Belcher, R.J., Phys. Fluids., 14, 1821 (1971).

23. Bloor, M.I.G., and Ingham, D.B., Phys. Fluids., 20, 1228 (1977).

24. Taylor, G.I., Quart. Journ. Mech. and Applied. Math., 3, 129 (1950).

25. Ashton, C.J., Ph.D. Thesis, University of Aston. England (1980).

26. Binnie, A.M., Proc. Roy. Soc., A 205, 530 (1951).

27. Nissan, A.H., and Bresan, V.P., A. I. Ch. E.

Journ., 7, 543 (1961).

28. Harvey, J.K., Journ. Fluid Mech., 14, pt.4, 585 (1962).

29. Benjamin, T.B., Journ. Fluid Mech., 14, 593 (1962).

30. Sarpkaya, T., Journ. Fluid Mech., 45, pt.3, 545 (1971).

31. Gore, R.W., and Ranz, W.E., A. I. Ch. E. Journ., 10, 83 (1964).

32. Chanaud, R.C., Journ. Fluid Mech., 21, pt.1, 111 (1965).

33. Charpentier, J.C., Trans. Inst. Chem. Engrs., 60, 131 (1982).

34. Beenackers, A.A.C.M., and Van Swaaij, W.P.M., Chem. Eng. Journ., 15, 39 (1978).

35. Reynolds, O., Phil. Trans. Roy. Soc., London A 186, 123 (1894).

36. Taylor, G.I., Proc. Roy, Soc., A 151, 421 (1935).

37. Van Karman, T., and Howarth, L., Proc. Roy. Soc., A 164, 192 (1938).

38. Kolmogoroff, A.N., Compt. Rend. Acad. Sci., URSS 30, 301 (1941).

39. Heisenberg, W., Z. Physik., 124, 628 (1948).

40. Kraichnan, R.H., Phys. Fluid, 7, 1723 (1964).

41. Obukhov, A.M., Izv. Akad. Nauk, SSSR Ser Geograf. Geofiz. 13, 58 (1949).

42. Batchelor, G.K., J. Fluid Mech., 5, 113 (1957).

43. Beek, J., and Miller, R.S., Chem. Eng. Progr. Symp.

Ser., 55, No.25, 23 (1957).

44. Lee, J., Phys. Fluids., 8, 1647 (1965).

45. Corrsin, S.k, 'Proc. of the first Iowa Thermodynamics Symp.' Iowa State University, Ames (1953).

46. Corrsin, S., A. I. Ch. E. Journ., 10, 870 (1964).

47. Danckwerts, P.V., Appl. Sci. Research., A3, 279 (1953).

48. Sachs, J.P., and Rushton, J.H., Chem. Eng. Prog., 50, 597 (1954).

49. Cutter, L.A., A. I. Ch. E. Journ., 12, 35 (1966).

50. Manning, F.S., and Wilhelm, R.H., A. I. Ch. E. Journ., 9, 12 (1963).

51. Reith, I.T., A. I. Ch. E. - I. Chem. Eng Symp. Ser., No. 10, 14, 125 (1964).

52. Kim, W.J., and Manning, F.S., A. I. Ch. E J., 10.747 (1964).

53. Rao, M.A., and Brodkey, R.S., Chem. Eng. Sci., 27, 137 (1972).

54. Mujumdar, A.S., Huang, B., Wolf, D., Weber, M.E., and Douglas, W.J.M., Can. J. Chem. Eng., 48, 475 (1970).

55. Reed, X.B., Princz, M., and Hartland, S., Proc. Second Europ. Conf. on Mixing Cambridge, England (1977).

56. Donald, M.B., and Singer, H., Trans. Inst. Chem. Engrs., 37, 255 (1959).

57. Fossett, H., and Prosser, L.E., Proc. I. Mech. E., 160, 244 (1949).

58. Fossett, H., Trans. Inst. Chem. Engrs., 29, 322 (1951).

59. Taylor, J.F., Grimmett, H.L., and Comings, E.W., Chem. Eng. Prog., 47, 175 (1951).

60. Rosensweig, R.E., Hottel, H.C., and Williams, G.C., Chem. Eng. Sci., 15, 111 (1961).

61. Kristmanson, D., and Danckwerts, P.V., Chem. Eng. Sci., 16, 267 (1961).

62. Wilson, R.A.M., and Danckwerts, P.V., Chem. Eng. Sci., 19, 885 (1964).

63. Smith, J.M., Chemical Engineering Kinetics, 3rd. Edn. Mc. Graw - Hill, New York (1981).

64. Nauman, E.B., Chem. Eng. Sci., 32, 287 (1977).

65. Kataoka, K., and Takigawa,T., A. I. Ch. E. Journ., 27, 504 (1981).

66. Ajmera, P.V., Ph.D. Thesis, Carnegie - Mellon University, Pittsburgh, Pa (1969).

67. Vassilatos, G., and Toor, H.L., A. I. Ch. E. Journ. 11, 666 (1965).

68. Fisher, D.A., Ph.D. Thesis, University of Minnesota, Minneapolis (1974).

69. Ou, J.J., Ph.D. Thesis, University of Minnesota, Minneapolis (1980).

70. Ou, J.J., Lee, C.S., and Chen, S.H., Chem. Eng. Sci., 38, 1323 (1983).

71. Brodkey, R.S., Turbulence in Mixing Operations, Academic Press, Inc (1975).

72. Smoluchowski, M.V., Z. Phys. Chem., 92, 129 (1917).

73. Toor, H.L., A. I. Ch. E. Journ., 8, 70 (1962).

74. Toor, H.L., Ind. Eng. Chem. Fund., 8, 655 (1969).

75. Keeler, R.N., Petersen, E.E., and Prausnitz, J.M., A. I. Ch. E. Journ., 11, 221 (1965).

76. Toor, H.L., and Chiang, S.H., A. I. Ch. E. Journ., 5, 339 (1959).

77. Mao, K.W., and Toor, H.L., A. I. Ch. E. Journ., 16, 49 (1970).

78. Singh, M., Ph.D. Thesis, Carneigie - Mellon University Pittsburgh, Pa (1973).

79. Torrest, R.S., and Ranz, W.E., A. I. Ch. E. Journ., 16, 930 (1970).

80. Brodkey, R.S., Chem. Eng. Commun., 8, 1 (1981).

81. Mckelvey, K.N., Yieh, H.H., and Brodkey, R.S., A. I. Ch. E. Journ., 21, 1165 (1975).

82. Burke, S.P., and Schumann, T.E.W., Ind. Eng. Chem., 20, 998 (1928).

83. Caldin, E.F., Fast Reactions In Solution., Blackwell Scientific Publications Oxford (1964).

84. Hague, D.N., Fast Reactions., John Wiley & Sons. Inc (1971).

85. Frost, A.A., and Pearson, R.G., Kinetics and Mechanism. A Study of Homogeneous Chemical Reactions. 2nd Edn. John Wiley & Sons Inc. (1961).

86. Borne, J.R., The influence of mixing on fast, multiple chemical reactions I. Chem. E. Jubilee Symp. E.F.C.E. Pub. Ser., No. 21 (1982).

87. Hartiridge, H., and Roughton, F.J.W., Proc. Roy. Soc., A 104, 376, (1923).

88. Chance, B., J. Franklin Inst., 229, 455, 737 (1940).

89. Chance, B., Rev. Sci. Inst., 22, 619 (1951).

90. Gibson, Q.H., Disc. Faraday Soc., 17, 137 (1954).

91. Dalziel, K., Disc. Faraday Soc., 17, 128 (1954).

92. Pinsent, B.R.W., Disc. Faraday Soc., 17, 140 (1954).

93. Pearson, L., Pinsent, B.R.W., and Roughton, F.J.W., Disc. Faraday Soc., 17, 141 (1954).

94. Denbigh, K.G., and Page, F.M., Disc. Faraday Soc., 17, 145 (1954).

95. Young, H.H., and Hammett, L.P., J. Amer. Chem. Soc., 72, 280 (1950).

96. Stead, B., Page, F.M., and Denbigh, K.G., Disc. Faraday Soc., 2, 263 (1947).

97. Saldick, J., and Hammett, L.P., J. Amer. Chem. Soc., 72, 283 (1950).

98. Rand, M.J., and Hammett, L.P., J. Amer. Chem. Soc., 72, 287 (1950).

99. Eigen, M., Disc. Faraday Soc., 17, 194 (1954).

100. Nauman, E.B., Chem. Eng. Commun., 8, 53 (1981).

101. Mac Mullin, R.B., and Weber, M., Trans. Amer. Inst.

Chem. Engrs., 31, 409 (1935).

102. Bosworth, R.C.L., Phil. Mag., 39, 847 (1948).

103. Bosworth, R.C.L., Phi. Mag., 40, 314 (1949).

104. Danckwerts, P.V., Chem. Eng. Sci., 2, 1 (1953).

105. Hopkins, M.J., Sheppard, A.J., and Eisenklam, P., Chem. Eng. Sci., 24, 1131 (1969).

106. Petho, A., Chem. Eng. Sci., 23, 807 (1968).

107. Michelsen, M.L., and Ostergaard, K., Chem. Eng. Sci., 25, 583 (1970).

108. Bischoff, K., and Levenspiel, O., Adv. Chem. Eng., 4, 95 (1963).

109. Wen, C.Y., and Chung, S.F., Can. J. Chem. Eng., 43, 101 (1965).

110. Van de Vusse, J.G., Chem. Eng. Sci., 17, 507 (1962).

111. Clegg, G.T., and Coates, R., Chem. Eng. Sci., 22, 1177 (1967).

112. Moeller, W.G., and Dealy, J.M., Can. J. Chem. Eng., 48, 356 (1970).

113. Fox, E.A., and Gex, V.E., A. I. Ch. E. Journ., 2, 539 (1956).

114. Norwood, K.W., and Metzner, A.B., A. I. Ch. E. Journ., 6, 432 (1960).

115. Brennan, D.J., Trans. Inst. Chem. Engrs., 54, 209 (1976).

116. Coker, A.K., 14th Annual Dept. Chem. Eng. Symp. University of Aston, England (1983).

117. Sterbacek, Z., and Tausk, P., Mixing In The Chemical Industry, Pergamon Press (1965).

118. Okita, N., and Oyama, Y., Kagaku Kogaku., 27, 252 (1963).

119. Van de Vusse, J.G., Chem. Eng. Sci., 4, 178 (1955).

120. Hiby, J.M., and Modigell, M., Paper to 6th CHISA Congress, Prague (1978).

121. Lane, A.G.C., and Rice, P., Inst. Chem. Eng. Symp. Ser. No. 6, (1981).

122. Khang, S.J., and Levenspiel, O., Chem. Eng. Sci., 31, 569 (1976).

123. Maruyama, T., Ban, Y., and Mizushina, T., J. Chem. Eng. (Japan) 15, 342 (1982).

124. Kafarov, V.V., Ogorodnik, I.M., and Laskovenko, E.K., Int. Chem. Eng., 11, 41 (1971).

125. Brennan, D.J., and Lehrer, I.H., Trans. Inst. Chem. Engrs., 54, 139 (1976).

126. Denbigh, K.G., Dombrowski, N., Kisiel, A.J., and Place, E.R., Chem. Eng. Sci., 17, 573 (1962).

127. Danckwerts, P.V., and Wilson, R.A.M., J. Fluid Mech., 16, 412 (1963).

128. Coker, A.K., M.Sc. Thesis, University of Aston, England (1979).

129. Cooper, A.R., and Jeffreys, G.V., Chemical Kinetics and Reactor Design, Oliver & Boyd (1971).

130. Stainthorp, F.P., and Clegg, G.T., Chem. Eng. Sci, Suppl., 20, 167 (1965).

131. Sinclair, C.G., and Mc Naughton, K.J., Chem. Fund., 2, 287 (1963).

132. Wolf, D., and Resnick, W., Ind. Eng. Chem. Fund., 2, 287 (1963).

133. Bush, S.F., Trans. Inst. Chem. Engrs., 47, T59 (1969).

134. Wood, T., Chem. Eng. Sci., 23, 783 (1968).

135. David, R., Houzelot, J.L., and Villermaux, J., 3rd Europ. Conf. on Mixing, 113 (1979).

136. Syred, N., and Beer, J.M., Combustion and Flame 23, 143 (1974).

137. Beer, J.M., and Lee, K.B., Proc. 10th. Int. Symp. On Combustion, 1187 (1965).

138. Nauman, E.B., Chem. Eng. Commun., 8, 53 (1981).

139. Danckwerts, P.V., Chem. Eng. Sci., 8, 93 (1958).

140. Zwietering, TH.N., Chem. Eng. Sci., 11, 1 (1959).

141. Weinstein, H., and Adler, R.J., Chem. Eng. Sci., 22, 65 (1967).

142. Wen, C.Y., and Fan, L.T., Models For Flow Systems And Chemical Reactors, Marcel Dekker, Inc. New York (1975).

143. Ritchie, B.W., and Tobgy, A.H., Chem. Eng. Commun., 2, 249 (1978).

144. Bird, R.B., Stewart, W.E., and Lightfoot, E.N., Transport Phenomena, John Wiley & Sons. Inc. (1960).

145. Duncan, W.J., Thom, A.S., and Young, A.D.,

An Elementary Treatise On The Mechanics Of Fluids. Edwards Arnold (Publishers) Ltd. (1962).

146. Levenspiel, O., Chemical Reaction Engineering, 2nd Edn. John Wiley & Sons, Inc. (1972).

147. Himmelblau, D.M., and Bischoff, K.B., Process Analysis and Simulation: Deterministic Systems, John Wiley & Sons, Inc. (1968).

148. Sharma, M.M., and Danckwerts, P.V., Trans. Faraday Soc., 59, 386 (1963).

149. Denbigh, K.G., Chem. Eng. Sci., 14, 25 (1961).

15Ø. Jones,K., Basic Organic Chemistry, Part 5. Industrial Products John Wiley & Sons (1975).

151. Hinde, G.E., Anionic Surfactants Part 1. Surfactant Science Series 7, Marcel Dekker, Inc. New York and Basel (1977).

152. Heinerth, E., Anionic Surfactants Chemical Analysis, Surfactant Science Seris, 8, Marcel Dekker, Inc., New York and Basel (1977).

153. Grant, P.E., Ph.D. Thesis, University of Birmingham, (1971).

154. Milwidsky, B.M., and Gabriel, D.M., Detergent Analysis, 'A Handbook for Cost effective Quality Control, George Godwin, London (1981).

155. Peters, M.S., and Timmerhaus, K.D., Plant Design And Economics For Chemical Engineers 3rd. Edn.

Mc. Graw - Hill, Int. Book Co. (1981).

156. Dykes, D.J., Ph.D. Thesis, University of Aston, England, (1980).

157. Altiokka, M.R., Ph.D. Thesis, University of Aston, England, (1983).

158. Spencer, J.L., and Lunt, R.R., Ind. Eng. Chem. Fundam., 19, 142 (1980).